Study of diacylglycerol-activated TRPC6 channels in murine cortical neurons and their roles in the transport of transition metals

Peng Tu

UNIVERSITE JOSEPH FOURIER-GRENOBLE 1

THESE

Pour obtenir le grade de

DOCTEUR DE L'UNIVERSITE JOSEPH FOURIER

Discipline : BIOLOGIE

Présentée et soutenue publiquement le 23 septembre 2009

par

Peng TU

Etude des canaux TRPC6 sensibles au diacylglycérol dans les neurones de cortex de souris et de leurs rôles dans le transport de métaux de transition

---

Membres du jury :

Prof Claude FEUERSTEIN (Grenoble)	**Président**
Dr Thierry CAPIOD (Lille)	**Rapporteur**
Dr Jean-Yves CHATTON (Lausanne)	**Rapporteur**
Dr Janique GUIRAMAND (Montpellier)	**Examinateur**
Dr Isabelle MARTY (Grenoble)	**Examinateur**
Dr Alexandre BOURON (Grenoble)	**Directeur de thèse**

Study of diacylglycerol-activated TRPC6 channels in murine cortical neurons and their roles in the transport of transition metals

ABSTRACT

Transient Receptor Potential Canonical 6 (TRPC6) form diacylglycerol (DAG)-activated non-selective cation channels expressed in a variety of tissues and cells. They are for instance expressed in the cortex of embryonic (E13) mice. Cellular calcium imaging experiments show the existence of DAG-sensitive plasma membrane cation channels in cortical neurons kept in culture. These channels are permeable to Ca^{2+}, Na^{+}, Ba^{2+} and Mn^{2+}. The Ca^{2+} entry, not controlled by protein kinase C, is blocked by Gd^{3+} and SKF-96365 but potentiated by flufenamic acid. Hyperforin, which activates TRPC6 channels without acting on the other TRPC isoforms, triggers an entry of Ca^{2+} via non-selective cation channels. Although the exact molecular identity of the DAG-sensitive channels in cortical neurons has not yet been established, we suggest that TRPC6 form these channels.

Quantitative analyses with Inductively Coupled Plasma-Optical Emission Spectrometry, atomic absorption spectrometry and synchrotron microbeam X-ray fluorescence (μ-SXRF) show that over-expressing TRPC6 in HEK-293 cells elevates the intracellular contents of zinc, sulphur and manganese. Cellular iron and zinc imaging experiments indicate that TRPC6 channels, either over-expressed in HEK cells or endogenously present in cortical neurons, are permeable to iron and zinc when activated by DAG or hyperforin. The experiments with μ-SXRF further reveal that activating TRPC6 channels in the presence of iron leads to an intracellular iron accumulation in both HEK cells and cortical neurons.

In addition, during the time course of this study, we provided experimental evidence showing that flufenamic acid and hyperforin, two pharmacological tools used to manipulate the activity of TRPC6 channels, release Ca^{2+} and Zn^{2+} from mitochondria.

Key words: cortical neurons, HEK-293 cells, TRPC6, diacylglycerol, flufenamic acid, hyperforin, synchrotron microbeam X-ray fluorescence, iron, zinc, manganese, copper

REMERCIEMENTS / ACKNOWLEDGEMENTS

Ce travail a été réalisé au sein de l'équipe 'CaFe' du Laboratoire de Chimie et Biologie des Métaux (UMR 5249 CEA/CNRS/UJF) dirigé par le Prof Marc Fontecave au Commissariat à l'Énergie Atomique (CEA) Grenoble. Je souhaite remercier tous les membres du laboratoire de m'avoir accueillie et intégrée pendant ces trois années.

Je remercie Dr Thierry Capiod et Dr Jean-Yves Chatton pour l'honneur que vous m'avez fait en acceptant d'être rapporteurs de cette thèse. Je remercie aussi le Prof Claude Feuerstein, Dr Janique Guiramand et Dr Isabelle Marty qui ont bien voulu prendre part au jury.

Je te suis infiniment reconnaissante, Alexandre Bouron, mon directeur de thèse ! Merci de m'avoir encadrée tout au long de cette thèse et de m'avoir fait confiance. Merci pour ton aide constante et ta patience. J'ai beaucoup appris à ton contact, pendant nos discussions, pendant les préparations des articles, et non seulement dans le domaine des neurosciences. J'ai toujours admiré ton esprit scientifique et ton enthousiasme pour la recherche. Aussi, je n'oublierai pas ton dévouement à corriger, corriger et recorriger ce manuscrit. C'est tes corrections qui améliorent à chaque fois la précision et la clarté de cette thèse. Merci de tout cœur!

J'exprime toute ma reconnaissance à Jean-Marc Moulis. Il semblait que tu as toujours eu les réponses pour mes questions, non seulement sur le fer! C'était pour cette raison que je suis venue te voir lorsque j'avais besoin de conseils. J'admire ton regard critique et le recul que tu sais prendre sur les choses. Les discussions avec toi ont été très enrichisssantes et m'ont permis de gagner du temps. Tu m'as beaucoup apporté.

I would like to thank Dr Christiane Kunert-Keil, Dr Silke Lucke and Dr Heinrich Brinkmeier for our collaboration concerning the article on TRPC6, even though I haven't had the chance to meet you in person.

Un grand merci à Sylvain Bohic et Björn De Samber! Sylvain, j'admire ta gentillesse et tes grandes qualités de scientifique. Tu as passé des jours et des nuits sur la beamline et pour les analyses. Grâce à toi, j'ai pu montrer les très belles cartes de cellules dans la thèse. Björn, c'est un grand plaisir de passer le temps avec toi sur la beamline. Merci à toi pour les efforts que tu as faits sur notre travail au synchrotron. Tous les deux, même si des fois vous

avez parlé une langue (la physique) que je ne connaissais pas très bien, vous m'avez apprise autre chose que de la biologie.

Un grand merci à Pierre Richaud, Josiane Arnaud et Dr Sonia Levi. Merci à vous pour les efforts que vous avez faits pour mon projet de thèse.

Un grand merci à Gérard Brandolin pour ta gentillesse, ta patience, pour ton aide sur le travail de l'acide flufenamic et pour tes précieux conseils.

Et biensûr Julien Gibon! C'est dommage (pour moi) que tu sois arrivé si tard au labo. Pendant cette dernière année de ma thèse, il était toujours très agréable de discuter avec toi, pas seulement sur les manips, mais aussi sur la vie. Tu es très sympa et j'admire ta grande ouverture d'esprit. Je te remercie pour ton aide précieuse sur la fin. Tu feras une très belle thèse, j'en suis très sûre!

Je te remercie, Peggy Charbonnier, pour toute ton aide sur mes manips!

Je tiens à remercier les collègues qui m'ont aidée pendant ma thèse, Florent, Patrice, Serge, Christel, Estelle, Ely, Isabelle, Mohamed et Fabien.

I would like to thank you, Karthik. It is just so great to have you in the lab in these three years. I enjoyed all our discussions about China and India. Thank you for introducing to me the Indian music, the Bollywood films, and those dishes which I adore! It is a pity that I still can't say a word in Tamil, but in the future whenever someone speaks of Tamil Nadu (or India) to me, I can tell him instantly that I have a very good friend there.

Je tiens à remercier tous les autres amis dans le labo, Simon, Heidi, Caroline et Cheick.

最后的却是最重要的，谢谢我的家人，妈妈，爸爸，奶奶，爷爷，老婶，老伯，还有涂程。如果可以，很希望把论文翻译成中文，然后好好给你们讲讲我这三年来都做了些什么研究。不过这可是个不小的工程！就算不能看懂，希望你们可以感受到这论文里面饱含了你们对我的期望，鼓励，和长久的支持！再次感谢你们，也希望和你们分享这份成功的喜悦！

献给我的妈妈爸爸

Dedicated to my Mom and Dad

CONTENTS

LIST OF FIGURES

LIST OF TABLES

ABBREVIATIONS

$[Ca^{2+}]_i$	cytosolic concentration of free calcium
$[Ca^{2+}]_m$	mitochondrial concentration of free calcium
$[Ca^{2+}]_o$	extracellular concentration of free calcium
$[Na^{+}]_i$	cytosolic concentration of free sodium
$[Zn^{2+}]_i$	cytosolic concentration of free zinc
μ-SXRF	synchrotron microbeam X-ray fluorescence
20-HETE	20-hydroxyeicosatetraenoic acid
2-APB	2-aminoethyoxydiphenyl borane
AA	arachidonic acid
AD	Alzheimer's Disease
AMPA	α-amino-3-hydroxy-5-methyl-4-isoxazolepropionic-acid
BBB	blood brain barrier
BDNF	brain derived neurotrophic factor
Ca-A/K-receptor channels	Ca^{2+}-permeable AMPA/kainate channels
CaM	calmodulin
CaMKIV	Ca^{2+}/calmodulin-dependent kinase IV
CCE	capacitative Ca^{2+} entry
CIRB	calmodulin and inositol 1,4,5-triphosphate receptor-binding
CNS	central nervous system
CREB	cAMP-response-element binding protein
CSF	cerebrospinal fluid
DAG	diacylglycerol
DMSO	dimethyl sulfoxide
DMT1	divalent metal transporter 1
DTDP	2,2'-dithiodipyridine
EC_{50}	half maximal effective concentration
EET	epoxyeicosatrienoic acids
EGF	epidermal growth factor
ER	endoplasmic reticulum
FAC	ferric ammonium citrate
FCCP	carbonyl cyanide 4-(trifluoromethoxy)phenylhydrazone
FFA	flufenamic acid
GABA	gamma-aminobutyric acid
GPCR	G-protein-coupled-receptors
GSH	glutathione
GSSG	glutathione disulfide
HEK	human embryonic kidney
IC_{50}	half maximal inhibitory concentration
ICP-OES	Inductively Coupled Plasma-Optical Emission Spectrometry
I_{CRAC}	calcium release-activated current
IP_3	inositol 1,4,5-triphosphate
IP_3R	inositol 1,4,5-triphosphate receptor
IRE	iron responsive elements
IRP	iron regulatory proteins
JAK2	Janus Kinase 2
K_d	dissociation constant
MRE	metal-response element
MT	metallothioneins

MTF-1	metal-response element-binding factor-1
NCCE	non capacitative Ca^{2+} entry
NCX	Na^{+}/Ca^{2+} exchanger
NGF	nerve growth factor
NMDA	N-methyl-D-aspartate
NSCC	non-selective cation channels
NTBI	non-transferrin-bound iron
OAG	1-oleoyl-2-acetyl-sn-glycerol
PD	Parkinson's Disease
PDD	phorbol-12,13-didecanoate
PDGF	platelet-derived growth factor
PI3K	phosphoinositide 3-kinase
PIP	phosphatidylinositol phosphates
PIP_2	phosphatidylinositol 4,5-bisphosphate
PIP_3	phosphatidylinositol 3,4,5-trisphosphate
PKA	cAMP-dependent protein kinase
PKC	protein kinase C
PKG	cGMP-dependent protein kinase
PLC	phospholipase C
PMA	phorbol-12-myristoyl-13-acetate
PTK	protein-tyrosine kinases
PTP	permeability transition pore
PUFA	poly-unsaturated fatty acids
RNAi	RNA interference
ROC	receptor-operated channels
ROCE	receptor-operated Ca^{2+} entry
ROS	reactive oxygen species
RTK	receptor tyrosine kinases
RT-PCR	reverse-transcription polymerase chain reaction
SAG	1-stearoyl-2-arachidonoyl-sn-glycerol
SOC	store-operated channels
SOCE	store-operated Ca^{2+} entry
STIM	stromal interacting molecule
TBI	transferrin-bound iron
TCT	trivalent cation-specific transporter
Tf	transferrin
TfR	transferrin receptor
thermoTRP	temperature-sensitive TRP channels
TPEN	N,N,N′,N′-tetrakis(2-pyridylmethyl)ethylenediamine
TrkB	tyrosine kinase receptor B
TRPC	transient receptor potential canonical
VEGF	vascular endothelial growth factor
VGCC	voltage-gated Ca^{2+} channels
$\Delta\psi_m$	mitochondrial membrane potential

INTRODUCTION

TRPC6 can form diacylglycerol (DAG)-activated non-selective cation channels. They are expressed in a variety of tissues and cells. Experiments performed in the laboratory showed their expression in the cortex of embryonic (E13) mice. Since in the neuronal cell line PC12 TRPC6 channels can permit the uptake of Fe via a mechanism independent of transferrin and its receptor, we thought to verify whether this property was shared by neurons of the central nervous system.

During the first part of my thesis I checked for the presence of functional TRPC6 channels in cortical neurons. The DAG analogues 1-oleoyl-2-acetyl-sn-glycerol (OAG) and 1-stearoyl-2-arachidonoyl-sn-glycerol (SAG), as well as flufenamic acid and hyperforin were employed to characterize the properties of the channels. From a methodological point of view, the main techniques used were cellular calcium/sodium imaging with fluorescent probes and electrophysiology (whole-cell patch-clamp). The data obtained are summarized in the articles 1 (Chapter 7), 2 (Chapter 10) and 3 (Chapter 11).

After having established the existence of DAG-sensitive cation channels exhibiting TRPC6-like properties, I then determined if these channels could permit the transport of trace metal ions across the plasma membrane. To this aim, experiments were conducted on HEK-293 cells stably expressing TRPC6 channels and on cultured cortical neurons. Quantitative analyses were done with Inductively Coupled Plasma-Optical Emission Spectrometry and atomic absorption spectroscopy. Cellular imaging experiments with fluorescent indicators (Fura-2, calcein, FluoZin-3) were also carried out to gain further insight into the dynamics of the transport processes. In addition, topographic and quantitative analyses of intracellular trace metals were obtained by using synchrotron microbeam X-ray fluorescence. These results are summarized in Chapter 9.

In the Introduction (Chapters 1-4), I will give first a short overview of the different TRP channels. Then I will summarize the molecular mechanisms controlling iron and zinc entry into brain cells. Finally, I will present experimental data showing that distinct families of cation channels, including TRP channels, are involved in the transport of these elements across the plasma membrane. The Introduction part does not provide a complete and exhaustive discussion of these different topics but rather offers a short overview of our current knowledge.

1 TRPC6 channels

TRPC6, a non-selective cation channel (NSCC), is a member of the Canonical Transient Receptor Potential (TRPC) family. In the following Chapter 1, a short overview is given of the different families of TRP channels.

1.1 TRP

The TRP protein superfamily consists of a variety of cation channels that share structural similarities with *Drosophila* TRP. *Drosophila* carrying *trp* gene mutations exhibits a transient receptor potential instead of a sustained plateau-like receptor potential evoked in response to continuous light, which makes the *trp* flies behave as though blind (Cosens and Manning, 1969; Hardie and Minke, 1992). Accordingly, there came the name TRP. Unlike most ion channels, TRP channels are identified by their homology. They are involved in numerous biological processes.

1.1.1 Classification

TRP channels are expressed and functional in many organisms including flies, worms, fish, tunicates, mouse and human. Based on their amino acid sequence similarities, the TRP proteins fall into seven subfamilies: TRPC ('Canonical'), TRPV ('Vanilloid'), TRPM ('Melastatin'), TRPA ('Ankyrin'), TRPP ('Polycystin'), TRPML ('Mucolipin') and TRPN ('no mechanoreceptor potential C, NOMPC') (Clapham et al., 2005; Venkatachalam and Montell, 2007). There are now at least 28 mammalian TRP proteins which fall into the first six of the seven subfamilies (Flockerzi, 2007; Venkatachalam and Montell, 2007) (see Table 1-1). Figure 1-1 shows the phylogenetic tree of mammalian TRP.

1.1.2 Structure and permeability

To date, no structural information at the atomic level is available for any full-length TRP channel due to difficulties lying in overexpression, functional purification, and crystallization of eukaryotic transmembrane proteins. However, electron microscopy and X-ray crystallography have revealed the entire protein structure and the cytosolic domains of some TRP, respectively (Moiseenkova-Bell and Wensel, 2009). All TRP proteins have six putative transmembrane domains (S1-S6) with a cation-permeable pore region formed by a short hydrophobic stretch between S5 and S6 (Owsianik et al., 2006a) and cytosolic amino (N) and carboxy (C) termini. As they resemble voltage-gated K^+ channels (Clapham et al.,

2001), TRP channels are thought to form homo- or heterotetrameric channels (Clapham et al., 2001; Lepage and Boulay, 2007; Venkatachalam and Montell, 2007). Figure 1-2 shows the predicted protein structure and channel topology.

The degree of amino acid sequence similarity among members of one subfamily approaches up to more than 90%, but is limited between subfamilies. Within the cytoplasmic domains, some structural motifs have been identified by sequence comparisons such as an ankyrin repeat domain, a coiled-coil domain (Schindl and Romanin, 2007), and the so-called 'TRP domain', which is a highly conserved stretch of ~25 amino acids in the C-terminal region close to S6. It is found in all mammalian TRP subfamilies except TRPA and TRPP (Montell, 2005; Ramsey et al., 2006). In fact, amino acid sequences forming the pore are strongly conserved across different TRP subfamilies (Montell, 2005). S5, S6 and the TRP domain are similar even in distinct TRP channels (Ramsey et al., 2006).

All TRP channels are permeable to cations, only two TRP channels are impermeable to Ca^{2+} (TRPM4, TRPM5), and two others are highly Ca^{2+} permeable (TRPV5, TRPV6). The permeability ratios P_{Ca}/P_{Na} for these channels vary considerably, ranging from 0.1 to >100 (Owsianik et al., 2006a).

Table 1-1 The seven subfamilies of TRP channels

	Fly	***Worm***	***Mouse***	***Human***
TRPC	3	3	7	6
TRPV	2	5	6	6
TRPM	1	4	8	8
TRPA	4	2	1	1
TRPP	4	1	3	3
TRPML	1	1	3	3
TRPN	1	1	-	-
Total	16	17	28	27

Adapted from (Flockerzi, 2007).

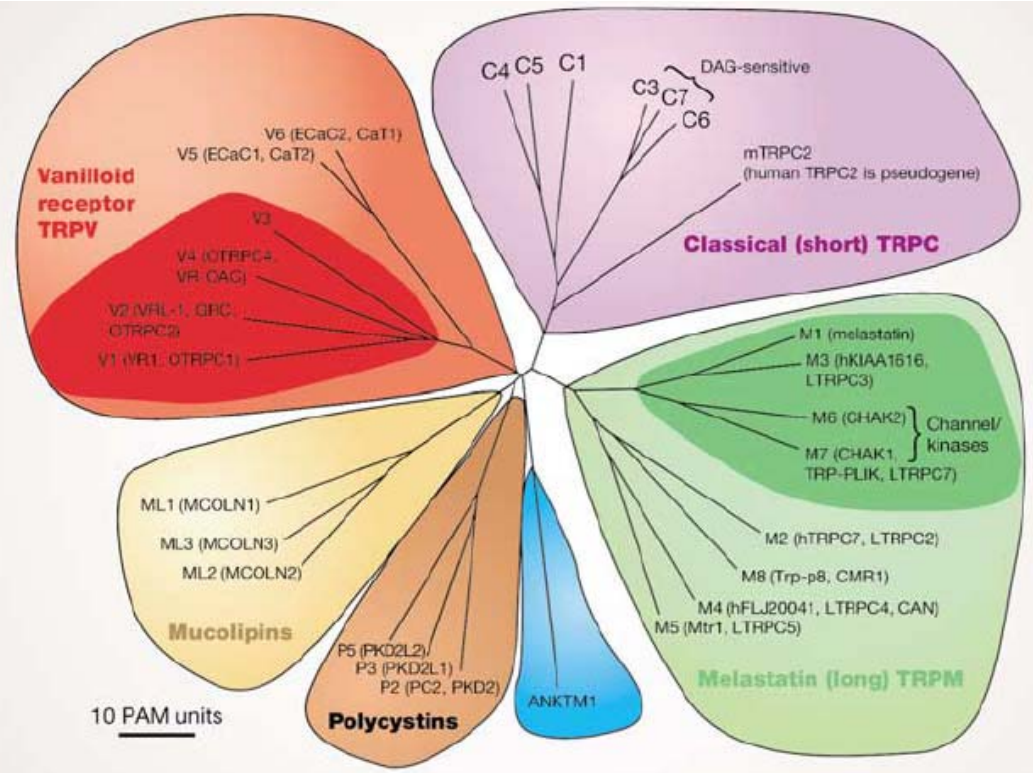

Figure 1-1 Phylogenetic tree of the mammalian TRP

The evolutionary distance is shown by the total branch lengths in point accepted mutations (PAM) units, which is the mean number of substitutions per 100 residues. *Adapted from (Clapham, 2003).*

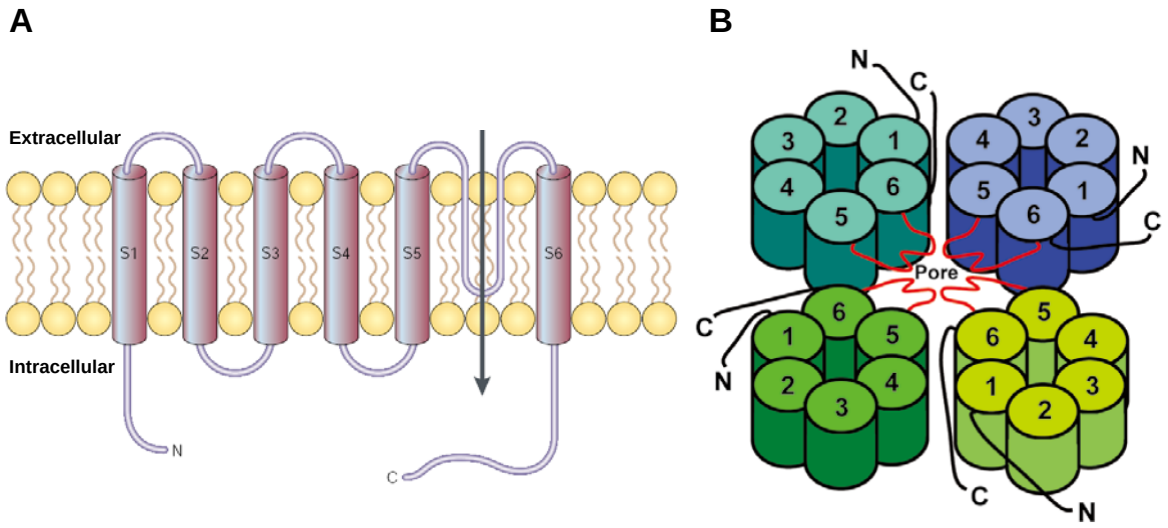

Figure 1-2 Predicted structure of TRP and topology of TRP channels

Panel A shows the putative structure of a TRP. It has 6 transmembrane helices (S1-S6) with a putative pore region between S5 and S6. *Adapted from (Clapham et al., 2001).* Panel B shows the proposed tetrameric channel structure. A TRP channel is composed of hetero or homo tetrameric TRP. *Adapted from (Watanabe et al., 2009).*

1.1.3 Activation and regulation

Several activation mechanisms have been established for TRP channels, including receptor activation, ligand activation, direct activation (Ramsey et al., 2006) as well as activation by calcium store depletion.

Receptor activation

Receptor activation is mediated by the phospholipase C (PLC) signaling pathway. G-protein-coupled-receptors (GPCR) or receptor tyrosine kinases (RTK) activate PLC, which catalyze the hydrolysis of phosphatidylinositol 4,5-bisphosphate (PIP_2) into diacylglycerol (DAG) and inositol 1,4,5-triphosphate (IP_3). Downstream from receptor activation, TRP channels are activated by one of the following mechanisms: (1) the decreased level of PIP_2; (2) the production of DAG; or (3) the release of Ca^{2+} from internal stores of the endoplasmic reticulum (ER) induced by IP_3 binding to IP_3 receptor (IP_3R). Of note, for some TRP channels such as TRPC4 and TRPC5, their gating mechanisms are currently unclear.

Ligand activation

Ligands that activate TRP channels may be divided into four categories: (a) endogenous lipid and lipid metabolites such as phosphoinositides (Nilius et al., 2008), DAG and poly-unsaturated fatty acids (PUFA) (Chyb et al., 1999); (b) exogenous small organic molecules such as 2-aminoethyoxydiphenyl borane (2-APB) and some natural compounds (Vriens et al., 2008) like capsaicin, menthol and hyperforin; (c) purine nucleotides and their metabolites such as ADP-ribose (Kolisek et al., 2005) and βNAD^+ (Hara et al., 2002); (d) inorganic molecules and ions such as Ca^{2+}, La^{3+} (Schaefer et al., 2000), Zn^{2+} (Hu et al., 2009) and H_2O_2 (Hara et al., 2002).

Direct activation

Putative direct activators include temperature, mechanical stimuli, conformational coupling to IP_3R, channel phosphorylation, osmolarity and pH.

Activation by calcium store depletion

There has been a long-time debate concerning the molecular identity of the store-operated channels (SOC). Store-operated Ca^{2+} entry (SOCE), also called capacitative Ca^{2+} entry (CCE), refers to a phenomenon in which the depletion of intracellular Ca^{2+} stores (primarily the ER) leads to the activation of plasma membrane Ca^{2+}-permeable channels. Ca^{2+} entering through SOC can then be pumped into the stores and thus permit their replenishment

(Putney, 1986; Parekh and Putney, 2005). Although some TRPC (see Section 1.1.5) may participate in SOCE, they exhibit biophysical properties distinct from SOC. For example, TRPC channels underline non selective cation currents which stands in contrast with the highly Ca^{2+}-selective SOC currents like I_{CRAC} (calcium release-activated current), (Putney, 2007a). The exact contribution of TRPC in SOCE remains currently debated.

It is worth mentioning that some TRP channels seem to have several modes of activation. Actually, many TRP channels function as polymodal sensors that integrate many of the signals mentioned above.

Concerning the regulation of TRP channels, their cytoplasmic parts play important regulatory roles influencing their function and trafficking (Pedersen et al., 2005; Owsianik et al., 2006b). Regulation of TRP channels includes: (1) posttranslational modifications such as phosphorylation, glycosylation and nitrosylation; (2) protein-protein interactions implying actors like calmodulin (CaM), IP_3R, stromal interacting molecule (STIM) and Orai proteins; (3) lipid interactions such as PIP_2 and cholesterol; and (4) trafficking.

1.1.4 TRP channels function as cellular sensors

TRP channels participate in a diversity of functions in both excitable and non-excitable cells. Something common and inherent shared by the superfamily of cation channels is that they function as cellular sensors integrating diverse signals, including intracellular and extracellular messengers, light, temperature, pain, pheromones, taste, touch, osmolarity. Thus, TRP channels play critical roles in sensory physiology (Clapham, 2003; Voets et al., 2005; Venkatachalam and Montell, 2007; Damann et al., 2008).

Phototransduction

Since the identification of the original *Drosophila* TRP channels (Montell and Rubin, 1989), these proteins have long been described as important channels involved in sensory transduction mechanisms. Recent studies suggest that TRP channels may function in mammalian photosensitive retinal ganglion cells: light activation of melanopsin, a GPCR from the opsin group, activates TRPC3 channels (Panda et al., 2005; Qiu et al., 2005).

Mechanosensation

Members of TRP channels are implicated in a wide range of mechanical transduction processes including the basic osmoregulation, complex hearing and touch (Christensen and Corey, 2007). Several TRP channels are putative stretch-activated channels, for example

TRPC1 (Maroto et al., 2005), TRPC6 (Spassova et al., 2006), TRPM7 (Numata et al., 2007a, b). Whether other components participate in the activation of TRP in response to membrane stretch is unknown. TRPV4 mediates the transduction of osmotic stimuli in many cell types and TRPV4$^{-/-}$ mice displays defects in osmoregulation (Liedtke and Friedman, 2003), while TRPA1 is involved in the auditory transduction process (Corey et al., 2004) and pain mechanosensation (Bautista et al., 2006).

Thermosensation

Six mammalian temperature-sensitive TRP channels (thermoTRP) have been identified, and they are the principal molecular thermometers in the peripheral sensory system (Patapoutian et al., 2003; Voets et al., 2005; Dhaka et al., 2006; Talavera et al., 2008). These thermoTRP have the potential to detect changes in temperature from <10°C to >50°C: TRPV1 and TRPV2 are sensors for uncomfortable warm (>43°C) (Caterina et al., 1997) and very hot (>52°C) (Caterina et al., 1999) temperatures, respectively; TRPV3 (>30-39°C) (Peier et al., 2002b; Smith et al., 2002; Xu et al., 2002) and TRPV4 (~25-34°C) (Guler et al., 2002) contribute to the perception of moderate temperatures; TRPM8 (<25°C) (McKemy et al., 2002; Peier et al., 2002a) and TRPA1 (<17°C) (Story et al., 2003) are activated upon cooling and function in sensing cold.

Chemosensation

TRPM5 is a candidate channel involved in taste sensation (Zhang et al., 2003). These channels expressed in taste receptor cells (Perez et al., 2002) are critical players in the signal transduction cascade downstream from the activation of sweet, bitter and umami tastes (Zhang et al., 2003; Damak et al., 2006). A recent study shows that TRPM5 and TRPV1 channels are involved in the transduction of the taste of complex tasting divalent salts (Riera et al., 2009). *trpc2* is a pseudogene in human, but murine TRPC2, expressed in the vomeronasal organ, is essential for the transmission of pheromone-mediated signals (Stowers et al., 2002; Lucas et al., 2003).

In addition to TRPM5 and TRPC2, thermoTRP contribute to the perception of chemical stimuli. ThermoTRP seem to be the favourite targets for plant-derived chemicals (Voets et al., 2005). This finding explains why we interpret food ingredients as thermal sensation, such as ‘hot’ chilli pepper and ‘cool’ mint (Voets et al., 2005).

1.1.5 TRPC

Among the TRP superfamily, the TRPC subfamily has the highest degree of homology to *Drosophila* TRP. Based on structural and functional similarities, the seven TRPC known to date can be subdivided into four groups: TRPC1, TRPC2, TRPC4/5 and TRPC3/6/7. TRPC channels are ubiquitously expressed, forming homomeric and heteromeric cation channels.

TRPC channels can be activated downstream from the PLC pathway. They are receptor-operated channels (ROC) and function as cellular effectors of hormones, neurotransmitters and growth factors. Homomeric (Hofmann et al., 1999; Okada et al., 1999) and heteromeric (Thebault et al., 2005; Maruyama et al., 2006; Peppiatt-Wildman et al., 2007) TRPC3/6/7 channels can be activated by DAG. In addition, homomeric TRPC1 (Lintschinger et al., 2000), TRPC2 (Lucas et al., 2003) and heteromeric TRPC1-TRPC3 (Lintschinger et al., 2000; Liu et al., 2005), TRPC3-TRPC4 (Poteser et al., 2006), TRPC3-TRPC5 (Liu et al., 2007) can also be activated by DAG. Although one group has reported that TRPC5 can be activated by DAG (Lee et al., 2003b), it is generally accepted that TRPC4 and TRPC5 are not DAG sensitive (Hofmann et al., 1999; Schaefer et al., 2000; Venkatachalam et al., 2003). The precise signal activating these channels remains unknown. Of note, direct binding of DAG to any TRPC channel has not yet been reported.

Although not possessing important Ca^{2+} selectivity, all TRPC channels have been proposed to be candidates for SOC. Store-depletion activates TRPC1 (Zitt et al., 1996; Liu et al., 2000), TRPC2 (Vannier et al., 1999), TRPC3 (Vazquez et al., 2003; Yildirim et al., 2005), TRPC4 (Philipp et al., 2000; Freichel et al., 2001; Fatherazi et al., 2007), TRPC5 (Xu et al., 2006; Ma et al., 2008), TRPC6 (Jardin et al., 2008; Jardin et al., 2009), TRPC7 (Riccio et al., 2002b; Lievremont et al., 2004), as well as heteromeric TRPC channels (Wu et al., 2000; Wu et al., 2004b; Zagranichnaya et al., 2005; Brechard et al., 2008). The different modes of activation (ROC versus SOC) observed depend on the expression system used and also depend on the expression level of the channel studied. Recently, new molecular players of SOCE, STIM and Orai, have been discovered and their interactions with TRPC channels has been demonstrated (Birnbaumer, 2009; Cahalan, 2009; Salido et al., 2009). STIM (Roos et al., 2005) is a transmembrane protein residing primarily in the ER and functions as a putative ER Ca^{2+} sensor. Orai proteins (Feske et al., 2006; Vig et al., 2006) are predicted to span the plasma membrane and form ion channels. The cytosolic C terminus of STIM interacts with Orai and TRPC channels. Indeed, all TRPC except TRPC7 are regulated directly or indirectly by STIM (Huang et al., 2006; Worley et al., 2007; Yuan et al., 2007). Concerning SOCE, one

hypothesis proposes that STIM senses the depletion of Ca^{2+} in the ER stores and activates SOC formed by Orai proteins (without TRPC channels) (Hewavitharana et al., 2007; Putney, 2007b). According to the second hypothesis, Orai and TRPC work in concert in mediating SOCE (Liao et al., 2008). Figure 1-3 illustrates these two models.

Besides the receptor-operated or store-operated modes of activation, TRPC channels can be modulated by lipids, covalent modifications and scaffolding proteins such as Homer and junctate (Kiselyov and Patterson, 2009).

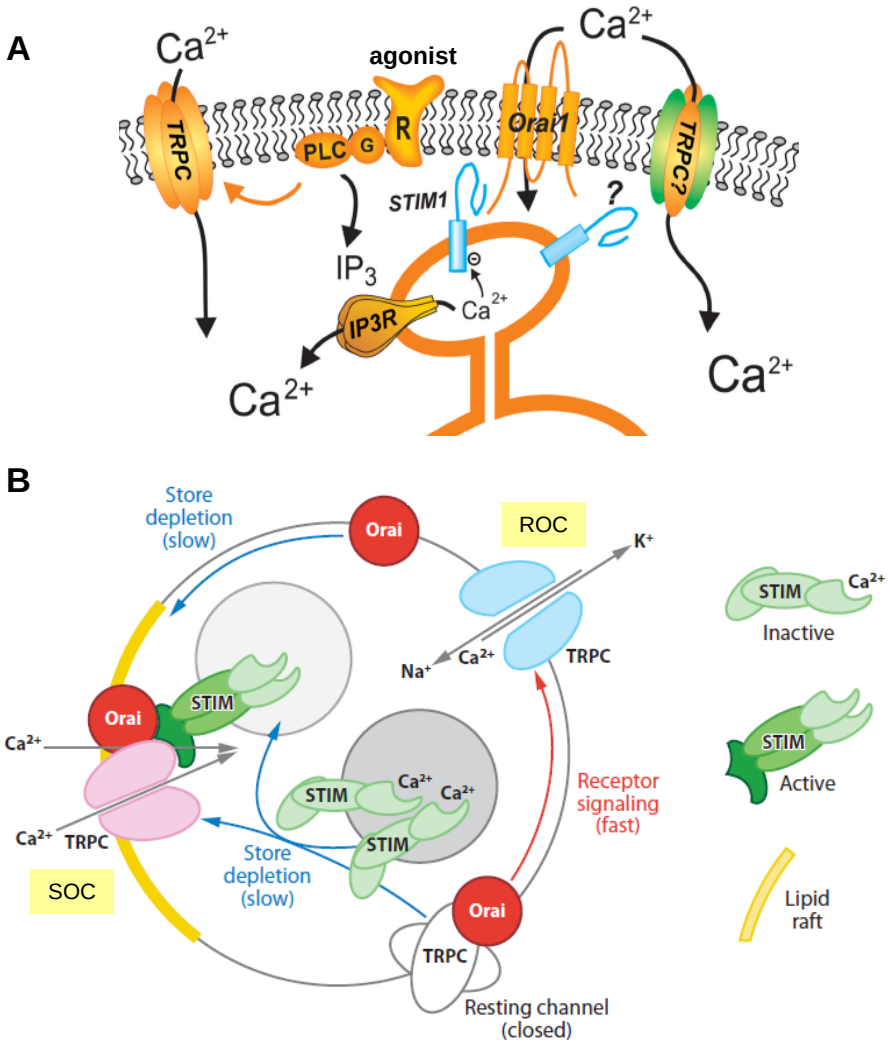

Figure 1-3 Proposed models of interaction among TRPC channels, STIM and Orai

Panel A shows a model in which STIM functions as a ER Ca^{2+} sensor and Orai proteins form SOC. *Adapted from (Putney, 2007b).* In panel B, the receptor-coupled PLC signaling pathway rapidly activates TRPC leading to receptor-operated Ca^{2+} entry (ROCE). Depletion of Ca^{2+} stores then activates STIM, causing the redistribution of Orai and TRPC and the assemblage of SOC complex in lipid raft domains of the plasma membrane. This leads to Ca^{2+} entry. *Adapted from (Birnbaumer, 2009).*

1.2 TRPC6

TRPC6 have been cloned from mouse brain (Boulay et al., 1997), human testis and placental (Hofmann et al., 1999). Full-length mouse and human TRPC6 proteins consist of 930 and 931 amino acids, respectively (Dietrich and Gudermann, 2007).

1.2.1 Structure of TRPC6 channels

TRPC6 (Figure 1-4) displays common structural features of the TRP superfamily of cation channels: cytoplasmic N- and C-termini, six transmembrane helices (S1-S6) and a putative pore region located between S5 and S6 (Clapham et al., 2001). TRPC6 possesses features of the TRPC subfamily, for example, N-terminal ankyrin-like repeats (Venkatachalam and Montell, 2007), a N-terminal (adjacent to S1) caveolin-1 binding site (Vazquez et al., 2004), C-terminal (adjacent to S6) highly conserved regions of TRP domain including TRP box 1 (Glu-Trp-Lys-Phe-Ala-Arg or EWKFAR) and TRP box 2 (a proline-rich motif) (Venkatachalam and Montell, 2007) and the CaM and IP_3R-binding (CIRB) site (Zhu, 2005).

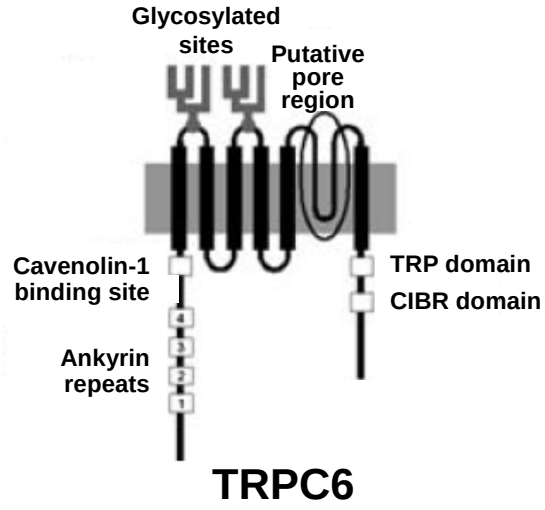

Figure 1-4 Structure of TRPC6 channels

The structural elements of TRPC6 channels include cytoplasmic N- and C-termini, six transmembrane helices (S1-S6), a putative pore region located between S5 and S6, the N-terminal ankyrin-like repeats and caveolin-1 binding site, and the C-terminal TRP domain CIRB domain. Two glycosylated sites in TRPC6 are indicated by covalently bound carbohydrates (in grey). *Adapted from (Dietrich et al., 2005a).*

In both recombinant and native systems, TRPC6 can assemble into homo- and heterotetramers not only within the TRPC3/6/7 subfamily (Goel et al., 2002; Hofmann et al., 2002; Bandyopadhyay et al., 2005), but also with combinations of TRPC1-TRPC4/5 (Strubing et al., 2003). Two domains responsible for the oligomerization of TRPC channels have been identified (Lepage et al., 2006).

1.2.2 Biophysical properties of TRPC6 channels

Currents through TRPC6 channels show a dual inward (at negative potentials) and outward (at positive potentials) rectification and the current-voltage relationship displays an S-shaped curve (Figure 1-5). The single-channel conductance is 28-37 pS (Hofmann et al., 1999; Inoue et al., 2001; Pedersen et al., 2005). The relative ion permeability P_{Ca}/P_{Na} of TRPC6 channels is around 5 (Hofmann et al., 1999; Inoue et al., 2001).

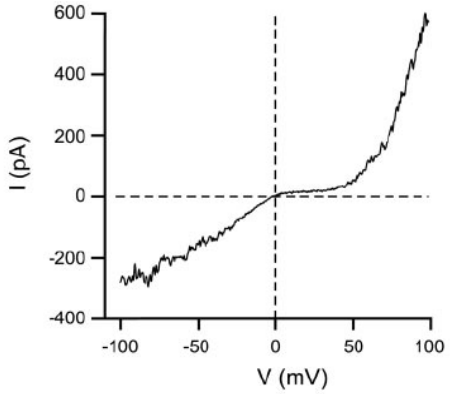

Figure 1-5 Current-voltage relationship of TRPC6 channels

The current-voltage relationship of the vasopressin-induced current via TRPC6-like channels in A7r5 smooth muscle cells is shown. It was obtained during a voltage ramp from -100 mV to + 100 mV. *Adapted from (Jung et al., 2002).*

In some cell types, other players like voltage-gated Ca^{2+} channels (VGCC), the plasmalemmal Na^+/Ca^{2+} exchanger (NCX) or ATPases participate in the entry of Ca^{2+} downstream from the activation of TRPC6 channels. For instance, in A7r5 smooth muscle cells, activation of endogenous TRPC6 channels by DAG increases cytosolic concentration of Ca^{2+} ($[Ca^{2+}]_i$). This response is blocked by the potent L-type Ca^{2+} channel inhibitor nimodipine. This indicates that the Na^+ entry via TRPC6 induces a depolarization which in turn activates VGCC (Soboloff et al., 2005). The model is illustrated in Figure 1-6. In human embryonic kidney (HEK)-293 cells stably expressing TRPC6, Ca^{2+}, in the presence of extracellular Na^+, contributes poorly (~4%) to the whole-cell currents (Estacion et al., 2004). It is concluded that in cells with a high input resistance, the primary effect of TRPC6 activation is to depolarize (due to the entry of Na^+), limiting Ca^{2+} entry via TRPC6 but facilitating Ca^{2+} entry via VGCC. In cells with a large inward-rectifier current or expressing Ca^{2+}-activated K^+ channels to hold the membrane potential negative, receptor-mediated activation of TRPC6 permits a sustained Ca^{2+} influx pathway (Estacion et al., 2004).

Another set of observations concerns the coupling between TRPC6 channels and the NCX. The NCX is an important Ca^{2+} extrusion mechanism requiring the energy of the transmembrane Na^+ gradient produced by the Na^+/K^+-ATPase, with a stoichiometry of 3 Na^+ : 1 Ca^{2+}. However, with elevated cytosolic concentration of Na^+ ($[Na^+]_i$) and at depolarized

membrane potentials, the NCX-mediated Ca^{2+} efflux decreases and can even switch from the forward (Ca^{2+} exit) to the reverse (Ca^{2+} entry) mode (Blaustein and Lederer, 1999). Indeed, Na^+ permeation through TRPC channels coupled with the reverse-mode of the NCX is an important event in Ca^{2+} signaling (Eder et al., 2005). Figure 1-7 is a model illustrating the putative link between TRPC channels and the NCX. Concerning TRPC6, the entry of Na^+ through these channels is shown to elevate $[Ca^{2+}]_i$ via the NCX operating in the reverse mode (Lemos et al., 2007; Poburko et al., 2007; Syyong et al., 2007; Fellner and Arendshorst, 2008; Meng et al., 2008).

A proteomics study shows that TRPC6 interact with the plasmalemmal Na^+/K^+-ATPase, in both kidney and brain, which indicates that they may form a functional complex involved in ion transport and homeostasis (Goel et al., 2005).

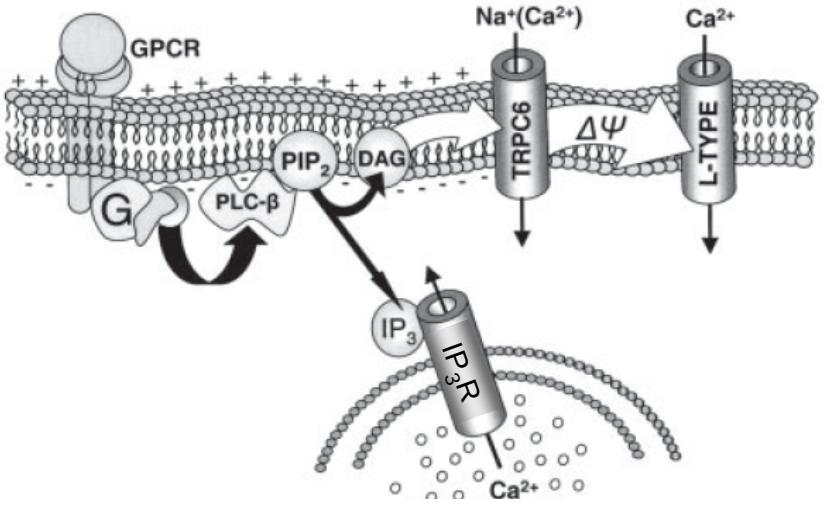

Figure 1-6 Model describing the activation of L-type Ca^{2+} channels via a TRPC6-mediated depolarization

GPCR activates PLC_β via G protein (G) and results in the formation of DAG and IP_3. IP_3 induces the release of Ca^{2+} from stores by its interaction with IP_3R, while DAG activates TRPC6 channels. The predominant entry of Na^+ (in addition to Ca^{2+}) depolarizes the membrane potential and activates voltage-sensitive L-type Ca^{2+} channels. *Adapted from (Soboloff et al., 2005).*

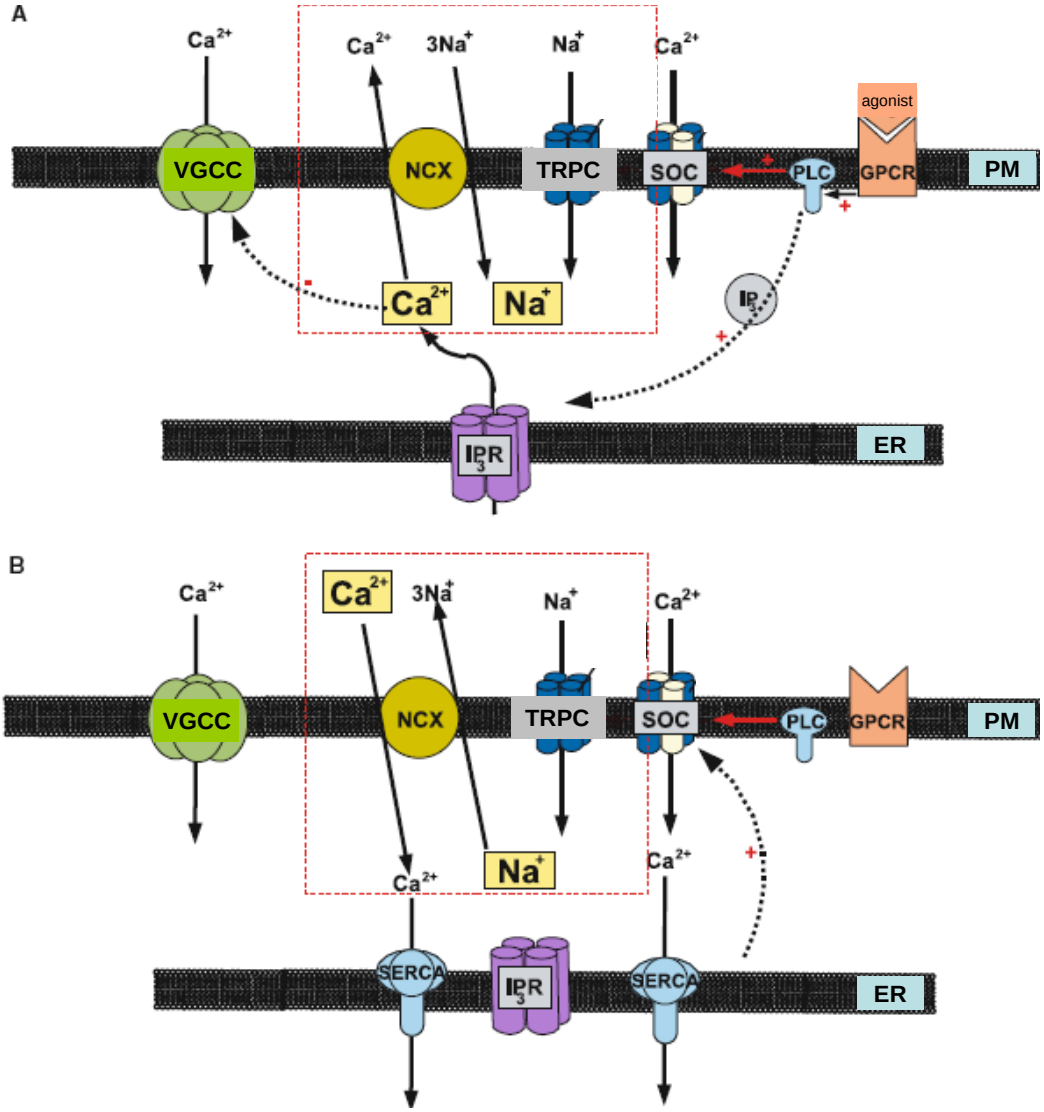

Figure 1-7 Hypothetical model of the relationship between TRPC channels and the NCX

Panel A: The activation of the PLC pathway increases $[Ca^{2+}]_i$, which drives the activation of the forward-mode of the NCX that cooperates with TRPC to produce intracellular Na^+ loading. VGCC is activated by depolarized membrane potentials but then inhibited by high local $[Ca^{2+}]_i$ levels. Panel B: Low $[Ca^{2+}]_i$ levels along with increasing $[Na^+]_i$ promote the reverse-mode of the NCX, which results in a local rise in $[Ca^{2+}]_i$ that may refill intracellular stores. Na^+ entry via TRPC channels is essential for this process. PM: plasma membrane. ER: endoplasmic reticulum. *Adapted from (Eder et al., 2005)*.

1.2.3 Activation of TRPC6 channels

1.2.3.1 Activation by diacylglycerol and related lipids

The members of the TRPC3/6/7 subfamily share 70-80% identity at the amino acid level. They all can be activated in response to the application of DAG or the DAG lipase inhibitor RHC80267 (Hofmann et al., 1999).

DAG can be metabolized by the DAG lipase to yield PUFA such as arachidonic acid (AA) and linolenic acid, which can activate or modulate a wide range of ion channels (Meves, 1994), like *Drosophila* TRP and TRPL (Chyb et al., 1999), TRPV4 (Watanabe et al., 2003), TRPM5 (Oike et al., 2006) and probably TRPC4 (Wu et al., 2002). TRPC6 has been reported to be activated by AA and 20-hydroxyeicosatetraenoic acid (20-HETE), the dominant AA metabolite (Basora et al., 2003). Epoxyeicosatrienoic acids (EET), another metabolite synthesized from AA by cytochrome P450 epoxygenases, stimulate the translocation of TRPC6 to the plasma membrane (Fleming et al., 2007; Keseru et al., 2008).

Phosphatidylinositol phosphates (PIP) have long been recognized for their roles in the regulation of TRP channels. For example, the DAG precursor and PLC substrate PIP_2, an essential modulator of various types of ion channels and transporters (reviewed by (Hilgemann et al., 2001; Suh and Hille, 2005, 2008)), positively or negatively regulates several TRP channels (Hardie, 2007; Qin, 2007; Rohacs and Nilius, 2007; Nilius et al., 2008; Large et al., 2009). The effects of PIP_2 on TRPC6 channels are still unclear. It was first reported that PIP_2 had no effect on TRPC6 activation (Hofmann et al., 1999), however recent observations show that PIP_2 can directly activate members of the TRPC3/6/7 subfamily (Lemonnier et al., 2008). PIP_2 may stimulate TRPC6 activity though the interactions with the CIRB site of TRPC6 (Kwon et al., 2007). Phosphatidylinositol 3,4,5-trisphosphate (PIP_3), a lipid product of PIP_2 catalyzed by phosphoinositide 3-kinase (PI3K), has positive effect on TRPC6 activation (Tseng et al., 2004). It disrupts the association of CaM with TRPC6, triggering the channel activation (Kwon et al., 2007). However, a recent study describes a powerful inhibitory action of PIP_2 on native TRPC6 channels expressed in mesenteric artery myocytes (Albert et al., 2008).

The regulation of TRPC6 channels by DAG and related lipids is summarized in Table 1-2.

Table 1-2 Regulation of TRPC6 channels by DAG and related lipids

Lipid		Action on TRPC6 channels	Tissue/Cell type	Techniques	References
DAG		Activation	CHO cells	Ca^{2+} imaging, Mn^{2+} quenching, electrophysiology	(Hofmann et al., 1999)
AA and its metabolites	AA 20-HETE	Activation	HEK-293 cells	Electrophysiology	(Basora et al., 2003)
	EET	Translocation	Vein endothelial cells	Ca^{2+} imaging, cell surface biotinylation and immunoblotting	(Fleming et al., 2007)
PIP_2		Activation	HEK-293 cells	Electrophysiology	(Lemonnier et al., 2008)
		Inhibition	Artery myocytes	Electrophysiology	(Albert et al., 2008)
PIP_3		Activation	HEK-293 cells	Electrophysiology	(Kwon et al., 2007)
			HEK-293 cells Jurkat T cells	Ca^{2+} imaging, pull down-analysis	(Tseng et al., 2004)

1.2.3.2 Activation by receptor stimulation

Many studies have proved that TRPC6 channels are activated in response to the stimulation of receptors including GPCR, RTK and cytokine receptor (Table 1-3). Activation of the first two groups of receptors activates the PLC signaling pathway leading to the production of DAG, while activation of interleukin-1 receptor, a cytokine receptor, also generates DAG (Beskina et al., 2007). Besides activation, stimulation of GPCR also induces the translocation of TRPC6 to the plasma membrane (Cayouette et al., 2004; Fleming et al., 2007).

Experiments with different cloned TRPC6 isoforms suggest that some amino acids present in the N terminus of TRPC6 are crucial for the activation by DAG but are not required for the activation by carbachol (Zhang and Saffen, 2001). Activation of muscarinic acetylcholine receptors stimulates the formation of a multiprotein complex containing

muscarinic acetylcholine receptors, TRPC6 channels, immunophilin FKBP12, calcineurin, CaM and protein kinase C (PKC) (Kim and Saffen, 2005). Accordingly, DAG alone may not fully account for the activation of TRPC6, and other receptor-mediated events may act synergistically with DAG to stimulate channel activity (Estacion et al., 2004).

Even though the ROC (but not SOC) identity of TRPC6 is quite clear, the high affinity interaction between IP_3R and TRPC6 has been proved biochemically (Tang et al., 2001). In fact, several studies have shown a direct interaction between the C-terminus of TRPC and the N-terminus of IP_3R (Kiselyov et al., 1998; Boulay et al., 1999; Lockwich et al., 2000; Tang et al., 2001), which is involved in the regulation of Ca^{2+} entry. Moreover, exocytotic insertion of TRPC6 channels into the plasma membrane takes place upon the depletion of intracellular Ca^{2+} stores (Cayouette et al., 2004). The latter response may be due to the conformational coupling between TRPC6 and IP_3R.

1.2.3.3 Activation by store depletion

Although TRPC6 is commonly described as a ROC, several authors have reported that it can function as a SOC. Expression of Orai in TRPC6-expressing HEK cells reconstitutes I_{CRAC} (Liao et al., 2008), while TRPC6, together with TRPC1 and Orai proteins, forms SOC in neutrophil-like HL-60 cells (Brechard et al., 2008). Moreover, in human platelets, TRPC6 plays a dual role, as a non capacitative Ca^{2+} entry (NCCE) channel regulated by DAG and as a component of SOC likely regulated by PIP_2 (Jardin et al., 2008). These latter authors further show that it is through its interaction with the Orai-STIM complex or TRPC3 that TRPC6 participates in SOCE or NCCE, respectively (Jardin et al., 2009). Interestingly, stimulation by thrombin or Ca^{2+} store depletion enhances the interaction between TRPC6 and Orai-STIM while DAG displaces TRPC6 from Orai and STIM and induces its association with TRPC3 (Jardin et al., 2009).

Table 1-3 Activation of TRPC6 by receptor stimulation

Receptor GPCR RTK cytokine receptor	**Tissue/Cell type**	**References**
H1 histamine receptor	CHO cells	(Hofmann et al., 1999)
M1 muscarinic receptor	Sympathetic neurons PC12 cells	(Delmas et al., 2002) (Zhang et al., 2006)
M3 muscarinic receptor	HEK293 cells	(Estacion et al., 2004)
M5 muscarinic receptor	COS cells	(Boulay et al., 1997; Zhang and Saffen, 2001)
B2 bradykinin receptor	Sympathetic neurons	(Delmas et al., 2002)
α1-adrenoceptor	Vascular smooth muscle	(Inoue et al., 2001)
V1 arginine vasopressin receptor	A7r5 smooth muscle cells	(Jung et al., 2002; Soboloff et al., 2005)
Serotonin receptor	A7r5 smooth muscle cells	(Jung et al., 2002)
Angiotensin II receptor (AT1)	HEK293 cells Mesenteric artery myocytes Cardiomyocytes	(Winn et al., 2005) (Saleh et al., 2006) (Onohara et al., 2006)
Protease activated receptor-1	Endothelial cells	(Singh et al., 2007)
Orexin type 1 receptor	Neuroblastoma cells	(Nasman et al., 2006)
Purinergic receptors (P2Y)	Aortic smooth muscle cells	(Lemos et al., 2007)
T-cell receptor	Jurkat T cells	(Tseng et al., 2004)
TrkB receptor	Cerebellar granule cells	(Li et al., 2005)
PDGF receptor	A7r5 smooth muscle cells	(Jung et al., 2002)
EGF receptor	COS cells	(Hisatsune et al., 2004)
VEGF receptor 2	HEK293 cells	(Pocock et al., 2004)
Interleukin-1 receptor	Astrocytes	(Beskina et al., 2007)

Abbreviations: TrkB: tyrosine kinase receptor B; PDGF: platelet-derived growth factor; EGF: epidermal growth factor; VEGF: vascular endothelial growth factor. *Adapted from (Abramowitz and Birnbaumer, 2009)*

1.2.3.4 Activation by mechanosensation

TRPC6 can be activated by mechanical stimuli independently of PLC, functioning as a sensor of mechanically and osmotically induced membrane stretch (Spassova et al., 2006). By cooperating with TRPC1 and TRPV4, TRPC6 mediates mechanical hyperalgesia and nociceptor sensitization in dorsal root ganglion neurons, but its precise role in the transduction of mechanical stimuli is unknown (Alessandri-Haber et al., 2009). However, some studies indicated that TRPC6 would not be stretch-activated channels (Gottlieb et al., 2008). In addition, some GPCR can be mechanically activated (Mederos y Schnitzler et al., 2008; Yasuda et al., 2008). They are the essential mechanosensing components in vascular smooth muscle cells and function as sensors of membrane stretch leading to the activation of TRPC6 (as well as TRPC3 and TRPC7) channels (Mederos y Schnitzler et al., 2008) (Figure 1-8). Moreover, a recent study shows that TRPC6 channels are not primarily activated by mechanical stimuli (Inoue et al., 2009). Instead, once receptor-activated, the channels become mechanosensitive via the production of 20-HETE (Inoue et al., 2009).

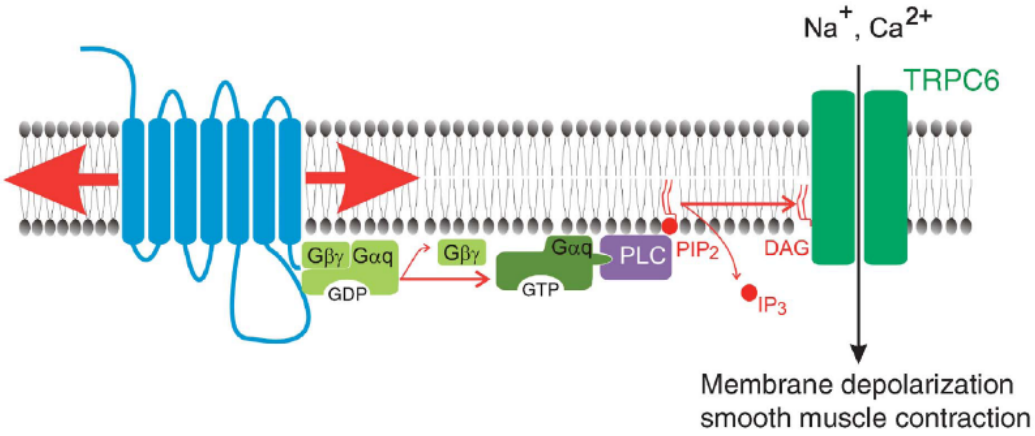

Figure 1-8 Proposed mechanism for stretch-induced activation of TRPC6 channels

In vascular smooth muscle cells, GPCR is mechanically activated, which induces the sequential activation of TRPC6 channels. *Adapted from (Voets and Nilius, 2009).*

1.2.4 Regulation of TRPC6 channels

1.2.4.1 Regulation by phosphorylation

Protein kinase C

Since DAG is the physiological activator of some PKC, the contribution of PKC to the effects of DAG on TRPC6 channels has been investigated. A PKC-independent effect of

DAG on TRPC6 has initially been shown: an acute challenge of TRPC6-expressing CHO cells with the PKC activators, phorbol-12,13-didecanoate (PDD) or phorbol-12-myristoyl-13-acetate (PMA), fails to evoke a Ca^{2+} rise; while downregulation of PKC by a long pre-treatment with these phorbol esters or inhibition with the PKC inhibitors, staurosporine, bisindolylmaleimide I or calphostin C does not affect TRPC6 activation by DAG (Hofmann et al., 1999). Although these results have been further confirmed (Inoue et al., 2001), some studies show the involvement of PKC in TRPC6 inactivation. By activating PKC, PMA blocks the activation of TRPC6 by DAG and carbachol (Zhang and Saffen, 2001). Interestingly, a later study shows a differential effect of PKC activation on DAG- and carbachol-induced TRPC6 currents: PMA has no significant effect on DAG-activated currents whereas it essentially eliminates the regulation by receptor stimulation (Estacion et al., 2004). In addition, the inactivation time course of TRPC6 currents is significantly retarded through PKC inhibition by calpostin C (Shi et al., 2004). Indeed, PKC phosphorylation at an identified phorsphorylation site located near TRPC6 channel C-terminus (Ser^{768}) is correlated with the channel inhibition (Kim and Saffen, 2005). The activity of TRPC6 can be fine-tuned through the phosphorylation/dephosphorylation cycles by the formation of a multiprotein complex centered on TRPC6 containing PKC and calcineurin, which respectively phosphorylate and dephosphorylate the channels (Kim and Saffen, 2005).

The PKC pathway activated by DAG may signify a feedback regulation of TRPC channels following activation by DAG. In mesenteric artery myocytes, low levels of DAG activate the channels whereas high levels of DAG inhibit them via a PKC-dependent pathway (Saleh et al., 2006). This dual PKC-independent and dependent action of DAG has also been seen in TRPC3 channels (Venkatachalam et al., 2003; Trebak et al., 2005).

Src family protein-tyrosine kinases

Tyrosine phosphorylation by Src family protein-tyrosine kinases (PTK) is involved in the modulation of TRPC6 channel activity (Hisatsune et al., 2004). Fyn, a member of Src family PTK, physically interacts with TRPC6 and increases the channel activity by tyrosine phosphorylation (Hisatsune et al., 2004). In addition, growth factors known to stimulate RTK such as EGF (Hisatsune et al., 2004) and PDGF (Jung et al., 2002) activate TRPC6 channels (Table 1-3). The former finding shows that the action of EGF on TRPC6 occurs via the stimulation of EGF receptors which in turn activate Src family PTK (Hisatsune et al., 2004). Moreover, the specific inhibition of Scr family of PTK by PP2 or SU6656 abolishes the activation of TRPC6 channels (Hisatsune et al., 2004; Soboloff et al., 2005; Aires et al.,

2007). Whether tyrosine phosphorylation directly affects the gating of TRPC6 channels remains unclear, since it is possible that DAG generated by PTK-activated PLC_γ pathway activates the channels (Jung et al., 2002; Large et al., 2009). Indeed, mutation in the tyrosine phosphorylation site of TRPC6 does not impair the channel activation, and TRPC6 can still be activated in Src family PTK-deficient cells (Kawasaki et al., 2006).

Other protein kinases

In human platelets, TRPC6 can be phosphorylated by a cAMP-dependent and a cGMP-dependent protein kinase (respectively PKA and PKG), but the phosphorylation does not seem to affect the channel activity (Hassock et al., 2002). In both a heterologous expression system (HEK-293 cells) and A7r5 vascular myocytes, TRPC6 channels are negatively regulated by the NO–cGMP–PKG pathway, probably via a phosphorylation site (Thr^{69}) of the N-terminal (Takahashi et al., 2008). In addition, a Ca^{2+}-CaM dependent phosphorylation involving CaM kinase II is essential for the activation of TRPC6 (Shi et al., 2004).

1.2.4.2 Regulation by Ca^{2+} and Calmodulin

Calcium

The effect of the extracellular concentration of calcium ($[Ca^{2+}]_o$) on TRPC6 currents remains controversial. Currents via endogenous TRPC6 channels of A7r5 smooth muscle cells are partially inhibited by physiological $[Ca^{2+}]_o$, while the complete removal of external Ca^{2+} decreases the amplitude of inward currents (Jung et al., 2002). This stands in contrast with other studies showing that $[Ca^{2+}]_o$ has a potentiating action on the TRPC6 currents in both HEK and vascular smooth muscle cells (Inoue et al., 2001). A later study reports biphasic effects of $[Ca^{2+}]_o$ on TRPC6 currents in HEK cells. It potentiates the currents in a submillimolar range (EC_{50} ~0.4 mM) but inhibits them in a higher concentration range (IC_{50} ~4 mM) (Shi et al., 2004).

Calmodulin

Calcium is also known to influence the activity of TRPC channels through the action of CaM. CaM, a small soluble Ca^{2+}-binding protein involved in the regulation of many cellular functions including channel activity (Saimi and Kung, 2002), binds directly to *Drosophila* TRP and TRPL (Phillips et al., 1992). Multiple CaM-binding sites are identified on different TRP proteins, for example, CaM binds to the C-terminus of all 7 TRPC (Tang et

al., 2001; Trost et al., 2001; Zhang et al., 2001; Boulay, 2002; Singh et al., 2002; Ordaz et al., 2005), namely the C-terminal CaM-binding sites. Interestingly, the first C-terminal CaM-binding site is also bound to an N-terminal region of IP_3R and was therefore named CIRB site (Tang et al., 2001; Zhang et al., 2001). The CIRB site is conserved among all TRPC proteins and *Drosophila* TRP proteins (Zhu, 2005). CaM and IP_3R compete with each other for the binding to the CIRB site of TRPC (Tang et al., 2001; Zhang et al., 2001). This competition is Ca^{2+}-dependent since CaM only binds to the CIRB site in the presence of Ca^{2+}. In some cases, CaM binding to the CIRB site can prevent TRPC channels from being activated, whereas the displacement of CaM by activated IP_3R or the inhibition by CaM antagonists activate the channels. This inhibitory effect of CaM has been found on TRPC1 (Vaca and Sampieri, 2002), TRPC3 (Zhang et al., 2001), TRPC4 (Tang et al., 2001), TRPC7 (Shi et al., 2004) as well as TRPC6 (Kwon et al., 2007). The latter study shows that mutations in TRPC6 that increase PIP_3-mediated disruption of CaM binding result in an enhancement of TRPC6 currents (Kwon et al., 2007). On the contrary, several studies show that CaM binding to TRPC6 is necessary for its activation. CaM inhibitors like calmidazolium and trifluoperazine, which dissociate CaM from TRPC6, inhibit TRPC6 activity in HEK-293 cells (Boulay, 2002; Shi et al., 2004).

1.2.5 Pharmacology of TRPC6 channels

1.2.5.1 Non-specific inhibitors

Unfortunately, there are no specific TRPC6 inhibitors available. TRPC6 can be blocked by cadmium (Cd^{2+}), lanthanum (La^{3+}) and gadolinium (Gd^{3+}) The 50% inhibitory concentration (IC_{50}) values for Cd^{2+}, La^{3+} and Gd^{3+} are 253µM, 4µM and 1.9µM, respectively (Inoue et al., 2001). TRPC6 can also be blocked by some organic blockers such as SKF-96365 (Inoue et al., 2001), amiloride (Inoue et al., 2001) and 2-APB (Clapham, 2007). In addition, the stretch activation of TRPC6 is inhibited by the tarantula peptide, GsMTx-4 (Spassova et al., 2006).

1.2.5.2 Flufenamic acid

Flufenamic acid (FFA), a non-steroidal anti-inflammatory drug belonging to the family of fenamates, is often used as a non-specific cation and anion channel blocker. In both HEK cells expressing TRPC6 and in rabbit portal vein smooth muscle cells, FFA reversibly enhances currents through TRPC6 whereas it dose-dependently inhibits currents through

TRPC3 and TRPC7 (Inoue et al., 2001). Since then, FFA represents a pharmacological tool to differentiate TRPC6 from TRPC3 and TRPC7 (Jung et al., 2002; Carter et al., 2006; Hill et al., 2006; Saleh et al., 2006; Fellner and Arendshorst, 2008). However, the potentiating effect of FFA on 20-HETE-triggered currents has not been found in TRPC6 expressing HEK cells (Basora et al., 2003). Although the use of FFA as a positive regulator of TRPC6 channels remains controversial (Chapter 10, article 2), a recent work has further confirmed that FFA is a tool for investigating TRPC6-mediated calcium signaling in human podocytes and HEK cells (Foster et al., 2009).

1.2.5.3 Hyperforin

Hyperforin, a bicyclic polyprenylated acylphloroglucionol derivative, is the major active constituent of *Hypericum perforatum* (St. John's wort) extract. Hyperforin has antidepressant properties. It is a broad-band neurotransmitter reuptake inhibitor affecting the synaptosomal uptake of serotonin, dopamine, noradrenalin, glutamate and gamma-aminobutyric acid (GABA) (Chatterjee et al., 1998; Beerhues, 2006). Other different cellular effects of hyperforin with potential pharmacological interest have been discovered, including its effects on β-amyloid precursor protein and on inflammation, as well as antibacterial, antitumoral and antiangiogenic effects (Medina et al., 2006).

At nanomolar concentrations, hyperforin induces significant inhibition of various ion channels (Chatterjee et al., 1999; Krishtal et al., 2001), but can activate NSCC (Treiber et al., 2005). The latter authors reveal that hyperforin activates TRPC6 channels in PC12 cells and HEK cells, without activating the other TRPC isoforms (Leuner et al., 2007). Hyperforin is now a potent pharmacological tool used to study TRPC6 channels (see Chapter 11, article 3).

1.2.6 Distribution and functions of TRPC6

TRPC6 is expressed in a wide variety of tissues including brain, kidney, lung, heart, ovary, testis … (Garcia and Schilling, 1997; Inoue et al., 2001; Hassock et al., 2002; Riccio et al., 2002a; Tseng et al., 2004). They participate in many biological processes ranging from cell proliferation to synaptogenesis. For a detailed description, see Table 1-4 and the following reviews: (Clapham, 2003; Schlondorff and Pollak, 2006; Dietrich and Gudermann, 2007; Nilius et al., 2007; Venkatachalam and Montell, 2007; Abramowitz and Birnbaumer, 2009).

Table 1-4 Functional roles of TRPC6 in different tissues

Tissue/Cell type		Physiological and pathophysiological responses	Functional roles of TRPC6	References
Vascular system	Vascular smooth muscle cells	Pressure-induced vasoconstriction (Bayliss effect [a]) and mechanosensitivity	Down-regulation of TRPC6 attenuates arterial smooth muscle depolarization and constriction caused by elevated intravascular pressure [1]. This may involve the stretch-induced activation of TRPC6 channels [2, 3] (see Section 1.2.3.4 for details).	(Welsh et al., 2002) [1] (Spassova et al., 2006) [2] (Mederos y Schnitzler et al., 2008) [3]
		Proliferation	Enhanced expression of TRPC6 and TRPC3 may be partially responsible for increased proliferation of pulmonary artery smooth muscle cells in idiopathic pulmonary arterial hypertension patients.	(Yu et al., 2004) [4]
		Vascular hypertension	Increased TRPC6 expression contributes to enhanced vascular smooth muscle cells reactivity and to vascular hypertension.	(Bae et al., 2007)
	Vascular endothelial cells	Permeability	Ca^{2+} entry via TRPC6 activates RhoA and in turn regulates endothelial cell contraction and the increase in endothelial permeability.	(Singh et al., 2007)
		Migration	Lysophosphatidylcholine translocates TRPC6 and TRPC5 to the plasma membrane, resulting in the inhibition of endothelial cell migration.	(Chaudhuri et al., 2008)

[a] Bayliss effect: Increasing intraluminal pressure in small arteries causes vasoconstriction (Bayliss, 1902).

Heart	Cardiac myocytes	Cardiac hypertrophy	Angiotensin II-induced cardiac hypertrophy is mediated by a Ca^{2+}-calcineuin-nuclear factor of activated T cells (NFAT) signaling pathway dependent on the activation of TRPC3 and TRPC6 [5]. Cardiac-specific overexpression of TRPC6 in transgenic mice results in cardiac hypertrophy [6].	(Onohara et al., 2006) [5] (Kuwahara et al., 2006) [6]
	Cardiac fibroblasts	Cardiac fibrosis	The endothelin-1-induced TRPC6 up-regulation in cardiac fibroblasts and the following NFAT activation negatively regulates endothelin-1-induced myofibroblast formation.	(Nishida et al., 2007)
Kidney	Glomerular podocytes	Glomerular filtration barrier dysfunction	Several mutations in TRPC6 are associated with the development of familial focal segmental glomerulosclerosis (FSGS) [7, 8]. Increased TRPC6 expression leads to disruption of podocytes cytoskeletal integrity causing proteinuria [9].	(Winn et al., 2005) [7] (Reiser et al., 2005) [8] (Moller et al., 2007) [9]
	Glomerular mesangial cells	Renal hyperfiltration (hyperglycemia)	High glucose incubation down-regulates TRPC6. Diabetic rats show a decrease in glomerular TRPC6 expression.	(Graham et al., 2007)
Lung	Pulmonary artery smooth muscle cells	Pulmonary hypertension	TRPC1 and TRPC6 are up-regulated by hypoxia in pulmonary artery smooth muscles, and these channels are implicated in hypoxia-induced pulmonary hypertension [10, 11]. TRPC6 expression is also enhanced in pulmonary artery smooth muscles from patients with idiopathic pulmonary arterial hypertension [4]. In addition, TRPC6 is essential for hypoxic pulmonary vasoconstriction and alveolar gas exchange [12].	(Lin et al., 2004) [10] (Wang et al., 2006) [11] (Weissmann et al., 2006) [12]

Blood	Platelets	Hyperglycemia	High glucose increases TRPC6 channel protein expression on the platelet surface. Platelets from patients with type 2 diabetes mellitus show increased TRPC6 expression.	(Liu et al., 2008)
	Erythrocytes	Eryptosis	TRPC6 contributes to the Ca^{2+} leak of human erythrocytes and participates in Ca^{2+}-induced erythrocyte death.	(Foller et al., 2008)
Nervous system (see Section 1.2.6.2)	Cerebral granule neuron	Neuronal survival	Ca^{2+} influx through TRPC3 and TRPC6 promotes cerebellar granule neuron survival via CREB activation.	(Jia et al., 2007)
		Axon guidance	Growth-cone turning induced by BDNF is abolished when TRPC3 and TRPC6 are inhibited by down-regulation or over-expression of their negative mutants.	(Li et al., 2005)
	Hippocampal neurons	Neuronal morphogenesis	TRPC6 promotes dendritic growth through a CaMKIV-CREB pathway.	(Tai et al., 2008)
		Synaptogenesis	TRPC6 is mainly localized to excitatory postsynaptic sites and is important for the development of dendritic spines and excitatory synapses.	(Zhou et al., 2008)
	Dorsal ganglion neurons	Mechanosensation	TRPC1 and TRPC6 channels cooperate with TRPV4 to mediate mechanical hyperalgesia and nociceptor sensitization.	(Alessandri-Haber et al., 2009)
Malignant cells	Prostate cancer epithelial cells	Proliferation	Phenylephrine stimulates cells proliferation via increased TRPC6 expression.	(Thebault et al., 2006)
	Hepatoma cells		Over-expressing TRPC6 increases cell proliferation.	(El Boustany et al., 2008)
	Breast adenocarcinoma		TRPC6 channels are strongly expressed and functional in breast cancer epithelial cells.	(Guilbert et al., 2008)

1.2.6.1 Distribution of TRPC6 in the brain

Human

All TRPC are widely expressed (Riccio et al., 2002a). Concerning TRPC6 (Figure 1-9), it is homogeneously expressed throughout the CNS and peripheral tissues with the highest levels in placenta and lung (Riccio et al., 2002a).

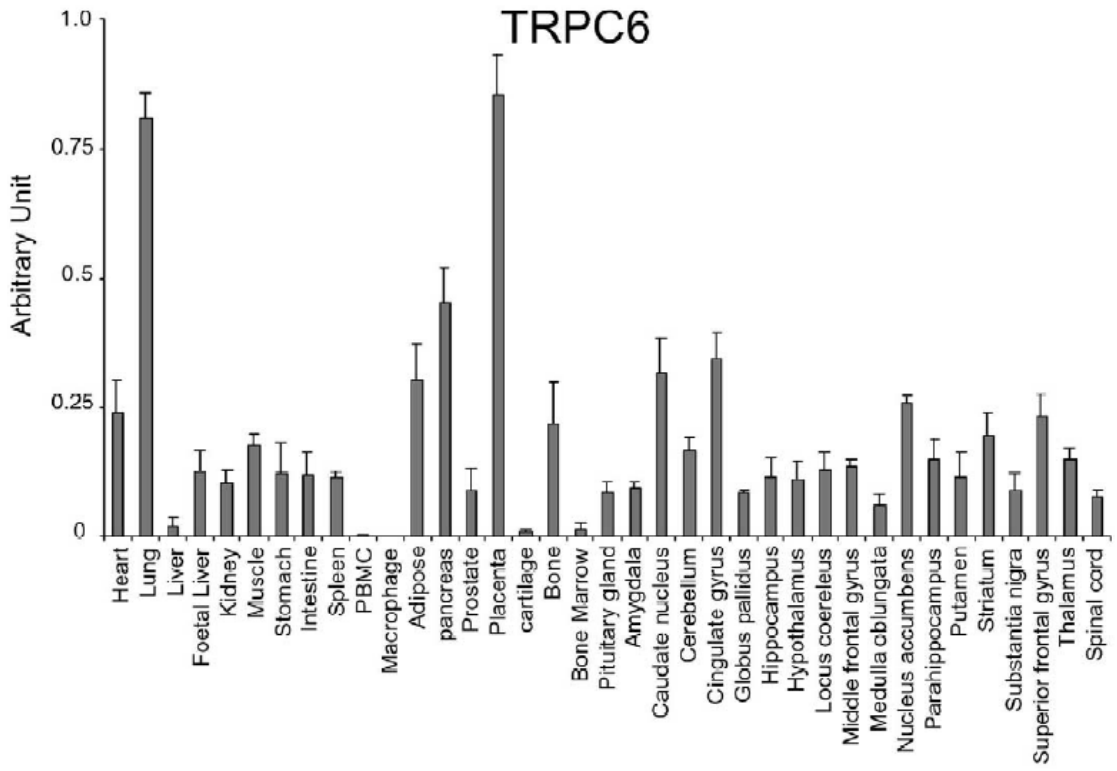

Figure 1-9 Expression of TRPC6 mRNA in human CNS and peripheral tissues

Data are expressed as arbitrary units normalized to cyclophilin to correct for RNA quantity and integrity. *Adapted from (Riccio et al., 2002a).*

Rat

TRPC6 is expressed in the brain of embryonic (embryonic day 18) rat but not in the brain of adult (postnatal days 40-45) rats (Strubing et al., 2003). Along with this finding, TRPC6 expression is down-regulated in rat cerebellum during the first six weeks after birth (Huang et al., 2007). TRPC6 mRNA is detected in hippocampus, cortex, and more weakly in olfactory bulb, cerebellum and midbrain (Mizuno et al., 1999; Bonaventure et al., 2002). TRPC6 was detected by immunohistochemistry in rat substantia nigra, with a postsynaptic

localization and associated with metabotropic glutamate receptor 1 in midbrain dopamine neurons (Giampa et al., 2007). Moreover, TRPC6, co-immunoprecipitating with TRPC3 and TRPC7, is also found in cerebellum synaptosomes (Goel et al., 2002; Zhou et al., 2008). TRPC6 is also abundant in sensory neurons of dorsal root ganglia (Kress et al., 2008).

Mouse

TRPC6 is expressed in both mouse brain and lung (Boulay et al., 1997). In the brain, TRPC6 is found in dentate gyrus granule cells (Otsuka et al., 1998). Previous results from our laboratory have shown a heterogeneous distribution of TRPC proteins in mouse embryonic (E13) cortex by means of immuno-histochemistry (Boisseau et al., 2009). In the immature cortical wall, both the first post-mitotic neurons and the dividing non-neuronal cells express TRPC6 (Boisseau et al., 2009). Figure 1-10 shows quantitative analyses of TRPC mRNA in murine embryonic brain and cortex. Figure 1-11 shows the expression of TRPC6 in murine embryonic cortex.

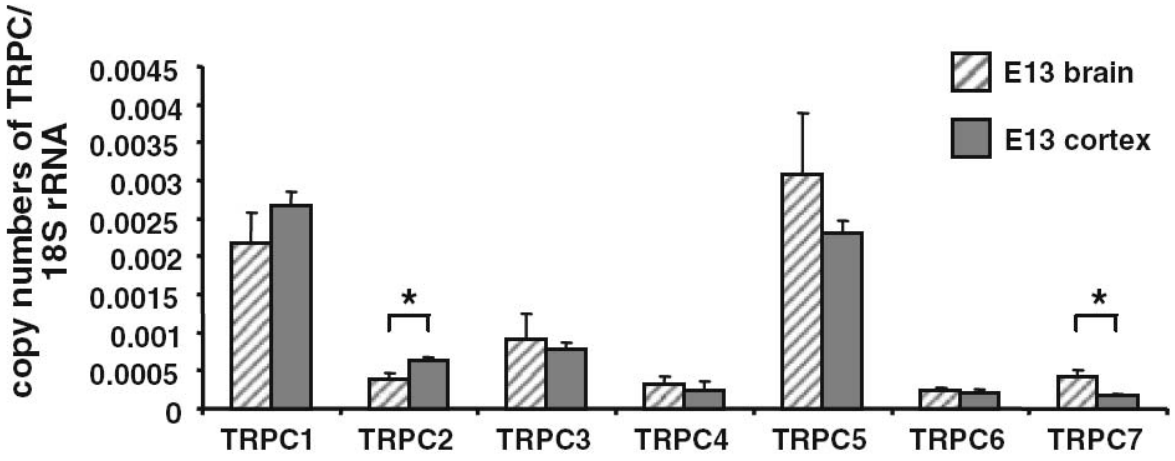

Figure 1-10 Expression and quantification of TRPC mRNAs in murine embryonic brain and cortex

Expression of TRPC1-7 mRNA was performed in E13 brain and cortex tissue samples using real-time RT-PCR. The mRNA levels of TRPC channels are given in relation to 18S rRNA. *Adapted from (Boisseau et al., 2009).*

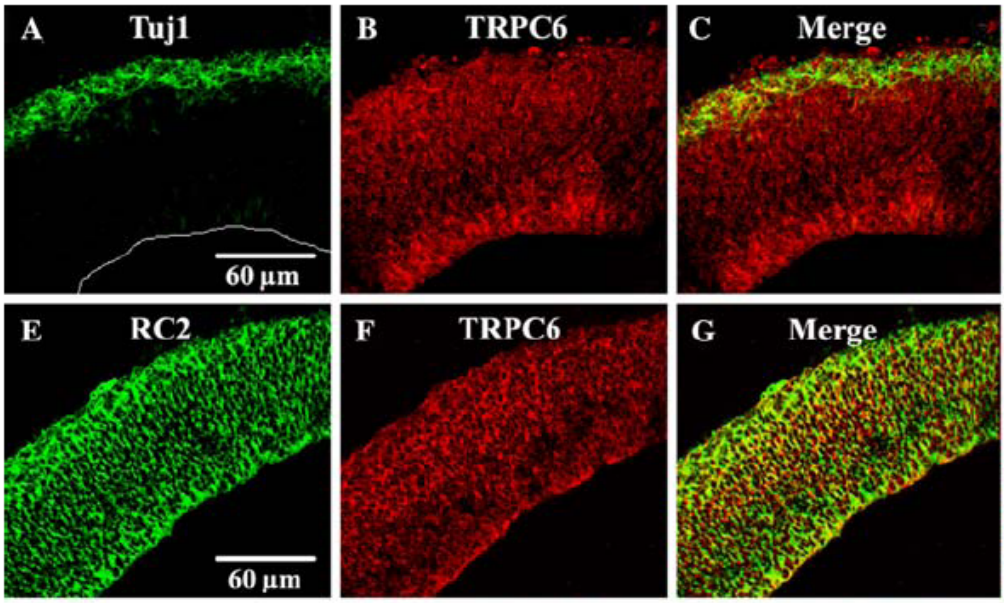

Figure 1-11 Expression of TRPC6 in murine embryonic cortex

Panels A-B: double immunostaining with Tuj1 (green, staining post-mitotic neurons) in panel A and anti-TRPC6 antibodies (red) in panel B. Panels E-F: double immunostaining with anti-RC2 (green, staining non-neuronal cells) in panel E and anti-TRPC6 antibodies (red) in panel F. Panels C and G: overlay of fluorescent confocal images. *Adapted from (Boisseau et al., 2009).*

1.2.6.2 Functions of TRPC6 in the brain

Role of TRPC6 in neurons

Members of TRPC subfamily have been proposed to play an important role in nerve growth cone guidance and neurite growth, for example, TRPC1 (Shim et al., 2005; Wang and Poo, 2005), TRPC3 (Li et al., 2005), TRPC5 (Greka et al., 2003) as well as TRPC6 (Li et al., 2005; Leuner et al., 2007; Tai et al., 2008). Growth cones, the hand-like structures at the tip of growing neurites, possess remarkable abilities to detect directional cues to help axons and dendrites to locate and recognize their appropriate synaptic partners, forming the appropriate connections between neurons and their target cells (Tessier-Lavigne and Goodman, 1996; Mueller, 1999; Dickson, 2002). The group of Wang first shows that the overexpression of a dominant-negative form or down-regulation of TRPC3 or TRPC6 inhibits brain-derived neurotrophic factor (BDNF) mediated growth-cone turning (Li et al., 2005). Then they find that TRPC3 and TRPC6 are required for BDNF-mediated neuronal protection, and promote cerebellar granule neuron survival via cAMP-response-element binding protein (CREB) activation (Jia et al., 2007). More recently, they prove that TRPC6 is highly expressed during

the period of maximal dendrite growth and stimulates dendritic growth through a Ca^{2+}/CaM-dependent kinase IV (CaMKIV)-CREB pathway (Tai et al., 2008), which is in line with the observation that hyperforin induces neurite outgrowth via TRPC6 activation (Leuner et al., 2007). In addition, TRPC6 is mainly localized to excitatory postsynaptic sites and that TRPC6 is important for the development of dendritic spines and excitatory synapses (Zhou et al., 2008).

In mouse cortical astrocytes, interleukin-1β, a cytokine acting in interleukin-1 receptors, enhances ROCE via TRPC6 channels (Beskina et al., 2007). Chronic treatment with interleukin-1β up-regulates the expression of TRPC6 (Beskina et al., 2007). This shows that TRPC6 channels are invovled in interleukin-1β-induced dysregulation of Ca^{2+} homeostasis.

Sections 1.2.6.1 and 1.2.6.2 present data describing the expression and the functions of TRPC6 in the brain. It is necessary to add that these channels are also present in the peripheral nervous system like in dorsal root ganglia (Elg et al., 2007). A recent work shows that TRPC1 and TRPC6 channels cooperate with TRPV4 to mediate mechanical hyperalgesia and nociceptor sensitization in rat dorsal root ganglion neurons (Alessandri-Haber et al., 2009). The authors point out that TRPC6 is a putative component of signaling complexes including TRPV4, integrins and Src tyrosine kinases, serving to transduce mechanical stimuli in the setting of inflammation or nerve injury (Alessandri-Haber et al., 2009).

Link between Alzheimer's disease and TRPC6

A major cause of the familial form of Alzheimer's disease (AD) is a missense mutation in one of three genes coding for amyloid precursor protein, presenilin 1 or presenilin 2 (Putney, 2000). In HEK-293 cells, presenilin 2 influences TRPC6-mediated Ca^{2+} entry (Lessard et al., 2005). Co-expression of wild-type presenilin 2 or AD-linked presenilin 2 mutants and TRPC6 in HEK-293 cells abolishes agonist-induced TRPC6 activation, while co-expression of a loss-of-function presenilin 2 mutant and TRPC6 in HEK-293 cells enhances TRPC6-mediated Ca^{2+} entry (Lessard et al., 2005). Thus, the crosstalk between TRPC6 and presenilin 2 may be linked to the onset and progression of AD. However, it remains unclear whether some intermediate proteins act between presenilin 2 and TRPC6.

2 Iron homeostasis in the brain

Adult men normally have ~35-45 mg of iron per kilogram of body weight. Most of this iron (~70%) is incorporated into hemoglobin in erythroid cells. Approximately ~10-15% is present in muscle fibers (in myoglobin) and other tissues (in enzymes and cytochromes). Most of the remaining iron is stored in liver and macrophages where it is recycled. There are no specific mechanisms for the secretion of iron out of the body, and iron loss can only occur via bleeding or cell desquamation. This non-specific iron loss is compensated by dietary iron absorption (~1-2 mg/day). Dietary iron, both inorganic iron and heme iron, is absorbed by duodenal enterocytes and then circulates in the plasma bound to transferrin (Andrews, 1999).

The chemical versatility of iron has made it one of the most commonly used metals in biological systems. It is required by all mammalian cells, executing its major roles in oxygen delivery and electron transport (Andrews, 2005). In neurons, iron is an essential cofactor for enzymes involved in energy metabolism, synthesis of neurotransmitters, mitochondrial electron transport chain, etc. Neurons seem to be more vulnerable to iron overload when compared to glial cells. In the brains of patients suffering from neurodegenerative diseases such as Parkinson's disease (PD), AD and Huntington's disease, neuronal iron accumulation is relatively higher than in the brain of age-matched controls (Moos and Morgan, 2004).

Before going further into the mechanisms controlling brain iron homeostasis, intercellular and intracellular iron transports are first introduced. Two pathways have been described to participate in the cellular iron uptake. The first is the transferrin-mediated iron (TBI) transport. Transferrin (Tf) is a ~80 kDa serum glycoprotein that binds in a reversible manner two atoms of Fe^{3+} with a high affinity (K_d ~10^{-23} M) (Wessling-Resnick, 2000). Diferric Tf binds to a highly specific Tf receptor (TfR), allowing a cellular uptake via receptor-mediated endocytosis. The acidic pH of the endosomes favours the release of Fe^{3+} from Tf, which is then reduced to Fe^{2+} and exported out of the endosomes via the divalent metal transporter 1 (DMT1, also known as Nramp2 and DCT1) or TRPML1 (Dong et al., 2008) (see Section 4.4.2). The Tf cycle is completed when the endosomes return to and fuse with the plasma membrane. Apo-Tf then returns to the circulation and TfR to the plasma membrane, and a new cycle of endocytosis/exocytosis can start again (Wessling-Resnick, 2000; Donovan et al., 2006). The transferrin cycle is illustrated in Figure 2-1.

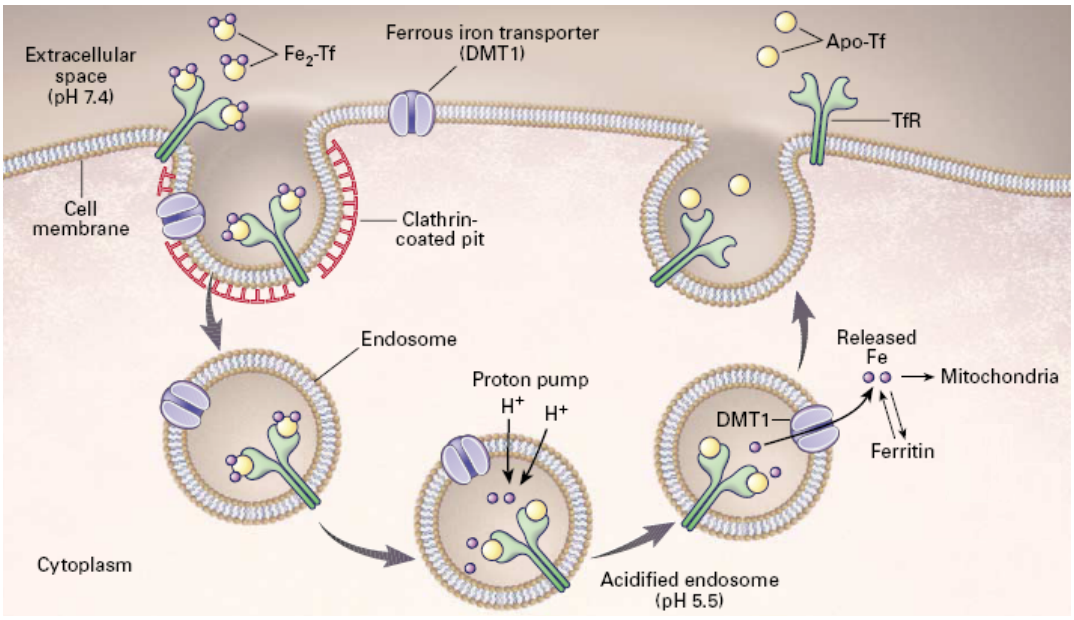

Figure 2-1 The transferrin cycle

Diferric Tf binds to TfR. TfR is a membrane glycoprotein that functions as a homodimer with each subunit binding one molecule of Tf. The Tf-TfR complexes localize to clathrin-coated pits, which facilitate the formation of the endosomes. The endosomal Na^+-H^+-ATPase permits the accumulation of H^+ in the lumen of these organelles. When the endosomal pH reaches ~5.5, iron dissociates from Tf. Fe^{3+} is reduced to Fe^{2+} by an endosomal reductase and Fe^{2+} is transported from the endosomes to cytoplasm by DMT1. The Tf cycle is completed when the endosomes return to and fuse with the plasma membrane. Apo-Tf returns to the circulation and TfR to the plasma membrane, allowing both molecules to start the cycle again. *Adapted from (Andrews, 1999).*

The second pathway is a non-transferrin-bound iron (NTBI) uptake. Candidates for NTBI uptake include DMT1 (Gunshin et al., 1997), the trivalent cation-specific transporter (TCT) (Attieh et al., 1999), Zip14 (Liuzzi et al., 2006), the Na^+/Mg^{2+} antiport system (Stonell et al., 1996), melanotransferrin (also known as p97) (Kennard et al., 1995), lactoferrin (McAbee, 1995), lipocalin (Yang et al., 2002) as well as VGCC (Oudit et al., 2003).

2.1 Brain iron homeostasis

2.1.1 Iron transport into the brain

To enter the brain, iron must cross the blood-brain barrier (BBB) or the blood-cerebrospinal fluid (CSF) barrier.

2.1.1.1 Iron transport across the blood-brain barrier

The BBB is a structure composed of brain capillary endothelial cells, a basal lamina, pericytes, and astrocytic end-feet processes. In the CNS, brain capillary endothelial cells are joined by tight junctions, protecting the brain from harmful substances circulating in the blood stream. By providing the required nutrients, brain capillary endothelial cells are necessary for a proper brain functioning.

Although iron crosses the BBB, the molecular mechanisms participating in the transport have not yet been completely clarified. The Tf/TfR pathway seems to be the major route of iron transport across the luminal membrane of the capillary endothelium (Bradbury, 1997; Moos and Morgan, 2000; Burdo et al., 2003). In addition, it has been suggested that pathways involving lactoferrin/lactoferrin receptor (Fillebeen et al., 1999), soluble melanotransferrin/glycosylphosphatidylinositol-anchored melanotransferrin (Rothenberger et al., 1996; Moroo et al., 2003) and ferritin/ferritin receptor (Fisher et al., 2007) might play a role in iron transport across the BBB. Moreover, low-molecular weight NTBI uptake, might be another pathway for iron to cross the BBB (Burdo et al., 2003; Deane et al., 2004).

In order to be available for the neural cells, iron needs to cross the abluminal membrane of the BBB and enter the interstitial fluid of the brain. Based on the similarity between the transport of dietary iron from intestinal enterocytes into the circulatory system and the iron transport across the BBB, ferroportin (Wu et al., 2004a) together with ceruloplasmin or hephaestin (Hahn et al., 2004) have been suggested to be involved in the transport of iron across the abluminal membrane of the BBB (Ke and Qian, 2007). In addition, astrocytes have probably the ability to import iron from endothelial cells through their end-feet processes on the abluminal surface of the capillary (Moos et al., 2007).

2.1.1.2 Iron transport across the blood-cerebrospinal fluid barrier

Choroid plexus epithelial cells constitute another barrier: the blood-CSF barrier. The choroid plexus is composed of CSF producing-choroidal capillaries and ventricular ependyma. The CSF is found within the ventricles of the brain and in the subarachnoid space around the brain and spinal cord. Thus, the choroid plexus which separates the blood from the CSF, acts as a filtration system that removes metabolic wastes or foreign substances from the CSF, maintaining the delicate extracellular neural environment.

When considering the mechanisms of iron into the brain, the blood-CSF barrier and the BBB are thought to share some common features. However, a major difference is that the choroid plexus of the lateral and third ventricles synthesizes Tf, which may be of significance for iron transport across the choroid plexus. In addition, NTBI is present in the CSF (Moos and Morgan, 1998). Together with the fact that ferric reductase stromal cell-derived receptor 2 (Vargas et al., 2003) and DMT1 are also present in the choroid plexus (Gunshin et al., 1997), NTBI uptake may be an alternative mechanism for iron transport across the blood-CSF barrier (Moos, 2002; Ke and Qian, 2007).

2.1.2 Circulation and storage of iron inside the brain

2.1.2.1 Iron circulation

After its transport across the BBB or the blood-CSF barrier, iron may bind quickly to the Tf secreted by the oligodendrocytes (Espinosa de los Monteros et al., 1990; Bradbury, 1997) and the choroid plexus (Dickson et al., 1985; Aldred et al., 1987; Bloch et al., 1987), two main Tf producing sites of the brain. However, brain Tf concentrations are about 10% of serum Tf concentrations, and measurements of interstitial iron concentrations imply that Tf may be highly saturated by iron. Thus, significant amount of NTBI may exist (Moos and Morgan, 1998), which is different from the serum where NTBI is rarely found due to the excess of Tf. NTBI in the brain includes iron complexed to smaller organic molecules like citrate, ascorbic acid, ATP or to proteins such as albumin, lactoferrin, soluble melanotransferrin and ferritin. Brain cells can acquire iron via pathways involving Tf/TfR (Dickinson and Connor, 1998), lactoferrin/lactoferrin receptor (Faucheux et al., 1995) and soluble melanotransferrin/glycosylphosphatidylinositol-anchored melanotransferrin (Qian and Wang, 1998), ferritin/ferritin receptor (Hulet et al., 1999; Hulet et al., 2000). Other low molecular-weight complexes of iron might enter the cells through channels (such as VGCC (Gaasch et al., 2007b)), via DMT1 or TCT (Attieh et al., 1999). A hypothetical scheme of brain iron homeostasis is shown in Figure 2-2.

2.1.2.2 Iron storage

One-third to three-fourths of the total iron of the brain is stored within glial cells (oligodendrocytes, astrocytes and microglia) (Morris et al., 1992). Molecularly, the main iron storage protein is ferritin which consists of an iron core and a shell of 24 subunits of two types, heavy (H) and light (L). The H and L subunits play complementary roles in iron

storage: the H subunit has a specific ferroxidase activity allowing rapid iron uptake while the L subunit is involved in the initiation and the stabilization of the ferritin-iron core. Ferritin is able to bind up to 4500 iron ions (Harrison and Arosio, 1996), indicating its important capacity in iron detoxification. Moreover, iron might be stored within the labile iron pool or within organelles. For example, iron can be sequestered by mitochondria in astrocytes (Schipper et al., 1999). Indeed, mitochondria are well-known sites for heme and iron-sulphur cluster synthesis, and ferritin is also expressed in these organelles (Levi et al., 2001).

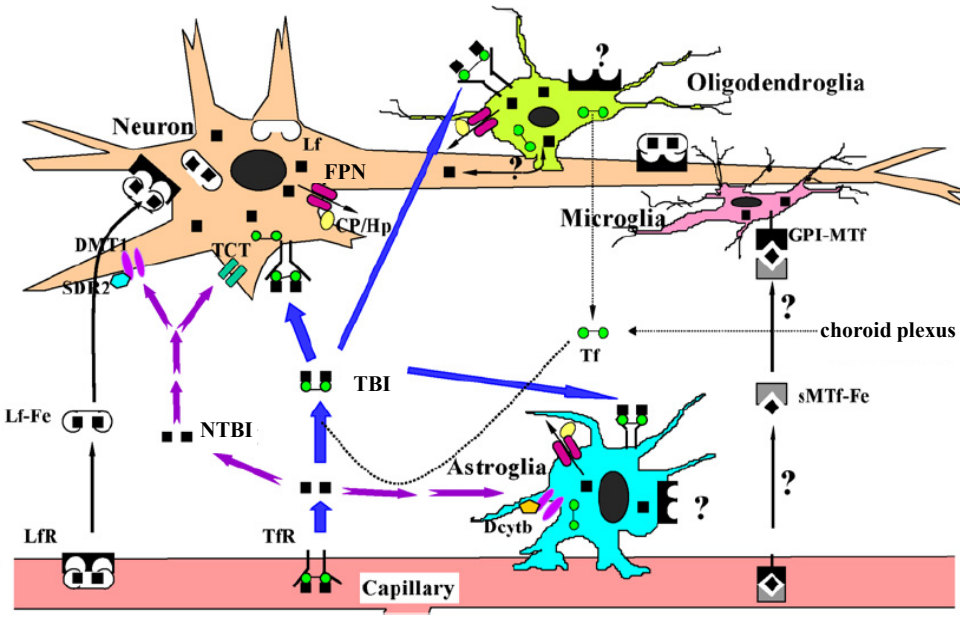

Figure 2-2 A hypothetical scheme of iron transport within the brain

Both TBI and NTBI exist in the brain. Oligodendrocytes and the choroid plexus are two main Tf producing sites of the brain. TBI occurs in neurons and glial cells by TfR-mediated endocytosis (blue arrows). NTBI, including iron complexed to proteins or to smaller organic molecules, is taken up via mechanisms involving lactoferrin (Lf)/lactoferrin receptor (LfR) and soluble melanotransferrin (sMTf)/glycosylphosphatidylinositol-anchored melanotransferrin (GPI-MTf) pathways (black arrows), DMT1 or TCT (purple arrows). Ferric reductases stromal cell-derived receptor 2 (SDR2) and duodenal cytochrome *b* (Dcytb) may facilitate DMT1-mediated NTBI uptake. Ferroportin (FPN), together with ceruloplasmin (CP) or hephaestin (Hp), can participate in the export of iron. *Adapted from (Ke and Qian, 2007).*

2.1.3 Iron transport out of the brain

As there is a constant influx of iron into the brain, there must be some export systems for iron to leave the brain and to maintain the brain iron homeostasis. TBI may exit the brain via the venous system and return to the systemic circulation through the arachnoid granulation (Bradbury, 1997; Rouault, 2001).The CSF and endothelial cells of the BBB have the potential

role to export iron, although this is poorly documented (Ke and Qian, 2007; Moos et al., 2007).

2.2 Neuronal iron homeostasis

2.2.1 Neuronal iron uptake

The neuronal expression of TfR (Dickinson and Connor, 1998) indicates that neurons can acquire iron via the TBI pathway. The neuronal expression of DMT1 (Gunshin et al., 1997) suggests that the iron-Tf complex undergoes dissociation in the endosomes and Fe^{3+} is then reduced to Fe^{2+} by a ferric reductase present within endosomes or at its membrane before being released into cytosol via the endosomal DMT1. The ferric reductase stromal cell-derived receptor 2 has for instance been identified in the choroid plexus, ependymal cells (Vargas et al., 2003) and in neurons of the substantia nigra (Ponting, 2001).

Beside the mechanism of TBI, neurons seem to take up iron via a NTBI uptake mechanism. This pathway may involve the following actors: DMT1, TCT, lactoferrin/lactoferrin receptor, ferritin/ferritin receptor (see Figure 2-2 and Figure 4-1). In addition, VGCC seem to participate in this NTBI uptake into neuronal cells (Gaasch et al., 2007b) (see Section 4.1). The quantitative importance of the two uptake pathways (TBI and NTBI) under physiological conditions remains unknown.

2.2.2 Neuronal iron storage

Neurons express ferritin (Hansen et al., 1999). Although the expression level is rather limited (Moos and Morgan, 2004), ferritin is mainly found in the axons (Zhang et al., 2005) and would be involved in the transport of iron from the neuronal cell body to the synapses (Rouault and Cooperman, 2006). Iron can also be stored in organelles such as lysosomes and mitochondria. By using light and electron microscopic histochemistry, iron deposits are mainly observed in lysosomes and occasionally in the cytosol, mitochondria, nucleus and axon, while large motor neurons are intensely stained for iron throughout the cytoplasm (Meguro et al., 2008). Mitochondria could play a role in transporting iron from the cell body to the axon terminal (Meguro et al., 2008).

2.2.3 Neuronal iron export

The ubiquitous expression of ferroportin in the brain (Burdo et al., 2001; Jiang et al., 2002; Wu et al., 2004a; Moos and Rosengren Nielsen, 2006) suggests that the ferroportin-

dependent export of iron is an important mechanism. Ferroportin is present in the soma, axons and dendrites of neurons, thus it probably plays an important role in regulating the axonal transport and the neuronal export of iron (Moos and Rosengren Nielsen, 2006). This latter aspect has been shown in SH-SY5Y neuroblastoma cells and hippocampal neurons where ferroportin participates in the efflux of iron (Aguirre et al., 2005). Ferroportin exports Fe^{2+}, which requires the presence of auxiliary ferroxidases like ceruloplasmin or hephaestin for oxidizing the toxic ferrous iron to ferric iron in the brain interstitial fluid. Indeed, ceruloplasmin is specifically expressed by astrocytes (Klomp et al., 1996; Patel and David, 1997), and the glycosylphosphatidylinositol-anchored form of ceruloplasmin physically interacts with ferroportin to export iron (Jeong and David, 2003). *Ceruloplasmin* gene-deficient mice have an increased iron deposition in the CNS (Patel et al., 2002). Hephaestin is expressed in different brain regions including cerebral cortex, hippocampus, striatum and substantia nigra (Qian et al., 2007). A recent study shows that ferroportin and hephaestin are co-localized in neurons and non-neuronal cells of the substantia nigra (Wang et al., 2007). The increased iron levels in this brain structure are correlated with a decreased expression level of the two proteins (Wang et al., 2007). Thus, it is possible that ferroportin, together with ceruloplasmin or hephaestin, is involved in the neuronal iron export. Ferroportin is also present in synaptic vesicles, suggesting that this metal could be released during exocytosis (Wu et al., 2004a), however, to our knowledge, the synaptic release of iron has never been documented.

2.3 Brain iron toxicity

Iron is indispensable for a proper development and function of the brain. This metal is indeed necessary for a wide range of biological processes including embryonic neuronal development (iron is a cofactor for ribonucleotide reductase), myelin formation, neurotransmitter synthesis and metabolism, and oxidative phosphorylation/ATP synthesis (iron is a key component of cytochromes a, b, and c, cytochrome oxidase and of the iron-sulphur complexes of the oxidative chain) (Gaasch et al., 2007a). The oxidation-reduction reactions of iron make it a significant cofactor; while free iron is highly toxic because of its ability to generate free radicals.

Iron carries out its toxicity via the Fenton Reaction:

$$Fe^{2+} + H_2O_2 \rightarrow Fe^{3+} + OH^- + OH^{\bullet} \quad (1)$$

Reduction of Fe^{3+} by cellular reducing agents (such as ascorbate, $O_2^{\bullet-}$…) regenerates the Fenton-active form of iron (Fe^{2+}) which re-enters the oxidation-reduction cycle:

$$Fe^{3+} + O_2^{\bullet-} \rightarrow Fe^{2+} + O_2 \quad (2)$$

When putting together the two reactions above, the net reaction acquired is called Haber-Weiss Reaction:

$$H_2O_2 + O_2^{\bullet-} \xrightarrow{Fe^{2+}/Fe^{3+}} O_2 + OH^- + OH^{\bullet} \quad (3)$$

In this cycle (Haber-Weiss reaction), iron acts as a catalyst in the continuous conversion of reactive oxygen intermediates, hydrogen peroxide (H_2O_2) and superoxide ($O_2^{\bullet-}$) – both by-products of aerobic metabolism – to highly reactive free radical species such as hydroxyl radical ($OH^{\bullet}$) (Stohs and Bagchi, 1995; Gaasch et al., 2007a).

As mentioned above, reactive oxygen species (ROS), including H_2O_2, $O_2^{\bullet-}$, $OH^{\bullet}$, etc., are produced under physiological conditions. They participate in the defense against infection and are coordinators of the inflammatory response (Halliwell, 2006). But excessive production of free radicals can induce severe oxidative cellular damages including lipid peroxidation, protein oxidation, and DNA/RNA oxidation.

The brain is particularly vulnerable to oxidative stress because of its specific characteristics (Thompson et al., 2001; Molina-Holgado et al., 2007):

- High oxygen consumption due to its high metabolic activities (20% of the basal body oxygen consumption);
- Membranes containing a high proportion of polyunsaturated fatty acids;
- High levels of Fenton-active metals such as iron and copper and the ability to accumulate these metals;
- High levels of pro-oxidant agents such as ascorbate, but low levels of protective antioxidant agents such as glutathione and catalase.

Iron progressively accumulates in the brain during life-span, and iron-induced oxidative stress can cause neurodegeneration (Thompson et al., 2001; Zecca et al., 2004). Iron-related neurodegenerative disorders are usually characterized by iron accumulation in specific brain regions or by defects in iron metabolism and/or homeostasis, although it remains unclear whether excessive iron in the brain is an initial event that causes neuronal

death or is a consequence of the disease process (Qian and Shen, 2001). Some iron-related neurological diseases are summarized in Table 2-1.

Table 2-1 Some neurological diseases and their associated alterations in iron status

Neurological disease	**Involvement of iron**
Parkinson's disease	Iron accumulation in substantia nigra, striatum, lateral globus pallidus and in neuromelanin-containing cells Decreased level of ferritin in substantia nigra, caudate, putamen Decreased level of TfR in substantia nigra Increased level DMT1 in substantia nigra
Alzheimer's disease	Iron accumulation in brain regions associated with neurodegeneration Increased iron level in amyloid plaques Decreased level of ferritin in areas that accumulate iron Decreased level of TfR in hippocampus Changes in IRP distribution and activity
Huntington's disease	Increased iron in striatum, occurs presymptomatically
Freidreich's ataxia	Increased mitochondrial iron in striatum and cerebellum Mutations in *frataxin* gene
Neurodegeneration with brain iron accumulation	Iron accumulation in globus pallidus and substantia nigra Mutations in pantothenate kinase 2
Neuroferritinopathy	Iron and ferritin accumulation in the basal ganglia Abnormal aggregates of ferritin and iron in globus pallidus and substantia nigra Low serum ferritin levels
Aceruloplasminemia	Increased basal ganglia and CSF iron
Hereditary hemochromatosis	Increased iron in choroid plexus and pituitary, basal ganglia Mutations in HFE (hemochromatosis) gene
Multiple sclerosis	High levels of iron and ferritin in oligodendrocytes Increase ferritin in CSF Loss of ferritin receptors in periplaque white matter

Adapted from (Burdo and Connor, 2003; Sadrzadeh and Saffari, 2004; Zecca et al., 2004).

3 Zinc homeostasis in the brain

Zinc is the second most abundant transition element in the human body, essential for the development and the function of the brain, skin, reproductive and digestive systems. Compared with the other organs, the brain has the highest zinc content. Approximately 90% of the total brain zinc binds to proteins, functioning as regulatory, structural or enzymatic components (Frederickson, 1989), and much of the remaining 10% is found in presynaptic vesicles, either loosely bound or free (Takeda, 2001). Total intracellular zinc concentration in the brain may be as high as 150 μM, although zinc concentration in the extracellular fluid is estimated to be ~0.15 μM (Takeda, 2000). The cytosolic concentration of free Zn^{2+} ($[Zn^{2+}]_i$) in cultured neurons ranges from nM to pM (Frederickson and Bush, 2001; Eide, 2006), whereas the zinc content in the synaptic vesicles is in the mM range (Frederickson and Bush, 2001).

3.1 Brain zinc homeostasis

Similarly to iron, zinc must cross the BBB or the blood-CSF fluid barrier. Nearly all serum zinc (~15 μM) is bound to protein (~98%) or low molecular weight ligands (~1-2%) , and a very small proportion (~1%) remains free (Takeda, 2001). Serum zinc bound to albumin is not essential for zinc transport into the brain, whereas zinc bound to amino acids (histidine and cysteine) is. Indeed, L-histidine seems to be involved in zinc transport into the brain across the brain barrier system. However, it is not sure how the histidine-bound zinc crosses the plasma membrane of brain capillary endothelial cells and choroid plexus epithelial cells. Some transport systems like DMT1 and the Zip family transporters may also be involved in this process (Takeda, 2000, 2001). The mechanism of zinc secretion from brain capillary endothelial cells to brain extracellular fluid or from choroidal epithelial cells to the CSF remains unknown (Takeda, 2000, 2001).

3.2 Neuronal zinc homeostasis

3.2.1 Neuronal zinc uptake

Although the entry routes participating in zinc uptake from extracellular fluids into neurons are not fully characterized, two types of pathways mainly account for Zn^{2+} entry: carriers and channels. The first includes the Zip family transporters (Colvin et al., 2003; Liuzzi and Cousins, 2004; Cousins et al., 2006), the main membrane zinc uptake transporters (Law et al., 2003) and DMT1 (Colvin et al., 2000a). The second zinc uptake pathway involves

voltage-gated L-type Ca^{2+} channels (Weiss et al., 1993; Freund and Reddig, 1994) and two types of glutamatergic receptors: the N-methyl-D-aspartate (NMDA) channels (Koh and Choi, 1994) and the Ca^{2+}-permeable α-amino-3-hydroxy-5-methyl-4-isoxazolepropionic-acid (AMPA) /kainate (Ca-A/K) channels (Yin and Weiss, 1995; Yin et al., 1998; Jia et al., 2002). Moreover, in cortical neurons, a Zn^{2+}/H^{+} antiporter seems to participate in the transport of Zn^{2+} across the plasma membrane (Colvin et al., 2000b; Colvin, 2002).

Besides these systems, the NCX can also transport zinc bidirectionally across the plasma membrane, mediating zinc influx and efflux (Sensi et al., 1997; Cheng and Reynolds, 1998). In addition, zinc can enter via a Na^{+}/Zn^{2+} exchanger distinct from the NCX (Ohana et al., 2004).

Compared with the less understood transporters (Colvin et al., 2003), the uptake of zinc via ion channels has been more studied (see Chapter 4 for a description of the ion channels involved in the transport of trace metal ions across the membranes).

3.2.2 Neuronal zinc storage

Once neurons uptake zinc, it can be transported and stored into synaptic vesicles by ZnT-3, another member of the family of zinc transporter proteins, or incorporated into zinc-binding proteins or sequestered by mitochondria

3.2.2.1 Metallothioneins

Metallothioneins (MT) form a family of ubiquitous low molecular weight (~7 kDa) metal-binding proteins with two cysteine-rich domains. They largely control zinc buffering within the cytoplasm (Hidalgo et al., 2001). MT display a high zinc binding affinity (K_d = 3.2 × 10^{13} M^{-1} at pH 7.4) (Jacob et al., 1998). They have also high affinities for copper, cadmium and mercury. Three of four MT isoforms are found in the CNS: MT-1 and MT-2 are widely expressed in astrocytes and spinal glia; MT-3 is mainly found in neurons (Hidalgo et al., 2001).

The zinc binding to MT is reversible, as the cysteine residues of MT are sensitive to cellular oxidants, especially disulphides such as glutathione disulfide (GSSG) or 2, 2'-dithiodipyridine (DTDP). Oxidants promote zinc release from MT, while a reduced intracellular environment facilitates zinc binding to MT (Maret and Vallee, 1998). For example, the glutathione redox state (i.e. the ratio between the reduced form [GSH] and oxidized form [GSSG]) regulates the zinc-MT interaction, as GSH binding to MT induces

GSSG-mediated zinc release (Maret, 1994). In addition, nitric oxide (NO) can also release zinc from MT (preferentially with MT-3), via *s*-nitrosylation (Chen et al., 2002; Spahl et al., 2003). This process is involved in the crosstalk between NO signaling and zinc signaling (Bossy-Wetzel et al., 2004). Hence, MT can mobilize zinc in response to oxidative or nitrosative stress, modulating zinc availability for other zinc-binding proteins.

3.2.2.2 Mitochondrial sequestration

Not only do mitochondria buffer Ca^{2+}, but they are important organelles involved in zinc buffering, exchange and trafficking. Mitochondria contain endogenous zinc (Sensi et al., 2003). On strong cytosolic zinc loading, zinc is taken up into these organelles, from which it can be subsequently released in a Ca^{2+}-dependent fashion (Sensi et al., 2000; Sensi et al., 2002). This cation interferes with the function of mitochondria: a rapid increase in $[Zn^{2+}]_i$ causes a loss of the neuronal mitochondrial membrane potential ($\Delta\psi_m$), generates ROS (Sensi et al., 1999), induces permeability transition pore (PTP) opening as well as the release of cytochrome c and apoptosis-inducing factors (Jiang et al., 2001).

Indeed, cytosolic zinc pool (zinc bound to cytosolic proteins, like MT) and mitochondrial zinc pool can be pharmacologically mobilized independently of each other, with zinc released from one resulting in apparent net zinc uptake in the other (Sensi et al., 2003). A strong mobilization of the endogenous cytosolic protein-bound zinc appears to induce a partial loss of $\Delta\psi_m$, suggesting a possible functional importance of this zinc movement between cytosolic and mitochondrial pools (Sensi et al., 2003).

Up to date, little is known about the pathways mediating zinc transport across mitochondrial membrane. Zinc may be uptaken by the mitochondrial calcium uniporter (Saris and Niva, 1994), via a non-identified ruthenium insensitive pathway (Malaiyandi et al., 2005) or it may also cross the mitochondrial membrane bound to MT (Ye et al., 2001).

3.2.3 Neuronal zinc export

Members of the ZnT family are responsible for the efflux of zinc from neurons as well as the vesicular zinc uptake (Liuzzi and Cousins, 2004; Cousins et al., 2006). Both ZnT-1 and ZnT-4 transport zinc out of the cells in order to avoid an increase in $[Zn^{2+}]_i$ (Cousins and McMahon, 2000). ZnT-1 mediates zinc efflux in astrocytes (Nolte et al., 2004) and PC12 cells (Kim et al., 2000). ZnT-3 serves to pump zinc into the synaptic vesicles, and ZnT-3 gene

knock-out mice have for instance no histochemically reactive zinc in their vesicles (Palmiter et al., 1996). Figure 3-1 depicts zinc homeostasis in neuron and at the synapse.

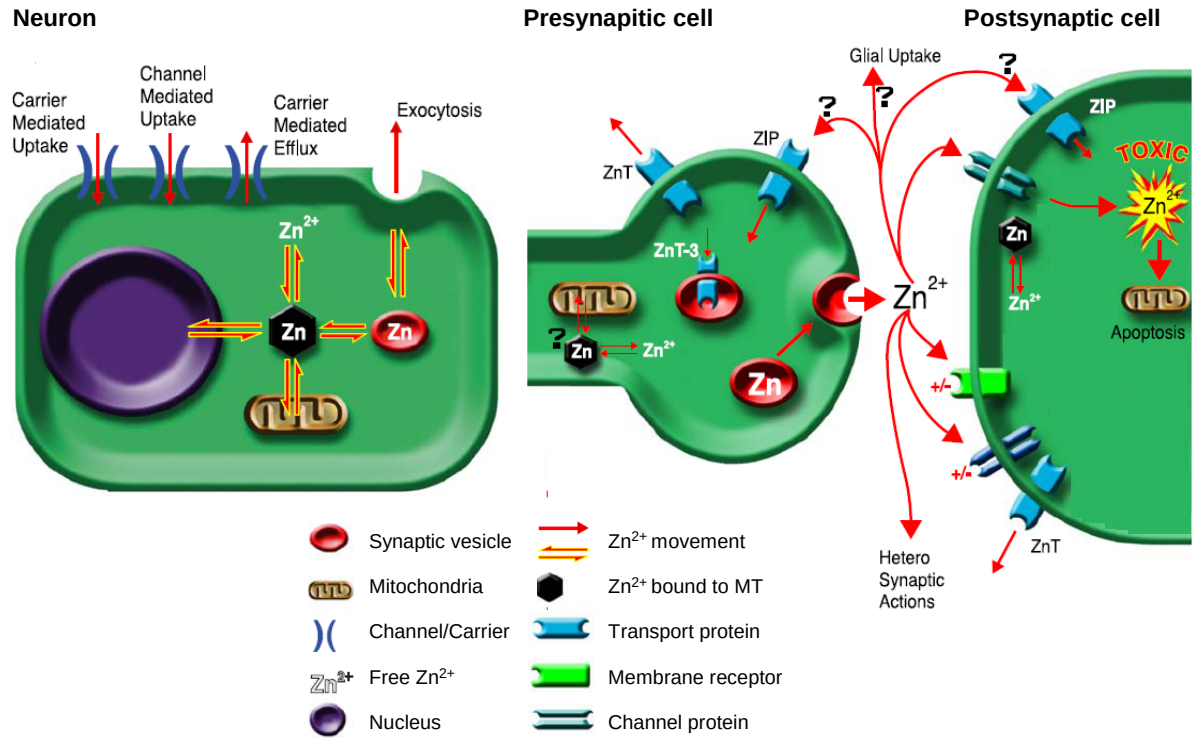

Figure 3-1 Neuronal zinc homeostasis

Neuronal zinc uptake is mediated by channels and carriers at the plasma membrane. $[Zn^{2+}]_i$ can be maintained at very low level since a large portion of zinc is incorporated into zinc-binding proteins such as MT, sequestered by mitochondria, or transported into synaptic vesicles. Some carriers can also mediate zinc efflux. At the synapse, presynaptic neurons release zinc during exocytosis, which can be reuptaken by presynaptic neurons, glia or postsynaptic neurons via carriers and channels. Excitotoxic stimulation induces the release of a large quantity of zinc into the synaptic cleft as well as the release of zinc from intracellular binding proteins. A high $[Zn^{2+}]_i$ causes toxicity to neurons. *Adapted from (Colvin et al., 2003).*

3.3 Brain zinc toxicity

Zinc seems to be less toxic when compared to other transition metals which have several oxidation states, but in fact it exerts lethal actions on neuronal cells. Adding 100-300 µM zinc into the culture medium is neurotoxic (Choi et al., 1988; Weiss et al., 1993; Sensi et al., 1999), and excessive increase in intracellular zinc have been found in degenerating neurons (Koh et al., 1996), reaching several hundred nanomolar (Canzoniero et al., 1999; Sensi et al., 1999).

Zinc can induce an oxidative stress and is thus involved in both apoptotic and necrotic processes (Capasso et al., 2005). Zinc neurotoxicity can be mediated by mitochondrial and extramitochondrial pathways (Lynes et al., 2007). In the former set of mechanisms, as mentioned before, a rapid and massive increase in $[Zn^{2+}]_i$ causes mitochondrial dysfunction displaying a loss of $\Delta\psi_m$ and an increased generation of ROS (Sensi et al., 1999). Submicromolar $[Zn^{2+}]_i$ in cortical neurons opens mitochondrial PTP and induces the release of cytochrome c as well as apoptosis-inducing factors (Jiang et al., 2001). In the latter set of mechanisms, zinc overload stimulates cytosolic ROS generation via NADPH oxidase activated by PKC (Noh and Koh, 2000) or nitrosative stress by activating neuronal nitric oxide synthase (Kim and Koh, 2002).

Not only does zinc trigger oxidative and nitrosative stress, but the stress can further increase $[Zn^{2+}]_i$, thus placing neurons in a lethal cycle, since ROS, NO or peroxynitrite ($ONOO^-$) produced by neuronal nitric oxide synthase in the presence of superoxide can detach zinc from MT (Maret and Vallee, 1998; Chen et al., 2002; Spahl et al., 2003).

Zinc is found to play an important role in the progression of several neurodegenerative diseases like AD, amyotrophic lateral sclerosis, cerebral ischemia, epilepsy and PD (Cuajungco and Lees, 1997; Frederickson et al., 2005; Mocchegiani et al., 2005). For example, *in vitro* experiments indicate that free zinc promotes the aggregation of the β-amyloid protein, a pathological hallmark of AD (Mantyh et al., 1993; Bush et al., 1994).

4 Cation channels are involved in the transport of metals

A wide diversity of channels can transport alkali and alkaline earth metals. But some of them seem to be involved in the transport of other metal ions like iron or zinc. This is the topic of the following chapter.

4.1 Roles of voltage-gated calcium channels in the transport of metals

4.1.1 Iron uptake via voltage-gated calcium channels

L-type VGCC can form a major pathway for ferrous iron (Fe^{2+}) entry into cardiomyocytes during iron-overload cardiomyopathy (Oudit et al., 2003). Fe^{2+} uptake through these channels could also be crucial in other excitable cells such as pancreatic beta cells, anterior pituitary cells and neurons (Oudit et al., 2006). Indeed, these channels play an important role in the transport of iron into neuronal cells (PC12 cells and murine neuroblastoma cells) and this role may be exacerbated under pathophysiologic conditions of iron overload (Gaasch et al., 2007b). By using radioactive isotopes, uptake of both Ca^{2+} and Fe^{2+} are observed in nerve growth factor (NGF)-differentiated PC12 cells stimulated with KCl. Similarly to Ca^{2+} uptake, iron uptake into neuronal cells is inhibited in a dose-dependent manner by the specific L-type VGCC blocker nimodipine and enhanced by the L-type VGCC activator FPL 64176. Uptake of Ca^{2+} is also inhibited in the presence of Fe^{2+} suggesting that these two cations compete for entry into neurons via L-type VGCC (Gaasch et al., 2007b). Another L-type VGCC blocker nitrendipine inhibits the uptake of iron in NGF-treated PC12 cells (Mwanjewe et al., 2001).

It is not surprising that in addition to their cardioprotective actions, L-type VGCC blockers also possess neuroprotective roles. For example nimodipine and S-312-d attenuate apoptosis in models evaluating cell death in AD (Yagami et al., 2004). Nimodipine and another dihydropyridine derivative PCA50938 exert neuroprotective actions in cerebral ischemia (Zapater et al., 1997). The L-type VGCC blockers also show antioxidant properties (Goncalves et al., 1991; Takei et al., 1994), for example they inhibit mitochondrial swelling and lipid peroxidation induced by $FeSO_4$ and ascorbic acid in the rat brain (Takei et al., 1994). Moreover, flunarizine, an antagonist of L-, T- and N-type VGCC, attenuates the neurotoxic effects of iron (Bostanci et al., 2006). The neuroprotective roles of such calcium channel antagonists can be explained, at least partially, by the fact that L-type VGCC form another uptake pathway of NTBI in the case of iron overload (Figure 4-1).

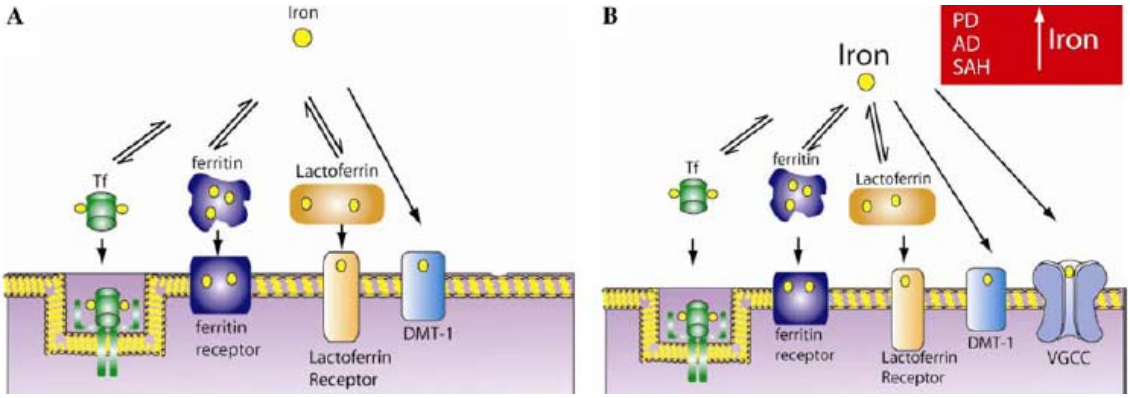

Figure 4-1 Iron entry into neuronal cells in homeostatic and pathophysiologic conditions

In homeostatic conditions (A), the primary routes for iron entry into neuronal cells are receptor-mediated endocytosis of TBI and lactoferrin-bound iron. Ferritin may be also involved in iron delivery. DMT-1 can actively transport iron into neuronal cells. In pathophysiological conditions (B) such as PD, AD and subarachnoid hemorrhage, the homeostatic iron uptake mechanisms are likely saturated and VGCC may play an important role in the transport of iron into neuronal cells. *Adapted from (Gaasch et al., 2007b).*

4.1.2 Zinc uptake via voltage-gated calcium channels

In cortical neurons AMPA-mediated depolarization facilitates Zn^{2+}-induced neurotoxicity (Weiss et al., 1993). L-type calcium channels are involved in this process (Freund and Reddig, 1994). By using the ratiometric fluorescent dye mag-fura-5, an entry of Zn^{2+} is visualized in neurons exposed to extracellular Zn^{2+} upon depolarization with high K^+ (Sensi et al., 1997). This increase in $[Zn^{2+}]_i$ is attenuated by Gd^{3+}, verapamil, ω-conotoxin GVIA, or nimodipine, indicating that Zn^{2+} enters through VGCC (Sensi et al., 1997). Compared to AMPA/Kainate channels, VGCC are less permeable to zinc (Sensi et al., 1999).

4.2 Zinc uptake via NMDA receptor-gated channels

Zn^{2+} is an effective blocker of NMDA receptors. In a concentration range of 10-100 μM, Zn^{2+} attenuates the activation of NMDA receptors and decreases the toxicity caused by NMDA-receptor activation and intracellular Ca^{2+} accumulation (Peters et al., 1987; Westbrook and Mayer, 1987; Legendre and Westbrook, 1990; Rassendren et al., 1990; Choi and Lipton, 1999). However, NMDA receptor contribute to Zn^{2+} toxicity by providing a route of Zn^{2+} influx into neurons (Koh and Choi, 1994; Cheng and Reynolds, 1998).

4.3 Zinc uptake via AMPA/Kainate channels

Most AMPA and kainate receptors are Ca^{2+} impermeable channels, but some neurons such as cortical and hippocampal neurons possess Ca^{2+}-permeable AMPA/kainate channels,

i.e. Ca-A/K-receptor channels (Yin et al., 1998; Jia et al., 2002). Ca-A/K-receptor channels produce rapid Ca^{2+} influx, resulting in mitochondrial Ca^{2+} overload and ROS generation (Carriedo et al., 1998). They are also highly permeable to Zn^{2+} (Yin and Weiss, 1995; Yin et al., 1998), displaying larger permeability than VGCC and NMDA-receptor channels (Jia et al., 2002). Thus, preferential zinc influx through Ca-A/K-receptor channels play an important role in triggering neuronal toxicity (Sensi et al., 1999).

4.4 Involvement of TRP channels in iron and zinc transport

4.4.1 TRPC6

Treatment of PC12 cells with NGF increases iron uptake (both NTBI and TBI, but predominately NTBI) (Mwanjewe et al., 2001). Several pathways other than DMT1 have been proposed to explain this NTBI uptake, like VGCC, ROC and/or SOC (Mwanjewe et al., 2001). Interestingly, the expression of TRPC6 mRNA (Figure 4-2A) and protein increases significantly upon the NGF treatment of PC12 cells, whereas the other TRPC isoforms remain unaffected (Mwanjewe and Grover, 2004). These results are in line with a previous study on TRPC6 in PC12 cells (Tesfai et al., 2001). In NGF-treated PC12 cells, DAG stimulates the NTBI entry (Figure 4-2B) (Mwanjewe and Grover, 2004). In addition, HEK-293 cells over-expressing TRPC6 have higher basal and DAG-dependent NTBI uptakes when compared to non transfected cells (Mwanjewe and Grover, 2004).

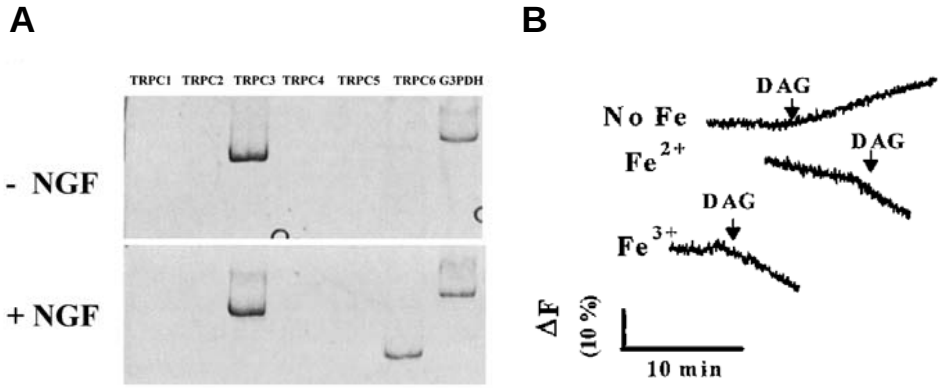

Figure 4-2 Role of TRPC6 in NTBI uptake in neuronal phenotype PC12 cells

Panel A shows the RT-PCR products of TRPC1–6 and control G3PDH in NGF-treated and control PC12 cells. An increase in the expression of TRPC6 mRNA is found after the NGF treatment. Panel B: Calcein fluorescence quenching experiments show that DAG triggers NTBI uptake in NGF-treated PC12 cells. *Adapted from (Mwanjewe and Grover, 2004).*

4.4.2 TRPML1

Release of iron from endosomes after TBI uptake (Hentze et al., 2004) or from lysosomes after lysosomal degradation of iron complexes (Kidane et al., 2006) are the main source of intracellular iron. In the former process, DMT1 was considered as the only endosomal Fe^{2+} transporter. However, a recent finding shows that TRPML1, primarily found in the late endosome and lysosome (Pryor et al., 2006; Venkatachalam et al., 2006; Nilius et al., 2007), functions as endolysosomal iron release channels (Dong et al., 2008). Indeed, TRPML1 and TRPML2 (but not TRPML3) are Fe^{2+} permeable. Moreover TRPML1 is also permeable to most other divalent trace metals with a permeability sequence of $Ba^{2+} > Mn^{2+} > Fe^{2+} \approx Ca^{2+} \approx Mg^{2+} > Ni^{2+} \approx Co^{2+} \approx Cd^{2+} > Zn^{2+} >> Cu^{2+}$ (pH 4.6), but not to Fe^{3+} (Dong et al., 2008). Mucolipidosis type IV disease (ML4) is caused by mutations in the human *trpml1* gene (Bassi et al., 2000; Sun et al., 2000). These mutations impair the channel permeability to Fe^{2+}, which is in line with the fact that ML4 cells ($TRPML1^{-/-}$) have a lower cytosolic Fe^{2+} content associated with an intra-lysosomal iron overload (Dong et al., 2008).

4.4.3 TRPM7

TRPM7 is a Ca^{2+}- and Mg^{2+}-permeable cation channel. The activity of TRPM7 is regulated by intracellular Mg^{2+} and Mg^{2+}-ATP. The TRPM7-mediated currents have thus been described as magnesium-nucleotide-regulated metal ion currents (Nadler et al., 2001). Interestingly, TRPM7 can conduct a variety of divalent cations with a permeability sequence of $Zn^{2+} \approx Ni^{2+} >> Ba^{2+} > Co^{2+} > Mg^{2+} \geq Mn^{2+} \geq Sr^{2+} \geq Cd^{2+} \geq Ca^{2+}$, even in the presence of physiological levels of Ca^{2+} and Mg^{2+} (Monteilh-Zoller et al., 2003). TRPM7 is a likely candidate participating in anoxic neuronal death. In cortical neurons, TRPM7 and TRPM2 seem to form heteromeric channels modulated by intracellular reactive oxygen/nitrogen species (Aarts et al., 2003). The ROS sensitivity and the permeability to trace metals may explain the neurotoxic properties of TRPM7.

4.4.4 TRPA1

TRPA1 is expressed in nociceptive neurons where it functions as a receptor for noxious stimuli (Patapoutian et al., 2009) and in diverse sensory processes including cold nociception, hearing, and inflammatory pain (Story et al., 2003; Corey et al., 2004; Bautista et al., 2006). Recent studies show that zinc ionophores activate TRPA1 by increasing $[Zn^{2+}]_i$ (Andersson et al., 2009). Moreover zinc can pass through and activate the channels (Hu et al.,

2009). Their constitutive activity allows an influx of Zn^{2+} which, in turn, enhances the channel activity via its interaction with intracellular cysteine and histidine residues of TRPA1 (Hu et al., 2009). TRPA1 is not only highly sensitive to intracellular Zn^{2+}, as nanomolar concentrations activate the channels, but also sensitive to Cu^{2+} and Cd^{2+} but not to Fe^{2+} (Corey et al., 2004; Hu et al., 2009).

The TRP channels that are permeable to trace metal ions are summarized in Table 4-1.

Table 4-1 TRP channels permeable to trace metal ions

TRP channels	Cell types	Permeation	Techniques	References
TRPM7	HEK-TRPM7 cells	$Zn^{2+} \approx Ni^{2+} >> Ba^{2+} > Co^{2+} > Mg^{2+} \geq Mn^{2+} \geq Sr^{2+} \geq Cd^{2+} \geq Ca^{2+}$	Patch-clamp Fura-2 quenching	(Monteilh-Zoller et al., 2003)
TRPC6	PC12 cells HEK-TRPC6 cells	Fe^{2+}, Fe^{3+}	^{55}Fe uptake Calcein quenching	(Mwanjewe and Grover, 2004)
TRPML1	HEK-TRPML1 cells	$Ba^{2+} > Mn^{2+} > Fe^{2+} \approx Ca^{2+} \approx Mg^{2+} > Ni^{2+} \approx Co^{2+} \approx Cd^{2+} > Zn^{2+} >> Cu^{2+}$ (pH 4.6)	Patch-clamp Fura-2 quenching ^{55}Fe uptake	(Dong et al., 2008)
TRPA1	Mouse dorsal root ganglia neurons HEK-TRPA1	Zn^{2+}, Cu^{2+}, Cd^{2+}	Zinc imaging with FluoZin-3	(Hu et al., 2009)

5 Research objective and proposal

The main research objective of my thesis was to determine (1) whether TRPC6 channels were functional in cortical neurons and (2) whether they could permit the entry of trace metal ions. This is of particular interest since an intraneuronal accumulation of metals such as iron and zinc is often noted in the brains of patients with neurodegenerative diseases. A complete understanding of the pathways involved in the uptake of metal ions by neuronal cells under pathophysiological conditions is still lacking.

Chapter 7 will present experimental data showing the existence of functional channels exhibiting TRPC6-like properties in cortical neurons (article 1). Chapter 9 addresses the second question of my thesis work: it is reported that TRPC6, endogenously present in cortical neurons or heterologously expressed in HEK-293 cells, could form metal-conducting channels. During the time course of my thesis we used flufenamic acid and hyperforin, two pharmacological tools currently employed to study native or heterogeneously expressed TRPC6 channels. We noticed that, besides their action of TRPC6 channels, flufenamic acid and hyperforin exerted also TRPC6-independent cellular responses that were not considered by the investigators working with these agents. We thus thought to further characterize the cellular responses induced by flufenamic acid and hyperforin. These results are summarized in Chapters 10 (article 2) and 11 (article 3). The data collected clearly show that these two TRPC6 modulators influence the cellular homeostasis of Zn^{2+} and Ca^{2+} by acting on mitochondria.

MATERIALS AND METHODS

6 Materials

The materials listed below are mainly those used in Section 8.3 and in Chapter 9. For those used in Sections 8.2, 10.2 and 11.2, please refer to the Materials and Methods section of the articles.

6.1 Cell cultures

6.1.1 Cortical neurons

The cortical neurons were dissociated from cerebral cortices isolated from embryonic (E13) C57BL6/J mice (vaginal plug was designated E0) according to procedures approved by the Ethical Committee of Rhône-Alpes Region (France). The cells have been prepared and kept up to 6 days in culture in a Neurobasal medium supplemented with 2% B27, 1% penicillin/streptomycin, and 0.25% glutamine (Bouron et al., 2006).

6.1.2 HEK and HEK-TRPC6 cells

HEK-293 cells were purchased from ATCC, LGC Promochem (France). They were grown in a DMEM medium supplemented with 10% foetal bovine serum and 1% penicillin/streptomycin under 95% O_2 and 5% CO_2 at 37°C. HEK-293 cells stably over-expressing TRPC6 (hereinafter designated HEK-TRPC6 cells) were a gift from Dr Guylain Boulay (Boulay et al., 1997). They were cultivated in the same medium as HEK cells, but supplemented with 0.8% Geneticin (G418) under 95% O_2 and 5% CO_2 at 37°C.

6.2 Antibody

The rabbit polyclonal anti-TRPC6 antibody (ACC-017) generated against the epitope RRNESQDYLLMDELG, corresponding to residues 24–38 of mouse TRPC6 was purchased from Alomone Labs (Jerusalem, Israel). The selectivity of this antibody has been shown previously (Strubing et al., 2003; Alessandri-Haber et al., 2009).

6.3 Reagents and solutions

6.3.1 Reagents

Calcein/AM was from Molecular Probes (Interchim, France). Ascorbic acid was from Fluka (Interchim, France). Zinc acetate was from Prolabo (France). $FeSO_4$ was from Aldrich

(France). Unless otherwise indicated, the other reagents (including ferric ammonium citrate, FAC) were from Sigma-Aldrich (France).

6.3.2 Tyrode's solutions

Tyrode's solutions	NaCl (mM)	KCl (mM)	$CaCl_2$ (mM)	$MgCl_2$ (mM)	HEPES (mM)	$FeSO_4$ (µM)	Ascorbic acid (mM)	FAC (µM)	Zinc acetate (µM)	Glucose (mM)
Normal	136	5	2	1	10	-	-	-	-	10
Ca^{2+} free	136	5	-	1	10	-	-	-	-	10
Fe^{2+} rich Ca^{2+} free	136	5	-	1	10	50 or 100	2.2 or 4.4	-	-	10
Fe^{3+} rich Ca^{2+} free	136	5	-	1	10	-	-	50	-	10
Zn^{2+} rich Ca^{2+} free	136	5	-	1	10	-	-	-	50	10
Zn^{2+} rich	136	5	2	1	10	-	-	-	50	10

pH is adjusted to 7.4 with NaOH.

Deionized and bidistilled water was used for the preparation of the Ca^{2+}-free Tyrode's solutions.

7 Methods

The methods listed below are mainly those used in Section 8.3 and in Chapter 9. For those used in Sections 8.2, 10.2 and 11.2, please refer to the Materials and Methods section of the articles.

7.1 Western Blot

Western blot experiments of TRPC6 were performed according to the protocol provided by the supplier of the anti-TRPC6 antibody (Alomone Labs). Proteins were extracted from cells in 50-100 µl lysis buffer (HEPES 10 mM, $MgCl_2$ 3 mM, KCl 40 mM, glycerol 2.5%, Triton-X100 1%, pH 7.5 with KOH) supplemented with 1% of the protease inhibitor cocktail (Sigma). The total protein concentration was measured with the Bio-Rad DC Protein Assay. Total protein extract (50 µg) was applied on an acrylamide gel (a concentration gel containing 4% acrylamide followed by a separation gel containing 8% acrylamide). The migration was run at 40 mA/gel for ~2 hours. The proteins were then transferred onto a nitrocellulose membrane (Bio-Rad) by using a semi dry system. The transfer was performed at 100 mA/gel for 3 hours. The membrane was blocked with a PBS solution containing 5% non-fat milk overnight at 4°C. It was then incubated with the anti-TRPC6 antibody (1 : 200 in the blocking solution) overnight at 4°C and with the antibody goat anti-rabbit IgG (Sigma, 1 : 5000 in the blocking solution) for 1 hour at room temperature. Chemiluminescence detection was performed with the ECL kit (Pierce).

7.2 Cellular fluorescence microscopy

7.2.1 Iron and zinc imaging with Fura-2

Cells (grown on 15 mm diameter glass coverslips) were incubated in a Tyrode's solution supplemented with 2.5 µM Fura-2 for 15 minutes at 20-22°C. They were then washed twice and kept in a Fura-2-free Tyrode's solution for 20 minutes at 20-22°C. Cover-slips were transferred on a perfusion chamber (RC-25F, Warner Instruments; Phymep, Paris, France) and placed on the stage of an Axio Observer A1 microscope (Carl Zeiss, Sartrouville, France) equipped with a CoolSnap HQ2 camera (Princeton Instruments; Roper Scientific) and a Fluar 40× oil immersion objective lens (1.3 NA) (Carl Zeiss). Light was provided by the DG-4 wavelength switcher (Princeton Instruments). A dual excitation at 340 and 380 nm was used and emission was collected at 515 nm. The software MetaFluor (Universal Imaging) was

used to acquire the images at a frequency 0.5 Hz and to analyze off-line the data. Stock solutions of SAG, hyperforin and TPEN were prepared in dimethyl sulfoxide (DMSO) and diluted at least 1000-fold into the Tyrode's solution immediately before use.

7.2.2 Iron imaging with calcein

Cells (grown on 15 mm diameter glass coverslips) were incubated in a Tyrode's solution supplemented with 0.125 μM calcein for 5 minutes at 20-22°C. They were then washed twice and the cover-slips were settled on the microscope as indicated in Section 7.2.1. The cells were excitated at 495 nm and the emission was collected at 515 nm.

7.2.3 Zinc imaging with FluoZin-3

Cells (grown on 15 mm diameter glass coverslips) were incubated in a Tyrode's solution supplemented with 5 μM FluoZin-3 for 30 minutes at 20-22°C. They were then washed twice and kept in a FluoZin-3-free Tyrode's solution for 30 minutes at 20-22°C. The cover-slips were settled on the microscope as indicated in Section 7.2.1. The cells were excitated at 495 nm and the emission was collected at 515 nm.

7.3 Quantification of intracellular zinc and sulphur by ICP-OES and copper and iron by atomic absorption spectroscopy

HEK-293 cells or HEK-TRPC6 cells were harvested by gentle pipetting and washed twice with PBS and once with PBS supplemented with 5 mM EDTA to remove metals non-specifically bound to membranes. In some cases, HEK and HEK-TRPC6 cells were pretreated with 50 μM $FeSO_4$ supplemented with ascorbic acid in the presence or absence of 100 μM OAG for 1 hour under 95% O_2 5% CO_2 at 37°C. The total protein concentration of each sample was measured by the Bio-Rad DC Protein Assay.

Pellets were dried by heating and vacuum and mineralized by incubating overnight in 70% nitric acid at 50°C, before analysis with Inductively Coupled Plasma-Optical Emission Spectrometry (ICP-OES) with a Varian, Vista MPX instrument. The zinc and sulphur contents were normalized to the amount of protein in each analyzed pellet.

Intracellular copper and iron were determined by atomic absorption spectroscopy. Dried pellets were homogenized by incubating overnight in tetramethylammonium hydroxide (Sigma) before analysis with electrothermal atomic absorption spectroscopy using external calibration curve and Zeeman background correction (Hitachi model 8270, Tokyo, Japan).

The copper and iron contents were normalized to the amount of protein in each analyzed pellet.

Data are presented as mean values +/- SEM, with n being the number of measurements.

7.4 Synchrotron microbeam X-ray fluorescence

An introduction on synchrotron radiation and X-ray fluorescence as well as a presentation of synchrotron microbeam X-ray fluorescence (μ-SXRF) experimental set-up and data processing methods is found in the appendix. Below is shown how the samples were prepared.

Cells were grown on a Si_3N_4 membrane (3 × 3 mm^2, thickness 500 nm, Silson Ltd., England). For HEK and HEK-TRPC6 cells, the membrane was first coated with poly-L-lysine (0.0025% in H_2O, 90 minutes at 37°C), while for primary culture of cortical neurons, it was first coated with poly-L-lysine (0.0033% in H_2O, 30 minutes at 37°C) following by poly-L-ornithine (0.0033% in H_2O, 90 minutes at 37°C). After coating, the membrane was washed twice with sterile deionized water. The cell suspension was added to the membrane and incubated under 95% O_2 5% CO_2 at 37°C for 48 hours. In some cases, after 48 hours, HEK and HEK-TRPC6 cells were exposed to 50 μM $FeSO_4$ supplemented with ascorbic acid in the presence or absence of 100 μM OAG for 1 hour, and cortical neurons were exposed to 10μM $FeSO_4$ supplemented with ascorbic acid in the presence or absence of 100 μM OAG or 10μM hyperforin for 1 hour or 5 minutes. After the treatments, cells were rinsed with a metal-free (no added $FeSO_4$) Neurobasal medium and then with PBS, cryofixed at -160°C by freezing into isopentane chilled with liquid nitrogen, freeze dried at -35°C in vacuum, and stored at room temperature in a desiccator. The protocol applied preserved the cellular morphology and the chemical element distribution integrity (Ortega et al., 1996).

Data are presented as mean values +/- SEM, with n being the number of cells tested.

RESULTS AND DISCUSSIONS

8 Cortical neurons express channels exhibiting TRPC6-like properties

8.1 Introduction

The protein TRPC6 is widely expressed in the brain. Together with its close homolog TRPC3, it plays an essential role in BDNF mediated growth-cone turning (Li et al., 2005) and BDNF-mediated neuronal protection (Jia et al., 2007). In addition, TRPC6 promotes neurite outgrowth (Leuner et al., 2007; Tai et al., 2008) and is important for the development of dendritic spines and excitatory synapses (Zhou et al., 2008). Whether TRPC6 channels exert additional roles in neuronal cells is unknown.

Unless otherwise indicated, the results described below were obtained on cultured cortical cells dissociated from cerebral cortices of embryonic (E13) mice. During corticogenesis, cortical neurons appear at E11-12 (Kriegstein and Noctor, 2004). The neurons found at E13 are thus the first post-mitotic neurons. They possess a large repertoire of functional plasma membrane Ca^{2+} channels including NMDA receptors (Platel et al., 2005), VGCC (Bouron et al., 2006), and SOC (Bouron et al., 2005). These neurons also express all TRPC isoforms including TRPC6 (Boisseau et al., 2009). The properties of native DAG-sensitive channels of cortical neurons were compared to those of TRPC6 channels over-expressed in HEK-293 cells.

As already mentioned, a previous work shows the presence of TRPC6 in the cortex at E13 (Boisseau et al., 2009). When I initiated this study, no data were yet available on the functional properties of these channels in this tissue. During the time course of my PhD thesis, a report showed the existence of DAG-sensitive channels of TRPC6 type in cortical astrocytes prepared from embryonic mice (Beskina et al., 2007).

8.2 Article 1: Diacylglycerol analogues activate second messenger-operated calcium channels exhibiting TRPC-like properties in cortical neurons

Journal of Neurochemistry

JOURNAL OF NEUROCHEMISTRY | 2009 | 108 | 126–138 doi: 10.1111/j.1471-4159.2008.05752.x

Diacylglycerol analogues activate second messenger–operated calcium channels exhibiting TRPC–like properties in cortical neurons

Peng Tu,*,†,‡ Christiane Kunert-Keil,§ Silke Lucke,§ Heinrich Brinkmeier§ and Alexandre Bouron*,†,‡

*CNRS UMR 5249, Grenoble, France

†CEA, DSV, IRTSV, Grenoble, France

‡Université Joseph Fourier, Grenoble, France

§EMAU Greifswald, Institut für Pathophysiologie, Karlsburg, Germany

Abstract

The lipid diacylglycerol (DAG) analogue 1-oleoyl-2-acetyl-*sn*-glycerol (OAG) was used to verify the existence of DAG-sensitive channels in cortical neurons dissociated from E13 mouse embryos. Calcium imaging experiments showed that OAG increased the cytosolic concentration of Ca^{2+} ($[Ca^{2+}]i$) in nearly 35% of the KCl-responsive cells. These Ca^{2+} responses disappeared in a Ca^{2+}-free medium supplemented with EGTA. Mn^{2+} quench experiments showed that OAG activated Ca^{2+}-conducting channels that were also permeant to Ba^{2+}. The OAG-induced Ca^{2+} responses were unaffected by nifedipine or omega-conotoxin GVIA (Sigma-Aldrich, Saint-Quentin Fallavier, France) but blocked by 1-[β-(3-(4-Methoxyphenyl)propoxy)-4-methoxyphenethyl]-1H-imidazole hydrochloride (SKF)-96365 and Gd^{3+}. Replacing Na^+ ions with *N*-methyl-D-glucamine diminished the amplitude of the OAG-induced Ca^{2+} responses showing that the Ca^{2+} entry was mediated via Na^+-dependent and Na^+-independent mechanisms. Experiments carried out with the fluorescent Na^+ indicator CoroNa Green showed that OAG elevated $[Na^+]i$. Like OAG, the DAG lipase inhibitor RHC80267 increased $[Ca^{2+}]i$ but not the protein kinase C activator phorbol 12-myristate 13-acetate. Moreover, the OAG-induced Ca^{2+} responses were not regulated by protein kinase C activation or inhibition but they were augmented by flufenamic acid which increases currents through C-type transient receptor potential protein family (TRPC) 6 channels. In addition, application of hyperforin, a specific activator of TRPC6 channels, elevated $[Ca^{2+}]i$. Whole-cell patch-clamp recordings showed that hyperforin activated non-selective cation channels. They were blocked by SKF-96365 but potentiated by flufenamic acid. Altogether, our data show the presence of hyperforin- and OAG-sensitive Ca^{2+}-permeable channels displaying TRPC6-like properties. This is the first report revealing the existence of second messenger-operated channels in cortical neurons.

Keywords: brain, calcium channels, cortex, neurons, transient receptor potential canonical.

J. Neurochem. (2009) **108**, 126–138.

The lipid diacylglycerol (DAG) is a second messenger involved in key cellular processes [for a review see (Carrasco and Merida 2007)]. Several DAG-sensitive proteins have been identified like some isoforms of the protein kinase C (PKC) family, Munc13 proteins (Brose *et al.* 2004) and ion channels of the C-type transient receptor potential protein family (TRPC). Seven TRPC are now identified and named TRPC1 to TRPC7. They all function as cation channels but they exhibit distinct gating and biophysical properties. For instance, homomeric TRPC1, TRPC3, TRPC6 or TRPC7 channels and heteromeric TRPC1–TRPC3 and TRPC3–TRPC4 channels can open in response to DAG application

Received June 24, 2008; revised manuscript received September 19, 2008; accepted October 20, 2008.

Address correspondence and reprint requests to Alexandre Bouron, Laboratoire de Chimie et Biologie des Métaux, UMR CNRS 5249, CEA, 17 rue des Martyrs, 38054 Grenoble, France.
E-mail: alexandre.bouron@cea.fr

Abbreviations used: ω-CTx, omega-conotoxin GVIA; DAG, diacylglycerol; DIG, digoxigenin; DIV, days *in vitro*; DMSO, dimethyl sulfoxide; FFA, flufenamic acid; MβCD, methyl-β-cyclodextrin; NMDG, *N*-methyl-D-glucamine; OAG, 1-oleoyl-2-acetyl-*sn*-glycerol; PKC, protein kinase C; PMA, phorbol 12-myristate 13-acetate; SAG, 1-stearoyl-2-arachidonoyl-sn-glycerol; SKF, 1-[β-(3-(4-Methoxyphenyl)propoxy)-4-methoxyphenethyl]-1H-imidazole hydrochloride; TRPC, C-type transient receptor potential protein family.

allowing an entry of Ca^{2+} into the cell (Hofmann *et al.* 1999; Lintschinger *et al.* 2000; Liu *et al.* 2005; Poteser *et al.* 2006). This DAG-dependent activation of TRPC channels occurs in a PKC-independent manner.

Several studies reported the existence of DAG-sensitive channels in neural cells. For instance, DAG activates Ca^{2+}-conducting channels in the neuronal cell lines PC12 (Mwanjewe and Grover 2004) and IMR-32 (Nasman *et al.* 2006), as well as in cortical astrocytes (Grimaldi *et al.* 2003; Beskina *et al.* 2007), vomeronasal neurons (Lucas *et al.* 2003), hippocampal neurons (Tai *et al.* 2008) and neural stem cells (Pla *et al.* 2005). In astrocytes from embryonic rat brains, TRPC3 channels mediate the DAG-induced cytosolic Ca^{2+} changes (Grimaldi *et al.* 2003) whereas in astrocytes prepared from embryonic murine brains TRPC6 forms the DAG-sensitive channels (Beskina *et al.* 2007). On the other hand, the Ca^{2+} responses are due to TRPC2 in vomeronasal neurons (Lucas *et al.* 2003) and to TRPC6 in the hippocampus (Tai *et al.* 2008). These latter findings suggest that the molecular identity of the DAG-sensitive channels seems species- and tissue-dependent. At E13, the immature cortex expresses all TRPC isoforms (Boisseau, Kunert-Keil, Lucke and Bouron; unpublished data). We thus tried to determine whether the first cortical neurons, which are generated at E11–12 (Kriegstein and Noctor 2004), express functional DAG-sensitive channels. By recording cytosolic Ca^{2+} changes we observed that the DAG analogues 1-oleoyl-2-acetyl-*sn*-glycerol (OAG) or 1-stearoyl-2-arachidonoyl-sn-glycerol (SAG) caused a Ca^{2+} influx via channels sensitive to Gd^{3+} and SKF-96365 but insensitive to nifedipine and omega-conotoxin GVIA (ω-CTx), (Sigma-Aldrich). The OAG-induced Ca^{2+} responses were observed in KCl-responding and KCl-insensitive cells. Similarly to OAG or SAG, the DAG lipase inhibitor RHC80267, used to prevent the degradation of DAG, elevated $[Ca^{2+}]i$ but not the PKC activator phorbol 12-myristate 13-acetate (PMA). Moreover, the OAG-induced responses were not altered by PKC activation or inhibition. This shows that OAG recruited SKF-96365-sensitive Ca^{2+}-conducting channels in a PKC-independent manner. Flufenamic acid (FFA) was used to further characterize the identity of the OAG-sensitive channels. FFA increases the amplitude of currents through TRPC6 channels but blocks TRPC3 and TRPC7 channels (Inoue *et al.* 2001). In cultured cortical neurons, FFA potentiated the OAG-induced Ca^{2+} responses suggesting that TRPC6 are key constituents of the OAG-sensitive channels. *In situ* hybridization experiments confirmed the presence of TRPC6, distributed throughout the cortical wall (preplate and ventricular zone) including in cortical neurons. Furthermore, Ca^{2+} imaging experiments and whole-cell patch-clamp recordings showed that hyperforin, a specific activator of TRPC6 channels (Leuner *et al.* 2007), activated non-selective cation channels blocked by SKF-96365. Currents through hyperforin-activated channels were increased by FFA. Altogether, these data suggest that OAG activated TRPC6 channels or channels exhibiting TRPC6-like properties. This is the first description of functional second messenger-operated channels in cortical neurons.

Materials and methods

Primary cell cultures

The cortical cells were dissociated from cerebral cortices isolated from embryonic (E13) C57BL6/J mice (vaginal plug was designated E0) according to procedures approved by the Ethical Committee of Rhône-Alpes Region (France). The cells have been prepared and kept up to 6 days in culture according to Bouron *et al.* (2006).

Calcium imaging experiments with Fluo-4

Cells were bathed in a Tyrode solution containing (in mM) 136 NaCl, 5 KCl, 2 $CaCl_2$, 1 $MgCl_2$, 10 HEPES, 10 glucose, pH 7.4 (NaOH) and 1.8 μM Fluo-4/AM for 10 min at 20–22°C. They were then washed twice with a Fluo-4/AM-free Tyrode solution, stored 20 min at 20–22°C and then placed on the stage of an upright Olympus BX51WI microscope equipped with a water immersion 20× objective lens (Olympus, 0.95 NA, Sartrouville, France). The emitted light, provided by a 100 W mercury lamp, was attenuated by a neutral density filter (U-25ND6, Olympus). Fluorescent images were captured by a cooled digital CCD MicroMax Princetown camera (Roper Scientific, Evry, France). The software MetaFluor (Universal Imaging; Roper Scientific) was used to acquire the images at a frequency of 0.2 or 0.5 Hz and to analyse off-line the data. The shutter was controlled by the shutter driver Uniblitz VMM-D1 (Vincent Associates; Roper Scientific). The excitation light for Fluo-4 was filtered through a 460–495 nm excitation filter and the emitted light was collected through a 510–550 nm filter. The Ca^{2+} imaging experiments were performed 2–5 h after the plating of the cells and on cells kept up to 6 days in culture. When indicated, cells were maintained in a nominally Ca^{2+}-free medium having the same composition as the Tyrode solution (see above) supplemented with 0.4 mM EGTA. The pH of the EGTA-containing solution was adjusted to pH 7.4 with NaOH. In some experiments, cells were stimulated with a K^+-rich solution containing 50 mM (instead of 5 mM) KCl. Under these conditions, the concentration of NaCl was reduced to 91 mM. All solutions were applied through a gravity-driven system perfusing the entire recording chamber. The fluorescence was collected from 10–40 cells simultaneously monitored. Only one field of view was used per dish. Data are presented as mean ± SEM, with *n* being the number of cell bodies tested. The experiments reported below were carried out at 20–22°C.

Calcium imaging experiments with fura-2

The uneven distribution of Fluo-4 and its photo-bleaching can limit the use of this Ca^{2+} indicator. To avoid these problems we used the ratiometric dye fura-2. Cells grown on 15 mm diameter glass cover-slips were incubated in a Tyrode solution supplemented with 2.5 μM fura-2 for 15 min at 20–22°C. They were then washed twice and kept in a fura-2-free Tyrode solution for 20 min at 20–22°C. Cover-slips were transferred on a perfusion chamber (RC-25F, Warner Instruments; Phymep, Paris, France) and placed on the stage of an Axio Observer A1 microscope (Carl Zeiss, Sartrouville,

France) equipped with a CoolSnap HQ2 camera (Princeton Instruments; Roper Scientific) and a Fluar 40× oil immersion objective lens (1.3 NA) (Carl Zeiss). Light was provided by the DG-4 wavelength switcher (Princeton Instruments). A dual excitation at 340 and 380 nm was used and emission was collected at 515 nm. The software MetaFluor (Universal Imaging) was used to acquire the images at a frequency 0.5 Hz and to analyse off-line the data. Stock solutions of OAG, SAG, nifedipine, hyperforin, cytochalasin D, PP2, RHC80267, GF 109203X and genistein were prepared in dimethyl sulfoxide (DMSO) and diluted at least 1000-fold into the Tyrode solution immediately before use so that the final concentration of DMSO never exceeded 0.1%. Control experiments were performed with DMSO alone (0.1%). At this concentration, the solvent never induced any cytosolic Ca^{2+} signal (not shown). All other stock solutions (SKF-96365, ω-CTx, Gd^{3+}, bethanechol, phenylephrine, histamine hydrochloride and α-methyl-5-hydroxytryptamine) were prepared in water and also diluted at least 1000-fold into the Tyrode solution immediately before use.

Sodium imaging experiments with CoroNa Green

The effect of OAG on the cytosolic concentration of Na^+ was assayed with the fluorescent Na^+ indicator CoroNa Green. Cells were incubated with 5 μM CoroNa Green/AM for 30 min at 20–22°C. They were rinsed and placed on the stage of an Axio Observer A1 microscope (Carl Zeiss). These experiments were carried out with the fura-2 Ca^{2+} imaging setup described above, except that a single excitation at 495 nm was used and emission was collected at 525 nm.

Electrophysiological recordings

The whole-cell configuration of the patch-clamp technique (Hamill *et al.* 1981) was used to record currents activated by hyperforin. The experiments were conducted according to protocols and recording solutions already described (Hill *et al.* 2006). The external medium contained (in mM): 140 NaCl, 4 KCl, 10 TEACl, 1 $CaCl_2$, 1 $MgCl_2$, 10 HEPES, 5 D-glucose, pH 7.4 (NaOH). The patch pipettes were fabricated by means of the DMZ Universal pipette puller (Zeitz Instruments, München, Germany) from thick wall borosilicate glass capillaries (1.5 mm o.d. × 0.86 mm i.d., Clark Electromedical Instruments; Phymep). When filled with the following intracellular solution (in mM): 140 CsCl, 1 $MgCl_2$, 5 D-glucose, 10 HEPES, 0.1 EGTA, 4 ATP, 0.2 GTP, pH 7.2 (CsOH), pipettes had a resistance of 2.5–3.8 MΩ. Currents were measured with an Axoclamp 200B amplifier (Axon Instruments, Dipsi, Chatillon, France), filtered at 1 kHz, and analysed off-line using the pClamp software (version 9.0, Axon Instruments). Unless otherwise indicated, the holding membrane potential was set at 0 mV to inactivate voltage-gated Na^+ and Ca^{2+} channels. Whole-cell currents, recorded at 20–22°C 1–3 days after the plating of the cells, were triggered at a frequency of 0.2 Hz by 2 s voltage ramps from −100 to +40 mV. Capacitive transients were cancelled and the cell capacitance value was read from the amplifier dials.

Standard RT-PCR

Total RNA was isolated using guanidinium-isothiocyanate (RNeasy Mini Kit; Qiagen, Hilden, Germany) and RNA concentration was determined by UV absorbance measurements. An amount of 200 ng total RNA was reverse transcribed using random hexamer primers and the TaqMan Reverse Transcription Reagents (PE Applied Biosystems, Weiterstadt, Germany). PCR was performed with Taq Polymerase for 40 cycles as described previously (Kunert-Keil *et al.* 2006). Amplification of a TRPC6 cDNA fragment was done with murine specific TRPC6 primers (Assay-on-Demand Mm00443441_m1; PE Applied Biosystems).

In situ hybridization

Non-radioactive *in situ* hybridization was performed with cryo sections (4 μm) which had been fixed in 4% paraformaldehyde. Sections were rehydrated and permeabilized with 0.2 M HCl. Post-fixation (paraformaldehyde 4%, 20 min, 4°C) was followed by acetylation using 0.4% acetic anhydride in triethanolamine (0.1 M, pH 8.0, 15 min). After washing with 50% formamide in 1.5% sodium-sodium phosphate-EDTA buffer (20x sodium-sodium phosphate-EDTA buffer: 3.6 M NaCl, 0.2 M NaH_2PO_4, 0.2 M EDTA, pH 7.4) the sections were pre-hybridized for 1 h at 56°C in a solution containing 50% formamide and 50% solution D (4 M guanidine thiocyanate, 25 mM sodium citrate, pH 7.0), 0.5% blocking reagent (Roche Biochemicals, Mannheim, Germany) and 210 μg/mL t-RNA. For TRPC6, a cDNA fragment (GenBank: NM_013838; position nt +2181 to + 2507) was cloned into the pGEM-T-Easy cloning vector (Promega, Mannheim, Germany) (Kunert-Keil *et al.* 2006). After hybridization for 12–16 h with pre-hybridization solution containing 125 ng digoxigenin (DIG)-labelled cRNA probe (Kunert-Keil *et al.* 2006) and washing with 2x saline sodium citrate buffer (20x saline sodium citrate buffer: 3 M NaCl, 0.3 M sodium citrate; pH 7.4) sections were incubated with blocking reagent (Roche Biochemicals). Bound riboprobe was visualized by incubation with alkaline phosphatase-conjugated anti-DIG antibody (Roche Biochemicals) and subsequent substrate reaction containing 5-bromo-4-chloro-3-indolyl phosphate/nitro-blue-tetrazolium chloride.

Materials

GF 109203X (bisindolylmaleimide I (2-[1-[3-(dimethylamino)propyl]-1H-indol-3-yl]-4-(1H-indol-3-yl)-1H-pyrrole-2,5-dione, or Go 6850) and PP2 were purchased from Calbiochem (VWR, Fontenay sous Bois, France). The fluorescent Ca^{2+} and Na^+ indicators Fluo-4, fura-2, CoroNa Green were from Molecular Probes (Interchim, France). The alkaline phosphatase-conjugated anti-DIG antibody and the blocking reagent were from Roche Biochemicals. All other chemicals including PMA, OAG, SAG, FFA, RHC80267 and *N*-methyl-D-glucamine (NMDG), genistein, methyl-β-cyclodextrin (MβCD), cytochalasin D, bethanechol, phenylephrine, serotonin, α-methyl-5-hydroxytryptamine were from Sigma-Aldrich. Hyperforin is a kind gift from Dr Willmar Schwabe GmbH & Co (Karlsruhe, Germany).

Results

OAG evoked Ca^{2+} responses

Most of the freshly dissociated or cultured E13 cortical cells express β_{III}-tubulin, a marker of early post-mitotic neurons (Bouron *et al.* 2005) and possess functional voltage-gated Ca^{2+} channels (Bouron *et al.* 2006). The external application

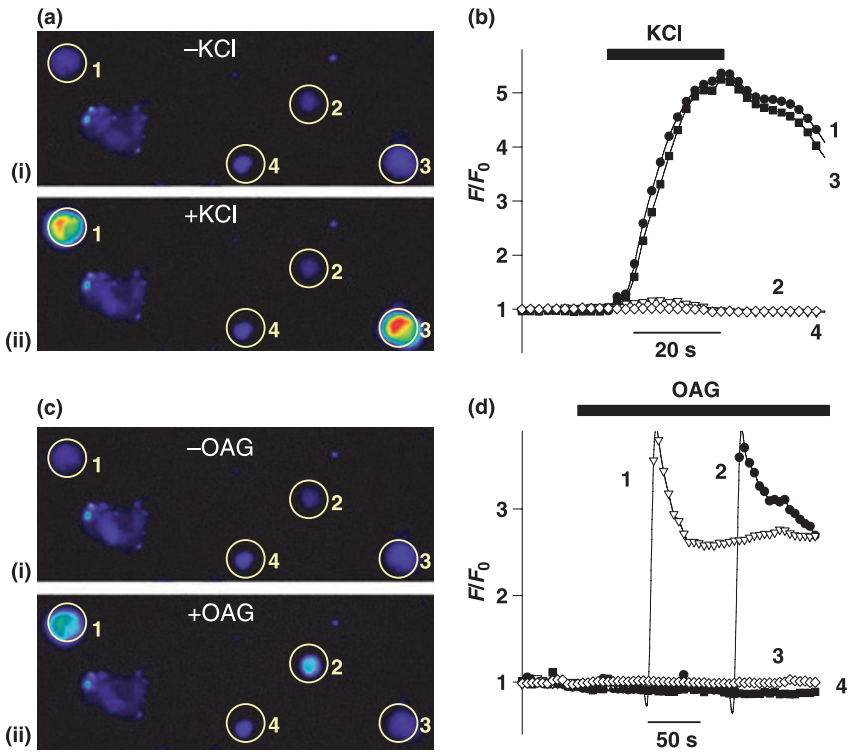

Fig. 1 1-oleoyl-2-acetyl-*sn*-glycerol (OAG) induced Fluo-4 signals in KCl-responsive and KCl-unresponsive cells. Fluo-4 loaded cells are shown before (a-i) and after (a-ii) the application of a depolarizing medium containing 50 mM KCl (instead of 5 mM for the control medium). In this example, KCl triggered a Fluo-4 increase in cells 1 and 3 whereas cells 2 and 4 failed to respond to KCl. (b) Shows the time course of the Fluo-4 signals (F/F_0) as a function of time, with F being the Fluo-4 fluorescence and F_0 the baseline Fluo-4 fluorescence. In these experiments, KCl was applied, washed away and then OAG was added after the Fluo-4 fluorescence had returned to the baseline. The same Fluo-4 loaded cells as in (a) are shown before (c-i) and after (c-ii) the addition of OAG (100 μM). OAG-induced Ca^{2+} responses were noted in cells 1 and 2. The horizontal bars in (b) and (d) indicate when KCl and OAG were present in the bath respectively. Unless noted otherwise, throughout this study, for each experiment, a KCl challenge was applied before adding OAG. We only studied the properties of the KCl responsive cells.

of OAG (100 μM) evoked Ca^{2+} responses in some KCl-responding and KCl-insensitive cells as shown in Fig. 1. In this report, we only analysed the properties of cells where a KCl-induced depolarization evoked a transient Ca^{2+} rise. These KCl-responsive cells were considered as neurons (Bouron *et al.* 2006). In contrast to the KCl responses, the OAG-induced Ca^{2+} responses were asynchronous and displayed a diversity of shapes as illustrated in Fig. 2(a). Similar experiments were carried out after 1, 2, 4, 5 and 6 days *in vitro* (DIV). OAG evoked Ca^{2+} responses in freshly dissociated cells (Fig. 2a) as well as in cells kept up to 6 days in primary culture (data not shown). These Ca^{2+} responses had roughly the same amplitude regardless of the age of the cells, at least up to six DIV. The total number of KCl-responsive cells used in the present study was 1129. Only 389 of them (35%) displayed OAG-induced Ca^{2+} responses. Schematically, based on their time course three types of OAG-induced Ca^{2+} responses were identified: (i) cells with transient Fluo-4 responses (15%), (ii) cells exhibiting a sustained elevation of Ca^{2+} (23%) and (iii) cells with oscillatory Ca^{2+} responses (62%, total 100%). These three phenotypes could be seen in distinct cells from the same dish, whether freshly dissociated cells or cells kept several days in culture.

OAG controlled an entry of Ca^{2+} and Na^+

The OAG-induced Ca^{2+} responses were not observed when the cells were bathed in a Ca^{2+}-free medium (supplemented with 0.4 mM EGTA) (n = 65 cells) (Fig. 2b). Thus, OAG did not release Ca^{2+} from stores but rather promoted an entry of Ca^{2+}. Furthermore, the OAG-induced Ca^{2+} responses were unaffected by the voltage-gated Ca^{2+} channel inhibitors nifedipine (5 μM, n = 40) or ω-CTx (1 μM, n = 37) but they were strongly attenuated in the presence of Gd^{3+} (5 μM, n = 106) and SKF-96365 (20 μM, n = 82) (Fig. 2b). A recent study showed that DAG can promote an entry of Na^+ through TRPC6 channels which, in turn, elevates the cytosolic concentration of Ca^{2+} via the Na^+/Ca^{2+} exchanger operating in the reverse mode (Lemos *et al.* 2007). As Gd^{3+} blocks the Na^+/Ca^{2+} exchanger (Zhang and Hancox 2000),

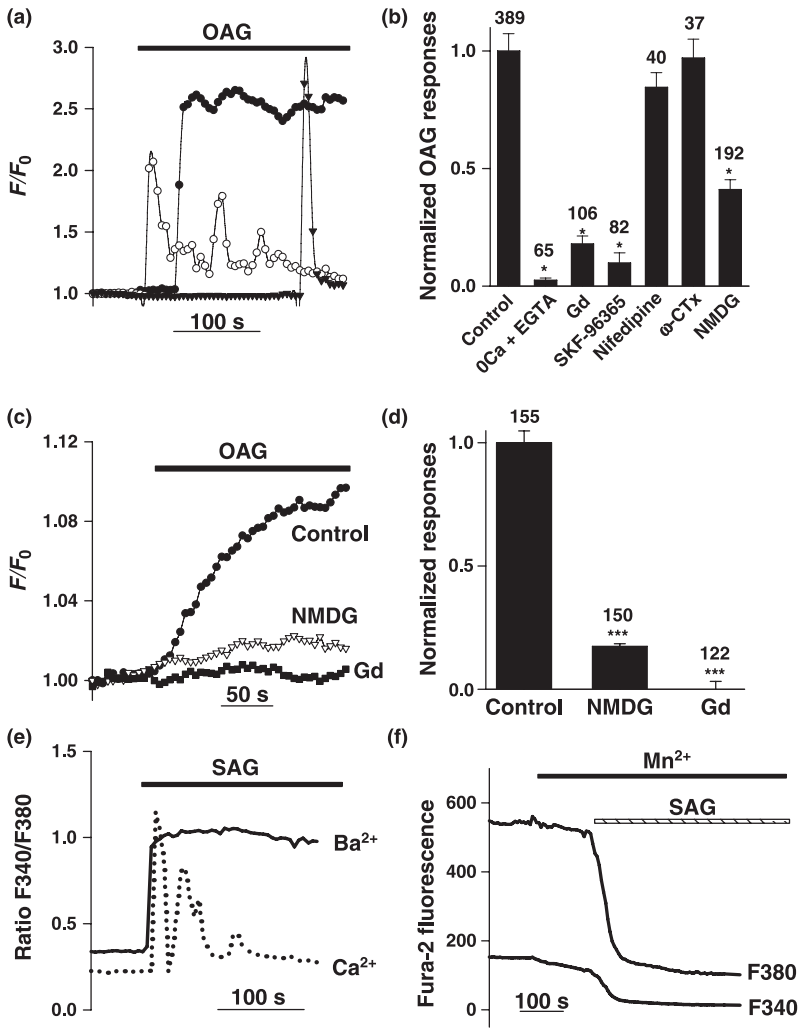

Fig. 2 1-oleoyl-2-acetyl-*sn*-glycerol (OAG) triggered an entry of Ca^{2+} via Gd^{3+}- and SKF-96365-sensitive channels. (a) Shows representative Fluo-4 signals from three KCl-responsive cells. It illustrates the diversity of the OAG responses: transient, long-lasting and oscillatory. In (b) is shown the normalized increase in Fluo-4 fluorescence (mean ± SEM) induced by OAG (100 μM) under different conditions. Control: maximal amplitudes (normalized data) of the Fluo-4 responses observed during an acute application of OAG (100 μM) (n = 389 cells). Experiments were also performed when the cells were kept in a Ca^{2+}-free medium supplemented with 0.4 mM EGTA (0Ca + EGTA) (n = 65 cells) or in a normal (2 mM Ca^{2+}) recording medium containing either 5 μM Gd^{3+} (n = 106 cells), 20 μM SKF-96365 (n = 82 cells), 5 μM nifedipine (n = 40 cells), 1 μM ω-conotoxin GVIA (ω-CTx, n = 37 cells) or 140 mM *N*-methyl-D-glucamine (NMDG, n = 192 cells) (in this latter case NaCl was omitted). *p < 0.001 versus control (one-way ANOVA followed by a Tukey test). The fluorescent Na^+ indicator CoroNa Green was used to verify whether OAG increased $[Na^+]_i$. (c) Shows representative CoroNa Green responses. The application of OAG (100 μM) induced a time-dependent increase in CoroNa Green fluorescence (F/F_0) (control) which was not observed in the presence of Gd^{3+} (5 μM) or when Na^+ was replaced with $NMDG^+$. These experiments are summarized in (d) with the number of cells tested indicated above each bar. ***p < 0.001 (Student's t-test). For each cell, the maximum change in fluorescence (F/F_0) was determined and compared with the normalized CoroNa Green responses obtained in control conditions. The horizontal bar in (c) indicates when OAG was present. (e) Shows fura-2 recordings from two different cells. The Tyrode solution contained 2 mM Ca^{2+} or Ba^{2+} and the cells were stimulated when indicated by the horizontal black bar with 50 μM SAG. The graph shows the changes in fura-2 fluorescence (ratio F340 nm/F380 nm) as a function of time. In the presence of Ba^{2+} the responses are sustained. In (f) are shown representative fura-2 responses at 340 and 380 nm from a cortical neuron kept in a Ca^{2+}-free medium. The addition of 100 μM Mn^{2+} had almost no effect. But the subsequent application of 50 μM SAG (still in the presence of 100 μM Mn^{2+} and no added Ca^{2+}) provokes a clear quench of the fura-2 fluorescence at both wavelengths.

experiments were performed with a Na^+-free Tyrode solution where Na^+ was replaced with the large organic cation $NMDG^+$. Under these conditions, OAG-induced Ca^{2+} responses were still observed but, on average, their amplitudes were reduced by nearly 50% (n = 192) (Fig. 2b). This latter result thus suggests that two mechanisms contributed to

the OAG-induced Ca^{2+} entry: OAG triggers a Gd^{3+}- and SKF-96365-sensitive Ca^{2+} rise via Na^+-dependent and Na^+-independent mechanisms. The effects of OAG on $[Na^+]_i$ was assayed by means of the fluorescent Na^+ indicator CoroNa Green (Poburko *et al.* 2007). Figure 2(c) shows representative CoroNa Green responses obtained in three different experimental conditions. OAG induced a time-dependent increase in CoroNa Green fluorescence, an effect that was not observed in the presence of Gd^{3+} or when Na^+ was replaced with $NMDG^+$ (Fig. 2c and d). Thus, OAG elevated $[Na^+]_i$ via a Gd^{3+}-sensitive process. This response depends on the extracellular concentration of Na^+.

Some experiments were performed with the ratiometric Ca^{2+} indicator fura-2 and with SAG, another DAG analogue. SAG induced Ca^{2+} transients (Fig. 2e). Similar fura-2 signals were obtained with OAG (not shown). When replacing 2 mM $CaCl_2$ with 2 mM $BaCl_2$, SAG elevated the cytosolic concentration of Ba^{2+} (Fig. 2e). These Ba^{2+} signals were sustained, not transient as seen with Ca^{2+} because Ba^{2+} is weakly pumped out of the cells or into the organelles (Yamaguchi *et al.* 1989). To further verify the presence of DAG-activated Ca^{2+} channels, we checked whether Mn^{2+} could quench the fura-2 fluorescence. Mn^{2+} ions readily enter cells through Ca^{2+}-conducting channels. The results of these experiments are summarized in Fig. 2(f). Cells were kept in a Ca^{2+}-free medium. The addition of Mn^{2+} (100 μM) weakly diminished the fura-2 fluorescence at 340 and 380 nm. However, a subsequent addition of SAG was accompanied by a clear quench of the fura-2 fluorescence at both wavelengths (Fig. 2f). Altogether, these experiments showed that DAG analogues like OAG or SAG activated SKF-96365-sensitive channels permeable to Ca^{2+}, Ba^{2+} and Mn^{2+}. Based on our data, it is proposed that in embryonic cortical neurons OAG activates SKF-96365-sensitive cation channels allowing an entry of Ca^{2+} and Na^+. This OAG-induced Na^+ entry thus stimulates the Na^+/Ca^{2+} exchanger which, when operating in the reverse mode, allows an entry of Ca^{2+}. According to this hypothesis, OAG elevates the cytosolic concentrations of Ca^{2+} by activating OAG-sensitive Ca^{2+}-conducting channels and also by promoting an entry of Ca^{2+} via the Na^+/Ca^{2+} exchanger. These results are in agreement with recent data obtained on smooth muscle cells (Poburko *et al.* 2007; Syyong *et al.* 2007). It is important to note that the Na^+/Ca^{2+} exchanger is already functional at E13 and mediates a Na^+-dependent Ca^{2+} entry (Platel *et al.* 2005). Both responses, namely the Na^+ and Ca^{2+} entries, disappeared in the presence of Gd^{3+}, a potent blocker of calcium channels and of the Na^+/Ca^{2+} exchanger (Zhang and Hancox 2000).

The DAG lipase inhibitor RHC80267 induced Ca^{2+} responses

The DAG lipase inhibitor RHC80267 (50 μM), used to prevent the degradation of DAG, can elevate $[Ca^{2+}]_i$ (Hofmann *et al.* 1999). When acutely applied, RHC80267 elicited a weak Fluo-4 increase (8%, n = 133 cells) (Fig. 3a). However, this RHC80267 treatment, done at 20–22°C, was probably too short to significantly alter the intracellular concentration of DAG and therefore to promote robust Ca^{2+} responses. Experiments were then realized after a longer RHC80267 treatment during which the cells were maintained at 37°C. This was performed as follows: Fluo-4-loaded cells were kept in a Ca^{2+}-free medium containing 0.4 mM EGTA + 50 μM RHC80267 for 20 min at 37°C. They were then placed on the stage of the microscope and superfused with a recording medium containing 2 mM Ca^{2+}. The readmission of Ca^{2+} was accompanied by large Fluo-4 signals (Fig. 3b). When similar experiments were conducted with RHC80267-untreated cells, the Ca^{2+} challenge was followed by much smaller Fluo-4 signals (Fig. 3b) which most likely reflect an entry of Ca^{2+} through store-operated channels. Thus, an entry of Ca^{2+} can be triggered by either inhibiting the DAG lipase with RHC80267 or by applying OAG (or SAG).

Protein kinase C neither mimicked nor affected OAG responses

Many cellular effects of DAG have been attributed to PKC, its major downstream effector. Among other responses, PKC can lead to cytosolic Ca^{2+} changes (Khoyi *et al.* 1999; Murthy *et al.* 2000; Rosado and Sage 2000; Albert and Large 2002). In order to determine whether OAG acted via a PKC-dependent mechanism, the phorbol ester PMA, a potent PKC activator, was used. The external application of PMA (1 μM) did not elevate $[Ca^{2+}]_i$ (Fig. 3c). We next tried to verify whether PKC regulated the OAG-induced Ca^{2+} entry. Figure 3(d) shows that PKC activation (with PMA), or PKC inhibition (with the PKC antagonist GF 109203X, also named bisindolylmaleimide I or Gö 6850) did not alter the OAG-induced Ca^{2+} entry. Thus, OAG promoted a PKC-independent entry of Ca^{2+}.

Flufenamic acid potentiated the OAG responses

In neural cells, the presence of a PKC-independent but OAG-sensitive entry of Ca^{2+} has been described in astrocytes (Grimaldi *et al.* 2003; Beskina *et al.* 2007), vomeronasal neurons (Lucas *et al.* 2003), hippocampal neurons (Tai *et al.* 2008) and neural stem cells (Pla *et al.* 2005). Depending on the tissue and the species (rat vs. mouse), TRPC2 (Lucas *et al.* 2003), TRPC3 (Grimaldi *et al.* 2003) or TRPC6 (Beskina *et al.* 2007; Tai *et al.* 2008) are the key elements of these OAG-sensitive channels but whatever their exact molecular identity, TRPC appear as likely candidates controlling OAG-sensitive channels (Hofmann *et al.* 1999; Lintschinger *et al.* 2000; Liu *et al.* 2005). FFA is an anti-inflammatory agent which, among other cellular actions, inhibits currents through TRPC3 and TRPC7 channels but increases currents through TRPC6 channels (Inoue *et al.* 2001; Jung *et al.* 2002). We thus took

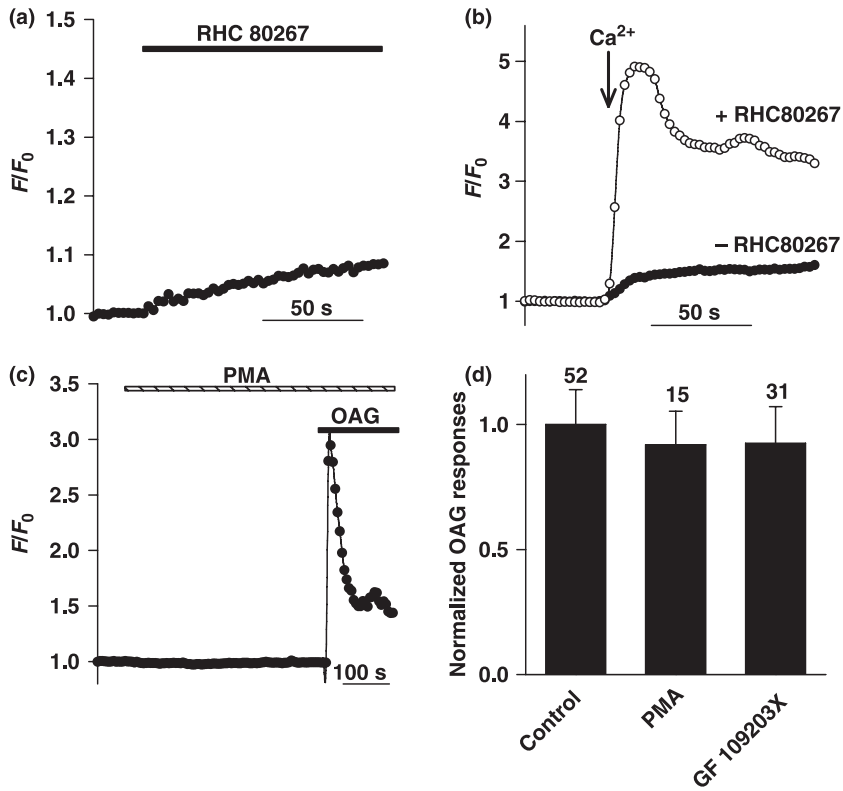

Fig. 3 In contrast to the PKC activator PMA, the DAG lipase inhibitor RHC80267 induced Fluo-4 responses. In this set of experiments, the DAG lipase inhibitor was used to determine whether DAG mediated the effects of OAG. (a) Shows a representative Fluo-4 recording from a cortical neuron illustrating that an acute application of RHC80276 (50 μM) induced a weak Ca^{2+} signal. In another set of experiments (b), Fluo-4-loaded cells were kept in a Ca^{2+}-free medium supplemented with 0.4 mM EGTA + 50 μM RHC80276 for 20 min at 37°C. They were then placed on the stage of the microscope and Fluo-4 signals were recorded (at 20–22°C). The re-introduction of 2 mM external Ca^{2+} was accompanied by large increases in fluorescence (open symbols) whereas RHC80276-untreated cells (filled symbols) poorly responded to the Ca^{2+} challenge. The arrow indicates when Ca^{2+} was added. C The phorbol ester PMA was used to verify whether the OAG-induced Ca^{2+} entry was under the control of PKC. The application of PMA (1 μM) did not induce any change in Fluo-4 fluorescence (c). When added after PMA, OAG was still able to promote an entry of Ca^{2+}. The horizontal bars indicate when PMA and OAG were present. Some experiments were carried out on cells pre-treated with the PKC inhibitor GF 109203X (5 μM) for 20 min at 20–22°C. (d) is a summary bar graph showing that the amplitude of the OAG-induced Fluo-4 responses (normalized data) was not affected by PMA and GF 109203X. For each cell, the maximal Fluo-4 signal induced by OAG was determined and compared with the normalized control values. The number of cells tested is indicated above each bar. PMA and GF 109203X were still present during the application of OAG.

advantage of this property to further characterize the OAG-sensitive channels. Applied alone (without OAG), FFA produced a modest but long-lasting elevation of the cytosolic concentration of Ca^{2+}. The Fluo-4 fluorescence increased by nearly 25% in the presence of FFA ($n = 14$ cells, $p < 0.05$, Student's t-test) (Fig. 4). When compared with OAG, FFA gave rise to weak Ca^{2+} responses having distinct kinetics properties. The FFA-induced Ca^{2+} rise also occurred when the cells were bathed in a Ca^{2+}-free medium (not shown) indicating that FFA promoted the release of Ca^{2+} from internal stores as already shown in non-neuronal (Poronnik *et al.* 1992; Cruickshank *et al.* 2003) and in neuronal cells (Lee *et al.* 1996). When added in the presence of FFA, OAG triggered larger Fluo-4 responses when compared with OAG alone (Fig. 4a). The amplitude of the Fluo-4 signals seen in the presence of FFA + OAG was larger than the sum of the two signals (the FFA-induced Ca^{2+} release + the OAG-induced Ca^{2+} entry). In addition, with FFA, the number of OAG responsive cells was > 60% instead of ~30% without FFA. Instead of blocking the OAG-induced Ca^{2+} entry, the channel blocker FFA increased the number of OAG responsive cells and potentiated the OAG-induced Ca^{2+} entry. As TRPC6 is the only known TRPC channel of which activity is up-regulated by FFA (Inoue *et al.* 2001; Jung *et al.* 2002), it seems that OAG activates TRPC6 channels or channels exhibiting TRPC6-like properties. We then addressed the question of the presence of TRPC6 in the cortex at E13.

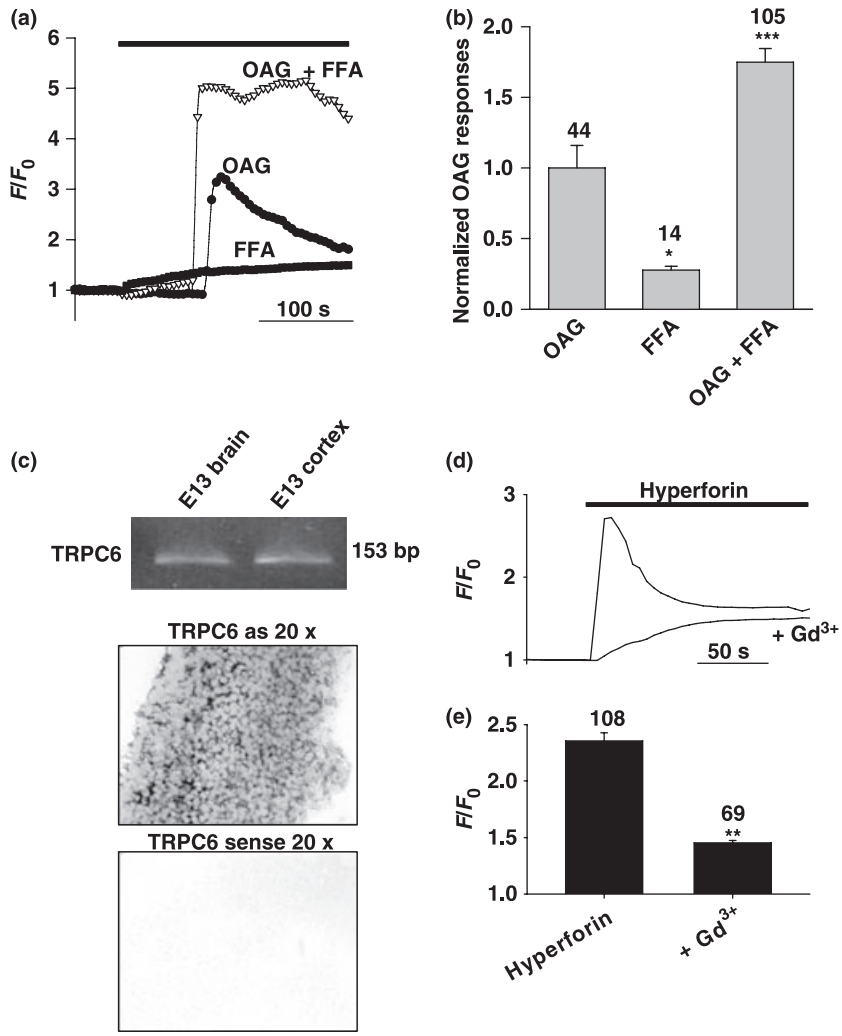

Fig. 4 Properties of the OAG-induced Ca^{2+} responses. (a) Three representative Fluo-4 responses from cells stimulated with OAG (100 μM), OAG + flufenamic acid (FFA, 85 μM) or with FFA (85 μM) alone are shown. The horizontal black bar indicates when these drugs were present in the bath. By itself, FFA increased the Fluo-4 fluorescence but when OAG was added together with FFA, the Fluo-4 responses were larger than without FFA. In (b) are shown normalized Fluo-4 signals under various experimental conditions. The number of cells tested is shown above each bar. $^*p < 0.05$ and $^{***}p < 0.001$, Student's *t*-test. (c) Reverse transcribed RNA (8 ng) from brain and cortex of E13 mice was added to the reaction mixtures and PCR products amplified in 40 cycles. The products were separated on agarose gels and stained with ethidium bromide. (b) *In situ* hybridization of TRPC6 was performed with tissue sections from brain of E13 mice. They were incubated with the antisense probe (upper panel) and the sense probe (lower panel) respectively. (d) The selective TRPC6 activator was used to better characterize the OAG-induced Ca^{2+} signals. Representative Fluo-4 signals elicited in response to the application of 10 μM hyperforin and 10 μM hyperforin + 5 μM Gd^{3+}. (e) Summary graph showing the Fluo-4 responses (F/F_0) recorded for each of the above experimental condition. The number of cells tested is indicated. $^{**}p < 0.001$, Student's *t*-test.

TRPC6 was found in the cortex of E13 mice

Using standard PCR, TRPC6 transcripts of expected size (153 bp) were detected in the brain and cortex from embryonic (E13) mice as shown in Fig. 4(c). The PCR products were exemplary sequenced and revealed the expected DNA sequence. *In situ* hybridization experiments with the antisense TRPC6 cRNA probe were carried out to better describe the expression of TRPC6 mRNA. It was found throughout the cortex, both in the preplate and in the ventricular zone (Fig. 4c). Sense probes applied as controls did not show positive results.

Hyperforin triggered an entry of Ca^{2+}

Cortical neurons express TRPC6 channels and OAG activates a Ca^{2+} entry pathway exhibiting TRPC6-like properties (up-regulation by FFA). If TRPC6 channels mediate these OAG-sensitive Ca^{2+} responses, hyperforin should mimic the effect of OAG. Indeed, hyperforin, the main active principle of St John's wort extract, specifically activates TRPC6 channels without activating TRPC1, TRPC3, TRPC4 and TRPC5 channels (Leuner *et al.* 2007). Like OAG, hyperforin triggers a massive entry of Ca^{2+} blocked by Gd^{3+} (Fig. 4d and e).

Hyperforin activated a non-selective cation current

When held at a holding potential of −50 mV, the external application of hyperforin elicited an inward current that transiently increased and then declined to baseline (Fig. 5a). On average, when measured at −50 mV, the maximal amplitude of the current induced by 5 μM hyperforin was 125 ± 17 pA ($n = 14$). In HEK293 cells over-expressing TRPC6 channels (Leuner *et al.* 2007) like in cortical neurons, hyperforin triggers a transient inward current. In neurons, this current was reduced by ∼80% in the presence of 20 μM SKF-96365 ($n = 4$, $p < 0.01$) (Fig. 5a) or 10 μM Gd^{3+} ($n = 5$) (not shown). Figure 5(b) shows representative current–voltage relationships obtained before and after the addition of 5 μM hyperforin. When recorded with a caesium-rich pipette solution, this antidepressant elicited an inward

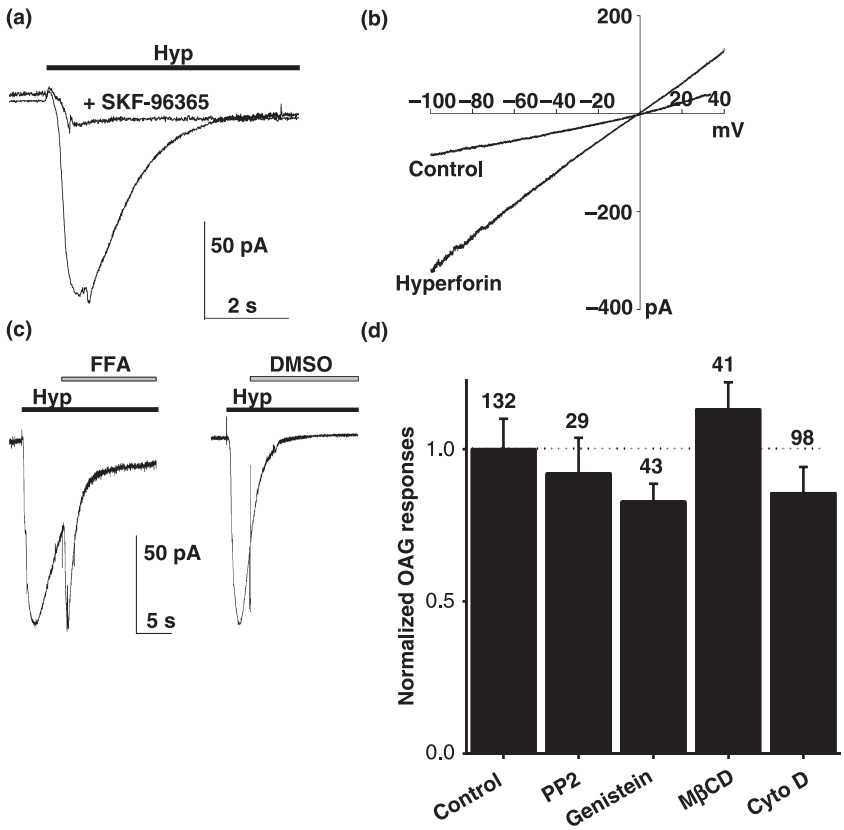

Fig. 5 Hyperforin activated SKF-96365- and FFA-sensitive cation channels. Whole-cell patch-clamp recordings were done to analyse the hyperforin-activated current. (a) Shows currents elicited from a holding potential of −50 mV. Hyperforin (5 μM) was bathed applied (horizontal black bar) either alone or in the presence of 20 μM SKF-96365. (b) Current–voltages (*I–V*) relationships. The cell was stimulated every 5 s by a 2 s ramp protocol from −100 to +40 mV applied from a holding potential of 0 mV. The *I–V* curves were obtained before and after the addition of 5 μM hyperforin. (c) Same experiments as in (a) except FFA (85 μM) or DMSO (0.1%) was added after hyperforin (5 μM). The horizontal bars indicate when hyperforin and FFA (or DMSO) were present. (d) In some experiments, cells were pre-treated with one of the following agent: PP2 (10 μM, 20 min at 20–22°C), genistein (50 μM, 20–30 min at 20–22°C), cytochalasin D (5 μM, 90 min at 37°C), methyl-β-cyclodextrin (MβCD, 10 μM, 20 min at 37 °C) before adding OAG (100 μM). (d) Shows the Ca^{2+} responses induced by OAG (normalized Fluo-4 responses). None of the agents used significantly altered the OAG-induced Ca^{2+} responses. The number of cells tested in indicated for each experimental condition.

and outward current having a reversal potential near 0 mV, indicating that hyperforin recruited non-selective cation channels. In addition, when added after hyperforin, FFA potentiated the current (n = 5/5 cells tested) (Fig. 5c). This enhancement was specific as its vehicle never affected the hyperforin-activated current (n = 5 cells tested). Thus, hyperforin activated SKF-96365- and Gd^{3+}-sensitive cation channels that were positively regulated by FFA.

Properties of the OAG-sensitive channels

The characterization of these cation channels was further investigated by comparing their properties to those of TRPC6 channels (Dietrich and Gudermann 2007). The activity of TRPC6 channels is under the control of PP2-sensitive src protein tyrosine kinases (Hisatsune *et al.* 2004; Aires *et al.* 2006). For instance, treating HEK293 cells over-expressing TRPC6 channels with the tyrosine kinase inhibitor PP2 attenuates the DAG-activated Ca^{2+} entry (Aires *et al.* 2006). It is however worth adding that TRPC6 channels over-expressed in HEK293 cells are insensitive to genistein, another tyrosine kinase inhibitor (Kawasaki *et al.* 2006). Cortical cells were incubated with PP2 (n = 29 cells) or genistein (n = 43) before adding OAG. Neither of these tyrosine kinase inhibitors affected the OAG-induced Ca^{2+} responses (Fig. 5d). Several studies have highlighted the importance of caveolae in Ca^{2+} homeostasis (Isshiki and Anderson 2003). The entry of Ca^{2+} through TRPC6 channels over-expressed in HEK293 cells is regulated by an exocytotic mechanism with TRPC6 channels present in caveolae-related microdomains (Cayouette *et al.* 2004). The application of OAG promotes the insertion of TRPC6 channels into the plasma membrane (Cayouette *et al.*

2004). Treating HEK293 cells over-expressing TRPC6 channels with MβCD, which disrupts lipid rafts, causes a complete suppression of the DAG-activated Ca^{2+} entry (Aires *et al.* 2006). Similar experiments were conducted with cortical neurons. MβCD did not affect the OAG-induced Ca^{2+} responses (n = 98 cells) (Fig. 5d). In another series of experiments, we verified whether the OAG-induced Ca^{2+} responses were controlled by an actin-dependent trafficking step. Cortical neurons were treated with cytochalasin D, a membrane-permeant inhibitor of actin polymerization. Here again, the OAG-induced Ca^{2+} responses were unaffected by cytochalasin D (n = 41 cells) (Fig. 5d). In a final set of experiments, cells were stimulated with one of the following neurotransmitter receptor agonists to gain further insight into the physiological relevance of these OAG-induced Ca^{2+} responses: bethanechol (10–100 μM, n = 50 cells), α-methyl-5-hydroxytryptamine (10 μM, n = 47 cells), phenylephrine (10 μM, n = 63 cells) and histamine (10 μM, n = 52 cells). These agonists recruit, respectively, muscarinic acetylcholine, serotonin 5-HT_2, α_1-adrenergic, and histamine receptors and promote the production of DAG. None of these agonists tested induced Ca^{2+} responses (not shown). Although the identity of the signalling pathway controlling the DAG-activated cationic channels remains unclear, this report clearly shows the existence of functional second messenger-operated cationic channels in cortical neurons from E13 mouse embryos.

Discussion

By performing Ca^{2+} imaging and electrophysiological experiments we have shown that in cortical cells from E13 mouse embryos OAG (or SAG) and hyperforin activate plasma membrane cation channels. These OAG-induced Ca^{2+} responses were observed in KCl-responsive and in KCl-unresponsive cells. This latter cell population, considered as non-neuronal cells, was not further analysed as recent studies already demonstrated that OAG triggers an entry of Ca^{2+} in cortical astrocytes. It develops via TRPC3 channels in cortical astrocytes prepared from E17 rat embryos (Grimaldi *et al.* 2003) and via TRPC6 channels in cortical astrocytes prepared from E17 mouse embryos (Beskina *et al.* 2007). In addition, an OAG-induced Ca^{2+} entry is found in neural stem cells prepared from E13 rat embryos (Pla *et al.* 2005). Thus, our data, showing a OAG-induced Ca^{2+} entry in KCl-unresponsive cells (e.g. cell 2 in Fig. 1) is in line with reports describing OAG-induced Ca^{2+} signals in non-neuronal cortical cells (Grimaldi *et al.* 2003; Beskina *et al.* 2007). Therefore, we focused our analysis on the KCl-responsive cells. To our knowledge, this is the first report showing second messenger-operated channels in cortical neurons.

Nearly 35% of the KCl-responsive cells responded to OAG. In most cases, OAG induced Ca^{2+} oscillations even in cells treated with caffeine to deplete the caffeine-sensitive Ca^{2+} pool of the endoplasmic reticulum (not shown). The OAG-induced Ca^{2+} signals, seen in freshly dissociated cells as well as in cultured isolated cells kept up to six DIV, disappeared when Ca^{2+} was omitted from the extracellular milieu. The entry of Ca^{2+} could be triggered by OAG, SAG or in the presence of the DAG lipase inhibitor RHC80267. This Ca^{2+} route was unaffected by the voltage-gated Ca^{2+} channel antagonists nifedipine and ω-CTx but it was strongly blocked by Gd^{3+} and SKF-96365. Replacing Na^+ ions with $NMDG^+$ did not suppress but attenuated the OAG-induced Ca^{2+} rise. Analysis of cytosolic Na^+ changes with the fluorescent Na^+ indicator CoroNa Green revealed that OAG caused an entry of Na^+. A similar observation was made in vascular smooth muscle cells (Poburko *et al.* 2007). Based on these findings it is proposed that DAG controls the activity of SKF-96365-sensitive channels allowing a Ca^{2+} entry via Na^+-dependent and Na^+-independent mechanisms. As the cytosolic Ca^{2+} rise partially depends on the extracellular concentration of Na^+, OAG controls the activity of Na^+- and Ca^{2+}-conducting channels. The intracellular load of Na^+ thus activates the Na^+/Ca^{2+} exchanger which, in turn, permits an entry of Ca^{2+} (Platel *et al.* 2005). This DAG-induced Ca^{2+} entry was blocked by Gd^{3+}. However, the broad spectrum Ca^{2+} channel antagonist Gd^{3+} also inhibits the Na^+/Ca^{2+} exchanger (Zhang and Hancox 2000) and the OAG-induced elevation of Na^+. PKC, a major downstream DAG effector, can increase the cytosolic concentration of Ca^{2+} in some cell types (Albert *et al.* 1987; Khoyi *et al.* 1999; Murthy *et al.* 2000; Rosado and Sage 2000; Albert and Large 2002). In contrast to OAG or SAG, the PKC activator PMA failed to trigger any Ca^{2+} response. Furthermore, stimulating or inhibiting PKC activity had no effect on the DAG-induced Ca^{2+} entry. Taken together, these results favour the existence of cation channels activated by DAG in a PKC-independent manner.

TRPC are Gd^{3+}- or SKF-96365-sensitive plasma membrane proteins forming voltage-independent cation channels. Some isoforms constitute DAG-sensitive Ca^{2+}-conducting channels. When heterogeneously expressed, homomeric TRPC3, TRPC6 or TRPC7 channels and heteromeric TRPC1–TRPC3, TRPC3–TRPC4 channels function as DAG-sensitive Ca^{2+}-conducting channels (Hofmann *et al.* 1999; Lintschinger *et al.* 2000; Liu *et al.* 2005; Poteser *et al.* 2006). Such DAG-sensitive channels have been described in the neuronal cell lines PC12 and IMR-32 (Mwanjewe and Grover 2004; Nasman *et al.* 2006) as well as in neural cells like cortical astrocytes (Grimaldi *et al.* 2003; Beskina *et al.* 2007), vomeronasal neurons (Lucas *et al.* 2003), hippocampal neurons (Tai *et al.* 2008) and neural stem cells (Pla *et al.* 2005). TRPC3 (in rats) (Grimaldi *et al.* 2003) or TRPC6 channels (in mice) (Beskina *et al.* 2007) participate in the DAG-induced cytosolic Ca^{2+} changes in astrocytes but the Ca^{2+} entry occurs through TRPC2 channels in vomeronasal

neurons (Lucas *et al.* 2003) and through TRPC6 channels in hippocampal neurons (Tai *et al.* 2008). Based on these findings, we suggest that TRPC channels or channels exhibiting TRPC-like properties are involved in the DAG-dependent Ca^{2+} entry of cortical neurons. Among the various TRPC isoforms described so far, only currents through TRPC6 channels are increased by FFA. This anti-inflammatory drug is a potent blocker of anion and cation channels including TRPC (Inoue *et al.* 2001). But heterogeneously expressed TRPC6 channels (in HEK cells) and native TRPC6 channels (in vascular smooth muscle cells) are up-regulated by FFA (Inoue *et al.* 2001; Jung *et al.* 2002). In smooth muscle cells, FFA inhibits native Ca^{2+}-conducting channels having TRPC3- and TRPC7-like properties with an IC_{50} value of 2.45 μM (Peppiatt-Wildman *et al.* 2007) but increases currents through native TRPC6-like channels (Hill *et al.* 2006). On the other hand, based on their electrophysiological and pharmacological studies, Carter *et al.* (2006) concluded that TRPC6 was involved in the ADP-dependent cation influx of murine megakaryocytes (Carter *et al.* 2006). Interestingly, this response was strongly enhanced by FFA (Carter *et al.* 2006). Therefore, TRPC6 (Inoue *et al.* 2001; Jung *et al.* 2002) and TRPC6-like channels (Carter *et al.* 2006; Hill *et al.* 2006) appear as the only TRPC channels up-regulated by FFA. In E13 cortical neurons, the OAG-induced Ca^{2+} entry was enhanced by FFA. Furthermore, hyperforin which selectively activates TRPC6 channels without activating TRPC1, TRPC3, TRPC4 and TRPC5 (Leuner *et al.* 2007) mimics the action of OAG. Electrophysiological measurements showed that this antidepressant activated non-selective cation channels blocked by Gd^{3+} (not shown) and SKF-96365. This in line with a recent study showing that hyperforin selectively activates non-selective cation TRPC6 channels (Leuner *et al.* 2007). In addition, hyperforin-activated currents were increased by FFA.

On the other hand, if the DAG-sensitive channels of cortical neurons exhibit TRPC6-like characteristics, they however display properties that are not found in other cells expressing TRPC6 channels. For instance, in HEK cells over-expressing TRPC6 channels, disruption of lipids rafts abolishes Ca^{2+} entry through TRPC6 channels (Aires *et al.* 2006) whereas the same treatment has no effect in cortical neurons. It is however possible that native and over-expressed TRPC6 channels exhibit distinct properties as already shown for TRPC3 where the mode of regulation of this TRPC isoform critically depends on its level of expression (Putney 2004). Another property of the DAG-sensitive channels of cortical neurons is their insensitivity to the tyrosine kinase inhibitors PP2 and genistein. Indeed, the src tyrosine kinase inhibitor PP2 abolishes endogenous TRPC6-dependent Ca^{2+} entry in cardiac myocytes (Nishida *et al.* 2007) and in HEK cells over-expressing TRPC6 channels (Aires *et al.* 2006) but has no effect on cortical neurons. Of note, Kawasaki *et al.* (2006) also reported that TRPC6 channels were unaffected by the tyrosine kinase inhibitor genistein.

Although the molecular identity of the DAG-sensitive channels of cortical neurons is not firmly established we exclude TRPC3 as the main candidate. This is based on the experiments carried out with PMA and showing that, after a PMA treatment, OAG was still able to promote an entry of Ca^{2+}. Indeed, PKC activation totally blocks TRPC3 in response to OAG (Trebak *et al.* 2003; Venkatachalam *et al.* 2003; Kwan *et al.* 2006). A key issue concerns the characterization of the physiological activator(s) of these channels. None of the neurotransmitter receptor agonist tested (bethanechol, α-methyl-5-hydroxytryptamine, phenylephrine and histamine) had an effect. Although a clear understanding of the signalling pathway controlling the DAG-activated cation channels remains unclear as well as their exact molecular identity, we provide experimental evidence for the existence of functional second messenger-operated cationic channels in cortical neurons from E13 mouse embryos. Inositol 1,4,5-trisphosphate and DAG are second messengers playing important roles in cell signalling. Inositol 1,4,5-trisphosphate links cell surface receptors and Ca^{2+} signalling whereas DAG is the physiological activator of protein kinase C and thus controls protein phosphorylation. This latter process is regarded as one of the most important molecular mechanisms by which extracellular signals produce their biological responses (Walaas and Greengard 1991). As already shown, DAG also regulates in a PKC independent manner the activity of some plasma membrane ion channels (Hofmann *et al.* 1999; Lintschinger *et al.* 2000; Poteser *et al.* 2006). By controlling the activity of various ion channels and the phosphorylation of a plethora of proteins, DAG is as a second messenger with a widespread biological importance.

Acknowledgements

We wish to thank D. Poburko for helpful comments and suggestions on a previous version of this work. We also wish to thank Dr Willmar Schwabe (Karlsruhe, Germany) for the kind gift of hyperforin. This study was supported by a grant from l'Agence Nationale de la Recherche (ANR-2006-SEST).

References

Aires V., Hichami A., Boulay G. and Khan N. A. (2006) Activation of TRPC6 calcium channels by diacylglycerol (DAG)-containing arachidonic acid: a comparative study with DAG-containing docosahexaenoic acid. *Biochimie* **89**, 926–937.

Albert A. P. and Large W. A. (2002) Activation of store-operated channels by noradrenaline via protein kinase C in rabbit portal vein myocytes. *J. Physiol.* **544**, 113–125.

Albert P. R., Wolfson G. and Tashjian A. H. Jr (1987) Diacylglycerol increases cytosolic free Ca^{2+} concentration in rat pituitary cells. Relationship to thyrotropin-releasing hormone action. *J. Biol. Chem.* **262**, 6577–6581.

Beskina O., Miller A., Mazzocco-Spezzia A., Pulina M. V. and Golovina V. A. (2007) Mechanisms of interleukin-1beta-induced Ca^{2+} signals in mouse cortical astrocytes: roles of store- and receptor-operated Ca^{2+} entry. *Am. J. Physiol. Cell Physiol.* **293**, C1103–C1111.

Bouron A., Altafaj X., Boisseau S. and De Waard M. (2005) A store-operated Ca^{2+} influx activated in response to the depletion of thapsigargin-sensitive Ca^{2+} stores is developmentally regulated in embryonic cortical neurons from mice. *Brain Res. Dev. Brain Res.* **159**, 64–71.

Bouron A., Boisseau S., De Waard M. and Peris L. (2006) Differential down-regulation of voltage-gated calcium channel currents by glutamate and BDNF in embryonic cortical neurons. *Eur. J. Neurosci.* **24**, 699–708.

Brose N., Betz A. and Wegmeyer H. (2004) Divergent and convergent signaling by the diacylglycerol second messenger pathway in mammals. *Curr. Opin. Neurobiol.* **14**, 328–340.

Carrasco S. and Merida I. (2007) Diacylglycerol, when simplicity becomes complex. *Trends Biochem. Sci.* **32**, 27–36.

Carter R. N., Tolhurst G., Walmsley G., Vizuete-Forster M., Miller N. and Mahaut-Smith M. P. (2006) Molecular and electrophysiological characterization of transient receptor potential ion channels in the primary murine megakaryocyte. *J. Physiol.* **576**, 151–162.

Cayouette S., Lussier M. P., Mathieu E.-L., Bousquet S. M. and Boulay G. (2004) Exocytotic insertion of TRPC6 channel into the plasma membrane upon Gq protein-coupled receptor activation. *J. Biol. Chem.* **279**, 7241–7246.

Cruickshank S. F., Baxter L. M. and Drummond R. M. (2003) The Cl(−) channel blocker niflumic acid releases Ca(2+) from an intracellular store in rat pulmonary artery smooth muscle cells. *Br. J. Pharmacol.* **140**, 1442–1450.

Dietrich A. and Gudermann T. (2007) Trpc6. *Handb. Exp. Pharmacol.* **179**, 125–141.

Grimaldi M., Maratos M. and Verma A. (2003) Transient receptor potential channel activation causes a novel form of $[Ca^{2+}]i$ oscillations and is not involved in capacitative Ca^{2+} entry in glial cells. *J. Neurosci.* **23**, 4737–4745.

Hamill O. P., Marty A., Neher E., Sakmann B. and Sigworth F. J. (1981) Improved patch-clamp techniques for high-resolution current recording from cells and cell-free membrane patches. *Pflugers Arch.* **391**, 85–100.

Hill A. J., Hinton J. M., Cheng H., Gao Z., Bates D. O., Hancox J. C., Langton P. D. and James A. F. (2006) A TRPC-like non-selective cation current activated by alpha 1-adrenoceptors in rat mesenteric artery smooth muscle cells. *Cell Calcium* **40**, 29–40.

Hisatsune C., Kuroda Y., Nakamura K., Inoue T., Nakamura T., Michikawa T., Mizutani A. and Mikoshiba K. (2004) Regulation of TRPC6 channel activity by tyrosine phosphorylation. *J. Biol. Chem.* **279**, 18887–18894.

Hofmann T., Obukhov A. G., Schaefer M., Harteneck C., Gudermann T. and Schultz G. (1999) Direct activation of human TRPC6 and TRPC3 channels by diacylglycerol. *Nature* **397**, 259–263.

Inoue R., Okada T., Onoue H., Hara Y., Shimizu S., Naitoh S., Ito Y. and Mori Y. (2001) The transient receptor potential protein homologue TRP6 is the essential component of vascular α1-adrenoceptor-activated Ca^{2+}-permeable cation channel. *Circ. Res.* **88**, 325–332.

Isshiki M. and Anderson R. G. (2003) Function of caveolae in Ca^{2+} entry and Ca^{2+}-dependent signal transduction. *Traffic* **4**, 717–723.

Jung S., Strotmann R., Schultz G. and Plant T. D. (2002) TRPC6 is a candidate channel involved in receptor-stimulated cation currents in A7r5 smooth muscle cells. *Am. J. Physiol. Cell Physiol.* **282**, C347–C359.

Kawasaki B. T., Liao Y. and Birnbaumer L. (2006) Role of Src in C3 transient receptor potential channel function and evidence for a heterogeneous makeup of receptor- and store-operated Ca^{2+} entry channels. *Proc. Natl Acad. Sci. USA* **103**, 335–340.

Khoyi M. A., Gregory L. G., Smith A. D., Keef K. D. and Westfall D. P. (1999) An unusual Ca(2+) entry pathway activated by protein kinase C in dog splenic artery. *J. Pharmacol. Exp. Ther.* **291**, 823–828.

Kriegstein A. R. and Noctor S. C. (2004) Patterns of neuronal migration in the embryonic cortex. *Trends Neurosci.* **27**, 392–399.

Kunert-Keil C., Bisping F., Kruger J. and Brinkmeier H. (2006) Tissue-specific expression of TRP channel genes in the mouse and its variation in three different mouse strains. *BMC Genomics* **7**, 159.

Kwan H. Y., Huang Y. and Yao X. (2006) Protein kinase C can inhibit TRPC3 channels indirectly via stimulating protein kinase G. *J. Cell. Physiol.* **207**, 315–321.

Lee R. J., Shaw T., Sandquist M. and Partridge L. D. (1996) Mechanism of action of the non-steroidal anti-inflammatory drug flufenamate on $[Ca^{2+}]i$ and Ca(2+)-activated currents in neurons. *Cell Calcium* **19**, 431–438.

Lemos V. S., Poburko D., Liao C. H., Cole W. C. and van Breemen C. (2007) Na^{+} entry via TRPC6 causes Ca^{2+} entry via NCX reversal in ATP stimulated smooth muscle cells. *Biochem. Biophys. Res. Commun.* **352**, 130–134.

Leuner K., Kazanski V., Muller M., Essin K., Henke B., Gollasch M., Harteneck C. and Muller W. E. (2007) Hyperforin – a key constituent of St. John's wort specifically activates TRPC6 channels. *FASEB J.* **21**, 4101–4111.

Lintschinger B., Balzer-Geldsetzer M., Baskaran T., Graier W. F., Romanin C., Zhu M. X. and Groschner K. (2000) Coassembly of Trp1 and Trp3 proteins generates diacylglycerol- and Ca^{2+}-sensitive cation channels. *J. Biol. Chem.* **275**, 27799–27805.

Liu X., Bandyopadhyay B. C., Singh B. B., Groschner K. and Ambudkar I. S. (2005) Molecular analysis of a store-operated and 2-acetyl-sn-glycerol-sensitive non-selective cation channel. Heteromeric assembly of TRPC1–TRPC3. *J. Biol. Chem.* **280**, 21600–21606.

Lucas P., Ukhanov K., Leinders-Zufall T. and Zufall F. (2003) A diacylglycerol-gated cation channel in vomeronasal neuron dendrites is impaired in TRPC2 mutant mice: mechanism of pheromone transduction. *Neuron* **40**, 551–561.

Murthy K. S., Yee Y. S., Grider J. R. and Makhlouf G. M. (2000) Phorbol-stimulated Ca(2+) mobilization and contraction in dispersed intestinal smooth muscle cells. *J. Pharmacol. Exp. Ther.* **294**, 991–996.

Mwanjewe J. and Grover A. K. (2004) Role of transient receptor potential canonical 6 (TRPC6) in non-transferrin-bound iron uptake in neuronal phenotype PC12 cells. *Biochem. J.* **378**, 975–982.

Nasman J., Bart G., Larsson K., Louhivuori L., Peltonen H. and Akerman K. E. (2006) The orexin OX1 receptor regulates Ca^{2+} entry via diacylglycerol-activated channels in differentiated neuroblastoma cells. *J. Neurosci.* **26**, 10658–10666.

Nishida M., Onohara N., Sato Y., Suda R., Ogushi M., Tanabe S., Inoue R., Mori Y. and Kurose H. (2007) Galpha12/13-mediated up-regulation of TRPC6 negatively regulates endothelin-1-induced cardiac myofibroblast formation and collagen synthesis through nuclear factor of activated T cells activation. *J. Biol. Chem.* **282**, 23117–23128.

Peppiatt-Wildman C. M., Albert A. P., Saleh S. N. and Large W. A. (2007) Endothelin-1 activates a Ca^{2+}-permeable cation channel with TRPC3 and TRPC7 properties in rabbit coronary artery myocytes. *J. Physiol.* **580**, 755–764.

Pla A. F., Maric D., Brazer S. C., Giacobini P., Liu X., Chang Y. H., Ambudkar I. S. and Barker J. L. (2005) Canonical transient receptor potential 1 plays a role in basic fibroblast growth factor (bFGF)/FGF receptor-1-induced Ca^{2+} entry and embryonic rat neural stem cell proliferation. *J. Neurosci.* **25**, 2687–2701.

Platel J. C., Boisseau S., Dupuis A., Brocard J., Poupard A., Savasta M., Villaz M. and Albrieux M. (2005) Na^+ channel-mediated Ca^{2+} entry leads to glutamate secretion in mouse neocortical preplate. *Proc. Natl Acad. Sci. USA* **102**, 19174–19179.

Poburko D., Liao C. H., Lemos V. S., Lin E., Maruyama Y., Cole W. C. and van Breemen C. (2007) Transient receptor potential channel 6-mediated, localized cytosolic [Na+] transients drive Na^+/Ca^{2+} exchanger-mediated Ca^{2+} entry in purinergically stimulated aorta smooth muscle cells. *Circ. Res.* **101**, 1030–1038.

Poronnik P., Ward M. C. and Cook D. I. (1992) Intracellular Ca^{2+} release by flufenamic acid and other blockers of the non-selective cation channel. *FEBS Lett.* **296**, 245–248.

Poteser M., Graziani A., Rosker C., Eder P., Derler I., Kahr H., Zhu M. X., Romanin C. and Groschner K. (2006) TRPC3 and TRPC4 associate to form a redox-sensitive cation channel. Evidence for expression of native TRPC3–TRPC4 heteromeric channels in endothelial cells. *J. Biol. Chem.* **281**, 13588–13595.

Putney J. W. Jr (2004) The enigmatic TRPCs: multifunctional cation channels. *Trends Cell Biol.* **14**, 282–286.

Rosado J. A. and Sage S. O. (2000) Protein kinase C activates non-capacitative calcium entry in human platelets. *J. Physiol.* **529**, 159–169.

Syyong H. T., Poburko D., Fameli N. and van Breemen C. (2007) ATP promotes NCX-reversal in aortic smooth muscle cells by DAG-activated Na^+ entry. *Biochem. Biophys. Res. Commun.* **357**, 1177–1182.

Tai Y., Feng S., Ge R., Du W., Zhang X., He Z. and Wang Y. (2008) TRPC6 channels promote dendritic growth via the CaMKIV–CREB pathway. *J. Cell Sci.* **121**, 2301–2307.

Trebak M., Vazquez G., Bird G. S. and Putney J. W. Jr (2003) The TRPC3/6/7 subfamily of cation channels. *Cell Calcium* **33**, 451–461.

Venkatachalam K., Zheng F. and Gill D. L. (2003) Regulation of canonical transient receptor potential (TRPC) channel function by diacylglycerol and protein kinase C. *J. Biol. Chem.* **278**, 29031–29040.

Walaas S. I. and Greengard P. (1991) Protein phosphorylation and neuronal function. *Pharmacol. Rev.* **43**, 299–349.

Yamaguchi D., Green J., Kleeman C. and Muallem S. (1989) Properties of the depolarization-activated calcium and barium entry in osteoblast-like cells. *J. Biol. Chem.* **264**, 197–204.

Zhang Y. H. and Hancox J. C. (2000) Gadolinium inhibits Na(+)–Ca(2+) exchanger current in guinea-pig isolated ventricular myocytes. *Br. J. Pharmacol.* **130**, 485–488.

8.3 Unpublished results

8.3.1 Cortical cells of E13 mice express TRPC6

Western blot experiments showed the expression of TRPC6 proteins in cultured cortical neurons from E13 mice (Figure 8-1). HEK and HEK-TRPC6 cells were used as negative and positive controls, respectively. Both HEK-TRPC6 cells and cortical neurons showed bands corresponding to TRPC6 (~100 kDa). A weak TRPC6 expression was found in HEK cells which is in agreement with previous reports showing the presence of endogenous TRPC channels (including TRPC6) in HEK cells (Garcia and Schilling, 1997; Wu et al., 2000; Zagranichnaya et al., 2005).

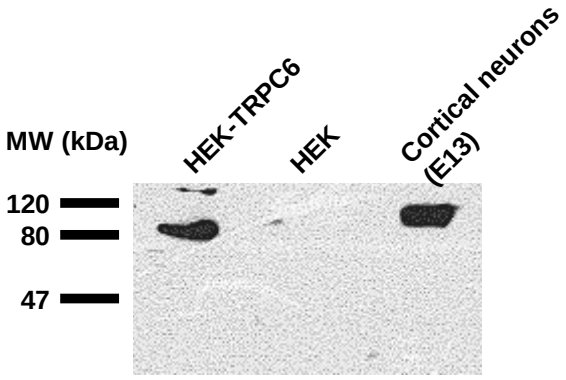

Figure 8-1 TRPC6 was found in cortical neurons

Expression of TRPC6 was analyzed by western blot in HEK cells, HEK-TRPC6 cells and E13 cortical neurons. Both HEK-TRPC6 cells and cortical neurons show bands corresponding to TRPC6 (~100 kDa). A weak TRPC6 expression is found in HEK cells.

8.3.2 OAG evokes Ca^{2+} responses regardless of the age of the cells

Calcium imaging experiments with Fluo-4 were carried out on freshly dissociated cortical cells as well as on cells kept 1, 2, 4, 5 and 6 days *in vitro* (DIV). OAG evoked Ca^{2+} responses regardless of the age of the cells, and these Ca^{2+} responses had roughly the same amplitude (Figure 8-2).

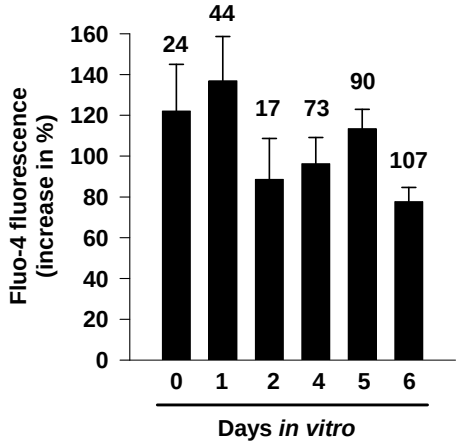

Figure 8-2 OAG evoked Ca^{2+} responses regardless of the age of neurons

OAG-induced Fluo-4 responses were observed in both freshly dissociated neurons (0 DIV) and neurons kept 1, 2, 4, 5 and 6 DIV. The maximal amplitude of the Fluo-4 response recorded during the application of OAG (100 μM) was measured for each cell. The number of neurons tested is indicated above each bar.

8.3.3 Cortical neurons display OAG- and RHC80267-induced Ca^{2+} responses

An acute application of RHC80267 (50 µM) at 20-22°C weakly increased $[Ca^{2+}]_i$. Such treatment was probably not efficient enough to significantly elevate the intracellular concentration of DAG. Therefore, experiments were performed after a longer RHC80267 treatment (50 µM, 20 minutes) at 37°C. Cells were kept in a Ca^{2+}-free medium. A subsequent admission of Ca^{2+} was accompanied by large Fluo-4 signals (see article 1, Section 8.2, Fig. 3(b), open circles). Similar experiments were conducted on RHC80267-untreated cells: the Ca^{2+} challenge was followed by much smaller Fluo-4 signals, which reflect most likely an entry of Ca^{2+} through SOC (see article 1, Section 8.2, Fig. 3(b), filled circles). The averaged maximal amplitudes of the Fluo-4 responses are shown in Figure 8-3. Interestingly, 35% of the neurons (59 out of 169) treated with RHC80267 produced large Fluo-4 signals after the readmission of Ca^{2+}, whereas 65% of them poorly responded to this protocol and presented Fluo-4 signals similar to those seen in RHC80267-untreated neurons. It is worth mentioning that this percentage of RHC80267-responsive neurons (35%) is similar to the percentage of OAG-sensitive neurons (see article 1, Section 8.2, Results section, part 'OAG evoked Ca^{2+} responses').

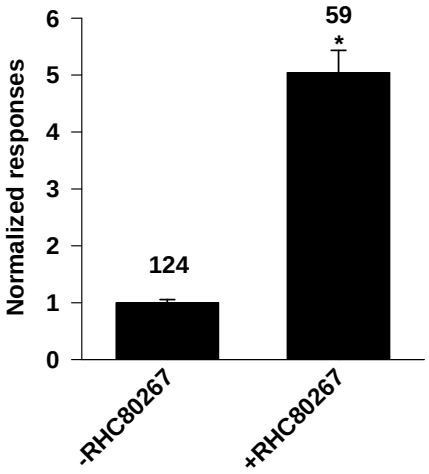

Figure 8-3 Treatment of cortical neurons with RHC80267 for 20 minutes at 37°C elicited a large Ca^{2+} signal on Ca^{2+} readmission

Fluo-4-loaded cells were kept in a Ca^{2+}-free medium supplemented with 0.4 mM EGTA in the absence or presence of 50 µM RHC80276 for 20 minutes at 37°C. They were then placed on the stage of the microscope and Fluo-4 signals were recorded (at 20-22 °C). The re-introduction of 2 mM external Ca^{2+} was accompanied by an increase of the Fluo-4 fluorescence. The maximal amplitudes (normalized data) of these Fluo-4 responses are shown. The number of neurons tested is indicated above each bar. * $p < 0.001$ (Student's t-test).

8.3.4 Properties of TRPC6 channels in HEK-TRPC6 cells

In HEK-TRPC6 cells, the addition of OAG (100 µM) evoked an entry of Ca^{2+}. These Ca^{2+} responses were asynchronous and displayed diverse kinetic patterns (transient or oscillatory Fluo-4 responses, Figure 8-4A). The OAG-induced Fluo-4 signals were not seen in the absence of extracellular Ca^{2+} or in HEK cells (results not shown). FFA was then used to verify whether this anti-inflammatory agent known to increase the amplitude of the currents through TRPC6 channels (Inoue et al., 2001) could enhance the OAG-induced Ca^{2+} entry in HEK-TRPC6 cells. Similarly to neurons (article 1, Fig. 4), FFA (85 µM) alone gave rise to a Fluo-4 response and the fluorescence augmented by 17% in HEK-TRPC6 cells (Figure 8-4A). This modest but long-lasting elevation of $[Ca^{2+}]_i$ was independent of $[Ca^{2+}]_o$, indicating that FFA promoted the release of Ca^{2+} from internal stores (see Chapter 10). It is worth mentioning that these FFA-induced Ca^{2+} responses were also present in HEK cells (results not shown). When OAG (100 µM) and FFA (85 µM) were added together, larger Fluo-4 responses were recorded (Figure 8-4A). Figure 8-4B shows that in the presence of OAG + FFA, the Fluo-4 signals were larger than the sum of the two signals (OAG-induced Fluo-4 signals + FFA-induced signals). This is in agreement with the data obtained on cortical neurons. Of note, the Fluo-4 signals elicited by OAG + FFA were synchronous and long-lasting (Figure 8-4A). This is clearly different from the Fluo-4 signals recorded without FFA (which are mainly oscillatory). Another way to analyze the data is to measure for each cell the area under the curve (Figure 8-4C). The results obtained clearly confirm that FFA enhances the OAG-sensitive Ca^{2+} responses (Figure 8-4D). In Chapter 10, we show that FFA alters the mitochondrial Ca^{2+} homeostasis. We suggest that these distinct Fluo-4 responses (long-lasting versus oscillatory) reflect the ability of mitochondria to buffer the entry of Ca^{2+} through DAG-sensitive channels (see Chapter 10 for further details).

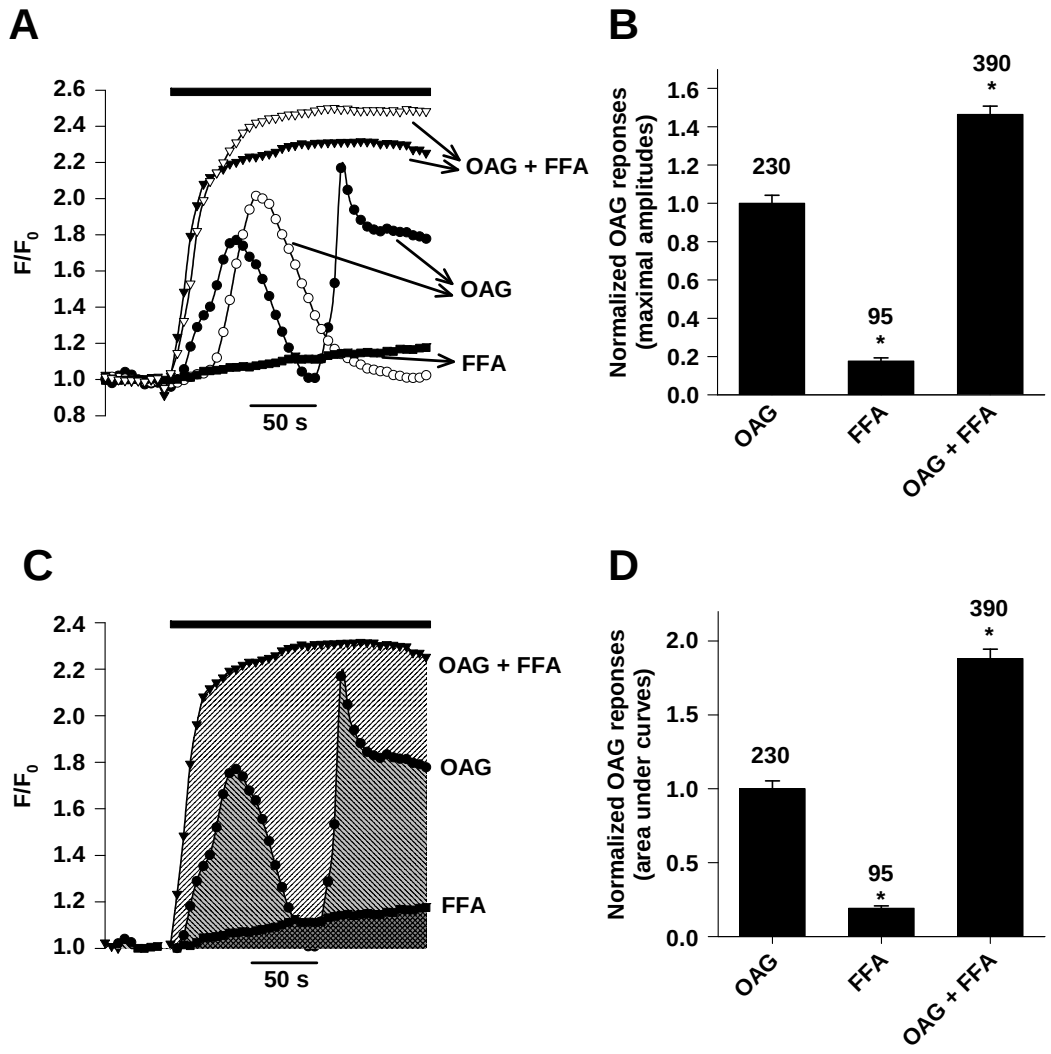

Figure 8-4 FFA increased the OAG-dependent Fluo-4 responses in HEK-TRPC6 cells

Panel A shows representative Fluo-4 responses from HEK-TRPC6 cells stimulated with OAG (100 μM) (● and ○), OAG (100 μM) + FFA (85 μM) (▼ and ▽) or FFA (85 μM) alone (◆). The horizontal black bar indicates when OAG, OAG + FFA or FFA was added in the bath. Panel B shows the maximal amplitudes (normalized data) of the Fluo-4 signals under various experimental conditions. Panel C shows the area under the curve for each cell. Panel D is a summary graph showing the area under the curves (normalized data). In these experiments, only the first 250 s of the recordings were analyzed. The number of cells tested is indicated above each bar. * $p < 0.001$ (Student's t-test).

8.4 Discussion

Calcium imaging and electrophysiological experiments show the existence of DAG (OAG or SAG)- and hyperforin-sensitive plasma membrane cation channels in cortical neurons. These channels are permeable to Ca^{2+}, Na^{+}, Ba^{2+} and Mn^{2+}. The Ca^{2+} entry is controlled by extracellular Na^{+}-independent and Na^{+}-dependent mechanisms. The latter one implies most likely the NCX. OAG-sensitive responses are blocked by Gd^{3+} and SKF-96365

but potentiated by FFA. The entry of Ca^{2+} can also be elicited by the DAG lipase inhibitor RHC80267. However, the OAG-induced responses are not affected by either PKC activation or inhibition. Although the exact molecular identity of these DAG-sensitive channels has not yet been established, we suggest that TRPC6 form the DAG-sensitive channels in E13 cortical neurons. Indeed, the DAG responses are mimicked by hyperforin, an activator of TRPC6 channels (Leuner et al., 2007). Furthermore, TRPC6 channels are the only TRPC channels of which activity is up-regulated by FFA (Inoue et al., 2001). RT-PCR, *in situ* hybridization and western blot experiments confirm the expression of TRPC6 in E13 cortex. Altogether, these data strongly support the idea that TRPC6 channels mediate the DAG-sensitive responses of cortical neurons.

FFA upregulates the OAG-induced Ca^{2+} entry in both cortical neurons and HEK-TRPC6 cells

FFA was used to characterize the DAG-activated cation channels. This non-specific anion and cation channel blocker has the property to enhance the amplitude of currents through TRPC6 channels (Inoue et al., 2001). It is a convenient pharmacological tool to characterize endogenous or heterogeneously expressed TRPC6 channels (Jung et al., 2002; Carter et al., 2006; Hill et al., 2006; Saleh et al., 2006; Fellner and Arendshorst, 2008; Foster et al., 2009). The OAG-induced Ca^{2+} entry is enhanced by FFA in both cortical neurons and HEK-TRPC6 cells. In electrophysiological experiments on cortical neurons, the current activated by hyperforin is potentiated by FFA. But, as already mentioned, during the time course of this study we noticed that FFA alone is able to increase $[Ca^{2+}]_i$. This latter result is the topic of the article 2 and will be discussed in Chapter 10.

Hyperforin activates non-selective cation channels in cortical neurons

Hyperforin was used to examine whether TRPC6 channels mediate the OAG-activated Ca^{2+} entry in cortical neurons. Calcium imaging experiments reveal that hyperforin triggers an entry of Ca^{2+} that is partially blocked by Gd^{3+}. Electrophysiological experiments show that hyperforin activates a non-selective cation current of which amplitude is strongly reduced in the presence of SKF-96365 but potentiated in the presence of FFA. Interestingly, the Ca^{2+} responses controlled by hyperforin and OAG exhibit distinct kinetic patterns. The OAG-activated Fluo-4 responses are asynchronous and either transient, oscillatory, or long-lasting. On the other hand, the hyperforin-activated Fluo-4 responses are synchronous (all the cells respond and all at the same time) characterized by a biphasic signal with a large transient peak

accompanied by a plateau-like phase of smaller amplitude. In fact, the transient peak reflects an entry of Ca^{2+}, whereas the plateau-like phase is insensitive to $[Ca^{2+}]_o$ and unaffected by the channel blocker Gd^{3+}. These latter observations are summarized in the article 3 and discussed in details in Chapter 11.

Perspectives

Pyr3, a pyrazole compound, has a selective inhibitory action on both recombinant and native TRPC3 channels without blocking the other TRPC isoforms (Kiyonaka et al., 2009). We have tested this TRPC3 blocker on cortical neurons. It fails to affect the OAG-sensitive Fluo-4 responses (unpublished data) further indicating that TRPC6 may mediate this entry of cations.

Besides pharmacological approaches, knocking out/down the expression of TRPC6 is another strategy that could be used to study the functions of TRPC6 channels. TRPC6-deficient ($TRPC6^{-/-}$) mice (Dietrich et al., 2005b) and transgenic mice overexpressing TRPC6 (Zhou et al., 2008) have been generated. They could be useful for the molecular identification of the OAG-sensitive channels of cortical neurons. It is however important to keep in mind that in $TRPC6^{-/-}$ mice, there is an up-regulation of TRPC3 (Dietrich et al., 2005b). This compensatory mechanism highlights the difficulty in identifying the physiological roles of a given TRPC. Of note, $TRPC6^{-/-}$ mice are viable and have no sign of neurologic dysfunction.

TRPC6 RNA interference (RNAi) can be achieved in cultured cells without significant compensation by other TRPC (Soboloff et al., 2005). However, after knocking down the expression of TRPC6, the DAG-induced non-selective cation current is effectively reduced (Soboloff et al., 2005) but not the DAG-induced Ca^{2+} entry (measured with fluorescent Ca^{2+} probes) (Soboloff et al., 2005; Godin and Rousseau, 2007). The latter observation may be due to the fact that the OAG-dependent Ca^{2+} entry occurs mainly via L-type VGCC or the NCX (the depolarization caused by the entry of Na^+ through TRPC6 channels in turn activates the entry of Ca^{2+} via L-type VGCC (Soboloff et al., 2005) or via the NCX working in the reverse mode (Poburko et al., 2007) (see Section 1.2.2)). But this mechanism does not seem to be universal since suppressing the expression of TRPC6 in keratinocytes diminishes the hyperforin-activated Ca^{2+} entry (Muller et al., 2008). It is also worth mentioning that RNAi constructs designed against TRPC6 are used in primary neuronal cultures such as rat cerebellar granule neurons (Jia et al., 2007) and hippocampal neurons (Tai et al., 2008; Zhou et al., 2008). These constructs could be used in cortical neurons.

9 TRPC6 channels form iron- and zinc-conducting channels

9.1 Introduction

Some cation channels including several TRP channels can transport metal ions across the plasma membrane (see Chapter 4). In Chapter 1, we showed the existence of DAG- and hyperforin-sensitive TRPC6-like channels (hereinafter designated TRPC6 channels) in E13 cortical neurons. These channels are permeable to Ca^{2+}, Na^{+}, Ba^{2+} and Mn^{2+}. Since in the neuronal cell line PC12 TRPC6 channels can mediate NTBI uptake (Mwanjewe and Grover, 2004), we thought to verify whether this property was also found in neurons of the CNS.

We first verified the consequences of the over-expression of TRPC6 channels on the intracellular contents of Fe and of a few selected elements (Zn, Cu, Mn, S). Quantitative analyses were performed with ICP-OES and atomic absorption spectroscopy. Cellular iron and zinc imaging were then carried out with various fluorescent indicators (Fura-2, calcein, FluoZin-3). Finally, topographic and quantitative analyses of intracellular trace metals were obtained by using μ-SXRF.

9.2 Results

9.2.1 HEK-TRPC6 cells have a higher zinc content than HEK cells

The intracellular contents of zinc and sulphur were determined by ICP-OES whereas the intracellular contents of copper and iron were determined by atomic absorption spectroscopy (but not by ICP-OES due to detection limits). It appears that over-expressing TRPC6 channels in HEK-293 cells increases the intracellular contents of zinc and sulphur but not of iron or copper (Table 9-1).

The intracellular content of iron of cells pretreated for 1 hour at 37°C with 50 μM Fe^{2+} ($FeSO_4$ supplemented with ascorbic acid) was quantified with atomic absorption spectrometry. $FeSO_4$ was added alone or in the presence of 100 μM OAG. Adding iron in the external medium increased the intracellular iron content. Activating TRPC6 channels with OAG (in the presence of iron) did not further increase the iron content (Figure 9-1A). Similarly, the intracellular content of zinc of cells pretreated for 1 hour at 37°C with 50 μM zinc acetate was quantified with ICP-OES. Adding zinc in the external medium or activating TRPC6 channels with OAG (in the presence of zinc) failed to increase the zinc content (Figure 9-1B).

Table 9-1 Quantification of some elements with ICP-OES and atomic absorption spectroscopy in HEK and HEK-TRPC6 cells

	HEK	HEK-TRPC6
Fe (µg/g protein)	127.4 ± 5.3 (4)	101.6 ± 15.0 (4)
Zn (µg/g protein)	301.6 ± 22.7 (10)	429.4 ± 24.6 (11)*
Cu (µg/g protein)	11.9 ± 1.8 (4)	7.8 ± 0.2 (5)
S (µg/g protein)	6989.5 ± 517.2 (10)	13215.4 ± 700.9 (11)*

The numbers in the brackets indicate the numbers of measurements. * $P \leq 0.001$ Student's t test.

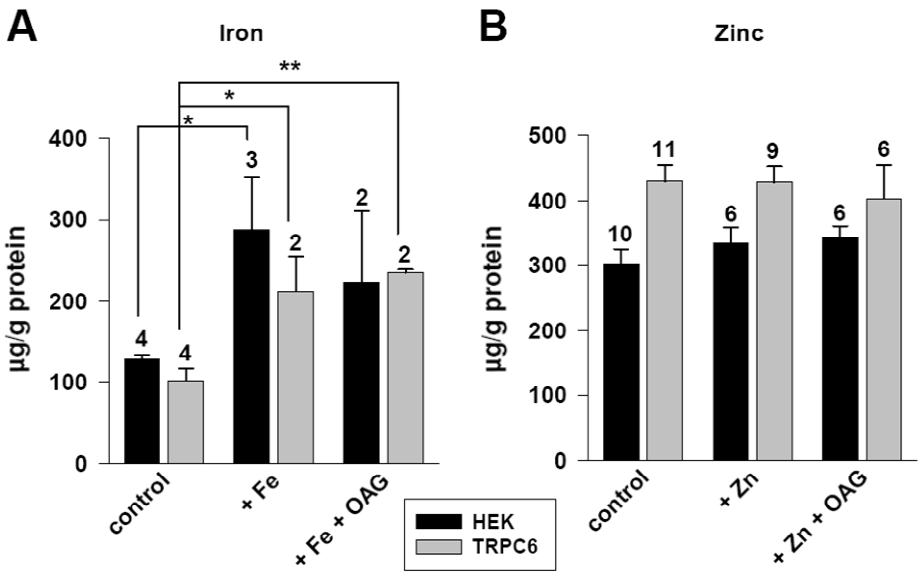

Figure 9-1 Quantification of iron with atomic absorption spectrometry and zinc with ICP-OES

Panel A: Intracellular iron was quantified in HEK (black) and HEK-TRPC6 (grey) cells by atomic absorption spectrometry after a 1-hour treatment at 37°C with 50 µM Fe^{2+} (Fe) in the presence or absence of 100 µM OAG. Panel B: Intracellular zinc was quantified in HEK (black) and HEK-TRPC6 (grey) cells by ICP-OES after a 1-hour treatment at 37°C with 50 µM Zn^{2+} (Zn) in the presence or absence of 100 µM OAG. * $p \leq 0.05$ and ** $p \leq 0.01$ (Student's t-test).

9.2.2 TRPC6 over-expressed in HEK cells form iron- and zinc-conducting channels

The calcium indicator Fura-2 is sensitive to transition metals (Grynkiewicz et al., 1985), like Zn^{2+} (Table 9-2). It has been used to monitor the changes in the intracellular concentration of free zinc ($[Zn^{2+}]_i$) in neurons (Cheng and Reynolds, 1998). Like Ca^{2+}, Zn^{2+} alters the excitation spectrum of Fura-2 and shifts the peak excitation wavelength from ~365

to ~340 nm, which provides the basis for ratiometric imaging approaches (Grynkiewicz et al., 1985; Kress et al., 2002). On the other hand, some metals produce a concentration-dependent quenching of the Fura-2 signal without altering the position of the excitation spectrum, such as Mn^{2+}, Fe^{2+} and Fe^{3+} (Grynkiewicz et al., 1985; Kress et al., 2002). Fura-2 has been used to detect cytosolic free iron in neurons, astrocytes, and oligodendrocytes kept in primary culture (Kress et al., 2002). Compared with Ca^{2+}, Zn^{2+} and Fe^{2+} have higher affinities for Fura-2 (Grynkiewicz et al., 1985; Atar et al., 1995; Kress et al., 2002). The calculated EC_{50} values of Fura-2 for Zn^{2+}, Fe^{2+} and Fe^{3+} are ~15.5 nM, ~5.03 nM and ~7.34 μM, respectively (Kress et al., 2002).

Iron imaging experiments with Fura-2 were first carried out on HEK and HEK-TRPC6 cells. In this set of experiments, cells were bathed in a Ca^{2+}-free Tyrode's solution supplemented with 100 μM Fe^{2+}. Fe^{2+} was chosen, since Fura-2 has a higher affinity to Fe^{2+} than to Fe^{3+} (Kress et al., 2002).

Figure 9-2 shows representative Fura-2 responses at 340 nm and 380 nm from a HEK-TRPC6 cell. When Fe^{2+} was added to the Ca^{2+}-free Tyrode's solution, no change was seen in the fluorescence. However, upon the addition of 50 μM SAG, a quenching of the fluorescence was noted at both wavelengths, showing the ability of TRPC6 channels to conduct Fe^{2+}. It is worth mentioning that the fluorescence quenching upon the addition of SAG (in the presence of Fe^{2+}) was only seen in 31% of HEK-TRPC6 cells tested (12 out of 39).

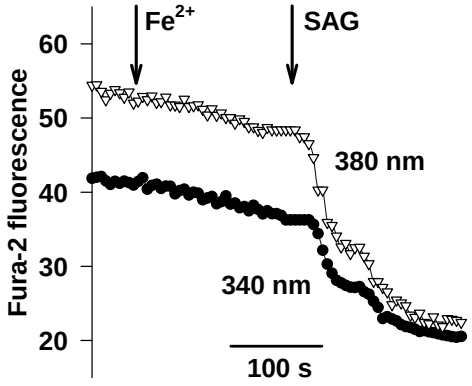

Figure 9-2 Iron imaging with Fura-2 in a HEK-TRPC6 cell

Fura-2 responses at 340 nm (●) and 380 nm (▽) from a HEK-TRPC6 cell bathed in a Ca^{2+}-free medium are shown. The fluorescence quenching upon the addition of SAG (in the presence of Fe^{2+}) was only seen in 31% of HEK-TRPC6 cells tested (12 out of 39). The arrows indicate when Fe^{2+} or SAG was added.

Similar experiments were carried out with 50 μM Zn^{2+} (zinc acetate). Figure 9-3A shows representative Fura-2 responses at 340 nm and 380 nm from a HEK-TRPC6 cell. When Zn^{2+} was added to the Ca^{2+}-free Tyrode's solution, the fluorescence remained unaffected. However, when 50 μM SAG was added in the Zn^{2+}-rich medium, a clear increase of the Fura-

2 fluorescence at 340 nm and a quenching at 380 nm were noted. The ratio of the fluorescence at 340 nm to that at 380 nm is shown in Figure 9-3B (open circles, n = 30). Of note, the responses upon the addition of SAG (in the presence of Zn^{2+}) were seen in practically all HEK-TRPC6 cells. These results show that TRPC6 channels over-expressed in HEK cells can form Zn^{2+}-conducting channels. Indeed, when compared with HEK cells (Figure 9-3B, filled circles, n = 52), HEK-TRPC6 cells showed a larger Zn^{2+} uptake. The weak Zn^{2+} entry seen in HEK cells may reflect the presence of endogenous TRPC6 channels. In conclusion, TRPC6 channels over-expressed in HEK cells can transport iron or zinc across the plasma membrane.

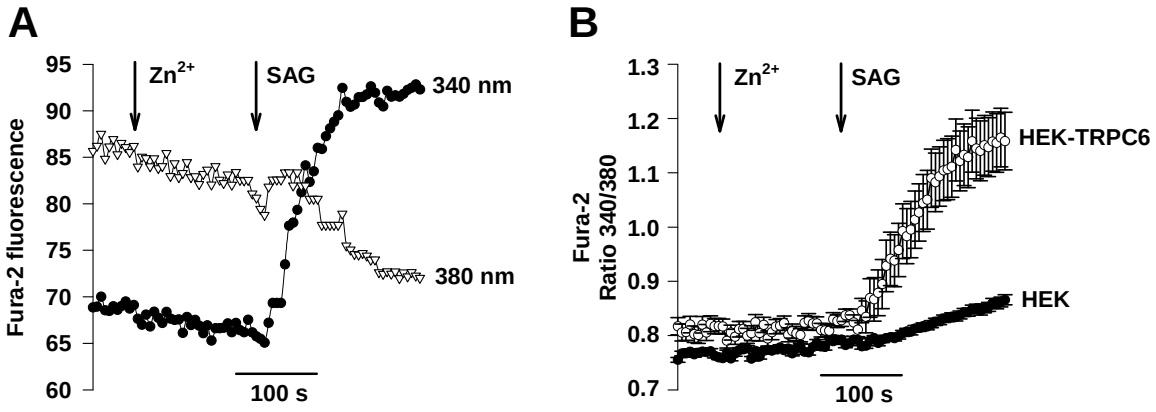

Figure 9-3 Zinc imaging with Fura-2 in HEK and HEK-TRPC6 cells

Panel A shows representative Fura-2 responses at 340 nm (●) and 380 nm (▽) from a HEK-TRPC6 cell bathed in a Ca^{2+}-free medium. The responses upon the addition of SAG (in the presence of Zn^{2+}) were seen in practically all HEK-TRPC6 cells. Panel B shows the changes in Fura-2 fluorescence (ratio F340 nm/F380 nm) in HEK cells (●, n = 52) and HEK-TRPC6 cells (○, n = 30) bathed in a Ca^{2+}-free medium. The arrows indicate when Zn^{2+} or SAG was added.

9.2.3 In cortical neurons TRPC6 channels form iron- and zinc-conducting channels

Iron and zinc imaging experiments were performed on cortical neurons loaded with Fura-2. By using the protocols illustrated in Figure 9-2 and Figure 9-3, we found that cortical neurons could permit the entry of iron or zinc after the activation of OAG-sensitive channels (Figure 9-4 and Figure 9-5).

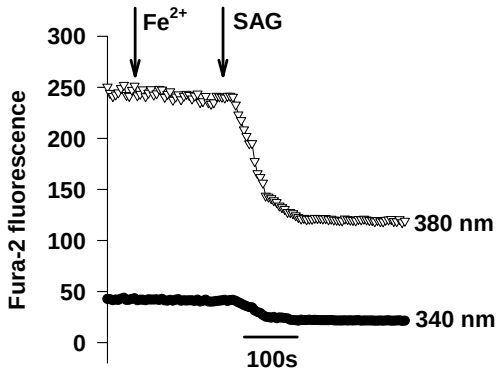

Figure 9-4 Iron imaging with Fura-2 in cortical neurons

Fura-2 responses at 340 nm (▽) and 380 nm (●) from a cortical neuron bathed in a Ca^{2+}-free medium are shown. The fluorescence quenching upon the addition of SAG (in the presence of Fe^{2+}) was seen in 24% of the neurons tested (10 out of 41). The arrows indicate when Fe^{2+} or SAG was added.

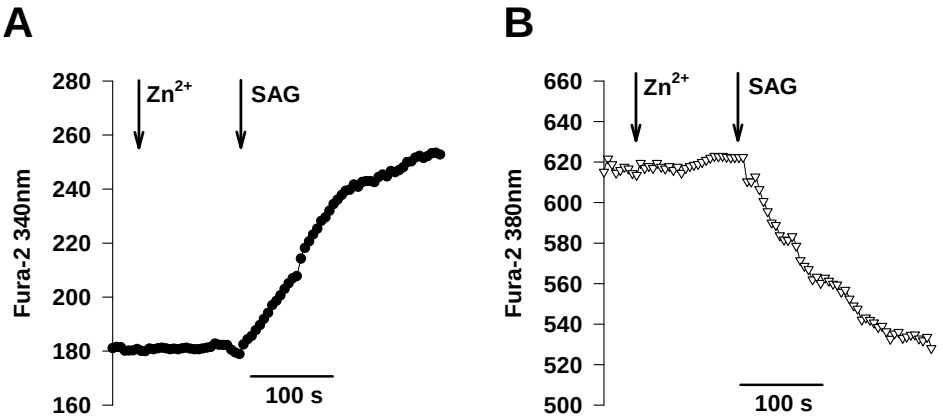

Figure 9-5 Zinc imaging with Fura-2 in cortical neurons

Fura-2 responses at 340 nm (●) and 380 nm (▽) from a cortical neuron bathed in a Ca^{2+}-free medium are shown. The responses upon the addition of SAG (in the presence of Zn^{2+}) were seen in practically all the neurons tested. The arrows indicate when Fe^{2+} or SAG was added.

Calcein is a derivative of fluorescein. Its fluorescence is quenched upon binding to iron. The affinities of calcein for Fe^{2+} and Fe^{3+} are identical to those of EDTA (affinity constants of $\sim 10^{-14}$ and 10^{-24} M, respectively) (Breuer et al., 1995). It is thus described as an iron probe. Since the fluorescence of calcein increases as $[Ca^{2+}]_i$ increases, external Ca^{2+} was omitted in order to monitor iron entry. Both Fe^{2+} and Fe^{3+} were tested. In Figure 9-6A, the addition of 50 μM Fe^{3+} (ferric ammonium citrate, FAC) to cortical neurons bathed in a Ca^{2+}-free Tyrode's solution caused no change in the calcein fluorescence, whereas the subsequent application of 50 μM SAG provoked a sudden decrease. In Figure 9-6B, a clear quench was seen upon the addition of 50 μM Fe^{2+} + SAG but not with Fe^{2+} alone. Here again, and

similarly to the experiments conducted with HEK-TRPC6 cells, the quenching of the calcein fluorescence was seen only in some cortical neurons.

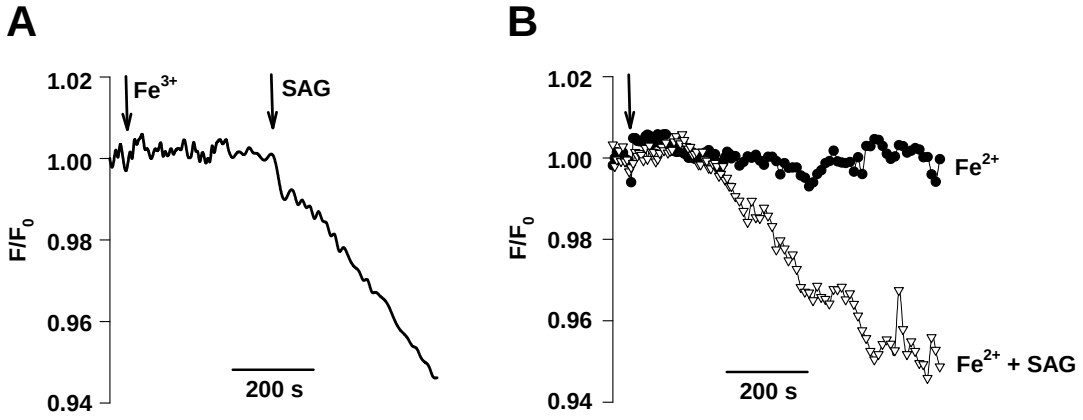

Figure 9-6 Iron imaging with calcein in cortical neurons

In panel A is shown the calcein fluorescence in a cortical neuron bathed in a Ca^{2+}-free Tyrode's solution. The fluorescence quenching upon the addition of SAG (in the presence of Fe^{3+}) was seen in 38% of the neurons tested (8 out of 21). The arrows indicate when Fe^{2+} or SAG was added. In panel B, 50 µM Fe^{2+} was added without (●) or with (▽) 50 µM SAG in a Ca^{2+}-free Tyrode's solution. The fluorescence quenching upon the addition of Fe^{2+} + SAG was seen in 27% of the neurons tested (7 out of 26). The arrow indicates when Fe^{2+} or Fe^{2+} + SAG were added.

New Zn^{2+}-selective fluorescent indicators have been synthesized (Gee et al., 2002b). FluoZin-3 is one of the most Zn^{2+}-sensitive and Zn^{2+}-specific probes. It exhibits a several hundred-fold increase in fluorescence upon saturation with Zn^{2+} occurring at ~100 nM Zn^{2+} *in vitro* with a K_d of 15 nM (Gee et al., 2002a; Gee et al., 2002b), and a >50-fold fluorescence increase upon saturation (~100 nM Zn^{2+}) in cells with an intracellular K_d of 3-4 nM (Gee et al., 2002b). It is important that Ca^{2+} ions do not interfere with Zn^{2+} measurements. Hence, the low K_d value for Zn^{2+} without detectable Ca^{2+} sensitivity (Table 9-2) makes FluoZin-3 an ideal Zn^{2+} probe (Gee et al., 2002b).

FluoZin-3 experiments were carried out on cortical neurons kept in a Ca^{2+}-free Tyrode's solution. Figure 9-7A shows that 50 µM Zn^{2+} elicited a weak FluoZin-3 response but a subsequent addition of 50 µM SAG provoked a strong elevation of the FluoZin-3 fluorescence. A different protocol was used to further compare the entry of Zn^{2+} induced by 50 µM Zn^{2+}, 50 µM Zn^{2+} + 50 µM SAG and 50 µM Zn^{2+} + 10 µM hyperforin (Figure 9-7B, C, red). The increase in FluoZin-3 fluorescence under these conditions is summarized in Figure

9-7D (red). The same set of experiments was carried out in a normal Tyrode's solution where 2 mM Ca^{2+} was present (Figure 9-7B, C, black) and the increase in FluoZin-3 fluorescence is shown in Figure 9-7D (black). The entry of Zn^{2+} in the absence of extracellular Ca^{2+} was larger than that in the presence of Ca^{2+}, showing Zn^{2+} and Ca^{2+} competed with each other. It is worth mentioning that for all the experiments performed, 50 μM N, N, N′, N′-tetrakis (2-pyridylmethyl) ethylenediamine (TPEN) was bath-applied at the end of the recording as illustrated in Figure 9-7A. This chelator with a strong affinity for Zn^{2+} (K_d = 0.26 fM, (Arslan et al., 1985)) fully reversed the Zn^{2+} responses and returned the FluoZin-3 fluorescence to the baseline (Figure 9-7A), which is in agreement with previous results (Gee et al., 2002b).

In conclusion, endogenous TRPC6 channels of cortical neurons form iron- and zinc-conducting channels.

Table 9-2 Comparison between Fura-2 and FluoZin-3

Probe	**λ_{ex} (nm)**	**λ_{em} (nm)**	**K_d**		**Reference**
			Zn^{2+}	**Ca^{2+}**	
Fura-2	340/380	510	1.6-3 nM	135-310 nM	(Grynkiewicz et al., 1985; Atar et al., 1995)
FluoZin-3	491	520	15 nM	NA[a]	(Gee et al., 2002b)

[a] No fluorescence response to ≤ 10mM Ca^{2+} was observed.

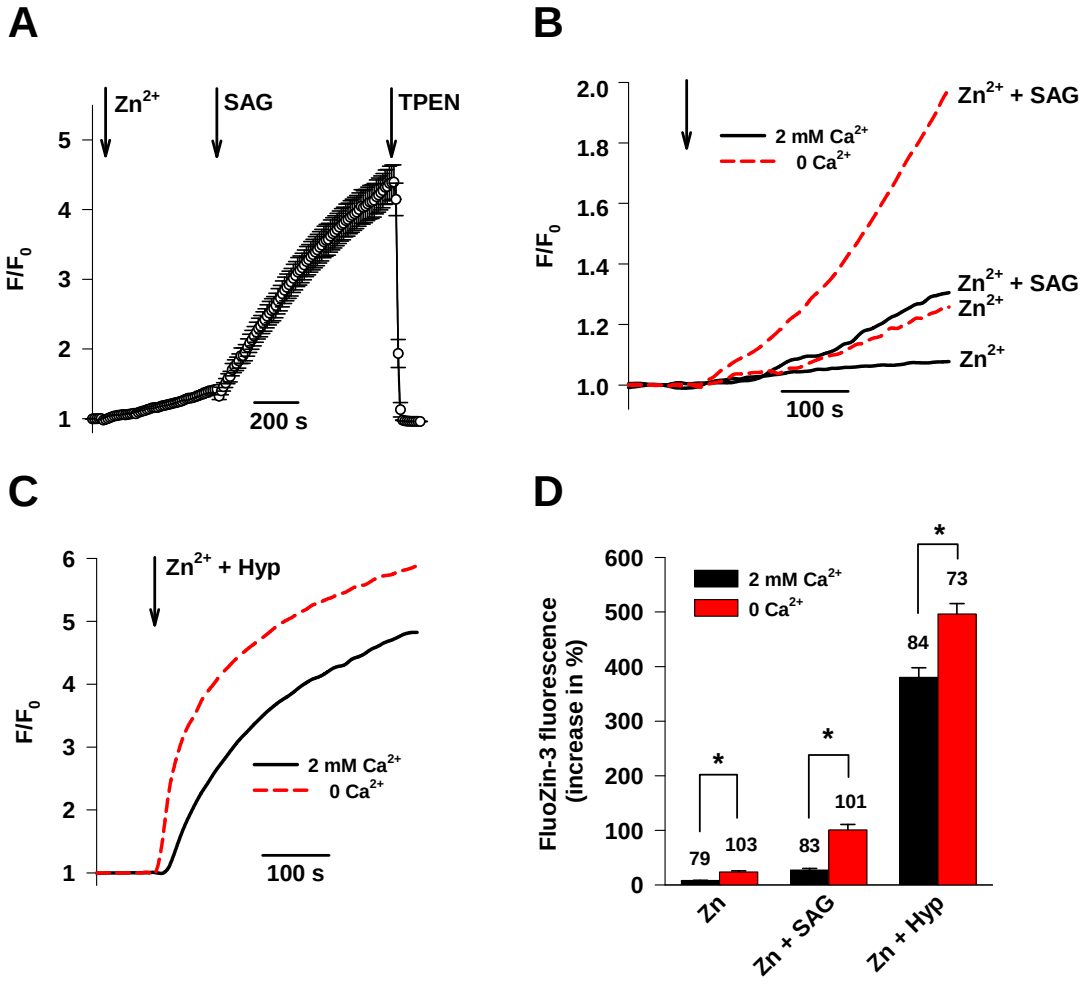

Figure 9-7 Zinc imaging with FluoZin-3 in cortical neurons

In panel A, cortical neurons (n = 59) were kept in a Ca^{2+}-free Tyrode's solution. The arrows indicate when Zn^{2+}, SAG or TPEN was added. In panel B are shown FluoZin-3 responses induced by 50 µM Zn^{2+}, 50 µM Zn^{2+} + 50 µM SAG and in panel C 50 µM Zn^{2+} + 10µM hyperforin (Hyp), in the presence (black) or absence (red) of Ca^{2+} in the medium. The arrows indicate when Zn^{2+}, Zn^{2+} + SAG or Zn^{2+} + hyperforin were added. Panel D is a summary graph with the black bars showing the experiments done in the presence of Ca^{2+} and the red bars in the absence of Ca^{2+}. For each cell, the maximal increase in FluoZin-3 fluorescence during the application (400 s) of Zn^{2+}, Zn^{2+} + SAG or Zn^{2+} + hyperforin was measured. The number of the cells tested is indicated above each bar. * $p \leq 0.001$ (Student's t-test followed by Mann-Whitney Rank Sum Test). There is a statistically significant difference among the black bars or the red bars with $p \leq 0.001$ (one-way ANOVA).

9.2.4 Topographic and quantitative analyses of metals in cortical neurons, HEK and HEK-TRPC6 cells

Synchrotron microbeam X-ray fluorescence (µ-SXRF) was applied for topographic and quantitative analyses of selected elements in HEK cells, HEK-TRPC6 cells and E13

cortical neurons. The aim of these experiments was to analyze the intracellular content and distribution of selected trace metals (Fe, Zn, Cu, Mn) without or with activating TRPC6 channels.

9.2.4.1 Quantitative analyses of selected trace metals in HEK and HEK-TRPC6 cells

Intracellular trace metals (Fe, Zn, Cu, Mn) were quantified and compared between HEK and HEK-TRPC6 cells. HEK-TRPC6 cells are enriched in zinc and manganese, while the contents of iron and copper are the same in HEK and HEK-TRPC6 cells (Table 9-3). The high manganese content of HEK-TRPC6 cells was not detected before with ICP-OES because of the detection limits (Section 9.2.1). The results of zinc, iron and copper are in line with those obtained with ICP-OES and with atomic absorption spectrometry (Table 9-1).

Table 9-3 Quantification of some trace metals by X-ray fluorescence in HEK and HEK-TRPC6 cells

	HEK	**HEK-TRPC6**
Fe (ng/cm^2)	93.1 ± 18.4	120.4 ± 25.4
Zn (ng/cm^2)	379.2 ± 61.0	560.7 ± 45.5 *
Cu (ng/cm^2)	8.5 ± 1.2	9.0 ± 1.3
Mn (ng/cm^2)	28.3 ± 2.9	93.0 ± 11.6 **

4 HEK cells and 5 HEK-TRPC6 cells were analyzed. * $P \leq 0.05$ Student's t-test, ** $P \leq 0.05$ Student's t-test followed by Mann-Whitney Rank Sum Test.

Figure 9-8 shows representative two-dimensional (2D) mappings of intracellular iron and zinc in HEK (A-B) and HEK-TRPC6 (C-D) cells. The iron distribution is heterogenous with numerous punctae while zinc is rather homogenously distributed all over the cell with a strong density in the nucleus.

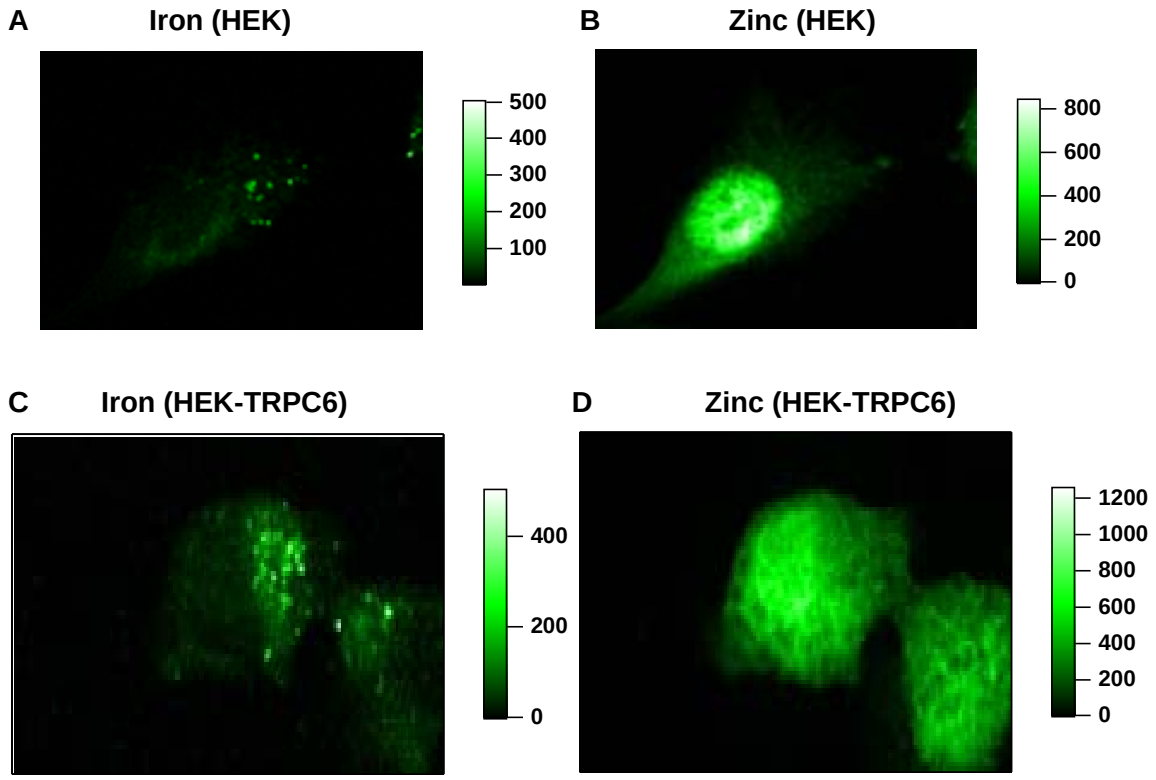

Figure 9-8 2D mappings of intracellular iron and zinc in HEK and HEK-TRPC6 cell

Representative 2D mappings of iron and zinc in a HEK cell (A: iron; B: zinc) and in a HEK-TRPC6 cell (C: iron; D: zinc) were obtained with µ-SXRF. The ladders on the right of the panels show the iron/ zinc intensity (counts).

9.2.4.2 Activation of TRPC6 channels in the presence of iron leads to an intracellular accumulation of iron in HEK-TRPC6 cells

HEK-TRPC6 cells were exposed to 50 µM Fe^{2+} in the presence or absence of 100 µM OAG for 1 hour at 37°C. After this treatment, the cells were washed, cryofixed and analyzed with µ-SXRF. The intracellular content of iron was quantified (Figure 9-9A). The iron content was not greatly affected after a 1-hour treatment with Fe. However, in the presence of OAG + Fe, the iron content was increased by 110% when compared to the control (OAG and Fe-untreated) cells and by 45% when compared to the Fe-treated cells. These results are different from those obtained with atomic absorption spectroscopy. In the latter case, activating TRPC6 channels with OAG (in the presence of Fe) did not further increase the iron content (Figure 9-1). This difference may be due to the limited number of experiments carried out and/or the detection limits of each methodology.

The intracellular contents of zinc, copper and manganese were also compared (Figure 9-9B, C, D). Interestingly, incubating HEK-TRPC6 cells in an iron-rich medium (without or with OAG) diminished the intracellular contents of zinc and manganese (for copper, the decrease is not statistically significant).

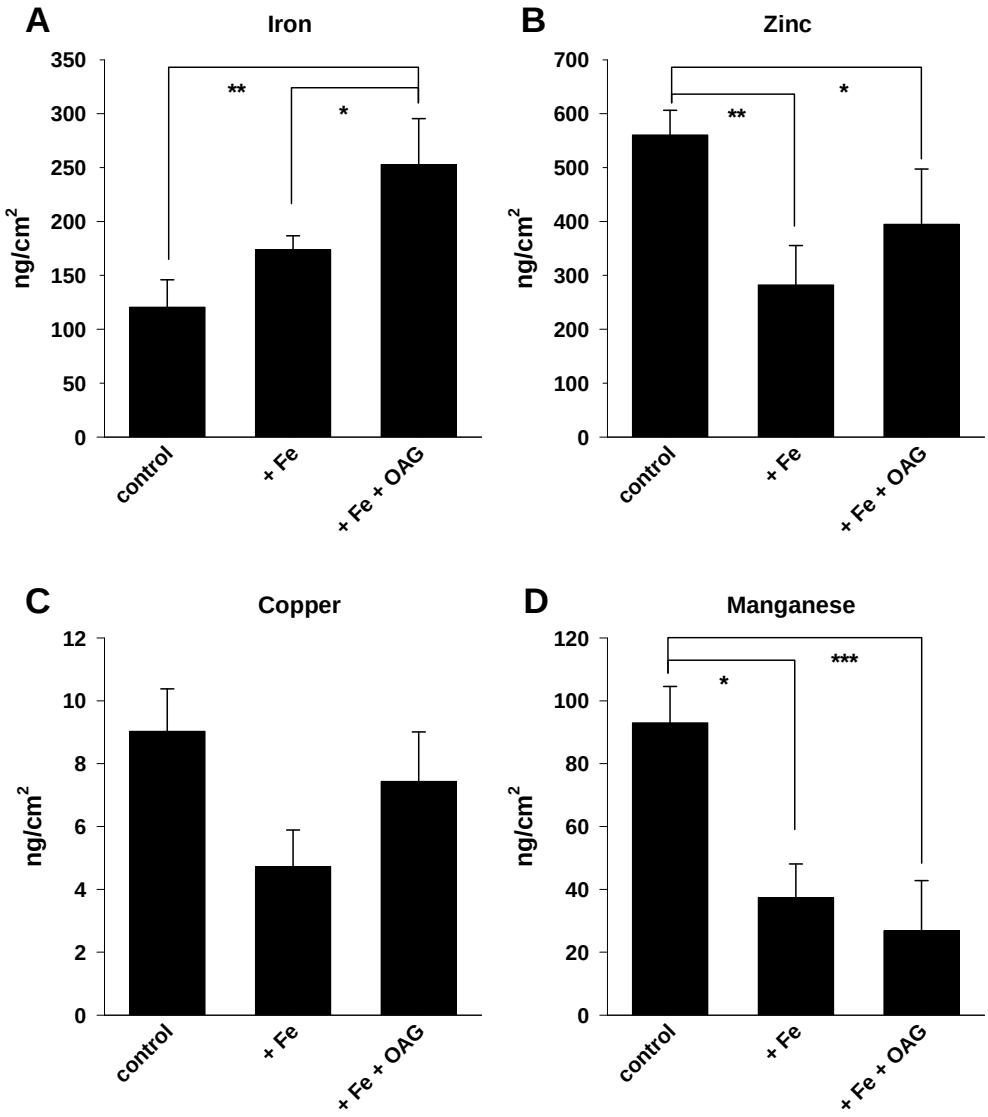

Figure 9-9 Activation of TRPC6 channels in an iron-rich extracellular medium induced an intracellular accumulation of iron in HEK-TRPC6 cells

HEK-TRPC6 cells were maintained for 1 hour (at 37°C) in a medium containing 50 µM Fe^{2+} (Fe) in the presence or absence of 100 µM OAG. After the treatment, the cells were washed, cryofixed and analyzed with µ-SXRF. Panels A, B, C and D show the intracellular contents of iron, zinc, copper and manganese, respectively. The number of cells analyzed for each condition (control, + Fe and + Fe + OAG) is 5, 3 and 4, respectively. * $P \leq 0.05$, ** $P \leq 0.01$, *** $P \leq 0.005$, Student's t-test.

9.2.4.3 OAG and hyperforin have distinct effects on the intracellular iron content of cortical neurons

μ-SXRF experiments were also carried out on cortical neurons. Figure 9-10 shows the 2D mapping of intracellular iron and zinc in a cortical neuron.

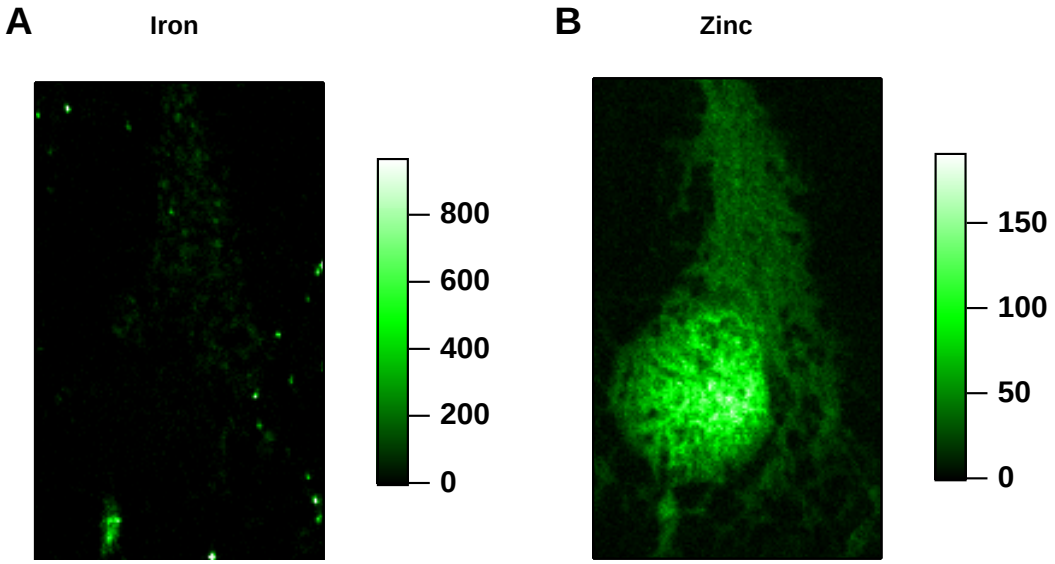

Figure 9-10 2D mappings of intracellular iron and zinc in a cortical neuron

Representative 2D mappings of iron (A) and zinc (B) in a cortical neuron were obtained with μ-SXRF. The ladders on the right of the panels show the iron/zinc intensity (counts).

The same experiments as the ones illustrated in Figure 9-9 were carried out on cortical neurons to verify whether activating TRPC6 channels in an iron-rich medium caused an intraneuronal accumulation of this metal. Cortical neurons were treated for 5 minutes or 1 hour (at 37°C) with 10 μM Fe^{2+} in the presence or absence of 100 μM OAG (or 10 μM hyperforin). The concentration of Fe used (10 μM) was smaller than with HEK-cells (50 μM) in order to avoid neurotoxic effects. The intracellular contents of iron, zinc, copper and manganese are shown in Figure 9-11. A short treatment (5 minutes) with Fe + OAG increased the intracellular iron content, which was accompanied by an augmentation of the intracellular zinc, copper and manganese contents. The contents of these metals after a 5-minute treatment with Fe + OAG were of the same levels as those after 1-hour treatment with Fe alone. However, a longer treatment (1 hour) with Fe + OAG failed to further increase the intracellular iron content. Surprisingly, the cellular contents of all metals (except copper) after this 1-hour treatment returned to their corresponding control levels. In the case of hyperforin, the cellular contents of all four metals were increased after the treatment with Fe + hyperforin.

Unlike OAG, the intracellular contents of the metals (especially iron) were positively correlated to the duration of the treatment: a 1-hour treatment causes a stronger accumulation than a 5-minute treatment.

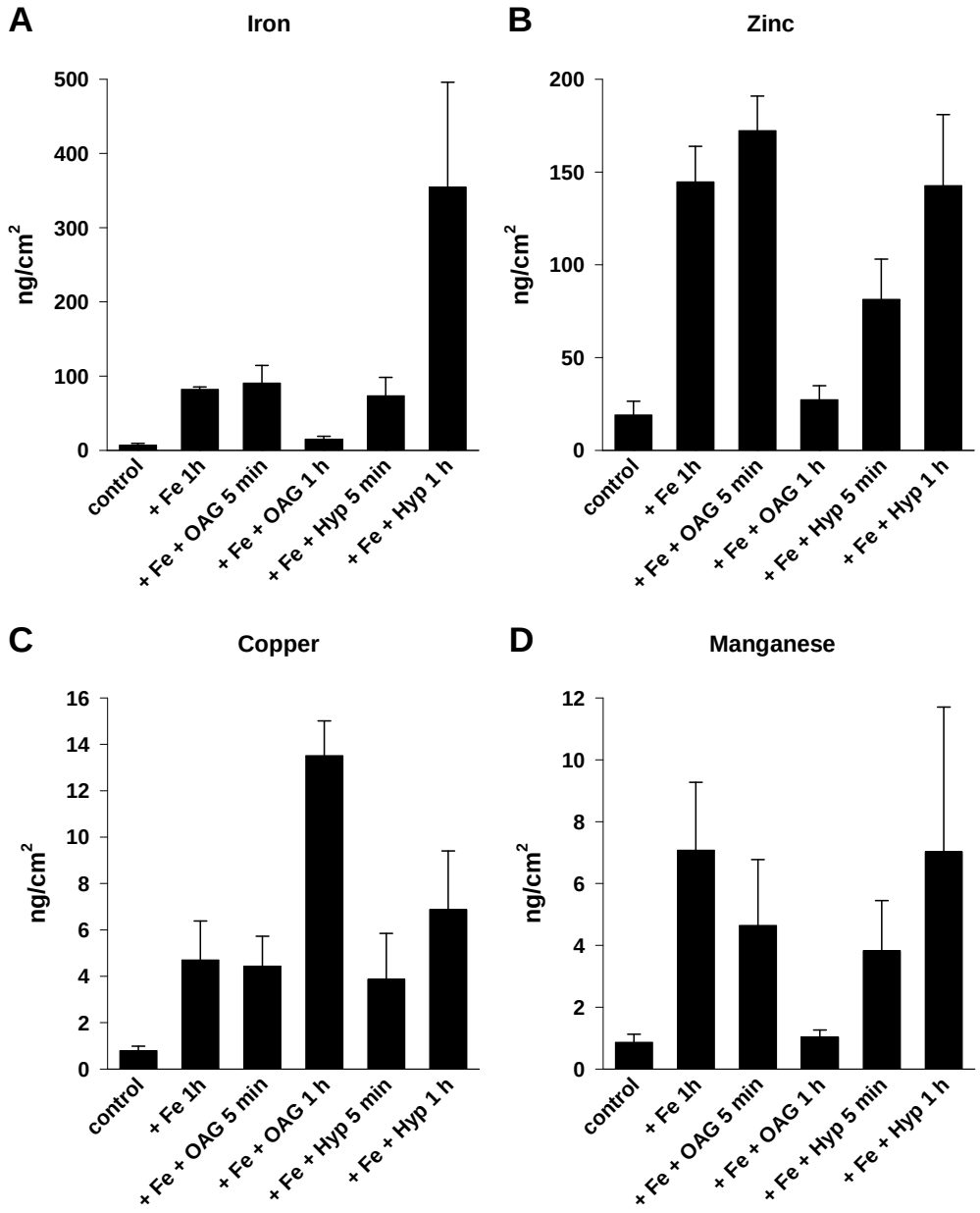

Figure 9-11 The intracellular contents of Fe, Zn, Cu and Mn of cortical neurons after a 5-minute or 1-hour treatment with iron

Cortical neurons were maintained for 5 minutes (min) or 1 hour (h) (at 37°C) in a culture medium supplemented with 10 µM Fe^{2+} (Fe) in the absence or presence of 100 µM OAG (or 10 µM hyperforin (Hyp)). After the treatment, neurons were washed, cryofixed and analyzed with µ-SXRF. Panels A, B, C and D show the intracellular contents of iron, zinc, copper and manganese respectively. The number of cells analyzed for each condition (control, + Fe 1 h, + Fe + OAG 5 min, + Fe + OAG 1 h, + Fe + Hyp 5 min and + Fe + Hyp 1 h) is 7, 4, 5, 5, 4 and 8, respectively.

9.3 Discussion

Our results reveal that TRPC6 channels can permit the entry of iron and zinc. Quantitative analyses with ICP-OES and atomic absorption spectrometry show that over-expressing TRPC6 in HEK cells is accompanied by an enhancement of the intracellular contents of zinc and sulphur whereas the contents of iron and copper remain unaffected. Iron and zinc imaging experiments indicate that TRPC6 channels, either overexpressed in HEK cells or endogenously present in cortical neurons, are permeable to iron and zinc when activated by SAG or hyperforin. The state-of-art technique μ-SXRF was used for topographic and quantitative analyses of selected elements (iron, zinc, copper and manganese) in HEK cells, HEK-TRPC6 cells and cortical neurons. These experiments further show that activating TRPC6 channels in the presence of iron leads to an intracellular iron accumulation in both HEK-TRPC6 cells and cortical neurons.

HEK-TRPC6 cells are enriched in zinc, sulphur and manganese

By using different quantitative analysis techniques (ICP-OES, atomic absorption spectrometry and μ-SXRF), we show that overexpressing TRPC6 channels in HEK cells increases the intracellular contents of some elements such as zinc, sulphur and manganese (Table 9-1 and Table 9-3) without altering the iron and copper status (Table 9-1 and Table 9-3). Zinc imaging experiments carried out on HEK-TRPC6 cells show that TRPC6 form zinc-conducting channels (Figure 9-3B), which can explain why HEK-TRPC6 cells are enriched in zinc. The enhancement of the sulphur content probably reflects an increased expression of sulphur-containing proteins, like MT. MT are the main zinc-binding proteins. They are rich in cysteine and their expression level is up-regulated by high $[Zn^{2+}]_i$ via a posttranscriptional regulation system (Langmade et al., 2000; Andrews, 2001). Indeed, a zinc finger domain containing metal-response element-binding factor-1 (MTF-1) has been identified as a cellular sensor of zinc status, controlling the expression of MT by binding their specific gene promoters, termed metal-response element (MRE) (Langmade et al., 2000; Andrews, 2001). We are planning to compare the expression level of MT in HEK and HEK-TRPC6 cells. Finally, it is not surprising to see a manganese overload in HEK-TRPC6 cells, since TRPC6 channels form Mn^{2+}-conducting channels (Hofmann et al., 1999; Boulay, 2002). The DAG-sensitive channels of cortical neurons are permeable to Mn^{2+} (article 1, Section 8.2). However, no change is observed for iron in HEK-TRPC6 cells, although TRPC6 channels are permeable to iron. This may indicate that cells control more tightly the content of this redox metal than their zinc content.

TRPC6 channels form iron-conducting channels

Although quantitative analyses show that the intracellular iron content of HEK and HEK-TRPC6 cells are of the same level (Table 9-1 and Table 9-3), iron imaging experiments demonstrate that TRPC6 channels over-expressed in HEK cells are permeable to iron (Figure 9-2). This finding is in agreement with a previous report (Mwanjewe and Grover, 2004). In the presence of Fe^{2+} + OAG, HEK-TRPC6 cells are enriched in iron. Their intracellular iron content is increases by 110 % when compared to control (untreated) cells and by 45 % when compared to cells treated with Fe^{2+} alone (Figure 9-9A). These results obtained with µ-SXRF are different from those obtained with atomic absorption spectrometry (Figure 9-1), where OAG did not further enhance the iron content (when compared to OAG-untreated cells). It is important to know that some intrinsic differences exist among these techniques. The measurements with atomic absorption spectroscopy are based on a large quantity of cells, and the intracellular content of iron is normalized to the total protein quantity; while µ-SXRF carries out quantifications at the cellular level, and the intracellular content of iron is normalized to the surface of the cell analyzed. These two techniques quantify all the iron existing in the cells including cytosolic free iron, iron bound to proteins or ligands as well as iron stored in the organelles, while iron imaging shows the cytosolic variations of free iron. Another factor that may account for the discrepancies found between the results of µ-SXRF and of atomic absorption spectrometry is that the number of the measurements with atomic absorption spectrometry is limited (Figure 9-1). It is important to mention that the data collected by means of the synchrotron technique originate from 3 series of experiments (February, June and November 2008). The access to the **European Synchrotron Radiation Facility (ESRF) is limited**. The scientific project was submitted to the ESRF scientific committee in March 2007 and the decision allowing us some beam time in 2008 was taken (and announced) in June 2007. Obtaining new sessions would necessitate the resubmission of another proposal. Under these conditions, the additional experiments could not be performed before several months...

Taken together, it is concluded that TRPC6 channels form iron-conducting channels.

Effects of DAG on the intracellular iron content

Cellular iron imaging and µ-SXRF experiments were also carried out on cortical neurons. Iron imaging was performed with either Fura-2 (Figure 9-4) or calcein (Figure 9-6) in a calcium-free medium. The quenching of the fluorescence in the presence of Fe^{2+}/Fe^{3+} +

SAG indicates that TRPC6 channels of cortical neurons are permeable to iron. It is worth mentioning that in both HEK-TRPC6 cells and cortical neurons, the quenching of the fluorescence is only seen in some cells (31%). Quantitative analyses with μ-SXRF (Figure 9-11A) after a short treatment (5 minutes) with Fe^{2+} + OAG show a higher intracellular iron content: it reaches the same level as that seen after a 1-hour treatment with Fe^{2+} alone. However, a 1-hour treatment with Fe^{2+} + OAG fails to further increase the intracellular iron content but rather brings it back to the level seen in the control (untreated) neurons. This likely reflects the existence of regulatory mechanisms that protect the cells from iron overload. Several putative protective mechanisms have so far been reported. One is a posttranscriptional regulation implying two cytoplasmic iron regulatory proteins (IRP), IRP1 and IRP2. They interact with iron responsive elements (IRE) found in untranslated regions of mRNA encoding key proteins involved in the regulation of iron storage and metabolism. The cellular labile iron pool regulates the binding of IRP to IRE and affect either mRNA translation or mRNA stability, thus regulating the synthesis of specific proteins (Hentze et al., 2004; Pantopoulos, 2004; Andrews and Schmidt, 2007). When there is an iron overload, IRP are inactivated for IRE-binding, which up-regulates the expression of proteins involved in iron storage (ferritin) and export (ferroportin) but down-regulates the expression of those involved in iron uptake (TfR, DMT1) (Hentze et al., 2004). Another one is concerns a posttranslational regulatory mechanism involving hepcidin. Iron regulates the secretion of hepcidin, which in turn controls the concentration of ferroportin on the cell surface (Nemeth et al., 2004). In addtion, iron exposure to brain cells is known to produce pro-inflammatory cytokins such as interleukin-1β (Molina-Holgado et al., 2007). Interleukin-1β up-regulates the expressions of ceruloplasmin and ferroportin in astrocytes (di Patti et al., 2004). Of note, interleukin-1β enhances ROCE via TRPC6 channels in astrocytes and chronic treatment with interleukin-1β up-regulates the expression of TRPC6 (Beskina et al., 2007). Since TRPC6 can mediate the entry of iron and is up-regulated by interleukin-1β (which, on its side influences iron efflux systems), it would be interesting to determine more precisely how these actors regulate the neuronal homeostasis of iron

In our experiments, the augmentation of the intracellular iron content seen after a 5-minute treatment with Fe^{2+} + OAG reflects the iron entry via TRPC6 channels. But after a longer (1 hour) treatment, the iron content is similar to the one measured in control (untreated) cells. This indicates that during this 1 hour treatment, neuronal cells respond positively to an iron overload by decreasing the entry and/or (most likely) by promoting the efflux of the trace

metal. Interestingly, the existence of regulatory mechanisms intended to diminish the intracellular iron content has been suggested for SH-SY5Y neuroblastoma cells and hippocampal neurons (Aguirre et al., 2005). In this study, the authors show that iron accumulation kills some cells but that a sub-population respond to the iron exposure positively by decreasing the expression of DMT1 and increasing the expression of ferritin and ferroportin (Aguirre et al., 2005).

However, in our experiments, the intracellular iron content measured after a 1-hour incubation with Fe^{2+} alone is clearly larger than the control iron level. Moreover, when OAG is replaced by hyperforin, the intracellular iron content is positively correlated to the duration of the treatment (Figure 9-11A). These two observations seem to indicate that the mechanisms participating in neuronal regulation of iron homeostasis are rather DAG-dependent. Some PKC are activated by DAG, and PKC activation is known to directly phosphorylate IRP1 and to increase the binding of IRP1 to IRE resulting in an up-regulation of the expression of ferritin and TfR (Eisenstein et al., 1993; Schalinske and Eisenstein, 1996; Schalinske et al., 1997). In addition, the down-regulation of the expression of ferroportin induced by hepcidin is mediated by Janus Kinase 2 (JAK2), a nonreceptor tyrosine kinase (De Domenico et al., 2009). The binding of hepcidin to ferroportin triggers the binding of JAK2 to ferroportin and JAK2 phosphorylation, which in turn phosphorylates ferroportin and permits the internalization of ferroportin (De Domenico et al., 2009). Interestingly, JAK2 is also phosphorylated downstream from DAG/PKC (Rodriguez-Linares and Watson, 1994), and PKC is suggested to negatively regulate JAK2 (Kovanen et al., 2000; Rui et al., 2000). Thus, PKC activation induced by DAG might abolish the hepcidin-induced internalization of ferroportin, which could favour the iron export. The exact mechanism accounting for the DAG-dependent regulation of iron homeostasis seen in cortical neurons is unknown. But based on the experimental data published so far, it can be suggested that the low level of iron noted after a 1-hour treatment with Fe^{2+} + OAG indicates the existence of a DAG/PKC-dependent signaling pathway participating in the regulation of iron homeostasis in cortical neurons.

Interaction among iron, zinc, copper and manganese

In cortical neurons, the intracellular contents of iron, zinc, copper and manganese after different treatments are positively correlated (except copper after a 1 hour-treatment with $FeSO_4$ + OAG) (Figure 9-11). When the iron content increases, the contents of other metals increase, and *vice versa*. These results indicate that trace metals are present in the salt of

$FeSO_4$. On the contrary, in HEK-TRPC6 cells, the increase in iron is accompanied by decreases in the other metals (Figure 9-9). The reason accounting for the different results from these two types of cells remains unclear at present; whereas it is certain that the cellular iron status influences the other metals and this influence is cell type-dependent.

There exist some overlaps in the transport systems of metals. For example, the metals analyzed in the present study all share DMT1 for entering the cells. Iron and manganese compete for transferrin, DMT1, VGCC (Roth and Garrick, 2003) and maybe ferroportin (Wu et al., 2004a). Ceruloplasmin or hephaestin, responsible for iron export, are both copper-binding proteins that are involved in copper homeostasis. Iron and zinc share as well VGCC and Zip14 (Liuzzi et al., 2006) for entering the cells. As iron regulates the expression of a number of key proteins involved in divalent metal transport, the iron status may influence on the transport of other metals (Roth and Garrick, 2003). The covariance among these metals has been shown in several studies (Jones et al., 2008; Zhang et al., 2009).

TRPC6 channels form zinc-conducting channels

Cellular zinc imaging experiments with Fura-2 and FluoZin-3 show that TRPC6 channels form zinc-conducting channels in both HEK-TRPC6 cells (Figure 9-3) and cortical neurons (Figure 9-5 and Figure 9-7), even in the presence of physiological concentrations of Ca^{2+}. Zinc entry in the absence of extracellular Ca^{2+} is larger than in the presence of Ca^{2+}, indicating that Zn^{2+} and Ca^{2+} compete with each other. Of note, the zinc entry induced by OAG or hyperforin was observed in practically all the cells analyzed.

Perspectives

Here we show that native or overexpressed TRPC6 channels form iron- and zinc-conducting channels. However, the physiological and pathophysiological roles of the metal entry via these channels need to be further elucidated. In addition, whether exchangers like the NCX participate cooperatively in mediating this entry of iron or zinc remains unknown. Since we have found that a 1-hour treatment with Fe^{2+} + OAG fails to further increase the intracellular iron content but rather brings it back to the control level, analyses of the expression levels of the proteins involved in iron transport such as DMT1 and ferroportin after these treatments (Fe, Fe + OAG for 5 minutes or 1 hour) may provide new information. Moreover, quantitative analyses of the intracellular zinc content after various treatments (Zn, Zn + OAG or Zn + hyperforin for 5 minutes or 1 hour) may help understand more profoundly the cellular regulatory mechanisms of zinc homeostasis.

10 Flufenamic acid modulates store-operated and TRPC6 channels by altering mitochondrial calcium homeostasis

10.1 Introduction

FFA is a non-steroidal anti-inflammatory drug belonging to the family of fenamates. It is often used as a non-specific channel blocker but, a few reports have revealed that it also increases the amplitude of some currents. Table 10-1 provides an overview of its inhibitory and excitatory actions on ion channel currents. Interestingly, FFA reversibly enhances currents through TRPC6 channels, whereas it inhibits currents through TRPC3 and TRPC7 channels in a dose-dependent manner (Inoue et al., 2001; Jung et al., 2002; Carter et al., 2006; Hill et al., 2006; Saleh et al., 2006; Fellner and Arendshorst, 2008).

In addition, FFA is known to induce the release of Ca^{2+} from organelles (McDougall et al., 1988; Poronnik et al., 1992; Shaw et al., 1995; Jordani et al., 2000). Indeed, in our experiments we found that FFA could increase $[Ca^{2+}]_i$ in HEK cells and in cortical neurons. Since FFA is now commonly used to characterize TRPC6 channels, we decided to further analyze its effects on the Ca^{2+} homeostasis. It turned out that FFA acted intracellularly by releasing Ca^{2+} from mitochondria. We suggest that it indirectly regulates TRPC6 channels via its action on these organelles.

10.2 Article 2: The anti-inflammatory agent flufenamic acid depresses store-operated channels by altering mitochondrial calcium homeostasis

Table 10-1 The inhibitory and excitatory actions of flufenamic acid on ion channel currents

Action	Channels	Tissue/cell type	References
Inhibition of currents	Calcium-activated non-selective (CAN) cation channels	Exocrine pancreas cells	(Gogelein et al., 1990)
		Molluscan neuons	(Shaw et al., 1995)
		Sensory neurons	(Cho et al., 2003)
	SOC	Neutrophils	(Kankaanranta and Moilanen, 1995; Sandoval et al., 2007)
		Lymphocytes	(Kankaanranta et al., 1996)
	Voltage-gated Ca^{2+} channels	Smooth muscle cells	(Shimamura et al., 2002)
	Voltage-gated Na^{+} channels	Dorsal root ganglion neurons	(Lee et al., 2003a)
	Voltage-gated K^{+} channels	Oocytes	(Wang et al., 1997)
	Ca^{2+}-activated Cl^{-} channels	Oocytes	(White and Aylwin, 1990)
	Small-conductance Cl^{-} channels	T lymphocytes	(Schumacher et al., 1995)
	CFTR Cl^{-} channels	Oocytes	(McCarty et al., 1993)
	NMDA receptors	Spinal cord neurons	(Lerma and Martin del Rio, 1992)
	TRPC3	HEK cells	(Inoue et al., 2001)
	TRPC7	HEK cells	(Inoue et al., 2001)
	TRPC5	Myocytes and HEK cells	(Lee et al., 2003b)
	TRPM2	Insulinoma cell line	(Hill et al., 2004)
	TRPM4	HEK cells	(Ullrich et al., 2005)
	TRPM5	HEK cells	(Ullrich et al., 2005)
	TRPM7	Breast cancer cells	(Guilbert et al., 2009)
Augmentation of currents	Ca^{2+}-activated K^{+} channels	smooth muscle cells	(Ottolia and Toro, 1994)
	K^{+} channels	Smooth muscle and epithelial Cells	(Rae and Farrugia, 1992; Farrugia et al., 1993b; Farrugia et al., 1993a)
	TRPC6	HEK and smooth muscle cells	(Inoue et al., 2001)

Neuropharmacology 56 (2009) 1010–1016

Contents lists available at ScienceDirect

Neuropharmacology

journal homepage: www.elsevier.com/locate/neuropharm

The anti-inflammatory agent flufenamic acid depresses store-operated channels by altering mitochondrial calcium homeostasis

Peng Tu [a,b,d], Gérard Brandolin [b,c,d], Alexandre Bouron [a,b,d,*]

[a] UMR CNRS 5249, Grenoble, France
[b] CEA, DSV, IRTSV, Grenoble, France
[c] UMR CNRS 5092, Grenoble, France
[d] Université Joseph Fourier, Grenoble, France

ARTICLE INFO

Article history:
Received 22 May 2008
Received in revised form
13 January 2009
Accepted 12 February 2009

Keywords:
Calcium
Mitochondria
Neurons
TRP channels
HEK-293 cells

ABSTRACT

Fenamates like flufenamic acid (FFA) are anti-inflammatory drugs known to alter ion fluxes through the plasma membrane. They are for instance potent blockers of cation and anion channels, and FFA is now commonly used to block currents through TRP channels and receptor-operated channels. However, FFA exerts complex and multifaceted actions on ion transport systems and, in most instances, a molecular understanding of these FFA-dependent modulations is lacking. In addition, FFA is also to known to perturb the homeostasis of Ca^{2+}. In the present report, we investigated whether the FFA-induced alterations of the Ca^{2+} homeostasis could play a role in the FFA-dependent modulation of transmembrane ion fluxes. Experiments performed with the Ca^{2+} indicator Fluo-4 on cultured cortical neurons and HEK-293 cells showed that FFA increased the cytosolic concentration of Ca^{2+} even in cells kept in a Ca^{2+}-free medium or when the endoplasmic reticulum was depleted with thapsigargin. The FFA-dependent Ca^{2+} responses were, however, strongly reduced by bongkrekic acid, a specific ligand of the mitochondrial ADP/ATP carrier which, in addition, inhibits the permeability transition pore. Like FCCP, FFA released Ca^{2+} from isolated brain mitochondria and indirectly modulates store-operated Ca^{2+} channels. We suggest that some of the effects of FFA on plasma membrane ion channels could be explained, at least partially, by its ability to modulate the mitochondrial Ca^{2+} homeostasis.

1. Introduction

Flufenamic acid (FFA) is a non-steroidal anti-inflammatory agent altering the activity of some ion transport systems. FFA is for instance a potent blocker of anion and cation channels (Cho et al., 2003; Cousin and Motais, 1979; Gogelein et al., 1990; Lee et al., 1996; Shaw et al., 1995). More recently, FFA is becoming a useful pharmacological tool used to block currents through *t*ransient *r*eceptor *p*otential (TRP) channels, a superfamily of cation channels (Hill et al., 2004; Inoue et al., 2001; Naziroglu et al., 2007). But its actions of C-type TRP channels (TRPC) appear complex since FFA blocks currents through TRPC3 and TRPC7 channels whereas it increases currents through native and heterogeneously expressed TRPC6 channels (Inoue et al., 2001; Jung et al., 2002). Interestingly, some TRPC-independent conductances can also be potentiated by FFA (Ottolia and Toro, 1994; Rae and Farrugia, 1992; Wehner et al., 2006; Yamada et al., 1996). On the other hand, FFA has no effect on the Na/K pump activity (Cousin and Motais, 1979). Taken together, these data show that FFA differentially regulates ion transport systems.

Store-operated channels (SOC) are plasma membrane Ca^{2+}-conducting channels activated by emptying the endoplasmic reticulum (ER) Ca^{2+} pool. This store-dependent Ca^{2+} entry not only refills the depleted ER Ca^{2+} stores but is also involved in many cellular processes (Parekh and Putney, 2005). SOC are regulated by Ca^{2+} ions: Ca^{2+} entry through SOC causes a sub-plasma membrane Ca^{2+} accumulation depressing SOC activity (Duszynski et al., 2006). As a consequence, drugs inhibiting the mitochondrial Ca^{2+} uptake or the protonophore carbonyl cyanide 4-(trifluoromethoxy)phenylhydrazone (FCCP) are potent blockers of SOC (Duszynski et al., 2006; Hoth et al., 1997). Therefore, by buffering Ca^{2+} ions near SOC, mitochondria critically control this Ca^{2+}-dependent inactivation process and appear as important physiological regulators of SOC. In the present study we provide experimental evidence showing that FFA (i) releases Ca^{2+} from mitochondria, and (ii) strongly reduces Ca^{2+} entry through SOC.

* Corresponding author. Laboratoire de Chimie et Biologie des Métaux, UMR CNRS 5249, CEA, 17 rue des Martyrs, 38054 Grenoble, France. Tel.: +33 4 38 78 44 23; fax: +33 4 38 78 54 87.
E-mail address: alexandre.bouron@cea.fr (A. Bouron).

0028-3908/$ – see front matter © 2009 Elsevier Ltd. All rights reserved.
doi:10.1016/j.neuropharm.2009.02.004

2. Experimental

2.1. Embryonic cortical cells in primary cultures

Cortical cells were dissociated from cerebral cortices isolated from C57BL6/J mice embryos (vaginal plug was designated E0). Brains were collected in an ice-cold Ca^{2+}- and Mg^{2+}-free Hanks solution supplemented with gentamycin (10 mg/ml) and glucose (6 g/l). Cells were prepared and kept in culture according to a protocol already described (Bouron et al., 2006). All procedures have been approved by the Ethical Committee of Rhône-Alpes Region (France).

2.2. HEK-293 cell lines

Some experiments were carried out on HEK-293 cells (purchased from ATCC, LGC Promochem, France). They were grown in a DMEM medium supplemented with 10% foetal bovine serum and 1% penicillin/streptomycin. The Ca^{2+} imaging experiments (see below) were performed 2 or 3 days after the plating of the HEK-293 cells.

2.3. Calcium imaging experiments on cultured cells with Fluo-4

Cells (HEK-293 cells, neurons) were bathed in a Tyrode solution containing (in mM) NaCl 136, KCl 5, $CaCl_2$ 2, $MgCl_2$ 1, HEPES 10, glucose 10, pH 7.4 (NaOH) and 1.25 μM Fluo-4/AM for 10 min at room temperature. They were washed two times with a Fluo-4/AM-free Tyrode solution, stored 20 min at room temperature and then placed on the stage of an upright Olympus BX51WI microscope equipped with a water immersion 20× objective lens (Olympus, 0.95 NA). The emitted light, provided by a 100 W mercury lamp, was attenuated by a neutral density filter (U-25ND6, Olympus). Fluorescent images were captured by a cooled digital CCD MicroMax Princetown camera (782 × 582 pixels). The software MetaFluor (v4.5, Universal Imaging) was used to acquire the images at a frequency of 0.2 or 0.5 Hz and to analyze off-line the data. The shutter was controlled by the shutter driver Uniblitz VMM-D1 (Vincent Associates). The excitation light for Fluo-4 was filtered through a 460–495 nm excitation filter and the emitted light was collected through a 510–550 nm filter. Solutions were applied via a gravity-driven perfusing system (~2 ml/min). Mean values of Fluo-4 measurements are reported as means ± S.E.M., with *n* being the number of cell bodies tested. All the experiments were performed at room temperature. Throughout this study the amplitude of the FFA-induced Fluo-4 responses were analysed on soma and quantified 300 s after the application of the anti-inflammatory agent.

2.4. Mn^{2+} quench experiments with Fura-2

HEK-293 cells were grown on 16 mm diameter glass cover-slips and incubated in a Tyrode solution supplemented with 2.5 μM Fura-2 for 15 min, washed twice and kept in a Fura-2-free Tyrode solution for 20 min. Coverslips were placed on the stage of an Axio Observer A1 microscope equipped with a Fluar 40× oil immersion objective lens (1.3 NA) (Carl Zeiss, France). Light was provided by the DG-4 wavelength switcher (Princeton Instruments, Roper Scientific, France). Fura-2 loaded cells were excited at 360 nm and emission was collected at 515 nm. The software MetaFluor (Universal Imaging, Roper Scientific, France) was used to acquire the images at a frequency of 0.2 Hz by means of a CoolSnap HQ2 camera (Princeton Instruments, Roper Scientific, France) and to analyze the data off-line. The Fura-2 loading protocol as well as the Mn^{2+} quench experiments were carried out at room temperature.

2.5. Preparation of mouse brain mitochondria

Mitochondria were isolated from brains of 1-day-old neonatal mice according to Chinopoulos et al. (2003). They were collected in an ice-cold Ca^{2+}- and Mg^{2+}-free Hanks solution supplemented with gentamycin (10 mg/ml) and glucose (6 g/l). The brains were transferred to a medium containing (in mM): 75 sucrose, 225 mannitol, 1 EGTA, 10 HEPES, pH 7.4 (KOH). They were homogenized with a Potter homogenizer. The brain tissue homogenate was centrifuged at 1500 × *g* for 5 min at 4 °C. The supernatant was then centrifuged at 12,000 × *g* for 10 min at 4 °C and the pellet was resuspended in the same medium as above but without EGTA. The homogenate was centrifuged at 1500 × *g* for 3 min at 4 °C. The supernatant was then collected and centrifuged at 12,000 × *g* for 10 min at 4 °C. The pellet containing the mitochondria was resuspended in a medium containing (in mM): 5 DL-malic acid, 5 L-glutamic acid, 270 sucrose, 1 KH_2PO_4/K_2HPO_4 (pH 7.4), 10 Tris, pH 7.35 (KOH).

2.6. Calcium flux measurements from isolated mitochondria

Mitochondria were kept at 20–30 mg protein/ml. The protein content was determined by the BCA method using BSA as a standard. The calcium measurement experiments were carried out at 25 °C 1–6 h after the isolation of the organelles. Mitochondrial Ca^{2+} signals were recorded with the membrane impermeant fluorescent Ca^{2+} indicator Fluo-4 by means of a Fluoromax spectrofluorometer (Spex).

2.7. Assessment of mitochondrial membrane potential

The fluorescent cyanine dye 3,3′-dipropylthiodicarbocyanine (diS-C3-(5)) was used to follow the mitochondrial membrane potential (ΔΨ) changes induced upon addition of FFA. Isolated brain mitochondria were incubated in the presence of 10 μM diS-C3-(5). The experiments were carried out on a Fluoromax spectrofluorometer with excitation at 622 nm and emission at 670 nm.

2.8. Materials

Fluo-4/AM, 3,3′-dipropylthiodicarbocyanine (diS-C3-(5)) and Fluo-4 were from Molecular Probes (Interchim, France). Flufenamic acid, 3-(4,5-dimethyl thiazol-2-yl)-2,5-diphenyl tetrazolium bromide (MTT), carbonyl cyanide 4-(trifluoromethoxy)phenylhydrazone (FCCP), dantrolene and thapsigargin were from Sigma–Aldrich (France). All tissue culture media and reagents were obtained from Invitrogen (France).

3. Results

3.1. FFA induces Fluo-4 responses in neurons and HEK-293 cells

The effects of FFA on Ca^{2+} signalling were first tested on Fluo-4-loaded cortical neurons kept 1 day *in vitro* (DIV). In the presence of a Tyrode solution containing 2 mM Ca^{2+}, the external application of 85 μM FFA provoked a modest but clear increase of the Fluo-4 fluorescence, as illustrated in Fig. 1A. The FFA-induced Fluo-4 response had a slow onset and was observed in all cortical cells tested ($n = 394$). This FFA-induced Fluo-4 response was sustained (for at least up to 300 s) and perfectly reversible upon washout of the drug (Fig. 1A). Similar responses were observed on HEK-293 cells (Fig. 1B) showing that FFA could affect the Ca^{2+} homeostasis of murine (cortical neurons) and human (HEK-293 cells) cells. Experiments were carried out with a nominally Ca^{2+}-free medium (instead of the normal Tyrode medium containing 2 mM Ca^{2+}).

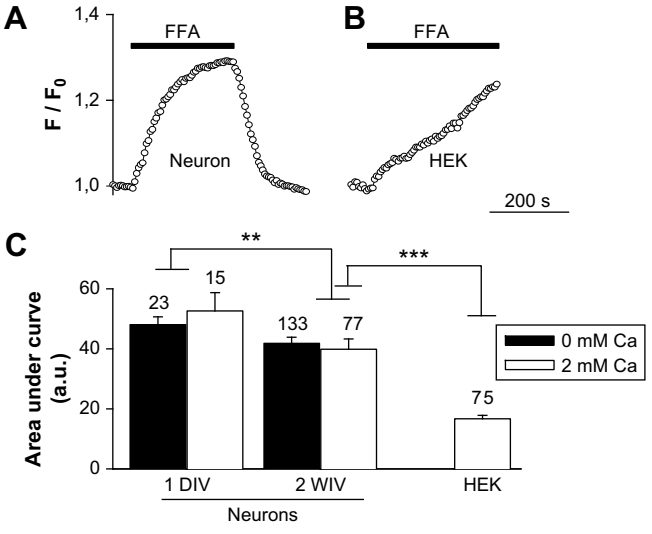

Fig. 1. FFA elicits intracellular Ca^{2+} responses. Representative Fluo-4 signals observed in response to the application of FFA (85 μM) on a neuron kept 1 DIV (A) and a HEK-293 cell (B). These cells were bathed in a normal (2 mM Ca^{2+}) Tyrode solution. The graph shows the time course of the changes of the Fluo-4 fluorescence (F/F_0) as a function of time, with F being the Fluo-4 fluorescence and F_0 the baseline Fluo-4 fluorescence. FFA was added when indicated by the horizontal black bars (A, B) and washed away (A). (C) is a summary graph of experiments performed on cortical neurons kept 1 DIV and 2 weeks in vitro (WIV). The FFA-induced Ca^{2+} signals were quantified by determining, for each cell, the area under the curve. Unless otherwise indicated, only the first 300 s of the recordings were analyzed. FFA was added in a nominally Ca^{2+}-free medium (open bar) or in the presence of 2 mM Ca^{2+} (solid bar). The number of cells tested is indicated for each experimental condition. This graph shows that the FFA-induced Fluo-4 signals were present in immature neurons (i.e. with short and thin processes) as well as in fully morphologically differentiated neurons, regardless of the external concentration of Ca^{2+}.

Under these conditions, FFA was still able to elicit a Fluo-4 response (Fig. 1C), even when the Ca^{2+}-free medium was supplemented with 0.4 mM EGTA (not shown). Cortical neurons kept 2 weeks *in vitro* also exhibited FFA-dependent Fluo-4 responses not influenced by the external concentration of Ca^{2+} (Fig. 1C). On average, 85 μM FFA produced a 20–30% increase of the Fluo-4 fluorescence. The FFA-induced Ca^{2+} signals were quantified by determining, for each cell, the area under the curve. Unless otherwise indicated, only the first 300 s of the recording were analyzed. Under these conditions, the FFA-induced Ca^{2+} signals were of similar amplitude, regardless of the age of the cortical neurons (i.e. after 1 day or 2 weeks in vitro) (Fig. 2C). When compared to neurons, HEK 293 cells displayed weaker FFA-induced Ca^{2+} signals (Fig. 2C). Thus, the FFA-induced Ca^{2+} rise, which occurred either with or without external Ca^{2+}, is most likely due to the release of stored Ca^{2+}. It was observed in HEK-293 cells and in neurons, regardless of their differentiation state (immature or fully morphologically differentiated neurons).

3.2. FFA releases Ca^{2+} from internal stores

The results reported above indicated that FFA did not trigger an entry of Ca^{2+} but rather favoured the release of Ca^{2+} from stores. To gain further insight into the FFA-sensitive Ca^{2+} pool, the following experiments were performed. Cortical neurons were treated with thapsigargin (Tg, 1 μM), a blocker of some intracellular Ca^{2+} pumps before adding FFA (85 μM). Tg-untreated and Tg-treated cells had FFA-induced Fluo-4 responses of similar amplitude (Fig. 2A). In another set of experiments we determined whether ryanodine receptors (RyR), a family of intracellular Ca^{2+} release channels mainly located in the ER, could play a role in the FFA-dependent Fluo-4 responses. At E13, cortical cells express three RyR isoforms with RyR2 being the predominant isoform whereas RyR1 and RyR3 are only weakly expressed (Faure et al., 2001). Surprisingly, when cells were incubated with the RyR inhibitor dantrolene (30 μM), the FFA-induced Fluo-4 responses were of larger amplitude (Fig. 2B). Thus, preventing the release of Ca^{2+} from RyR potentiated the FFA-induced Ca^{2+} responses. Altogether, these experiments showed that depleting (with Tg) or preventing (with dantrolene) the release of Ca^{2+} from the ER did not inhibit the FFA-induced Ca^{2+} signals. This implied that FFA (85 μM) mobilized Ca^{2+} from non ER Ca^{2+} pools. In order to assess the contribution of mitochondria, cells were pre-treated with bongkrekic acid before applying FFA. Bongkrekic acid is a well-known and highly specific ligand of the ADP/ATP carrier which also blocks the mitochondrial permeability transition pore (Kroemer et al., 2007). On average, the maximal amplitude of the FFA-induced Ca^{2+} signal was attenuated by bongkrekic acid by ~50% (Fig. 2B). In another set of experiments, bongkrekic acid was applied when the cells were bathed in a Tyrode solution with a pH of 6.8 because the inhibition of the mitochondrial ADP/ATP carrier is pH dependent (Kemp et al., 1971). Reducing the pH of the bathing solution is known to facilitate the entry of bongkrekic acid (Lauquin and Vignais, 1976). Bongkrekic acid was applied at pH 6.8 and then washed away with the normal Tyrode solution (pH 7.4). A subsequent addition of FFA also elicited Fluo-4 responses but, like at pH 7.4, they were attenuated by only 50% ($n = 62$, $P < 0.05$) (not shown). These latter results indicate that FFA perturbs the mitochondrial Ca^{2+} homeostasis. Fig. 2C is a summary graph showing that thapsigargin and dantrolene failed to inhibit the FFA-induced Ca^{2+} signals whereas they were depressed by bongkrekic acid.

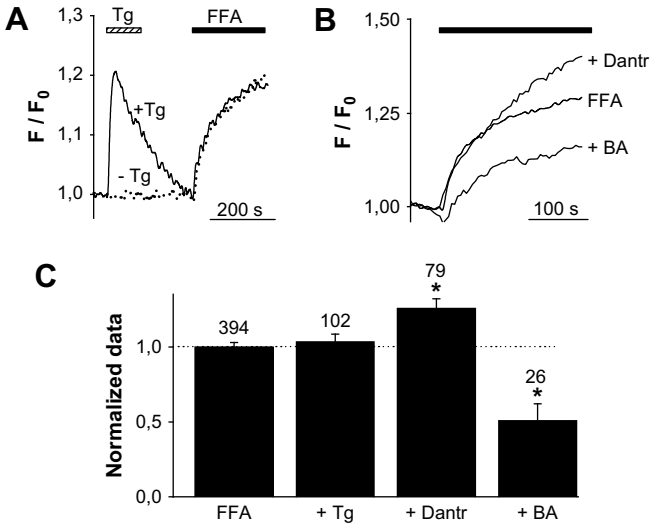

Fig. 2. FFA releases Ca^{2+} from stores. The identity of the FFA-sensitive Ca^{2+} pool was determined according to the protocol illustrated in Fig. 1A. (A) shows representative Fluo-4 signals from two different cortical cells. The external application of thapsigargin (Tg, 1 μM) induced a transient Fluo-4 response due to the passive leakage of Ca^{2+} from Tg-sensitive Ca^{2+} pools. A subsequent application of FFA evoked a Ca^{2+} rise (solid line) as in Tg-untreated cells (dotted line). (B) shows Fluo-4 responses from three cortical cells. FFA (85 μM) was added either alone or on cells pre-treated with dantrolene (30 μM, 20 min at room temperature) or with bongkrekic acid (BA, 48 μM, 40 min at room temperature). (C) is a summary bar graph showing the amplitude of the Fluo-4 responses (normalized data) induced by FFA alone (85 μM) or after one of the following agents: thapsigargin (Tg), bongkrekic acid (BA), and dantrolene (Dantr). The number of cells tested is indicated above each bar. $^*P < 0.001$ (one-way ANOVA followed by a Tukey test). The horizontal bars in A and B indicate when Tg and FFA were present.

3.3. FFA releases Ca^{2+} from mitochondria

To further analyze the actions of FFA, we checked whether it altered the mitochondrial Ca^{2+} handling of isolated brain mitochondria. Previously, we first verified their ability to sequester Ca^{2+}, a sign of functional integrity. The addition of 25 μM Ca^{2+} into the medium provoked a transient fluorescence increase which declined to the basal value (Fig. 3A). This decrease in fluorescence reflected the mitochondrial Ca^{2+} uptake. The addition of the protonophore FCCP, which collapses the mitochondrial Ca^{2+} gradient, produced a large increase in fluorescence reflecting the release of mitochondrial Ca^{2+} which can no longer be taken up by these organelles. Thus, this protonophore gives rise to a sustained extramitochondrial Ca^{2+} response (Ichas et al., 1997). FCCP was also able to release Ca^{2+} from mitochondria even if added without a prepulse of Ca^{2+} (not shown). When applied on cultured cortical neurons, FCCP evoked a robust and long-lasting Ca^{2+} rise (Fig. 3B). This was observed on all cells tested ($n > 50$) showing that mitochondria of embryonic cortical neurons contain FCCP-sensitive Ca^{2+} pools.

We next addressed the question of the action of FFA on mitochondrial Ca^{2+} homeostasis. Experiments similar to that described in Fig. 3A were carried out with FFA. Like FCCP, FFA released Ca^{2+} in a concentration dependent manner from isolated brain mitochondria when added either without (Fig. 3C) or with a prior Ca^{2+} prepulse (not shown). FCCP (1 μM) was applied at the end of each experiment and the FFA-induced mitochondrial Ca^{2+} release was compared to the FCCP-induced Ca^{2+} signal. Fig. 3D is a dose–response curve showing that FFA triggers the release of Ca^{2+} from isolated mitochondria with an EC_{50} of 18 μM. This FFA-induced mitochondrial Ca^{2+} release was reduced by bongkrekic acid and cyclosporin A by ~20% ($n = 3$) and ~50% ($n = 4$), respectively (Fig. 3E) but was potentiated by dantrolene (1 μM) ($n = 3$). The fluorescent cyanine dye diS-C3-(5) was used to determine the effect of FFA on the mitochondrial membrane potential. Similarly to FCCP, FFA (17 μM) elicited a rapid increase in diS-C3-(5) fluorescence,

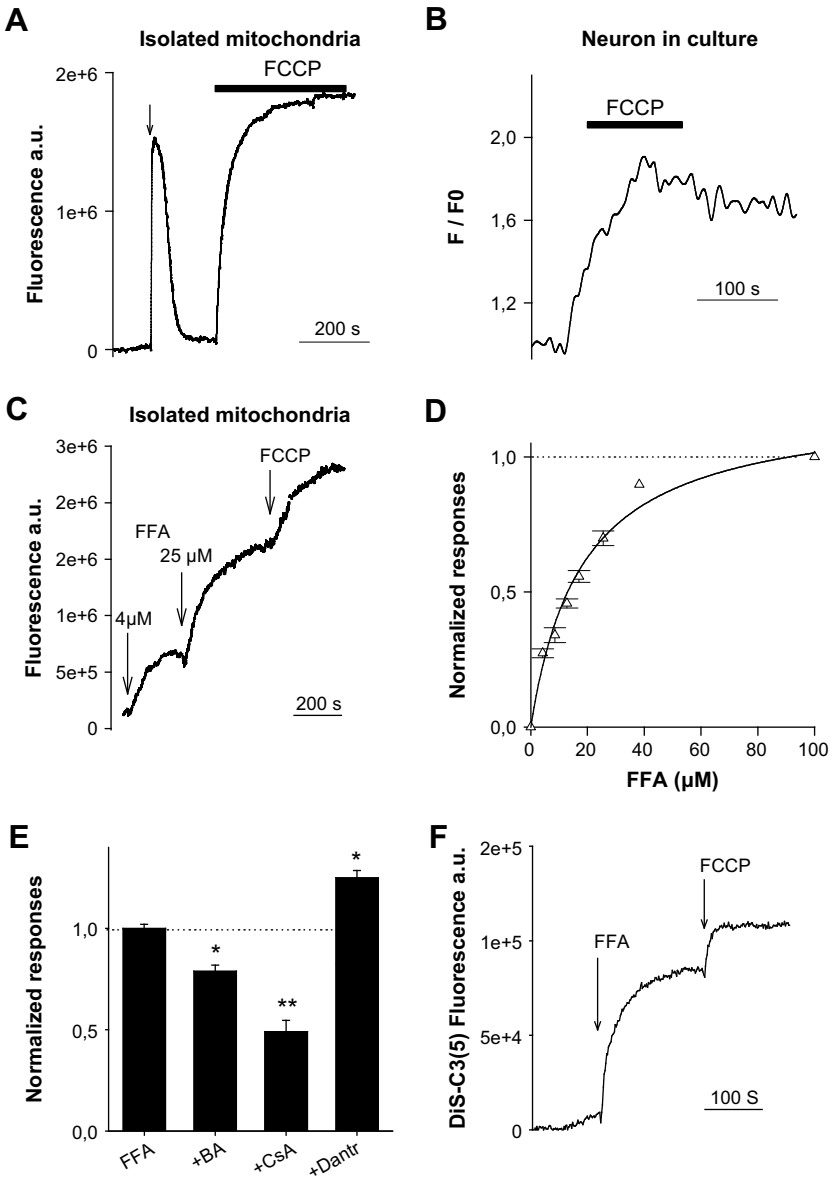

Fig. 3. FFA releases Ca^{2+} from isolated mitochondria. Isolated mitochondria were prepared from whole brains. (A) shows the changes in fluorescence (in arbitrary unit) as a function of time. Mitochondria were first loaded with Ca^{2+} (arrow, 25 µM $CaCl_2$). (A) The addition of Ca^{2+} gives rise to a transient response: the concentration of Ca^{2+} in the extra-mitochondrial compartment first increases (due to the $CaCl_2$ challenge) and then decreases (which reflects the mitochondrial Ca^{2+} uptake). FCCP (0.6 µM) was added as indicated by the horizontal black bar after the completion of the Ca^{2+} uptake. (B) Similar experiments were conducted on Fluo-4 loaded cortical neurons in culture but in this case no $CaCl_2$ challenge was applied before the addition of FCCP (2 µM). The external application of the protonophore (indicated by the horizontal black bar) provoked a robust Fluo-4 signal that slowly declined to basal value upon washing of the protonophore. (C) Like FCCP, FFA triggered the release of Ca^{2+} from isolated mitochondria. The figure shows a representative trace with 4 and 25 µM FFA. FCCP (1 µM) was applied at the end of each experiment and the FFA-induced mitochondrial Ca^{2+} release was compared to the FCCP-induced Ca^{2+} signal (normalized values). (D) is a dose–response curve showing that FFA triggers the release of Ca^{2+} from isolated mitochondria (EC_{50} 18 µM). Three to ten experiments were performed for each concentration of FFA. Mean ± S.E.M. (E) is a summary graph showing the effect of bongkrekic acid (BA, 40 µM), cyclosporin A (CsA, 5 µM) and dantrolene (1 µM) on the FFA-induced mitochondrial Ca^{2+} release (normalized data). Mean ± S.E.M. from at least three experiments. $^{*}P < 0.05$ and $^{**}P < 0.01$, respectively (one-way ANOVA followed by a Tukey test). (F) The effect of FFA on the mitochondrial membrane potential was assessed by means of the fluorescent cyanine dye 3,3′-dipropylthiodicarbocyanine (diS-C3-(5)). Similarly to FCCP, the addition of FFA (17 µM) caused a rapid increase in diS-C3-(5) fluorescence which indicates that FFA produced a collapse of the mitochondrial membrane potential.

showing that it caused a collapse of the mitochondrial membrane potential ($\Delta\Psi$) (Fig. 3F). Collectively, our experiments show that FFA, like FCCP, causes a collapse of $\Delta\Psi$ and releases Ca^{2+} from embryonic cortical neurons as well as from isolated brain mitochondria.

3.4. FFA indirectly blocks store-operated channels

Mitochondria play important roles in regulating Ca^{2+} signalling. Due to their close proximity with the ER, they influence ER Ca^{2+} signals and function as efficient Ca^{2+} buffers (Pizzo and Pozzan, 2007). In addition, mitochondria can shape plasma membrane Ca^{2+} signals. By buffering Ca^{2+} ions near SOC, mitochondria regulate SOC activity and are therefore physiological regulators of these channels (Duszynski et al., 2006; Hoth et al., 1997). To further characterize the action of FFA on Ca^{2+} signalling, we verified whether it could influence SOC responses. This was performed on HEK-293 cells. To this aim, thapsigargin (Tg, 1 µM), applied in the presence of a nominally Ca^{2+}-free medium, was used to empty the ER. The re-admission of Ca^{2+} was followed by a large Ca^{2+} influx through SOC

($n = 120$ cells) (Fig. 4A). The same experiments were carried out with the protonophore FCCP (0.5 μM) which disrupts the mitochondrial membrane potential. The Tg-activated Ca^{2+} release was reduced by nearly 50% ($n = 66$ cells, $P < 0.05$) when compared to FCCP-untreated cells (Fig. 4B). In addition, FCCP-treated cells had a smaller depletion-activated Ca^{2+} entry (Fig. 4C). This is in agreement with previous studies showing that FCCP depresses SOC by altering mitochondrial functions (Glitsch et al., 2002; Hoth et al., 1997). Similar experiments were then performed with FFA. Under these conditions, the amplitude of the Tg-activated Ca^{2+} release was also diminished by ~55% ($n = 54$ cells, $P < 0.05$) when compared to FFA-untreated cells (Fig. 4B). Like FCCP, FFA reduced the amplitude of the Fluo-4 signals observed in response to the re-admission of Ca^{2+} by 70–80% ($n = 54$ cells, $P < 0.05$) (Fig. 4C). To look for a direct effect of FFA on SOC, Mn^{2+} quench experiments were carried out. Cells were loaded with the fluorescent dye Fura-2 and treated as described in Fig. 4A. Mn^{2+}(100 μM) was used as a surrogate of Ca^{2+}. Its entry into cells via plasma membrane Ca^{2+} channels causes a quench of the Fura-2 fluorescence. If FFA exerts a direct inhibitory action on SOC, it should prevent the quenching of the Fura-2 fluorescence by Mn^{2+}. The results of these experiments are shown in Fig. 4D. Thisindicates that FFA weakly blocked SOC. Similar experiments were repeated with La^{3+}, instead of FFA. La^{3+} ions are potent blockers of SOC and, in contrast to FFA, completely prevented the entry of Mn^{2+}. These results indicate that the inhibitory action exerted by FFA on the Tg-activated Ca^{2+} entry cannot be explained by a direct blockade of the SOC. In conclusion, these data show that, like FCCP, FFA exerts a negative regulation on SOC. We propose that the FFA-induced inhibition of SOC most likely reflects its ability to alter the mitochondrial Ca^{2+} homeostasis.

4. Discussion

Fenamates like FFA, niflumic acid or meclofenamic acid are non-steroidal anti-inflammatory agents known to potently block plasma membrane ion channels and gap junctions. However, they cannot be described as unspecific blockers of ion fluxes because they exert a wide diversity of actions on ion transport systems. For instance, niflumic acid or FFA potentiates currents through some anion (Picollo et al., 2007) and cation (Ottolia and Toro, 1994; Rae and Farrugia, 1992; Yamada et al., 1996) channels. In fact, the effects of these anti-inflammatory agents on channel-mediated ion transport systems appear rather complex, which can be further illustrated by their actions on the hypertonicity-induced cation channels (HICC) and on the Ca^{2+}-conducting TRPC channels. Two major groups of HICC have been identified. The first one, blocked by amiloride, comprises FFA-insensitive channels whereas the second group contains FFA-sensitive and amiloride-insensitive HICC (Wehner

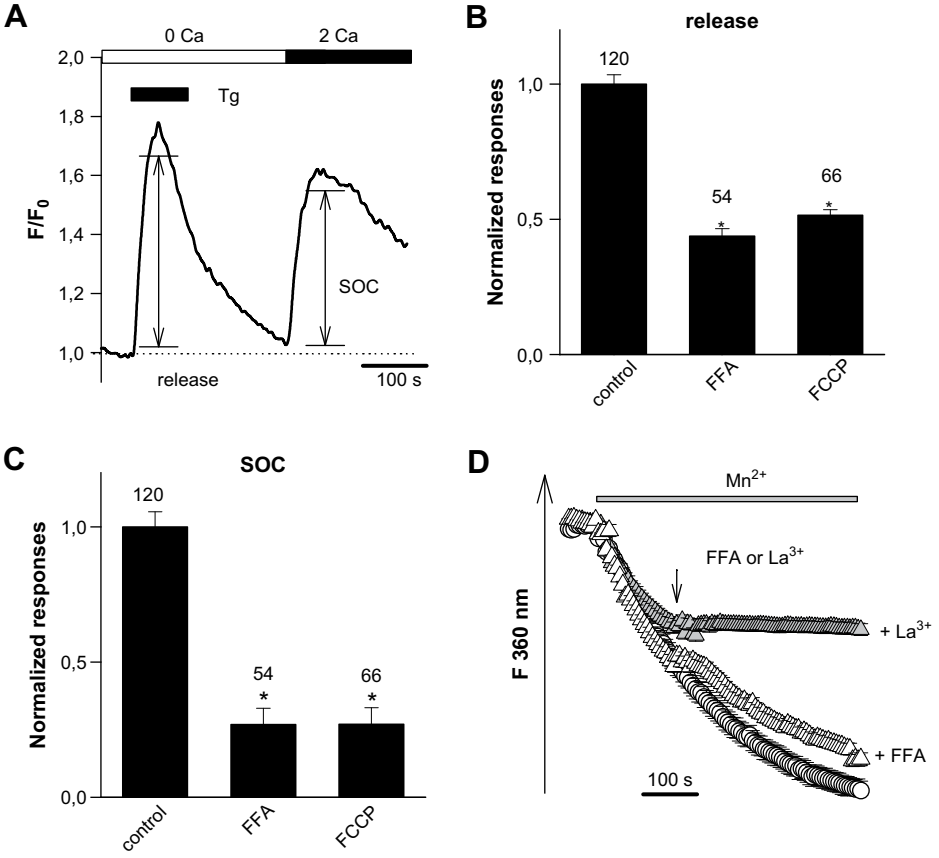

Fig. 4. FFA indirectly blocks store-operated Ca^{2+} channels. (A) shows a representative recording illustrating the change in fluorescence (F/F_0) from a Fluo-4 loaded HEK-293 cell as a function of time. The cell was first kept in a nominally Ca^{2+}-free medium. The addition of thapsigargin (Tg, 2 μM) was followed by a transient Ca^{2+} rise due to the passive release of Ca^{2+} from Tg-sensitive Ca^{2+} pools. A second Ca^{2+} rise (due to the Ca^{2+} entry through SOC) was seen upon the re-admission of 2 mM Ca^{2+} in the external medium (control). Some cells were pre-treated with FFA (85 μM, 5 min at room temperature) or FCCP (0.5 μM, 5 min at room temperature) before the beginning of the recording. Both drugs reduced the Tg-activated release (B) and entry (C) of Ca^{2+}. FFA or FCCP were maintained in the milieu during the recording. The horizontal bars indicated when Tg and Ca^{2+} were present. (B) and (C) are summary bar graphs showing the normalized Tg-dependent release of Ca^{2+} and the normalized SOC responses from control cells (FFA-untreated and FCCP-untreated), FFA-treated cells and FCCP-treated cells. The total number of HEK-293 cells used is indicated above each bar. *$P < 0.01$, Student's t-test. (D). Fura-2 loaded HEK-293 cells were kept in Ca^{2+}-free medium and treated with 1 μM Tg for 5 min to deplete the internal Ca^{2+} stores. Tg was washed away prior to the beginning of the recording. The addition of 100 μM Mn^{2+} was followed by a quench of the Fura-2 fluorescence (excitation at 360 nm). The arrow indicates when FFA (85 μM, $n = 22$) or La^{3+} (100 μM, $n = 24$) was added into the recording medium (Mean ± S.E.M.). In contrast to the SOC inhibitor La^{3+}, which completely prevented the Mn^{2+} quench, FFA poorly affected the entry of Mn^{2+}.

et al., 2006). FFA blocks current through TRPC3 and TRPC7 but increases currents through native and heterogeneously expressed TRPC6 channels (Inoue et al., 2001; Jung et al., 2002). Moreover, FFA can even differentially regulate distinct cation channels expressed within the same cell type. For instance, in rat cerebellar neurons, it produces a bidirectional modulation of the transient outward potassium currents (I_A): at 0.1–10 μM, FFA increases I_A whereas it reversibly decreases it at 50–1000 μM but augments the amplitude of the current through delayed rectifier potassium channels (I_K) (Shimamura et al., 2002; Zhao et al., 2007). On the other hand, kainate receptors (White and Aylwin, 1990) and the Na/K pump (Cousin and Motais, 1979) are not affected by FFA. Taken together, these results show the complex and multifaceted action of fenamates on transmembrane ion fluxes. In most instances, a molecular understanding of these distinct FFA-dependent modulations of ion transport systems is lacking.

The FFA-induced cellular responses are far from being limited to the plasma membrane. In addition to their well-known inhibition of cyclo-oxygenases, fenamates can alter calcium signalling. The present report clearly shows that, in neurons and HEK-293 cells, FFA elevates the cytosolic free Ca^{2+} concentration by releasing Ca^{2+} from Tg-insensitive internal Ca^{2+} stores. This effect is fully reversible upon washout of the drug. Based on the experiments performed on isolated brain mitochondria we conclude that FFA promotes the release of Ca^{2+} from these organelles and not from the ER. Previous works showed that FFA or related compounds release stored Ca^{2+} in many cell types like the mandibular cell line ST_{885}, parotid secretory cells, mandibular secretory cells, parathyroid cells, unfertilized oocytes, cultured insulinoma (RINm5F), cardiac myocytes (Poronnik et al., 1992) and smooth muscle cells (Cruickshank et al., 2003). In neurons, fenamates influence the homeostasis of Ca^{2+} by releasing Ca^{2+} from Tg-sensitive compartments in molluscan neurons (Lee et al., 1996; Shaw et al., 1995) and from Tg-insensitive Ca^{2+} compartments in hippocampal (Partridge and Valenzuela, 1999) and cortical neurons (present study).

We provide experimental evidence for a FFA-induced alteration of the mitochondrial Ca^{2+} homeostasis in neurons of the central nervous system. This response is highly relevant since it occurs at a concentration (85 μM) lower than that commonly used to inhibit TRPM2, TRPC and receptor-operated channels ($\geq$100 μM). The release of Ca^{2+} triggered by FFA was attenuated by bongkrekic acid, a specific inhibitor of the ADP/ATP carrier known to block the mitochondrial permeability transition pore (Kroemer et al., 2007). Moreover, in isolated mitochondria the FFA-induced Ca^{2+} release was partially reduced by cyclosporin A, which acts on cyclophylin D, another putative key element of the mitochondrial permeability transition pore (Kroemer et al., 2007). The effect of cyclosporin A appears modest but is in line with a previous study showing that the mitochondrial permeability transition is poorly affected by cyclosporine A in brain mitochondria (Chinopoulos et al., 2003). Our data suggest that FFA promotes the release of Ca^{2+} by altering the function and/or the integrity of the mitochondrial permeability transition pore complex. The mitochondrial permeability transition is defined as a sudden increase of the permeability of the inner mitochondrial membrane. By allowing the release of small solutes and molecules having a molecular mass of $<$1.5 kDa it can exert a pro-apoptotic action (Kroemer et al., 2007). Our results on central nervous system neurons support the view that the main effect of FFA on cellular Ca^{2+} homeostasis resides in its ability to uncouple mitochondria and to alter mitochondrial Ca^{2+} fluxes (Jordani et al., 2000; McDougall et al., 1988).

In cultured cells like in isolated mitochondria, the ryanodine receptor antagonist dantrolene enhances the release of Ca^{2+} induced by FFA. Several authors have reported the existence of mitochondrial ryanodine receptors (Altschafl et al., 2007; Brookes et al., 2004). Although we do not have any evidence for the presence of mitochondrial ryanodine receptors in cortical neurons from mice, our data could support the presence of these Ca^{2+}channels in brain tissue.

Mitochondria can buffer Ca^{2+} entering through the plasma membrane whether this entry occurs via the Na^+/Ca^{2+} exchanger (Poburko et al., 2006) or via channels like voltage-gated Ca^{2+} channels (Greenwood et al., 1997) or SOC (Hoth et al., 1997). Therefore, by controlling transmembrane Ca^{2+} fluxes mitochondria are physiological regulators shaping Ca^{2+} signals (Pizzo and Pozzan, 2007). Like many, if not all, Ca^{2+}-channels, SOC exhibit a Ca^{2+}-inactivation process: the accumulation of Ca^{2+} in the close vicinity of the pore exerts a negative feedback regulatory control on channel activity. Inhibiting the Ca^{2+} buffering capacity of mitochondria depresses Ca^{2+} entry through SOC (Duszynski et al., 2006). For instance, the protonophore FCCP indirectly inhibits Ca^{2+} entry through SOC by altering the mitochondrial Ca^{2+} handling (Glitsch et al., 2002; Hoth et al., 1997). Like FCCP, FFA is a potent inhibitor of SOC in HEK-293 cells (present report) and in human polymorphonuclear leukocytes (Kankaanranta and Moilanen, 1995). Due to their ability to accumulate Ca^{2+} at restricted microdomains exhibiting a high spatio-temporal free Ca^{2+} concentration (like near Ca^{2+} release sites or Ca^{2+}-conducting channels), mitochondria critically shape in size and duration intracellular Ca^{2+} signals (Pizzo and Pozzan, 2007). FFA reduces the size of the Tg-sensitive Ca^{2+} pool (Fig. 4). Although a direct inhibitory effect of FFA on the "leak" Ca^{2+} channels of the ER cannot be excluded, the reduced Ca^{2+} pool resulting from the inhibition of the mitochondrial Ca^{2+} handling with FFA underscores the role of these organelles in maintaining the filling state of the ER. Indeed, part of the Ca^{2+} captured by mitochondria is recycled back to the ER (Arnaudeau et al., 2001). Mitochondria are thus essential for the maintenance of Ca^{2+} entry through SOC (Duszynski et al., 2006; Pizzo and Pozzan, 2007) and for the Ca^{2+} refilling of the ER (Malli et al., 2005).

In summary, our data shed new light on the cellular actions of fenamates. FFA, commonly used to block TRPM, TRPC and receptor-operated channels, alters Ca^{2+} homeostasis by releasing Ca^{2+} from Tg-insensitive internal stores. The experiments carried out on isolated brain mitochondria showed that FFA triggers the release of Ca^{2+} from these organelles and not from the ER. Furthermore, our data indicate that the FFA-induced inhibition of SOC is due to its ability to perturb the mitochondrial Ca^{2+} homeostasis. Previous studies reported that FFA differentially regulates TRPC channels since it blocks currents through TRPC3 or TRPC7 and potentiates currents through TRPC6 channels (Inoue et al., 2001; Jung et al., 2002). Although FFA can directly act on some plasma membrane channels as shown with electrophysiological experiments performed with the cell-excised membrane patch method (Gogelein et al., 1990), we propose that the FFA-induced alteration of the mitochondrial Ca^{2+} homeostasis could explain, at least partially, some of the effects of this anti-inflammatory agent on plasma membrane channels.

Acknowledgement

This work was supported by a grant from l'Agence Nationale de la Recherche (ANR-SEST-2006).

References

Altschafl, B.A., Beutner, G., Sharma, V.K., Sheu, S.S., Valdivia, H.H., 2007. The mitochondrial ryanodine receptor in rat heart: a pharmaco-kinetic profile. Biochim. Biophys. Acta 1768, 1784–1795.

Arnaudeau, S., Kelley, W.L., Walsh Jr., J.V., Demaurex, N., 2001. Mitochondria recycle Ca(2+) to the endoplasmic reticulum and prevent the depletion of neighboring endoplasmic reticulum regions. J. Biol. Chem. 276, 29430–29439.

Bouron, A., Boisseau, S., De Waard, M., Peris, L., 2006. Differential down-regulation of voltage-gated calcium channel currents by glutamate and BDNF in embryonic cortical neurons. Eur. J. Neurosci 24, 699–708.
Brookes, P.S., Yoon, Y., Robotham, J.L., Anders, M.W., Sheu, S.S., 2004. Calcium, ATP, and ROS: a mitochondrial love-hate triangle. Am. J. Physiol. Cell Physiol 287, C817–833.
Chinopoulos, C., Starkov, A.A., Fiskum, G., 2003. Cyclosporin A-insensitive permeability transition in brain mitochondria: inhibition by 2-aminoethoxydiphenyl borate. J. Biol. Chem. 278, 27382–27389.
Cho, H., Kim, M.S., Shim, W.S., Yang, Y.D., Koo, J., Oh, U., 2003. Calcium-activated cationic channel in rat sensory neurons. Eur. J. Neurosci 17, 2630–2638.
Cousin, J.L., Motais, R., 1979. Inhibition of anion permeability by amphiphilic compounds in human red cell: evidence for an interaction of niflumic acid with the band 3 protein. J. Membr. Biol. 46, 125–153.
Cruickshank, S.F., Baxter, L.M., Drummond, R.M., 2003. The Cl(−) channel blocker niflumic acid releases Ca(2+) from an intracellular store in rat pulmonary artery smooth muscle cells. Br. J. Pharmacol 140, 1442–1450.
Duszynski, J., Koziel, R., Brutkowski, W., Szczepanowska, J., Zablocki, K., 2006. The regulatory role of mitochondria in capacitative calcium entry. Biochim. Biophys. Acta 1757, 380–387.
Faure, A.V., Grunwald, D., Moutin, M.J., Hilly, M., Mauger, J.P., Marty, I., De Waard, M., Villaz, M., Albrieux, M., 2001. Developmental expression of the calcium release channels during early neurogenesis of the mouse cerebral cortex. Eur. J. Neurosci 14, 1613–1622.
Glitsch, M.D., Bakowski, D., Parekh, A.B., 2002. Store-operated Ca2+ entry depends on mitochondrial Ca2+ uptake. EMBO J 21, 6744–6754.
Gogelein, H., Dahlem, D., Englert, H.C., Lang, H.J., 1990. Flufenamic acid, mefenamic acid and niflumic acid inhibit single nonselective cation channels in the rat exocrine pancreas. FEBS Lett. 268, 79–82.
Greenwood, I.A., Helliwell, R.M., Large, W.A., 1997. Modulation of Ca(2+)-activated Cl− currents in rabbit portal vein smooth muscle by an inhibitor of mitochondrial Ca2+ uptake. J. Physiol 505 (Pt 1), 53–64.
Hill, K., Benham, C.D., McNulty, S., Randall, A.D., 2004. Flufenamic acid is a pH-dependent antagonist of TRPM2 channels. Neuropharmacology 47, 450–460.
Hoth, M., Fanger, C.M., Lewis, R.S., 1997. Mitochondrial regulation of store-operated calcium signaling in T lymphocytes. J. Cell Biol. 137, 633–648.
Ichas, F., Jouaville, L.S., Mazat, J.P., 1997. Mitochondria are excitable organelles capable of generating and conveying electrical and calcium signals. Cell 89, 1145–1153.
Inoue, R., Okada, T., Onoue, H., Hara, Y., Shimizu, S., Naitoh, S., Ito, Y., Mori, Y., 2001. The transient receptor potential protein homologue TRP6 is the essential component of vascular {{alpha}}1-adrenoceptor-activated Ca2+-permeable cation channel. Circ. Res. 88, 325–332.
Jordani, M.C., Santos, A.C., Prado, I.M., Uyemura, S.A., Curti, C., 2000. Flufenamic acid as an inducer of mitochondrial permeability transition. Mol. Cell. Biochem 210, 153–158.
Jung, S., Strotmann, R., Schultz, G., Plant, T.D., 2002. TRPC6 is a candidate channel involved in receptor-stimulated cation currents in A7r5 smooth muscle cells. Am. J. Physiol. Cell Physiol 282, C347–359.
Kankaanranta, H., Moilanen, E., 1995. Flufenamic and tolfenamic acids inhibit calcium influx in human polymorphonuclear leukocytes. Mol. Pharmacol 47, 1006–1013.
Kemp, A.J., Souverijn, J.H.M., Out, T.A., 1971. Energy Transduction in Respiration and Photosynthesis. Adriatica Editrice, Bari, Italy, pp. 959–969.
Kroemer, G., Galluzzi, L., Brenner, C., 2007. Mitochondrial membrane permeabilization in cell death. Physiol. Rev. 87, 99–163.
Lauquin, G.J., Vignais, P.V., 1976. Interaction of (3H) bongkrekic acid with the mitochondrial adenine nucleotide translocator. Biochemistry 15, 2316–2322.
Lee, R.J., Shaw, T., Sandquist, M., Partridge, L.D., 1996. Mechanism of action of the non-steroidal anti-inflammatory drug flufenamate on [Ca2+]i and Ca(2+)-activated currents in neurons. Cell Calcium 19, 431–438.
Malli, R., Frieden, M., Trenker, M., Graier, W.F., 2005. The role of mitochondria for Ca2+ refilling of the endoplasmic reticulum. J. Biol. Chem. 280, 12114–12122.
McDougall, P., Markham, A., Cameron, I., Sweetman, A.J., 1988. Action of the nonsteroidal anti-inflammatory agent, flufenamic acid, on calcium movements in isolated mitochondria. Biochem. Pharmacol 37, 1327–1330.
Naziroglu, M., Luckhoff, A., Jungling, E., 2007. Antagonist effect of flufenamic acid on TRPM2 cation channels activated by hydrogen peroxide. Cell Biochem. Funct 25, 383–387.
Ottolia, M., Toro, L., 1994. Potentiation of large conductance KCa channels by niflumic, flufenamic, and mefenamic acids. Biophys. J. 67, 2272–2279.
Parekh, A.B., Putney Jr., J.W., 2005. Store-operated calcium channels. Physiol. Rev. 85, 757–810.
Partridge, L.D., Valenzuela, C.F., 1999. Ca2+ store-dependent potentiation of Ca2+-activated non-selective cation channels in rat hippocampal neurones in vitro. J. Physiol. 521 Pt 3, 617–627.
Picollo, A., Liantonio, A., Babini, E., Camerino, D.C., Pusch, M., 2007. Mechanism of interaction of niflumic acid with heterologously expressed kidney CLC-K chloride channels. J. Membr. Biol. 216, 73–82.
Pizzo, P., Pozzan, T., 2007. Mitochondria-endoplasmic reticulum choreography: structure and signaling dynamics. Trends Cell Biol. 17, 511–517.
Poburko, D., Potter, K., van Breemen, E., Fameli, N., Liao, C.H., Basset, O., Ruegg, U.T., van Breemen, C., 2006. Mitochondria buffer NCX-mediated Ca2+-entry and limit its diffusion into vascular smooth muscle cells. Cell Calcium 40, 359–371.
Poronnik, P., Ward, M.C., Cook, D.I., 1992. Intracellular Ca2+ release by flufenamic acid and other blockers of the non-selective cation channel. FEBS Lett. 296, 245–248.
Rae, J.L., Farrugia, G., 1992. Whole-cell potassium current in rabbit corneal epithelium activated by fenamates. J. Membr. Biol. 129, 81–97.
Shaw, T., Lee, R.J., Partridge, L.D., 1995. Action of diphenylamine carboxylate derivatives, a family of non-steroidal anti-inflammatory drugs, on [Ca2+]i and Ca(2+)-activated channels in neurons. Neurosci. Lett. 190, 121–124.
Shimamura, K., Zhou, M., Ito, Y., Kimura, S., Zou, L.B., Sekiguchi, F., Kitramura, K., Sunano, S., 2002. Effects of flufenamic acid on smooth muscle of the carotid artery isolated from spontaneously hypertensive rats. J. Smooth Muscle Res. 38, 39–50.
Wehner, F., Bondarava, M., ter Veld, F., Endl, E., Nurnberger, H.R., Li, T., 2006. Hypertonicity-induced cation channels. Acta Physiol 187, 21–25 (Oxf.).
White, M.M., Aylwin, M., 1990. Niflumic and flufenamic acids are potent reversible blockers of Ca2(+)-activated Cl− channels in Xenopus oocytes. Mol. Pharmacol 37, 720–724.
Yamada, K., Waniishi, Y., Inoue, R., Ito, Y., 1996. Fenamates potentiate the alpha 1-adrenoceptor-activated nonselective cation channels in rabbit portal vein smooth muscle. Jpn J. Pharmacol 70, 81–84.
Zhao, Z.G., Zhang, M., Zeng, X.M., Fei, X.W., Liu, L.Y., Zhang, Z.H., Mei, Y.A., 2007. Flufenamic acid bi-directionally modulates the transient outward K(+) current in rat cerebellar granule cells. J. Pharmacol. Exp. Ther 322, 195–204.

10.3 Discussion

Our results show that FFA increases $[Ca^{2+}]_i$ in both HEK cells and cortical neurons. These Ca^{2+} responses are unaffected by depleting the ER or by preventing the Ca^{2+} release from the ER. However, they are strongly reduced by bongkrekic acid, a specific ligand of the mitochondrial ADP/ATP carrier known to inhibit mitochondrial PTP. Experiments on isolated mouse brain mitochondria indicate that FFA promotes the release of Ca^{2+} from mitochondria in a dose-dependent manner and that it collapses $\Delta\psi_m$. Furthermore, incubation with FFA but not acute application of FFA inhibits SOC. This latter result raises the possibility that the modulation of plasma membrane ion channels by FFA is partially due to its action on mitochondrial Ca^{2+} homeostasis.

FFA releases Ca^{2+} from mitochondria

FFA has various actions on mitochondria. It is an inhibitor of the mitochondrial ATPase (Chatterjee and Stefanovich, 1976), an uncoupler of the mitochondrial oxidative phosphorylation (McDougall et al., 1983), an inducer of the mitochondrial permeability transition (Jordani et al., 2000), and it releases Ca^{2+} from these organelles (McDougall et al., 1988; Jordani et al., 2000). Along the same line, we confirm that FFA promotes the release of Ca^{2+} from isolated brain mitochondria.

On the other hand, the FFA-induced Fluo-4 responses are sustained even when the cells maintained in a Ca^{2+}-free Tyrode's solution. The amplitude of the FFA-induced Fluo-4 responses are unaffected by the external concentration of Ca^{2+} (article 2, Section 10.2, Fig. 1C), suggesting that FFA may also prevent the efflux of Ca^{2+} as reported by previous authors (Poronnik et al., 1992; Shaw et al., 1995).

Taken together, FFA collapses $\Delta\psi_m$, promotes mitochondrial Ca^{2+} release and inhibits mitochondrial Ca^{2+} uptake. Meanwhile it may also block the efflux of Ca^{2+} at the plasma membrane. These actions account for the sustained $[Ca^{2+}]_i$ increase in the presence of FFA.

The FFA-dependent modulation of plasma membrane ion channels may reflect its actions on mitochondria

Mitochondria are in close proximity to the plasma membrane and internal Ca^{2+} channels. They play an important role in buffering cytosolic Ca^{2+} (Rizzuto et al., 2000; Carafoli, 2003). Plasma membrane ion channels including SOC, VGCC, TRP channels, Ca^{2+}-activated K^+ and Cl^- channels are regulated by mitochondria (Poburko et al., 2004; Chalmers

et al., 2007; Demaurex et al., 2009). For example, Ca^{2+} buffering by mitochondria reduces Ca^{2+}-dependent inactivation of SOC (Duszynski et al., 2006) and VGCC (Sanchez et al., 2001); mitochondrial buffering of Ca^{2+} that enters via VGCC regulates negatively the activation of Ca^{2+}-sensitive K^+ (Cheranov and Jaggar, 2004) and Cl^- channels (Greenwood et al., 1997). Since FFA has various actions on mitochondria, its inhibitory and excitatory actions on ion channel currents (Table 10-1) may be exerted, at least partially, via mitochondria. In article 2 (Section 10.2) we show that FFA inhibits SOC. The inhibition is probably not due to a direct interaction between the drug and the channels. Similarly the protonophore carbonyl cyanide 4-(trifluoromethoxy)phenylhydrazone (FCCP) inhibits Ca^{2+} entry through SOC by altering mitochondrial handling (Hoth et al., 1997; Glitsch et al., 2002).

The activation of some TRP channels can induce mitochondrial Na^+ and Ca^{2+} overload (Yang et al., 2006; Hacker and Medler, 2008; Medvedeva et al., 2008), meanwhile, some TRP channels are regulated by mitochondria (Agam et al., 2000; Perraud et al., 2005; Kim et al., 2007). For instance, depleting ATP from mitochondria with mitochondrial uncouplers activates *Drosophila* TRP and TRPL channels (Agam et al., 2000); accumulation of cytosolic ADP-ribose released from mitochondria is required for oxidative- and nitrosative-stress-induced gating of TRPM2 channels(Perraud et al., 2005); $\Delta\psi_m$ and the F_1/F_0-ATP synthase of mitochondria play an important role in regulating the activity of TRPM7 channels (Kim et al., 2007). As mentioned above (Section 8.3.4), the modulation of TRPC6 channels by FFA are noted in HEK-TRPC6 cells. The presence of FFA not only potentiates the OAG-induced Fluo-4 signals but also changes their kinetic patterns (Figure 8-4). Indeed, the Fluo-4 signals in the presence of OAG + FFA (Figure 8-4A, ▼ and ▽) are long-lasting, whereas OAG alone triggers oscillatory Ca^{2+} responses (Figure 8-4A, ● and ○). The suppression of the Ca^{2+} oscillations by FFA suggests that mitochondria are involved in these responses. It could also be envisaged that the suppression is due to the FFA-dependent inhibition of the Ca^{2+} efflux mechanisms (Poronnik et al., 1992; Shaw et al., 1995). In order to gain more information on the role played by mitochondria in DAG-sensitive Ca^{2+} responses, it would be interesting to carry out simultaneous measurements of $[Ca^{2+}]_i$/whole cell currents and mitochondrial concentration of calcium ($[Ca^{2+}]_m$) as done previously by different authors (Collins et al., 2001; Gerasimenko and Tepikin, 2005; Young et al., 2008). These latter studies reveal a crosstalk between $[Ca^{2+}]_i$ and $[Ca^{2+}]_m$.

Thus, the fact that FFA acts on mitochondria needs to be kept in mind when interpreting its actions on channels.

11 The TRPC6 channel activator hyperforin releases zinc and calcium from mitochondria

11.1 Introduction

As hyperforin, the major active constituent of *Hypericum perforatum* (St. John's wort) extract, can activate TRPC6 channels without activating the other TRPC isoforms (Leuner et al., 2007), we have used this agent to characterize the DAG-sensitive calcium channels of cortical neurons (article 1, section 8.2). Besides its effect on TRPC6 channels (Treiber et al., 2005; Leuner et al., 2007), hyperforin blocks a wide range of ion channels, including voltage-gated (Ca^{2+}, Na^{+} and K^{+}) (Chatterjee et al., 1999; Fisunov et al., 2000) and ligand-gated (GABA, NMDA, AMPA) channels (Chatterjee et al., 1999; Kumar et al., 2006).

Interestingly, hyperforin increases $[Ca^{2+}]_i$ by mobilizing Ca^{2+} from internal stores (Koch and Chatterjee, 2001; Feisst and Werz, 2004). It can also abolish the GPCR activation-induced liberation of Ca^{2+} from the ER (Feisst and Werz, 2004). Along the same line, we found that in cortical neurons, the addition of Gd^{3+}, a potent blocker of TRPC channels, reduced but did not abolish the hyperforin-induced Ca^{2+} rise (article 1, Section 8.2), suggesting that it could release Ca^{2+} from internal stores. We thus decided to further characterize the cellular actions of this TRPC6 channel activator. Our data revealed that hyperforin displays protonophore-like properties, triggering the release of Ca^{2+} and Zn^{2+} from mitochondria.

11.2 Article 3: The TRPC6 channel activator hyperforin induces the release of zinc and calcium from mitochondria

THE TRPC6 CHANNEL ACTIVATOR HYPERFORIN INDUCES THE RELEASE OF ZINC AND CALCIUM FROM MITOCHONDRIA

Peng TU [1,2,3], Julien GIBON [1,2,3] and Alexandre BOURON [1,2,3]

[1] UMR CNRS 5249, Grenoble, France.

[2] CEA, DSV, IRTSV, Grenoble.

[3] Université Joseph Fourier, Grenoble.

Corresponding author :

Alexandre Bouron

Laboratoire de Chimie et Biologie des Métaux

UMR CNRS 5249

CEA

17 rue des Martyrs

38054 Grenoble

France

Phone : 00 33 4 38 78 44 23 - FAX : 00 33 4 38 78 54 87– E-mail : alexandre.bouron@cea.fr

Key words: Hyperforin, Cortex, Calcium, Zinc, TRPC6 channels

Running title: Hyperforin alters the homeostasis of Zn and Ca

Abstract

Hyperforin, an extract of the medicinal plant *hypericum perforatum* (also named St John's wort), possesses antidepressant properties. Recent data showed that it elevates the intracellular concentration of Ca^{2+} by activating diacylglycerol-sensitive TRPC6 channels without activating the other isoforms (TRPC1, TRPC3, TRPC4, TRPC5, and TRPC7). So far, the mechanisms by which hyperforin exerts its antidepressant action are largely unknown. The present study was undertaken to further characterize the cellular neuronal responses induced by hyperforin. Experiments conducted on cortical neurons in primary culture and loaded with fluorescent probes for Ca^{2+} (Fluo-4) and Zn^{2+} (FluoZin-3) showed that it not only controls the activity of plasma membrane channels but it mobilizes these two cations from internal pools. Experiments conducted on isolated brain mitochondria indicated that hyperforin, like the inhibitor of oxidative phosphorylation, carbonylcyanide-4-(trifluoromethoxy)-phenylhydrazone (FCCP), collapses the mitochondrial membrane potential. Furthermore, it promotes a massive release of Ca^{2+} and Zn^{2+} from these organelles via a ruthenium red-sensitive transporter. In addition, chronically applied, hyperforin decreases the intracellular pools of Ca^{2+} and Zn^{2+}. In fact, this antidepressant exerts complex actions on central nervous system neurons. Hyperforin not only triggers the entry of cations via plasma membrane TRPC6 channels but it displays protonophore-like properties. Since this antidepressant is now use to probe the functions of native TRPC6 channels, our data indicate that caution is required when interpreting results obtained with hyperforin.

1. Introduction

Hyperforin, an extract of the medicinal plant *hypericum perforatum* (also named St John's wort) exhibits antidepressant properties [1]. Indeed, hyperforin alleviates symptoms of mild to moderate depression and is now commonly prescribed worldwide [2-4]. *In vitro* experiments showed that hyperforin inhibits the synaptic uptake of various neurotransmitters, including serotonin and noradrenaline [5]. However, the mechanisms by which it exerts its antidepressive actions remain elusive [2].

Hyperforin, known to change membrane fluidity [6], influences cell functions by altering the activity of some plasma membrane channels. For instance, it is a potent blocker of many voltage-gated (Ca, Na and K) channels [7, 8] and ligand-gated (GABA, NMDA, AMPA) channels [8, 9]. Besides inhibiting proteins involved in the transport of ions through the plasma membrane, hyperforin activates an inward cationic current in a dose-dependent manner [8, 10]. TRPC6, a member of the C-class of transient receptor potential (TRPC) proteins, is the key molecular component of these hyperforin-activated channels [11]. TRPC6 is activated by hyperforin but the other TRPC isoforms (TRPC1, TRPC3, TRPC4, TRPC5 and TRPC7) are insensitive to the antidepressant [11].

Several authors took advantage of this property to study the functions and properties of native TRPC6 channels [11-13]. In cortical neurons, whole cell patch-clamp recordings showed that hyperforin elicits an inward current displaying TRPC6-like properties. Additional imaging experiments carried out with the Ca^{2+} sensitive probe Fluo-4 confirmed that hyperforin gave rise to an entry of cations [13]. However, the addition of Gd^{3+}, a potent blocker of TRPC

channels, reduced but did not abolish the hyperforin-induced Ca^{2+} rise [13], suggesting that it could release Ca^{2+} from internal stores.

The present study was undertaken to further characterize the effects of hyperforin on neurons from the central nervous system. Our data show that this antidepressant exerts complex actions on cortical neurons. Hyperforin not only triggers an entry of cations via plasma membrane TRPC6 channels [11] but displays protonophore-like properties, triggering the release of Ca^{2+} and Zn^{2+} from mitochondria.

2. Materials and methods

2.1 Primary cultures of embryonic cortical cells

Cortical cells were prepared from isolated cerebral cortices of C57BL6/J mice embryos (vaginal plug was designated E0). Brains were removed and kept in an ice-cold Ca^{2+}- and Mg^{2+}-free Hank's solution containing gentamycin (10 mg/ml) and glucose (6 g/l). Cells were mechanically isolated by means of successive aspirations through a fire-polished sterile Pasteur pipette. They were plated on 16 mm diameter glass cover-slips and kept up to 4 days in a 5% CO_2/95% O_2 atmosphere at 37°C [14]. The procedures used have been approved by the Ethical Committee of Rhône-Alpes Region (France).

2.2 Calcium imaging experiments with Fluo-4

The culture medium was removed and the cortical cells were washed twice with a Tyrode solution containing (in mM): 136 NaCl, 5 KCl, 2 $CaCl_2$, 1 $MgCl_2$, 10 HEPES, 10 glucose, pH 7.4 (NaOH). After a 10 min incubation period (at room temperature) in a Tyrode solution supplemented with 1.25 μM Fluo-4/AM, cells were washed twice with a Fluo-4/AM-free Tyrode solution and kept at room temperature ≥20 min to allow the de-esterification of the dye. Glass cover-slips, inserted into a perfusion chamber (RC-25F, Warner Instruments, Phymep, France), were placed on the stage of an Axio Observer A1 microscope (Carl Zeiss, France) equipped with a Fluar 40x oil immersion objective lens (1.3 NA) (Carl Zeiss, France). Light was provided by the DG-4 wavelength switcher (Princeton Instruments, Roper Scientific, France). The excitation light for Fluo-4 was filtered through a 470-495 nm excitation filter and the emitted light was collected through a 525 nm filter. Images, acquired by means of a high speed cooled CCD camera (CoolSnap HQ2, Princeton Instruments, Roper Scientific, France) were analyzed using the software MetaFluor (Universal Imaging, Roper

Scientific, France). Mean Fluo-4 values are reported as means ± SEM, with *n* indicating the number of cell bodies analyzed. All the experiments were performed at room temperature.

2.3 Zinc imaging experiments with FluoZin-3

Changes in the intracellular concentration of Zn^{2+} were recorded with the specific fluorescent Zn^{2+} indicator FluoZin-3 [15]. The experimental conditions were as described above except that the cells were incubated with 5 µM FluoZin-3/AM for 30 min at room temperature. Afterwards, they were washed twice and kept for 30 min in a FluoZin-3-free Tyrode solution before starting the recordings. The Fluo-4 and FluoZin-3 recordings were performed as follows: images were captured every 5 s. The baseline Fluo-4 (or FluoZin-3) fluorescence was recorded for ≥1 min before adding hyperforin and averaged (F0). Unless otherwise indicated, the changes in Fluo-4 (or FluoZin-3) fluorescence as a function of time were expressed as F/F0, with F being the Fluo-4 (or FluoZin-3) fluorescence.

2.4 Calcium fluxes measurements from isolated brain mitochondria

Some experimented were conducted on isolated brain mitochondria. These organelles were prepared from brains of 1-day-old neonatal mice according to [16]. The experimental procedures used in the present study were described previously [17].

2.5 Changes of the mitochondrial membrane potential

The changes of the mitochondrial membrane potential ($\Delta\Psi$) induced by hyperforin were assayed using the fluorescent cyanine dye 3,3'-dipropylthiodicarbocyanine (diS-C3-(5)) [18] according to experimental conditions already described [17].

2.6 Materials

FluoZin-3/AM, Fluo-4, Fluo-4/AM, and 3,3'-dipropylthiodicarbocyanine (diS-C3-(5)) were from Molecular Probes (Interchim, France). Glycyl-phenylalanine-2-naphthylamide (GPN), carbonyl cyanide 4-(trifluoromethoxy)phenylhydrazone (FCCP), ruthenium red, N,N,N',N'-tetrakis(2-pyridylmethyl)ethylene-diamine (TPEN), and thapsigargin were from Sigma-Aldrich (France). Bafilomycin A was from Tocris (Lucerna Chem AG, Switzerland). Cyclosporin A was purchased from Calbiochem (France). Tissue culture media were obtained from Invitrogen (VWR, France). Hyperforin was a kind gift from Dr. Willmar Schwabe GmbH & Co (Karlsruhe, Germany).

3. Results

Hyperforin releases Ca^{2+} from internal compartments

The antidepressant hyperforin promotes the entry of cations (including Ca^{2+}) through TRPC6 channels [11] or channels exhibiting TRPC6-like properties [13]. The hyperforin-induced Fluo-4 signals were biphasic with a large and transient response followed by a plateau phase (Figure 1A, filled circles). Even in the presence of a high concentration of Gd^{3+} (50 µM), a potent blocker of TRPC channels, hyperforin was still able to increase the cytosolic concentration of Ca^{2+} ($[Ca^{2+}]i$) as illustrated in Figure 1A (open circles). In this case, Gd^{3+} specifically suppressed the transient phase leaving the plateau unaffected. The latter result suggested that hyperforin elicited a transient influx of Ca^{2+} followed by a release of Ca^{2+} from internal stores. In the following experiments, the hyperforin-induced Ca^{2+} responses were recorded when the cells were kept either in a 2 mM Ca^{2+} Tyrode solution (Figures 1B) or in a Ca^{2+}-free solution (Figures 1C), thus excluding a Ca^{2+} entry via Gd^{3+}-insensitive channels. In both instances, hyperforin increased $[Ca^{2+}]i$ in a dose-dependent manner (Figure 1D). The half-maximal effective concentrations were 3.3 and 3.5 µM when measured in Ca^{2+}-free and in normal (2 mM Ca^{2+}) Tyrode solutions, respectively. Thus, hyperforin not only triggers the entry of Ca^{2+} through plasma membrane channels but it causes the release of Ca^{2+} from internal compartments. The blocker of TRPC channels Gd^{3+} prevents the entry of cations through the hyperforin-activated channels without altering the hyperforin-induced release of Ca^{2+}.

Hyperforin elevates the cytoplasmic concentration of Zn^{2+}

Fluo-4 is a well-known fluorescent Ca^{2+} indicator [19] but it can not be regarded as a specific sensitive Ca^{2+} probe because a plethora of metals like Zn, Cu, or Cd interfere with the

fluorescence of Ca^{2+} sensitive dyes [20-22]. Cations of metals like Fe or Mn quench the fluorescence of Ca^{2+} probes whereas the binding of Zn^{2+} gives rise to prominent fluorescent signals. An easy way to check for the contribution of Ca^{2+} in the Fluo-4 response is to use TPEN. Indeed, TPEN is a membrane permeant heavy metal chelator having a low affinity for cations like Ca^{2+} and Mg^{2+} but a very high affinity for transition, mainly Zn^{2+}, metals ions [23]. Since $Fe^{2+}$and Mn $^{2+}$ do not increase but rather quench the Fluo-4 fluorescence we hypothesized that the hyperforin-induced Fluo-4 signals could reflect cytosolic changes in the concentration of chelatable Zn^{2+} and/or Ca^{2+}. To check whether hyperforin elevated $[Zn^{2+}]i$, the experiments illustrated in Figure 1C were repeated but this time in the presence of TPEN. When extracellular Ca^{2+} was omitted, hyperforin increased the Fluo-4 fluorescence as already shown (Figure 1C) but this hyperforin-induced Fluo-4 signal was markedly attenuated by TPEN (Figure 2A). On average, the maximal increases in Fluo-4 fluorescence induced by a 250 s application of 10 µM hyperforin (added in a Ca^{2+}-free Tyrode solution) were 63 +/- 1 % (n= 285) and 20 +/- 1 % (n= 278), without and with TPEN (10 µM), respectively ($p<0.001$, Student' t test). Thus, the antidepressant mobilizes Ca^{2+} and Zn^{2+} from internal pools. To further verify the effect of hyperforin on the chelatable Zn^{2+}, we used the specific fluorescent Zn^{2+} indicator FluoZin-3 [15]. To prevent any hyperforin-induced Zn^{2+} entry, cortical neurons were maintained in a Tyrode medium supplemented with Ca-EDTA in order to chelate extracellular Zn^{2+} [24]. The addition of hyperforin gave rise to a robust elevation of the FluoZin-3 fluorescence (Figure 2B). A subsequent addition of TPEN (10 µM) totally eliminated the hyperforin-induced FluoZin-3 response (Figure 2B), providing further support to the idea that the antidepressant alters the homeostasis of Zn^{2+}. Taken together, these experiments show that hyperforin increases the cytosolic concentrations of free Ca^{2+} and Zn^{2+}.

Characterisation of the intracellular pools of Ca^{2+} and Zn^{2+}

We next addressed the question of the intracellular sources of Ca^{2+} and Zn^{2+}. To this aim, we first check the involvement of the endoplasmic reticulum (ER). Any release of Zn^{2+} from the ER could contribute to the hyperforin-induced Fluo-4 (or FluoZin-3) signals observed in Figure 2. The application of thapsigargin (Tg), an inhibitor of the ER Ca^{2+} pumps, elicited a transient Fluo-4 signal (Figure 3A, n= 47 cells). However, FluoZin-3 loaded cells failed to respond to Tg (Figure 3B, n= 75 cells) showing that the Tg-dependent depletion of the ER did not cause the release of Zn^{2+} but specifically reflected the leakage of Ca^{2+} out of this store. The contribution of additional intracellular stores was verified by using glycyl-phenylalanine-2-naphthylamide (GPN). It provokes the osmotic lysis of lysosomes or lysosome-related organelles [25]. These acidic compartments are known to store cations like Ca^{2+} [26, 27] including in neural cells [28, 29]. Similar to Tg, GPN (200 µM) caused a transient Fluo-4 response (Figure 3C) (n=81 cells) but did not induce any FluoZin-3 signal (Figure 3D) (n= 65 cells). The vacuolar ATPase inhibitor bafilomycin A [30, 31] was also used. It blocks proton pumps located in endosomes and lysosomes [31] and thus promotes the release of cations out of these compartments [32, 33]. Regardless of the probe used, Fluo-4 (n=33 cells) or FluoZin-3 (n=109 cells), 0.5 µM bafilomycin A never elicited any fluorescent signal (Figures 3 E-F). In a last series of experiments, the protonophore carbonyl cyanide 4-(trifluoromethoxy)phenylhydrazone (FCCP) was tested to further characterize the intracellular pools of Zn^{2+} and Ca^{2+}. FCCP alters the Ca^{2+} homeostasis by collapsing the mitochondrial membrane potential and it triggers the release of Ca^{2+} from these organelles [17, 34]. The addition of FCCP (2 µM) produced strong Fluo-4 (Figure 3G) and FluoZin-3 signals (Figure 3H) in all cells tested (n>100 for Fluo-4 and n=64 cells for FluoZin-3). Altogether, the results depicted in Figure 3 indicate that cortical neurons possess i) Tg-, GPN- and FCCP-sensitive Ca^{2+} stores and ii) FCCP-sensitive Zn^{2+} stores. Since FCCP is a potent mitochondrial

uncoupler, hyperforin was applied on isolated brain mitochondria to verify whether it effectively releases Zn^{2+} from these organelles.

Hyperforin releases Zn^{2+} from isolated brain mitochondria

The application of FCCP to isolated brain mitochondria preincubated with the non-permeant form of Fluo-4 gave rise to a strong Fluo-4 signal (Figure 4A) as already shown [17]. A subsequent addition of hyperforin (1 µM) had no additional effect (Figure 4A). However, if hyperforin was added without FCCP, it produced a strong elevation of the Fluo-4 fluorescence (Figure 4B). The hyperforin-induced Fluo-4 signals were strongly reduced in the presence of the Zn^{2+} chelator TPEN (2.5 µM, n= 4) (Figure 4B) confirming that the antidepressant releases this metal from mitochondria. It is worth noting that hyperforin elicited a TPEN-resistant Fluo-4 signal which most likely reflected the release of Ca^{2+} from mitochondria. Cyclosporin A (CsA), acting on cyclophylin D, a putative component of the mitochondrial permeability transition pore [35], and ruthenium red, a blocker of the mitochondrial Ca^{2+} uniporter [36], were used. CsA (5 µM, n=4) had no effect but ruthenium red (3 µM, n=4) completely blocked the hyperforin-induced Fluo-4 signal (Figure 4B). Previous reports showed that hyperforin has protonophore-like properties [37]. Its action on the mitochondrial membrane potential was assessed by using the fluorescent cyanine dye 3,3'-dipropylthiodicarbocyanine (diS-C3-(5)) [17, 18]. The addition of hyperforin (2 µM) to isolated brain mitochondria enhanced the diS-C3-(5) fluorescence (Figure 4C), showing that it collapsed the mitochondrial membrane potential [18]. A subsequent addition of FCCP had no additional effect. In summary, these experiments show that hyperforin probably exerts an uncoupling action on isolated mitochondria by collapsing the membrane potential. This is accompanied by the release of Ca^{2+} and Zn^{2+} via a ruthenium red-sensitive mechanism.

Chronically applied, hyperforin alters the intracellular pools of Ca^{2+} and Zn^{2+}

Hyperforin is used to assess the functions of native TRPC6 channels [12]. However, since it is a potent protonophore altering the homeostasis of zinc and calcium, we determined whether a chronic application of this antidepressant could modify the intracellular pools of Ca^{2+} and Zn^{2+}. Cortical neurons were incubated for 48 h with 1 µM hyperforin. The antidepressant was washed away and the cells were loaded with Fluo-4 (or FluoZin-3) as described (see Materials and Methods). To specifically analyse the hyperforin-induced Ca^{2+} release, Fluo-4 loaded cells were maintained in a Ca^{2+}-free Tyrode solution supplemented with TPEN (10 µM). Under these conditions, the hyperforin-induced Fluo-4 signals from hyperforin-treated cells were significantly smaller when compared to the hyperforin-untreated (control) cells (Figures 5A-B). Similar experiments were conducted with FluoZin-3 loaded cells. Here again, the application of hyperforin elicited smaller FluoZin-3 signals in hyperforin-treated cells when compared to the control cells (untreated) (Figures 5C-D). On average, after a 48 h treatment, the amplitude of the Fluo-4 and of FluoZin-3 signals were reduced, respectively by 31 % ($p<0.001$) and 28 % ($p<0.001$). It shows that maintaining cells in a culture medium supplemented with a low concentration of hyperforin (1 µM) alters the intracellular pools in Ca^{2+} and Zn^{2+}.

4. Discussion

The antidepressant hyperforin exerts multiple cellular actions but it is now currently used to explore the properties and functions of TRPC6 channels. Indeed, hyperforin activates TRPC6, giving rise to a non selective cation current [11]. Experiments conducted on cultured cortical neurons loaded with the sensitive Ca^{2+} probe Fluo-4 showed that hyperforin induced cytosolic Ca^{2+} changes [13]. However, the hyperforin-induced Fluo-4 signals were incompletely eliminated by Gd^{3+}, a potent blocker of TRPC channels, even when present at very high concentrations (e.g. 50 µM). Based on this observation we hypothesised that the Gd^{3+}-resistant Fluo-4 responses triggered by hyperforin could reflect the release of Ca^{2+} from internal stores. But, as pointed out by other authors [38], caution is required when interpreting data obtained with fluorescent Ca^{2+} probes because they are sensitive to metals like Zn or Fe endogenously present in all living cells. This difficulty has for instance been recently illustrated in lymphocytes where thymerosal, described as a Ca^{2+} mobilising agent, releases Zn^{2+} but no Ca^{2+} from internal compartments [39]. These data prompted us to determine whether hyperforin could alter the intracellular homeostasis of cations like Ca^{2+} and Zn^{2+}.

FluoZin-3 is a specific fluorescent Zn^{2+} indicator [15], insensitive to Ca^{2+} and Mg^{2+} [40]. It has become a very useful tool for studying Zn^{2+} homeostasis. Our data clearly show that hyperforin enhanced the FluoZin-3 fluorescence in living neurons. This hyperforin-dependent FluoZin-3 signal could reflect an uptake of Zn^{2+} because this cation is a common contaminant present in physiological solutions but a chelator like Ca-EDTA minimizes this drawback [24]. However, even when the cells were kept in a Tyrode solution supplemented with Ca-EDTA, hyperforin was still able to elevate the FluoZin-3 fluorescence. Moreover, the amplitudes of the hyperforin-induced FluoZin-3 signals were not affected by Ca-EDTA (not shown). This

demonstrates that hyperforin did not promote the entry of Zn^{2+} but rather mobilized this cation from intracellular pools.

In neurons, the main likely sources of intracellular Zn^{2+} are metallothioneins, an important family of Zn^{2+}-binding proteins which reversibly bind this metal [41], mitochondria [42, 43], and synaptic vesicles [44, 45]. It is however important to mention that all the data reported in the present study were obtained on immature cortical neurons kept for only 2 to 4 days in culture, before synaptogenesis and the establishment of a mature synaptically connected neuronal network. Experiments conducted with bafilomycin A and GPN, known to act on acidic compartments (including synaptic vesicles), suggested that these stores did not contribute to the mobilization of Zn^{2+} observed in response to the addition of hyperforin. Besides synaptic vesicles, various intracellular membrane-delimited compartments can store cations (e.g the ER, lysosomes and lysosomes-like organelles, peroxisomes, mitochondria). Inhibiting the Ca^{2+} pumps of the ER with Tg released Ca^{2+} but not Zn^{2+}. A similar observation was recently made on lymphocytes [39]. Except for FCCP, none of the agents used (Tg, GPN and bafilomycin A) elevated the FluoZin-3 fluorescence, pointing to mitochondria as the putative hyperforin-sensitive Zn^{2+} pool. This was confirmed by experiments carried out on isolated brain mitochondria. Hyperforin caused a robust Fluo-4 signal that was strongly attenuated by TPEN. These results are in agreement with previous studies showing the presence of a mitochondrial pool of Zn^{2+} in cortical neurons [42, 43]. The mitochondrial Zn^{2+} uptake occurs via the Ca^{2+} uniporter (in a ruthenium-sensitive manner) and via a non identified ruthenium red-insensitive pathway [42]. On the other hand, the mechanisms controlling the mitochondrial Zn^{2+} efflux are still not characterized [42]. In isolated murine brain mitochondria, ruthenium red, a blocker of the mitochondrial Ca^{2+} uniporter [36, 46], strongly attenuated the hyperforin-induced release of Zn^{2+}. Ruthenium red can however

influence the activity of other intracellular targets like ryanodine receptors (RyRs), the voltage-dependent anion channels VDAC [47] and the so-called “rapid-mode” uptake (or RaM) [48]. Interestingly, under certain conditions, RyRs can mediate a release of Ca^{2+} from mitochondria [36]. But, to our knowledge, the presence of these Ca^{2+} channels in brain mitochondria has never been documented. Whatever the exact molecular identity of the hyperforin-sensitive mitochondrial target allowing the efflux of cations, our data show that this antidepressant releases Zn^{2+} and Ca^{2+} from mitochondria via a ruthenium red-sensitive process. Hyperforin collapses the mitochondrial membrane potential which is in agreement with a previous report demonstrating that, similarly to FCCP, the antidepressant has protonophore properties [37]. The hyperforin-induced loss of the mitochondrial potential permits the passive release of Ca^{2+} and Zn^{2+} out of these organelles.

Hyperforin is a potent uptake inhibitor of various neurotransmitters [1, 3]. However, this latter characteristic does not seem to explain its antidepressant action. So far, the molecular mechanisms by which hyperforin alleviates mild depressions are unknown. Interestingly, it alters the neuronal homeostasis of zinc. Of note, clinical data show that subjects suffering from depression exhibit lower zinc serum levels than non-depressed control subjects [49]. As importantly, zinc has antidepressant properties [50]. Synthetic antidepressants like imipramine and citalopram affect zinc concentration in the blood serum and in the brain [50]. Moreover, zinc supplementation exerts an antidepressant-like activity and enhances the effects of synthetic antidepressants [50]. *In vitro* experiments, data collected from animal studies as well as clinical and post-mortem studies point to a role of zinc in the physiopathology of depression and in its treatment. Whether the hyperforin-induced alteration of the neuronal homeostasis of Zn^{2+} is involved in its antidepressant action remains to be shown.

In conclusion, this report reveals that hyperforin collapses the mitochondrial membrane potential and releases Ca^{2+} and Zn^{2+} from these organelles via a ruthenium red-sensitive mechanism. Hyperforin is now commonly used to understand the functions and properties of native TRPC6 channels. However, when considering its large number of targets located either in the plasma membrane or intracellularly, caution is needed when interpreting data obtained with this protonophore-like agent disturbing Ca^{2+} and Zn^{2+} homeostasis.

Acknowledgments

We wish to thank Drs. G. Brandolin for his help with the experiments on isolated brain mitochondria, J-M Moulis for a critical reading of this manuscript. We also wish to thank W. Schwabe (Karlsruhe, Germany) for the kind gift of hyperforin. This study was supported by a grant from l'Agence Nationale de la Recherche.

REFERENCES

1. Chatterjee SS, Bhattacharya SK, Wonnemann M, Singer A, Muller WE. (1998) Hyperforin as a possible antidepressant component of hypericum extracts. Life Sci, 63, 499-510.
2. Mennini T, Gobbi M. (2004) The antidepressant mechanism of Hypericum perforatum. Life Sci, 75, 1021-7.
3. Nathan P. (1999) The experimental and clinical pharmacology of St John's Wort (Hypericum perforatum L.). Mol Psychiatry, 4, 333-8.
4. Zanoli P. (2004) Role of hyperforin in the pharmacological activities of St. John's Wort. CNS Drug Rev, 10, 203-18.
5. Muller WE. (2003) Current St John's wort research from mode of action to clinical efficacy. Pharmacol Res, 47, 101-9.
6. Eckert GP, Keller JH, Jourdan C, Karas M, Volmer DA, Schubert-Zsilavecz M, Muller WE. (2004) Hyperforin modifies neuronal membrane properties in vivo. Neurosci Lett, 367, 139-43.
7. Fisunov A, Lozovaya N, Tsintsadze T, Chatterjee S, Noldner M, Krishtal O. (2000) Hyperforin modulates gating of P-type Ca2+ current in cerebellar Purkinje neurons. Pflugers Arch, 440, 427-34.
8. Chatterjee S, Filippov V, Lishko P, Maximyuk O, Noldner M, Krishtal O. (1999) Hyperforin attenuates various ionic conductance mechanisms in the isolated hippocampal neurons of rat. Life Sci, 65, 2395-405.
9. Kumar V, Mdzinarishvili A, Kiewert C, Abbruscato T, Bickel U, van der Schyf CJ, Klein J. (2006) NMDA receptor-antagonistic properties of hyperforin, a constituent of St. John's Wort. J Pharmacol Sci, 102, 47-54.

10. Treiber K, Singer A, Henke B, Muller WE. (2005) Hyperforin activates nonselective cation channels (NSCCs). Br J Pharmacol, 145, 75-83.

11. Leuner K, Kazanski V, Muller M, Essin K, Henke B, Gollasch M, Harteneck C, Muller WE. (2007) Hyperforin--a key constituent of St. John's wort specifically activates TRPC6 channels. Faseb J, 21, 4101-11.

12. Muller M, Essin K, Hill K, Beschmann H, Rubant S, Schempp CM, Gollasch M, Boehncke WH, Harteneck C, Muller WE, Leuner K. (2008) Specific TRPC6 channel activation, a novel approach to stimulate keratinocyte differentiation. J Biol Chem, 283, 33942-54.

13. Tu P, Kunert-Keil C, Lucke S, Brinkmeier H, Bouron A. (2009) Diacylglycerol analogues activate second messenger-operated calcium channels exhibiting TRPC-like properties in cortical neurons. J. Neurochem, 108, 126-138.

14. Bouron A, Altafaj X, Boisseau S, De Waard M. (2005) A store-operated Ca2+ influx activated in response to the depletion of thapsigargin-sensitive Ca2+ stores is developmentally regulated in embryonic cortical neurons from mice. Brain Res Dev Brain Res, 159, 64-71.

15. Gee KR, Zhou ZL, Ton-That D, Sensi SL, Weiss JH. (2002) Measuring zinc in living cells. A new generation of sensitive and selective fluorescent probes. Cell Calcium, 31, 245-51.

16. Chinopoulos C, Starkov AA, Fiskum G. (2003) Cyclosporin A-insensitive permeability transition in brain mitochondria: inhibition by 2-aminoethoxydiphenyl borate. J Biol Chem, 278, 27382-9.

17. Tu P, Brandolin G, Bouron A. (2009) The anti-inflammatory agent flufenamic acid depresses store-operated channels by altering mitochondrial calcium homeostasis. Neuropharmacology.

18. Waggoner AS. (1979) The use of cyanine dyes for the determination of membrane potentials in cells, organelles, and vesicles. Methods Enzymol, 55, 689-95.

19. Gee KR, Brown KA, Chen WN, Bishop-Stewart J, Gray D, Johnson I. (2000) Chemical and physiological characterization of fluo-4 Ca(2+)-indicator dyes. Cell Calcium, 27, 97-106.

20. Grynkiewicz G, Poenie M, Tsien RY. (1985) A new generation of Ca2+ indicators with greatly improved fluorescence properties. J Biol Chem, 260, 3440-50.

21. Marchi B, Burlando B, Panfoli I, Viarengo A. (2000) Interference of heavy metal cations with fluorescent Ca2+ probes does not affect Ca2+ measurements in living cells. Cell Calcium, 28, 225-31.

22. Rousselet E, Richaud P, Douki T, Chantegrel JG, Favier A, Bouron A, Moulis JM. (2008) A zinc-resistant human epithelial cell line is impaired in cadmium and manganese import. Toxicol Appl Pharmacol, 230, 312-9.

23. Arslan P, Di Virgilio F, Beltrame M, Tsien RY, Pozzan T. (1985) Cytosolic Ca2+ homeostasis in Ehrlich and Yoshida carcinomas. A new, membrane-permeant chelator of heavy metals reveals that these ascites tumor cell lines have normal cytosolic free Ca2+. J Biol Chem, 260, 2719-27.

24. Kay AR. (2004) Detecting and minimizing zinc contamination in physiological solutions. BMC Physiol, 4, 4.

25. Berg TO, Stromhaug PE, Berg T, Seglen PO. (1994) Separation of lysosomes and autophagosomes by means of glycyl-phenylalanine-naphthylamide, a lysosome-disrupting cathepsin-C substrate. Eur J Biochem, 221, 595-602.

26. Haller T, Dietl P, Deetjen P, Volkl H. (1996) The lysosomal compartment as intracellular calcium store in MDCK cells: a possible involvement in InsP3-mediated Ca2+ release. Cell Calcium, 19, 157-65.

27. Srinivas SP, Ong A, Goon L, Bonanno JA. (2002) Lysosomal Ca(2+) stores in bovine corneal endothelium. Invest Ophthalmol Vis Sci, 43, 2341-50.

28. McGuinness L, Bardo SJ, Emptage NJ. (2007) The lysosome or lysosome-related organelle may serve as a Ca2+ store in the boutons of hippocampal pyramidal cells. Neuropharmacology, 52, 126-35.

29. Singaravelu K, Deitmer JW. (2006) Calcium mobilization by nicotinic acid adenine dinucleotide phosphate (NAADP) in rat astrocytes. Cell Calcium, 39, 143-53.

30. Bowman EJ, Siebers A, Altendorf K. (1988) Bafilomycins: a class of inhibitors of membrane ATPases from microorganisms, animal cells, and plant cells. Proc Natl Acad Sci U S A, 85, 7972-6.

31. Drose S, Altendorf K. (1997) Bafilomycins and concanamycins as inhibitors of V-ATPases and P-ATPases. J Exp Biol, 200, 1-8.

32. Lloyd-Evans E, Morgan AJ, He X, Smith DA, Elliot-Smith E, Sillence DJ, Churchill GC, Schuchman EH, Galione A, Platt FM. (2008) Niemann-Pick disease type C1 is a sphingosine storage disease that causes deregulation of lysosomal calcium. Nat Med, 14, 1247-55.

33. Camacho M, Machado JD, Alvarez J, Borges R. (2008) Intravesicular calcium release mediates the motion and exocytosis of secretory organelles: a study with adrenal chromaffin cells. J Biol Chem, 283, 22383-9.

34. Ichas F, Jouaville LS, Mazat JP. (1997) Mitochondria are excitable organelles capable of generating and conveying electrical and calcium signals. Cell, 89, 1145-53.

35. Kroemer G, Galluzzi L, Brenner C. (2007) Mitochondrial membrane permeabilization in cell death. Physiol Rev, 87, 99-163.

36. O'Rourke B. (2007) Mitochondrial ion channels. Annu Rev Physiol, 69, 19-49.

37. Roz N, Rehavi M. (2003) Hyperforin inhibits vesicular uptake of monoamines by dissipating pH gradient across synaptic vesicle membrane. Life Sci, 73, 461-70.

38. Martin JL, Stork CJ, Li YV. (2006) Determining zinc with commonly used calcium and zinc fluorescent indicators, a question on calcium signals. Cell Calcium, 40, 393-402.

39. Haase H, Hebel S, Engelhardt G, Rink L. (2009) Zinc ions cause the thimerosal-induced signal of fluorescent calcium probes in lymphocytes. Cell Calcium, 45, 185-91.

40. Devinney MJ, 2nd, Reynolds IJ, Dineley KE. (2005) Simultaneous detection of intracellular free calcium and zinc using fura-2FF and FluoZin-3. Cell Calcium, 37, 225-32.

41. West AK, Hidalgo J, Eddins D, Levin ED, Aschner M. (2008) Metallothionein in the central nervous system: Roles in protection, regeneration and cognition. Neurotoxicology, 29, 488-502.

42. Malaiyandi LM, Vergun O, Dineley KE, Reynolds IJ. (2005) Direct visualization of mitochondrial zinc accumulation reveals uniporter-dependent and -independent transport mechanisms. J Neurochem, 93, 1242-50.

43. Sensi SL, Ton-That D, Weiss JH. (2002) Mitochondrial sequestration and Ca(2+)-dependent release of cytosolic Zn(2+) loads in cortical neurons. Neurobiol Dis, 10, 100-8.

44. Paoletti P, Vergnano AM, Barbour B, Casado M. (2009) Zinc at glutamatergic synapses. Neuroscience, 158, 126-36.

45. Palmiter RD, Cole TB, Quaife CJ, Findley SD. (1996) ZnT-3, a putative transporter of zinc into synaptic vesicles. Proc Natl Acad Sci U S A, 93, 14934-9.

46. Demaurex N, Poburko D, Frieden M. (2009) Regulation of plasma membrane calcium fluxes by mitochondria. Biochim Biophys Acta.

47. Hajnoczky G, Csordas G, Das S, Garcia-Perez C, Saotome M, Sinha Roy S, Yi M. (2006) Mitochondrial calcium signalling and cell death: approaches for assessing the role of mitochondrial Ca2+ uptake in apoptosis. Cell Calcium, 40, 553-60.

48. Gunter TE, Sheu SS. (2009) Characteristics and possible functions of mitochondrial Ca(2+) transport mechanisms. Biochim Biophys Acta.

49. Nowak G, Szewczyk B, Pilc A. (2005) Zinc and depression. An update. Pharmacol Rep, 57, 713-8.

50. Szewczyk B, Poleszak E, Sowa-Kucma M, Siwek M, Dudek D, Ryszewska-Pokrasniewicz B, Radziwon-Zaleska M, Opoka W, Czekaj J, Pilc A, Nowak G. (2008) Antidepressant activity of zinc and magnesium in view of the current hypotheses of antidepressant action. Pharmacol Rep, 60, 588-9.

Figure legends

FIGURE 1 : Hyperforin releases Ca^{2+} from internal compartments

A Fluo-4 recordings from isolated cortical neurons kept 2 days in culture. The graph shows that the external application of 10 µM hyperforin causes a strong enhancement of the Fluo-4 fluorescence. This response was never totally abolished by the TRPC channel blocker Gd^{3+} used at 50 µM (n= 53 cells).

B-C shown representative Fluo-4 recordings from distinct cultured cortical neurons. Cells were kept in a normal (2 mM Ca^{2+}) Tyrode (**B**) or in a Ca^{2+}-free Tyrode solution (**C**). The external application of hyperforin (0.2, 1, 10 µM) (indicated by the horizontal black bars) triggered a Fluo-4 response in a concentration-dependent manner. In these experiments, cells experienced only one application of hyperforin.

D Dose-response curves obtained when hyperforin was added in the absence (open circles) or presence (filled circles) of external Ca^{2+} (2 mM). The number of cells tested is given for each concentration. Mean +/- SEM.

FIGURE 2 : Hyperforin increases the cytosolic concentration of free Ca^{2+} and Zn^{2+}

Representative Fluo-4 recordings from cortical neurons kept in a Ca-free Tyrode solution without (filled circles) or with 10 µM TPEN (open circles) (**A)**. Similar experiments were performed with FluoZin-3-loaded cells (**B)**. In both instances, hyperforin (10 µM) was added when indicated (horizontal black bar). The hyperforin-induced FluoZin-3 response was observed in all cortical cells tested and was totally abolished by TPEN (10 µM) (n=491 cells).

FIGURE 3 : Intracellular pools of Ca^{2+} and Zn^{2+}

Cortical neurons were loaded with Fluo-4 (**A**, **C**, **E**, **G**) or FluoZin-3 (**B**, **D**, **F**, **H**). The horizontal black bars indicated when the following agents were added: thapsigargin (Tg, 2 µM A: n= 45 cells, B: n= 75) ; glycyl-phenylalanine-2-naphthylamide (GPN, 200 µM, C: n= 81, D: n= 65) ; bafilomycin A (Baf A, 0.5 µM, E: n= 33, F: n= 109) ; and carbonyl cyanide 4-(trifluoromethoxy)phenylhydrazone (FCCP, 2 µM, G: n>100, H: n=64).

FIGURE 4 : Hyperforin releases Zn^{2+} from isolated brain mitochondria

To assess the functional state of the isolated mitochondria, Ca^{2+} (1 µM) was added to the medium. This provoked a rapid increase in Fluo-4 fluorescence followed by a delayed decline reflecting the mitochondrial Ca^{2+} uptake [17]. Panel **A** shows that FCCP (2 µM) produced a strong elevation of the Fluo-4 fluorescence. A subsequent addition of hyperforin (2.5 µM) had no effect. (**B**) Without FCCP, hyperforin (1 µM) caused a robust Fluo-4 signal insensitive to CsA (5 µM) but strongly blocked by ruthenium red (3 µM) (**B**). In the presence of TPEN (2.5 µM), hyperforin caused a smaller Fluo-4 response (**B**). In these experiments, CsA, ruthenium red or TPEN were added to the recording medium (containing the isolated mitochondria) at least 2 min before hyperforin. **C** shows the effect of hyperforin on the mitochondrial membrane potential. The addition of the antidepressant on isolated brain mitochondria strongly enhanced the diS-C3-(5) fluorescence (**C**). A subsequent application of FCCP (2 µM) had no additional effect, indicating that the mitochondrial membrane was completely depolarised. Representative traces from 4 independent experiments are shown.

FIGURE 5 : A chronic hyperforin treatment diminishes the intracellular pools of Ca^{2+} and Zn^{2+}

Cortical neurons were kept for 48 h in a Neurobasal medium supplemented with 1 µM hyperforin. After this treatment, hyperforin was washed away and the cells were loaded with either Fluo-4 (**A-B**) or FluoZin-3 (**C-D**) and kept in a Ca^{2+}-free Tyrode solution to specifically monitor intracellular responses without the contamination of any hyperforin-dependent Ca^{2+} entry. Of note, Fluo-4 signals were recorded in the presence of TPEN (10 µM) to eliminate the contribution of Zn^{2+}. These Fluo-4 signals were then considered as reflecting the hyperforin-dependent release of Ca^{2+}. Representative recordings showing that the external application of 10 µM hyperforin (horizontal black bars in **A** and **C**) elicited Fluo-4 (**A**) and FluoZin-3 (**C**) signals. Figures **B** and **D** are bar graphs summarizing these experiments. The averaged maximal amplitudes of the Fluo-4 (**B**) and FluoZin-3 (**D**) responses from control cells (not treated for 48 h with 1µM hyperforin) and hyperforin-treated cells (1 µM for 48 h) are also shown with the number of cells tested indicated above each bar. ** $p<0.001$ (Student's t test).

Figure 1

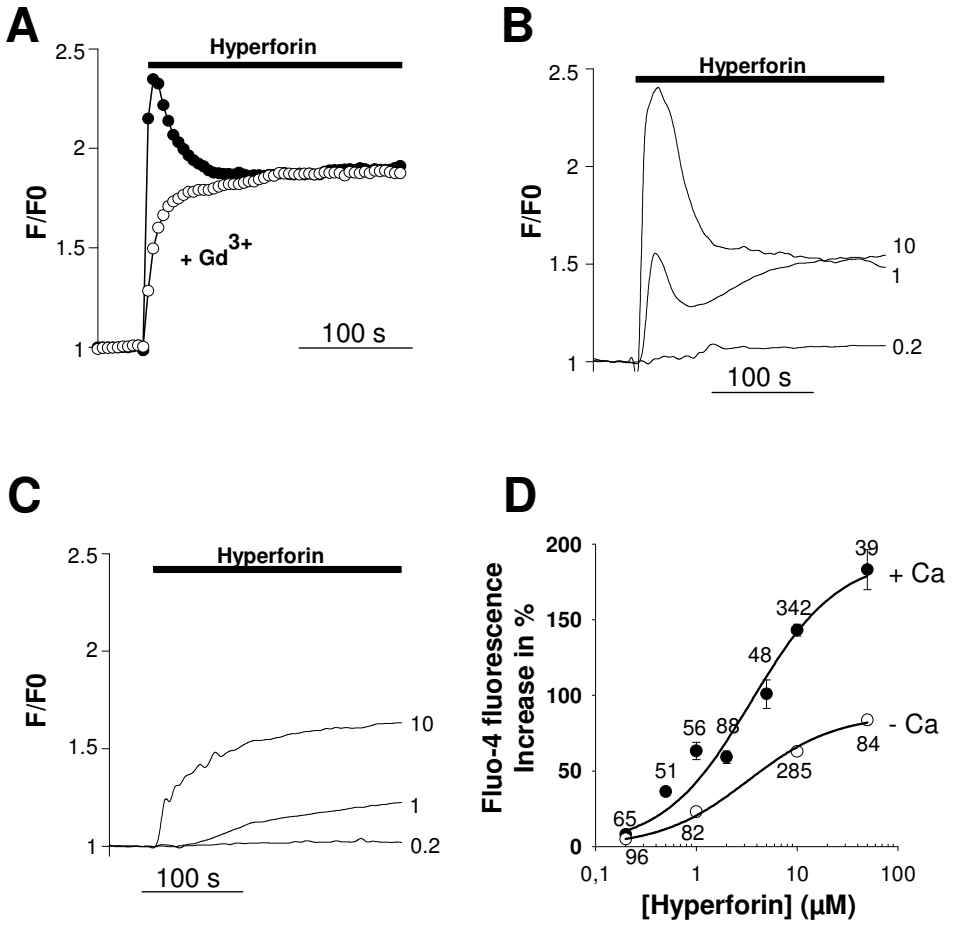

Tu et al, Hyperforin alters Zn and Ca homeostasis

Figure 2

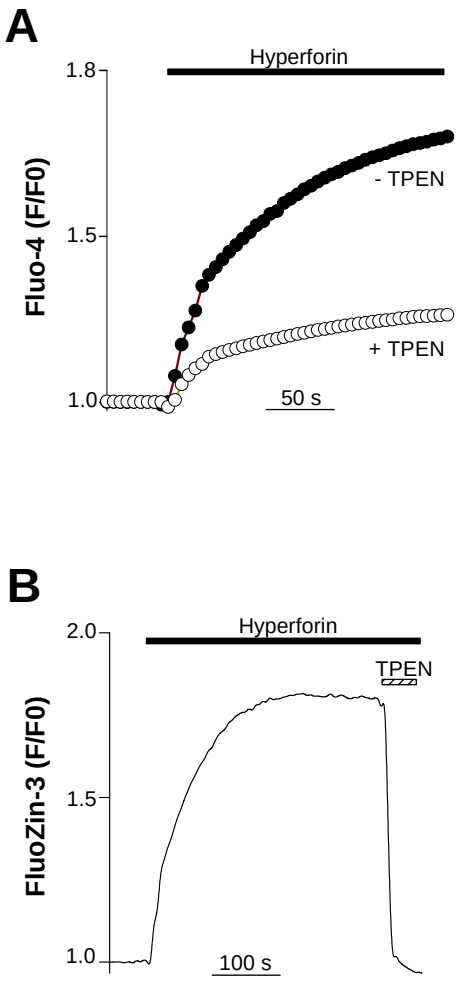

Tu et al, Hyperforin alters Zn and Ca homeostasis

Figure 3

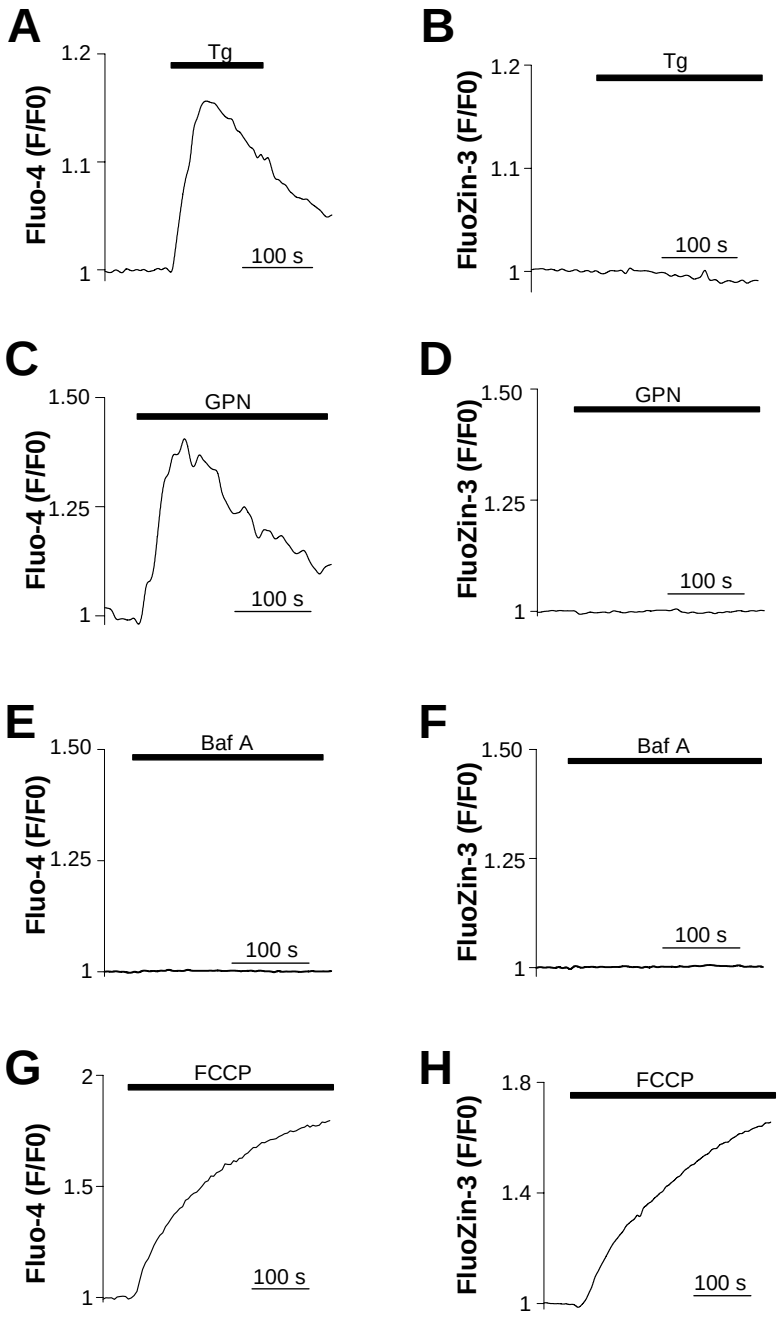

Tu et al, Hyperforin alters Zn and Ca homeostasis

Figure 4

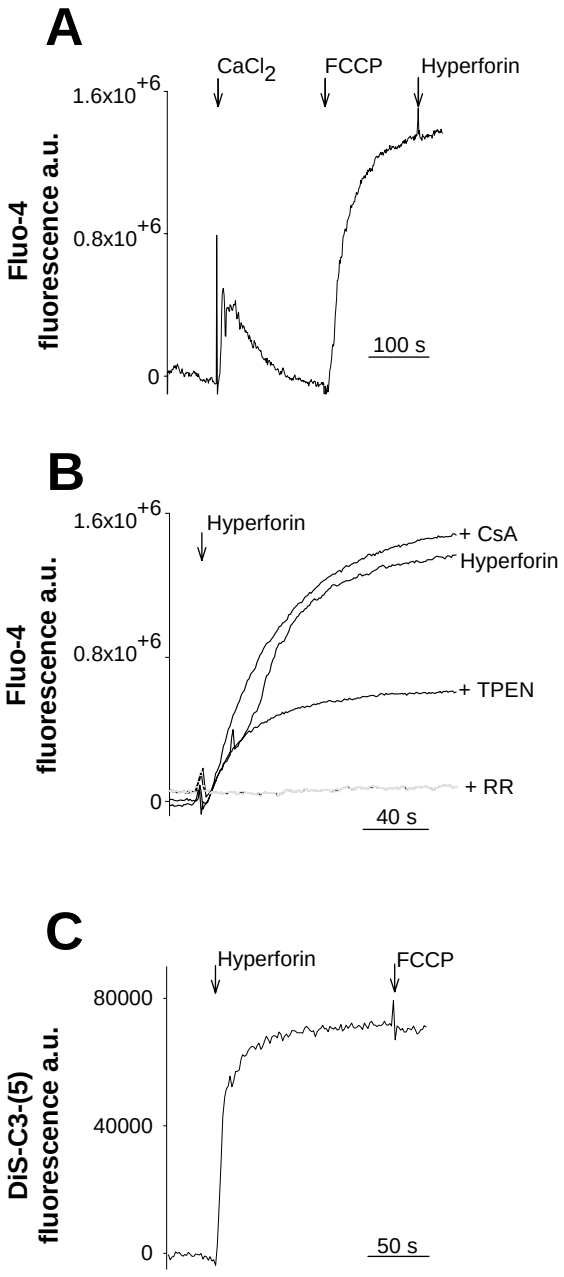

Tu et al, Hyperforin alters Zn and Ca homeostasis

Figure 5

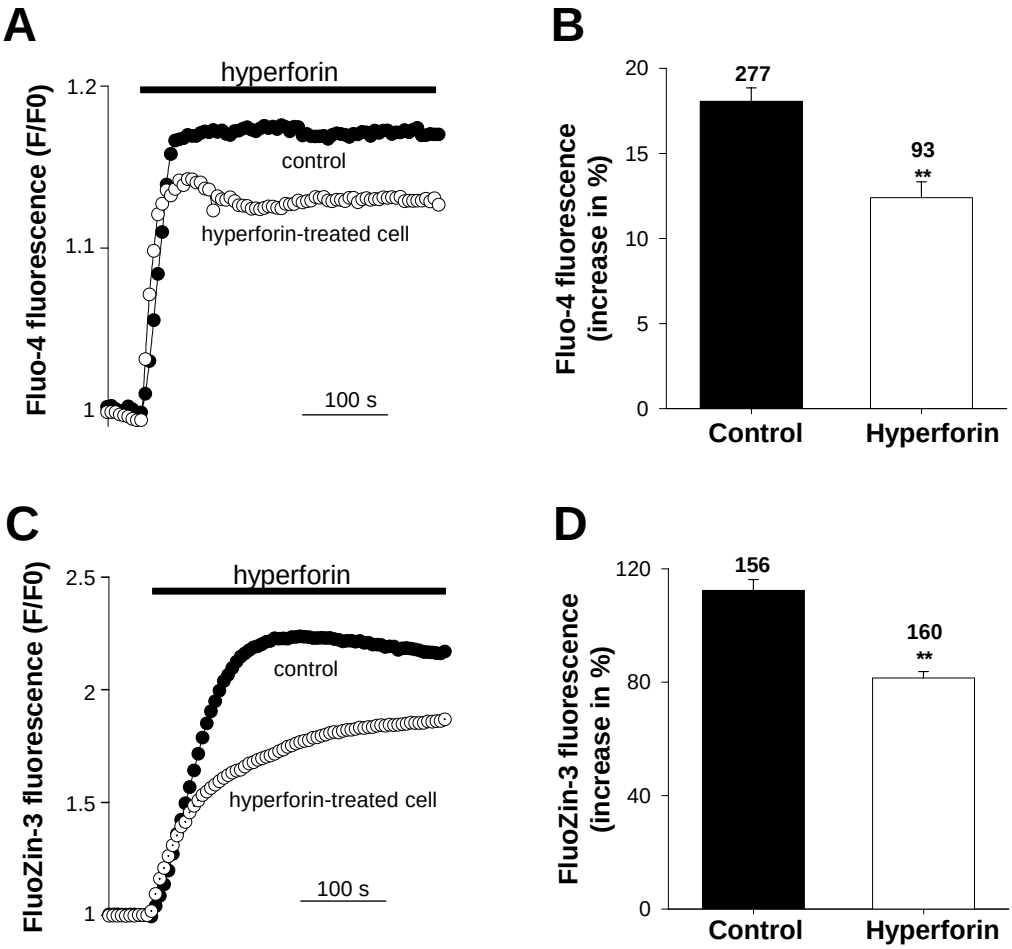

Tu et al, Hyperforin alters Zn and Ca homeostasis

11.3 Discussion

Hyperforin, a pharmacological tool used to activate TRPC6 channels, displays protonophore-like properties. It collapses $\Delta\psi_m$ and releases Ca^{2+} and Zn^{2+} from these organelles via a ruthenium red-sensitive mechanism. When chronically applied, hyperforin decreases the intracellular pools of Ca^{2+} and Zn^{2+}. Since hyperforin is now commonly used as an activator of TRPC6 channels, caution is required when interpreting the data obtained with this drug.

The results described above clearly show that hyperforin acts, among other targets, on mitochondria and causes the release of cations from these organelles. This finding incited us to reconsider the effects of FFA. Like hyperforin, this anti-inflammatory agent perturbs mitochondrial Ca^{2+} homeostasis. We thus thought to verify whether it could release Zn^{2+}.

This was achieved by realizing cellular imaging experiments with the specific zinc fluorescent probe FluoZin-3. The cells were bathed in a Ca^{2+}-free and Zn^{2+}-free Tyrode's solution. The addition of FFA increased the FluoZin-3 fluorescence (Figure 11-1), showing FFA elevated $[Zn^{2+}]_i$, probably due to a release of Zn^{2+} from mitochondria. Taken together, these results indicate that FFA (like FCCP and hyperforin) mobilizes mitochondrial Ca^{2+} and Zn^{2+}. However, it is important to note that both the FFA-dependent Fluo-4 and FluoZin-3 signals are much smaller than the ones observed with hyperforin (see Section 11.2). Of note, the concentration of FFA chosen (85 μM) provoks the maximal responses because increasing the concentration of FFA does not further increase the amplitude of the fluorescent responses. Although both FFA and hyperforin have the property to collapse $\Delta\psi_m$, the magnitudes of release of Ca^{2+} (or Zn^{2+}) associated to this effect are different (small with FFA, large with hyperforin). Another difference between the two agents is the fact that FFA acts in a reversible manner in contrast to hyperforin, the actions of which on $[Ca^{2+}]_i$ and $[Zn^{2+}]_i$ has never been reversed even during a continuous washing of this antidepressant. Whether FFA and hyperforin act on the same mitochondrial targets is unknown.

It is interesting to note that the pharmacological tools that are now commonly used to manipulate the activity of TRPC6 channels (FFA and hyperforin) have also the property to alter the mitochondrial homeostasis, triggering the release of cations from these organelles. The exact relationship between these organelles and this family of plasma membrane cation channels needs to be further clarified.

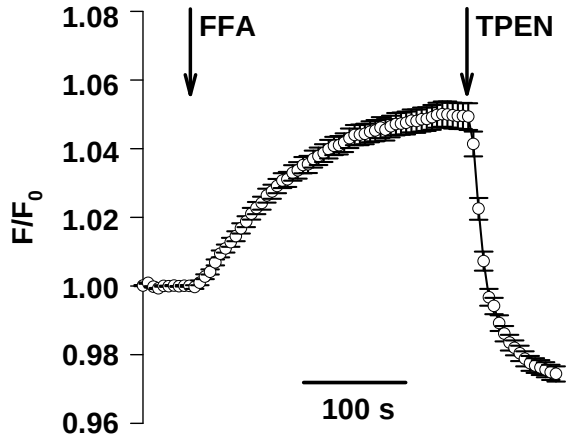

Figure 11-1 FFA mobilized intracellular zinc in cortical neurons

Cortical neurons (n = 52) were kept in a normal Tyrode's solution. The addition of 85 µM FFA increased the FluoZin-3 fluorescence. 50 µM TPEN was added to the bath in the end. It fully reversed the FluoZin-3 responses. The arrows indicate when FFA or TPEN was added.

CONCLUSION

A previous study carried out in the laboratory showed the presence of TRPC6 in the E13 cortex. Calcium imaging experiments indicate the existence of functional DAG-sensitive plasma membrane cation channels in cortical neurons. These channels, displaying TRPC6-like properties, are permeable to Ca^{2+}, Na^{+}, Ba^{2+} and Mn^{2+}. The Ca^{2+} entry is controlled by a Na^{+}-independent mechanism and a Na^{+}-dependent mechanism involving the NCX. The Ca^{2+} entry is blocked by Gd^{3+} and SKF-96365 but is potentiated by FFA. It can be stimulated by the DAG lipase inhibitor RHC80267. However, the OAG-induced responses are not affected by either PKC activation or inhibition. Hyperforin, an activator of TRPC6 channels, triggers an entry of Ca^{2+} via non-selective cation channels. Of note, the OAG-induced responses are insensitive to the TRPC3 channel blocker Pyr3 (unpublished data). Although the exact molecular identity of the DAG-sensitive channels in cortical neurons has not yet been established, we suggest that TRPC6 form these channels. RNAi constructs designed against TRPC6 could be used in cortical neurons in order to gain new information on the precise identity and functions of these channels.

Quantitative analyses with ICP-OES, atomic absorption spectrometry and μ-SXRF show that the over-expression of TRPC6 in HEK cells is accompanied by the elevation of the intracellular contents of zinc, sulphur and manganese, while the contents of iron and copper remain unaffected. Iron and zinc imaging experiments indicate that TRPC6 channels, either over-expressed in HEK cells or endogenously present in cortical neurons, are permeable to iron and zinc (and manganese) when activated by DAG or hyperforin. The experiments with the state-of-art technique μ-SXRF further reveal that activating TRPC6 channels in the presence of iron leads to an intracellular iron accumulation in both HEK-TRPC6 cells and cortical neurons. Thus, in both HEK cells and cortical neurons, TRPC6 channels form iron- and zinc-conducting channels. Analyses of the expression levels of the proteins involved in iron and zinc homeostasis such as DMT1, ferroportin and MT after activating the metal entry via TRPC6 channels may provide further insights into the neuronal regulatory processes participating in iron and zinc homeostasis.

FFA, a pharmacological tool used for distinguishing TRPC6 channels from the other members of the TRPC3/6/7 subgroup, increases $[Ca^{2+}]_i$ in both HEK cells and cortical neurons. These Ca^{2+} responses are unaffected by depleting the ER or by preventing the Ca^{2+} release from the ER. However, they are strongly reduced by bongkrekic acid, a specific ligand of mitochondrial ADP/ATP carrier which inhibits mitochondrial PTP. Experiments with isolated mouse brain mitochondria show that FFA promotes the release of Ca^{2+} from these

organelles and that it causes a collapse of $\Delta\psi_m$. Furthermore, an incubation with FFA but not an acute application of FFA inhibits SOC. Meanwhile, FFA suppresses the DAG-induced Fluo-4 oscillations in HEK-TRPC6 cells. These latter results raise the possibility that the modulation of plasma membrane ion channels by FFA reflects, at least partially, its actions on mitochondrial Ca^{2+} homeostasis. It would be interesting to carry out simultaneous measurements of $[Ca^{2+}]_i$ and $[Ca^{2+}]_m$. This may help us to understand the role played by mitochondria in buffering Ca^{2+} entering the cells via SOC or TRPC6 channels as well as the relationship between the FFA-induced perturbation of mitochondria and the FFA-dependent modulation of plasma membrane channels. Of note, recent experiments reveal that FFA also releases Zn^{2+} from mitochondria.

Hyperforin, which activates TRPC6 channels without activating the other isoforms (TRPC1, TRPC3, TRPC4, TRPC5 and TRPC7), mobilizes the intracellular Ca^{2+} and Zn^{2+}. Like the protonophore FCCP, hyperforin causes a collapse of $\Delta\psi_m$ and promotes a massive release of Ca^{2+} and Zn^{2+} from these organelles via a ruthenium red-sensitive transporter. In addition, chronically applied, hyperforin decreases the intracellular pools of Ca^{2+} and Zn^{2+}. Thus, hyperforin not only triggers the entry of cations via plasma membrane TRPC6 channels but displays protonophore-like properties.

In conclusion, TRPC6 is the putative protein that forms the DAG- and hyperforin-sensitive channels in cortical neurons. TRPC6 channels, both heterologously or endogenously expressed, form cation channels allowing the entry of iron, zinc or manganese. Although the molecular mechanisms favouring the intraneuronal accumulation of metals are far from being understood, this thesis shows that TRPC6 channels can be a candidate pathway allowing the neuronal uptake of trace metal ions. The pathophysiological significance of this TRPC6-dependent entry of metals remains to be clarified. FFA and hyperforin, two pharmacological tools used to, respectively, enhance the activity and trigger the opening of TRPC6 channels, release Ca^{2+} and Zn^{2+} from mitochondria. Caution is thus required when interpreting results obtained with these drugs.

REFERENCES

Aarts M, Iihara K, Wei WL, Xiong ZG, Arundine M, Cerwinski W, MacDonald JF, Tymianski M (2003) A key role for TRPM7 channels in anoxic neuronal death. Cell 115:863-877.

Abramowitz J, Birnbaumer L (2009) Physiology and pathophysiology of canonical transient receptor potential channels. Faseb J 23:297-328.

Agam K, von Campenhausen M, Levy S, Ben-Ami HC, Cook B, Kirschfeld K, Minke B (2000) Metabolic stress reversibly activates the Drosophila light-sensitive channels TRP and TRPL in vivo. J Neurosci 20:5748-5755.

Aguirre P, Mena N, Tapia V, Arredondo M, Nunez MT (2005) Iron homeostasis in neuronal cells: a role for IREG1. BMC Neurosci 6:3.

Aires V, Hichami A, Boulay G, Khan NA (2007) Activation of TRPC6 calcium channels by diacylglycerol (DAG)-containing arachidonic acid: a comparative study with DAG-containing docosahexaenoic acid. Biochimie 89:926-937.

Albert AP, Saleh SN, Large WA (2008) Inhibition of native TRPC6 channel activity by phosphatidylinositol 4,5-bisphosphate in mesenteric artery myocytes. J Physiol 586:3087-3095.

Aldred AR, Dickson PW, Marley PD, Schreiber G (1987) Distribution of transferrin synthesis in brain and other tissues in the rat. J Biol Chem 262:5293-5297.

Alessandri-Haber N, Dina OA, Chen X, Levine JD (2009) TRPC1 and TRPC6 channels cooperate with TRPV4 to mediate mechanical hyperalgesia and nociceptor sensitization. J Neurosci 29:6217-6228.

Andersson DA, Gentry C, Moss S, Bevan S (2009) Clioquinol and pyrithione activate TRPA1 by increasing intracellular Zn2+. Proc Natl Acad Sci U S A 106:8374-8379.

Andrews GK (2001) Cellular zinc sensors: MTF-1 regulation of gene expression. Biometals 14:223-237.

Andrews NC (1999) Disorders of iron metabolism. N Engl J Med 341:1986-1995.

Andrews NC (2005) Molecular control of iron metabolism. Best Pract Res Clin Haematol 18:159-169.

Andrews NC, Schmidt PJ (2007) Iron homeostasis. Annu Rev Physiol 69:69-85.

Arslan P, Di Virgilio F, Beltrame M, Tsien RY, Pozzan T (1985) Cytosolic Ca2+ homeostasis in Ehrlich and Yoshida carcinomas. A new, membrane-permeant chelator of heavy metals reveals that these ascites tumor cell lines have normal cytosolic free Ca2+. J Biol Chem 260:2719-2727.

Atar D, Backx PH, Appel MM, Gao WD, Marban E (1995) Excitation-transcription coupling mediated by zinc influx through voltage-dependent calcium channels. J Biol Chem 270:2473-2477.

Attieh ZK, Mukhopadhyay CK, Seshadri V, Tripoulas NA, Fox PL (1999) Ceruloplasmin ferroxidase activity stimulates cellular iron uptake by a trivalent cation-specific transport mechanism. J Biol Chem 274:1116-1123.

Bae YM, Kim A, Lee YJ, Lim W, Noh YH, Kim EJ, Kim J, Kim TK, Park SW, Kim B, Cho SI, Kim DK, Ho WK (2007) Enhancement of receptor-operated cation current and TRPC6 expression in arterial smooth muscle cells of deoxycorticosterone acetate-salt hypertensive rats. J Hypertens 25:809-817.

Bandyopadhyay BC, Swaim WD, Liu X, Redman RS, Patterson RL, Ambudkar IS (2005) Apical localization of a functional TRPC3/TRPC6-Ca2+-signaling complex in polarized epithelial cells. Role in apical Ca2+ influx. J Biol Chem 280:12908-12916.

Basora N, Boulay G, Bilodeau L, Rousseau E, Payet MD (2003) 20-hydroxyeicosatetraenoic acid (20-HETE) activates mouse TRPC6 channels expressed in HEK293 cells. J Biol Chem 278:31709-31716.

Bassi MT, Manzoni M, Monti E, Pizzo MT, Ballabio A, Borsani G (2000) Cloning of the gene encoding a novel integral membrane protein, mucolipidin-and identification of the two major founder mutations causing mucolipidosis type IV. Am J Hum Genet 67:1110-1120.

Bautista DM, Jordt SE, Nikai T, Tsuruda PR, Read AJ, Poblete J, Yamoah EN, Basbaum AI, Julius D (2006) TRPA1 mediates the inflammatory actions of environmental irritants and proalgesic agents. Cell 124:1269-1282.

Bayliss WM (1902) On the local reactions of the arterial wall to changes of internal pressure. J Physiol 28:220-231.

Beerhues L (2006) Hyperforin. Phytochemistry 67:2201-2207.

Beskina O, Miller A, Mazzocco-Spezzia A, Pulina MV, Golovina VA (2007) Mechanisms of interleukin-1beta-induced Ca2+ signals in mouse cortical astrocytes: roles of store- and receptor-operated Ca2+ entry. Am J Physiol Cell Physiol 293:C1103-1111.

Birnbaumer L (2009) The TRPC class of ion channels: a critical review of their roles in slow, sustained increases in intracellular Ca(2+) concentrations. Annu Rev Pharmacol Toxicol 49:395-426.

Blaustein MP, Lederer WJ (1999) Sodium/calcium exchange: its physiological implications. Physiol Rev 79:763-854.

Bloch B, Popovici T, Chouham S, Levin MJ, Tuil D, Kahn A (1987) Transferrin gene expression in choroid plexus of the adult rat brain. Brain Res Bull 18:573-576.

Boisseau S, Kunert-Keil C, Lucke S, Bouron A (2009) Heterogeneous distribution of TRPC proteins in the embryonic cortex. Histochem Cell Biol 131:355-363.

Bonaventure P, Guo H, Tian B, Liu X, Bittner A, Roland B, Salunga R, Ma XJ, Kamme F, Meurers B, Bakker M, Jurzak M, Leysen JE, Erlander MG (2002) Nuclei and subnuclei gene expression profiling in mammalian brain. Brain Res 943:38-47.

Bossy-Wetzel E, Talantova MV, Lee WD, Scholzke MN, Harrop A, Mathews E, Gotz T, Han J, Ellisman MH, Perkins GA, Lipton SA (2004) Crosstalk between nitric oxide and zinc pathways to neuronal cell death involving mitochondrial dysfunction and p38-activated K+ channels. Neuron 41:351-365.

Bostanci MO, Bagirici F, Canan S (2006) A calcium channel blocker flunarizine attenuates the neurotoxic effects of iron. Cell Biol Toxicol 22:119-125.

Boulay G (2002) Ca(2+)-calmodulin regulates receptor-operated Ca(2+) entry activity of TRPC6 in HEK-293 cells. Cell Calcium 32:201-207.

Boulay G, Zhu X, Peyton M, Jiang M, Hurst R, Stefani E, Birnbaumer L (1997) Cloning and expression of a novel mammalian homolog of Drosophila transient receptor potential (Trp) involved in calcium entry secondary to activation of receptors coupled by the Gq class of G protein. J Biol Chem 272:29672-29680.

Boulay G, Brown DM, Qin N, Jiang M, Dietrich A, Zhu MX, Chen Z, Birnbaumer M, Mikoshiba K, Birnbaumer L (1999) Modulation of Ca(2+) entry by polypeptides of the inositol 1,4, 5-trisphosphate receptor (IP3R) that bind transient receptor potential (TRP): evidence for roles of TRP and IP3R in store depletion-activated Ca(2+) entry. Proc Natl Acad Sci U S A 96:14955-14960.

Bouron A, Altafaj X, Boisseau S, De Waard M (2005) A store-operated Ca2+ influx activated in response to the depletion of thapsigargin-sensitive Ca2+ stores is developmentally regulated in embryonic cortical neurons from mice. Brain Res Dev Brain Res 159:64-71.

Bouron A, Boisseau S, De Waard M, Peris L (2006) Differential down-regulation of voltage-gated calcium channel currents by glutamate and BDNF in embryonic cortical neurons. Eur J Neurosci 24:699-708.

Bradbury MW (1997) Transport of iron in the blood-brain-cerebrospinal fluid system. J Neurochem 69:443-454.

Brechard S, Melchior C, Plancon S, Schenten V, Tschirhart EJ (2008) Store-operated Ca2+ channels formed by TRPC1, TRPC6 and Orai1 and non-store-operated channels formed by TRPC3 are involved in the regulation of NADPH oxidase in HL-60 granulocytes. Cell Calcium 44:492-506.

Breuer W, Epsztejn S, Cabantchik ZI (1995) Iron acquired from transferrin by K562 cells is delivered into a cytoplasmic pool of chelatable iron(II). J Biol Chem 270:24209-24215.

Burdo JR, Connor JR (2003) Brain iron uptake and homeostatic mechanisms: an overview. Biometals 16:63-75.

Burdo JR, Antonetti DA, Wolpert EB, Connor JR (2003) Mechanisms and regulation of transferrin and iron transport in a model blood-brain barrier system. Neuroscience 121:883-890.

Burdo JR, Menzies SL, Simpson IA, Garrick LM, Garrick MD, Dolan KG, Haile DJ, Beard JL, Connor JR (2001) Distribution of divalent metal transporter 1 and metal transport protein 1 in the normal and Belgrade rat. J Neurosci Res 66:1198-1207.

Bush AI, Pettingell WH, Multhaup G, d Paradis M, Vonsattel JP, Gusella JF, Beyreuther K, Masters CL, Tanzi RE (1994) Rapid induction of Alzheimer A beta amyloid formation by zinc. Science 265:1464-1467.

Cahalan MD (2009) STIMulating store-operated Ca(2+) entry. Nat Cell Biol 11:669-677.

Canzoniero LM, Turetsky DM, Choi DW (1999) Measurement of intracellular free zinc concentrations accompanying zinc-induced neuronal death. J Neurosci 19:RC31.

Capasso M, Jeng JM, Malavolta M, Mocchegiani E, Sensi SL (2005) Zinc dyshomeostasis: a key modulator of neuronal injury. J Alzheimers Dis 8:93-108; discussion 209-115.

Carafoli E (2003) The calcium-signalling saga: tap water and protein crystals. Nat Rev Mol Cell Biol 4:326-332.

Carriedo SG, Yin HZ, Sensi SL, Weiss JH (1998) Rapid Ca2+ entry through Ca2+-permeable AMPA/Kainate channels triggers marked intracellular Ca2+ rises and consequent oxygen radical production. J Neurosci 18:7727-7738.

Carter RN, Tolhurst G, Walmsley G, Vizuete-Forster M, Miller N, Mahaut-Smith MP (2006) Molecular and electrophysiological characterization of transient receptor potential ion channels in the primary murine megakaryocyte. J Physiol 576:151-162.

Caterina MJ, Rosen TA, Tominaga M, Brake AJ, Julius D (1999) A capsaicin-receptor homologue with a high threshold for noxious heat. Nature 398:436-441.

Caterina MJ, Schumacher MA, Tominaga M, Rosen TA, Levine JD, Julius D (1997) The capsaicin receptor: a heat-activated ion channel in the pain pathway. Nature 389:816-824.

Cayouette S, Lussier MP, Mathieu EL, Bousquet SM, Boulay G (2004) Exocytotic insertion of TRPC6 channel into the plasma membrane upon Gq protein-coupled receptor activation. J Biol Chem 279:7241-7246.

Chalmers S, Olson ML, MacMillan D, Rainbow RD, McCarron JG (2007) Ion channels in smooth muscle: regulation by the sarcoplasmic reticulum and mitochondria. Cell Calcium 42:447-466.

Chatterjee S, Filippov V, Lishko P, Maximyuk O, Noldner M, Krishtal O (1999) Hyperforin attenuates various ionic conductance mechanisms in the isolated hippocampal neurons of rat. Life Sci 65:2395-2405.

Chatterjee SS, Stefanovich V (1976) Influence of anti-inflammatory agents on rat liver mitochondrial ATPase. Arzneimittelforschung 26:499-502.

Chatterjee SS, Bhattacharya SK, Wonnemann M, Singer A, Muller WE (1998) Hyperforin as a possible antidepressant component of hypericum extracts. Life Sci 63:499-510.

Chaudhuri P, Colles SM, Bhat M, Van Wagoner DR, Birnbaumer L, Graham LM (2008) Elucidation of a TRPC6-TRPC5 channel cascade that restricts endothelial cell movement. Mol Biol Cell 19:3203-3211.

Chen Y, Irie Y, Keung WM, Maret W (2002) S-nitrosothiols react preferentially with zinc thiolate clusters of metallothionein III through transnitrosation. Biochemistry 41:8360-8367.

Cheng C, Reynolds IJ (1998) Calcium-sensitive fluorescent dyes can report increases in intracellular free zinc concentration in cultured forebrain neurons. J Neurochem 71:2401-2410.

Cheranov SY, Jaggar JH (2004) Mitochondrial modulation of Ca2+ sparks and transient KCa currents in smooth muscle cells of rat cerebral arteries. J Physiol 556:755-771.

Cho H, Kim MS, Shim WS, Yang YD, Koo J, Oh U (2003) Calcium-activated cationic channel in rat sensory neurons. Eur J Neurosci 17:2630-2638.

Choi DW, Yokoyama M, Koh J (1988) Zinc neurotoxicity in cortical cell culture. Neuroscience 24:67-79.

Choi YB, Lipton SA (1999) Identification and mechanism of action of two histidine residues underlying high-affinity Zn2+ inhibition of the NMDA receptor. Neuron 23:171-180.

Christensen AP, Corey DP (2007) TRP channels in mechanosensation: direct or indirect activation? Nat Rev Neurosci 8:510-521.

Chyb S, Raghu P, Hardie RC (1999) Polyunsaturated fatty acids activate the Drosophila light-sensitive channels TRP and TRPL. Nature 397:255-259.

Clapham DE (2003) TRP channels as cellular sensors. Nature 426:517-524.

Clapham DE (2007) SnapShot: mammalian TRP channels. Cell 129:220.

Clapham DE, Runnels LW, Strubing C (2001) The TRP ion channel family. Nat Rev Neurosci 2:387-396.

Clapham DE, Julius D, Montell C, Schultz G (2005) International Union of Pharmacology. XLIX. Nomenclature and structure-function relationships of transient receptor potential channels. Pharmacol Rev 57:427-450.

Collins TJ, Lipp P, Berridge MJ, Bootman MD (2001) Mitochondrial Ca(2+) uptake depends on the spatial and temporal profile of cytosolic Ca(2+) signals. J Biol Chem 276:26411-26420.

Colvin RA (2002) pH dependence and compartmentalization of zinc transported across plasma membrane of rat cortical neurons. Am J Physiol Cell Physiol 282:C317-329.

Colvin RA, Davis N, Nipper RW, Carter PA (2000a) Zinc transport in the brain: routes of zinc influx and efflux in neurons. J Nutr 130:1484S-1487S.

Colvin RA, Davis N, Nipper RW, Carter PA (2000b) Evidence for a zinc/proton antiporter in rat brain. Neurochem Int 36:539-547.

Colvin RA, Fontaine CP, Laskowski M, Thomas D (2003) Zn2+ transporters and Zn2+ homeostasis in neurons. Eur J Pharmacol 479:171-185.

Corey DP, Garcia-Anoveros J, Holt JR, Kwan KY, Lin SY, Vollrath MA, Amalfitano A, Cheung EL, Derfler BH, Duggan A, Geleoc GS, Gray PA, Hoffman MP, Rehm HL, Tamasauskas D, Zhang DS (2004) TRPA1 is a candidate for the mechanosensitive transduction channel of vertebrate hair cells. Nature 432:723-730.

Cosens DJ, Manning A (1969) Abnormal electroretinogram from a Drosophila mutant. Nature 224:285-287.

Cousins RJ, McMahon RJ (2000) Integrative aspects of zinc transporters. J Nutr 130:1384S-1387S.

Cousins RJ, Liuzzi JP, Lichten LA (2006) Mammalian zinc transport, trafficking, and signals. J Biol Chem 281:24085-24089.

Cuajungco MP, Lees GJ (1997) Zinc metabolism in the brain: relevance to human neurodegenerative disorders. Neurobiol Dis 4:137-169.

Damak S, Rong M, Yasumatsu K, Kokrashvili Z, Perez CA, Shigemura N, Yoshida R, Mosinger B, Jr., Glendinning JI, Ninomiya Y, Margolskee RF (2006) Trpm5 null mice respond to bitter, sweet, and umami compounds. Chem Senses 31:253-264.

Damann N, Voets T, Nilius B (2008) TRPs in our senses. Curr Biol 18:R880-889.

De Domenico I, Lo E, Ward DM, Kaplan J (2009) Hepcidin-induced internalization of ferroportin requires binding and cooperative interaction with Jak2. Proc Natl Acad Sci U S A 106:3800-3805.

Deane R, Zheng W, Zlokovic BV (2004) Brain capillary endothelium and choroid plexus epithelium regulate transport of transferrin-bound and free iron into the rat brain. J Neurochem 88:813-820.

Delmas P, Wanaverbecq N, Abogadie FC, Mistry M, Brown DA (2002) Signaling microdomains define the specificity of receptor-mediated InsP(3) pathways in neurons. Neuron 34:209-220.

Demaurex N, Poburko D, Frieden M (2009) Regulation of plasma membrane calcium fluxes by mitochondria. Biochim Biophys Acta.

Dhaka A, Viswanath V, Patapoutian A (2006) Trp ion channels and temperature sensation. Annu Rev Neurosci 29:135-161.

di Patti MC, Persichini T, Mazzone V, Polticelli F, Colasanti M, Musci G (2004) Interleukin-1beta up-regulates iron efflux in rat C6 glioma cells through modulation of ceruloplasmin and ferroportin-1 synthesis. Neurosci Lett 363:182-186.

Dickinson TK, Connor JR (1998) Immunohistochemical analysis of transferrin receptor: regional and cellular distribution in the hypotransferrinemic (hpx) mouse brain. Brain Res 801:171-181.

Dickson BJ (2002) Molecular mechanisms of axon guidance. Science 298:1959-1964.

Dickson PW, Aldred AR, Marley PD, Tu GF, Howlett GJ, Schreiber G (1985) High prealbumin and transferrin mRNA levels in the choroid plexus of rat brain. Biochem Biophys Res Commun 127:890-895.

Dietrich A, Gudermann T (2007) Trpc6. Handb Exp Pharmacol:125-141.

Dietrich A, Kalwa H, Rost BR, Gudermann T (2005a) The diacylgylcerol-sensitive TRPC3/6/7 subfamily of cation channels: functional characterization and physiological relevance. Pflugers Arch 451:72-80.

Dietrich A, Mederos YSM, Gollasch M, Gross V, Storch U, Dubrovska G, Obst M, Yildirim E, Salanova B, Kalwa H, Essin K, Pinkenburg O, Luft FC, Gudermann T, Birnbaumer L (2005b) Increased vascular smooth muscle contractility in TRPC6-/- mice. Mol Cell Biol 25:6980-6989.

Dong XP, Cheng X, Mills E, Delling M, Wang F, Kurz T, Xu H (2008) The type IV mucolipidosis-associated protein TRPML1 is an endolysosomal iron release channel. Nature 455:992-996.

Donovan A, Roy CN, Andrews NC (2006) The ins and outs of iron homeostasis. Physiology (Bethesda) 21:115-123.

Duszynski J, Koziel R, Brutkowski W, Szczepanowska J, Zablocki K (2006) The regulatory role of mitochondria in capacitative calcium entry. Biochim Biophys Acta 1757:380-387.

Eder P, Poteser M, Romanin C, Groschner K (2005) Na(+) entry and modulation of Na(+)/Ca(2+) exchange as a key mechanism of TRPC signaling. Pflugers Arch 451:99-104.

Eide DJ (2006) Zinc transporters and the cellular trafficking of zinc. Biochim Biophys Acta 1763:711-722.

Eisenstein RS, Tuazon PT, Schalinske KL, Anderson SA, Traugh JA (1993) Iron-responsive element-binding protein. Phosphorylation by protein kinase C. J Biol Chem 268:27363-27370.

El Boustany C, Bidaux G, Enfissi A, Delcourt P, Prevarskaya N, Capiod T (2008) Capacitative calcium entry and transient receptor potential canonical 6 expression control human hepatoma cell proliferation. Hepatology 47:2068-2077.

Elg S, Marmigere F, Mattsson JP, Ernfors P (2007) Cellular subtype distribution and developmental regulation of TRPC channel members in the mouse dorsal root ganglion. J Comp Neurol 503:35-46.

Espinosa de los Monteros A, Kumar S, Scully S, Cole R, de Vellis J (1990) Transferrin gene expression and secretion by rat brain cells in vitro. J Neurosci Res 25:576-580.

Estacion M, Li S, Sinkins WG, Gosling M, Bahra P, Poll C, Westwick J, Schilling WP (2004) Activation of human TRPC6 channels by receptor stimulation. J Biol Chem 279:22047-22056.

Farrugia G, Rae JL, Szurszewski JH (1993a) Characterization of an outward potassium current in canine jejunal circular smooth muscle and its activation by fenamates. J Physiol 468:297-310.

Farrugia G, Rae JL, Sarr MG, Szurszewski JH (1993b) Potassium current in circular smooth muscle of human jejunum activated by fenamates. Am J Physiol 265:G873-879.

Fatherazi S, Presland RB, Belton CM, Goodwin P, Al-Qutub M, Trbic Z, Macdonald G, Schubert MM, Izutsu KT (2007) Evidence that TRPC4 supports the calcium selective I(CRAC)-like current in human gingival keratinocytes. Pflugers Arch 453:879-889.

Faucheux BA, Nillesse N, Damier P, Spik G, Mouatt-Prigent A, Pierce A, Leveugle B, Kubis N, Hauw JJ, Agid Y, et al. (1995) Expression of lactoferrin receptors is increased in the mesencephalon of patients with Parkinson disease. Proc Natl Acad Sci U S A 92:9603-9607.

Feisst C, Werz O (2004) Suppression of receptor-mediated Ca2+ mobilization and functional leukocyte responses by hyperforin. Biochem Pharmacol 67:1531-1539.

Fellner SK, Arendshorst WJ (2008) Angiotensin II-stimulated Ca2+ entry mechanisms in afferent arterioles: role of transient receptor potential canonical channels and reverse Na+/Ca2+ exchange. Am J Physiol Renal Physiol 294:F212-219.

Feske S, Gwack Y, Prakriya M, Srikanth S, Puppel SH, Tanasa B, Hogan PG, Lewis RS, Daly M, Rao A (2006) A mutation in Orai1 causes immune deficiency by abrogating CRAC channel function. Nature 441:179-185.

Fillebeen C, Descamps L, Dehouck MP, Fenart L, Benaissa M, Spik G, Cecchelli R, Pierce A (1999) Receptor-mediated transcytosis of lactoferrin through the blood-brain barrier. J Biol Chem 274:7011-7017.

Fisher J, Devraj K, Ingram J, Slagle-Webb B, Madhankumar AB, Liu X, Klinger M, Simpson IA, Connor JR (2007) Ferritin: a novel mechanism for delivery of iron to the brain and other organs. Am J Physiol Cell Physiol 293:C641-649.

Fisunov A, Lozovaya N, Tsintsadze T, Chatterjee S, Noldner M, Krishtal O (2000) Hyperforin modulates gating of P-type Ca2+ current in cerebellar Purkinje neurons. Pflugers Arch 440:427-434.

Fleming I, Rueben A, Popp R, Fisslthaler B, Schrodt S, Sander A, Haendeler J, Falck JR, Morisseau C, Hammock BD, Busse R (2007) Epoxyeicosatrienoic acids regulate Trp channel dependent Ca2+ signaling and hyperpolarization in endothelial cells. Arterioscler Thromb Vasc Biol 27:2612-2618.

Flockerzi V (2007) An introduction on TRP channels. Handb Exp Pharmacol:1-19.

Foller M, Kasinathan RS, Koka S, Lang C, Shumilina E, Birnbaumer L, Lang F, Huber SM (2008) TRPC6 contributes to the Ca(2+) leak of human erythrocytes. Cell Physiol Biochem 21:183-192.

Foster RR, Zadeh MA, Welsh GI, Satchell SC, Ye Y, Mathieson PW, Bates DO, Saleem MA (2009) Flufenamic acid is a tool for investigating TRPC6-mediated calcium signalling in human conditionally immortalised podocytes and HEK293 cells. Cell Calcium.

Frederickson CJ (1989) Neurobiology of zinc and zinc-containing neurons. Int Rev Neurobiol 31:145-238.

Frederickson CJ, Bush AI (2001) Synaptically released zinc: physiological functions and pathological effects. Biometals 14:353-366.

Frederickson CJ, Koh JY, Bush AI (2005) The neurobiology of zinc in health and disease. Nat Rev Neurosci 6:449-462.

Freichel M, Suh SH, Pfeifer A, Schweig U, Trost C, Weissgerber P, Biel M, Philipp S, Freise D, Droogmans G, Hofmann F, Flockerzi V, Nilius B (2001) Lack of an endothelial store-operated Ca2+ current impairs agonist-dependent vasorelaxation in TRP4-/- mice. Nat Cell Biol 3:121-127.

Freund WD, Reddig S (1994) AMPA/Zn(2+)-induced neurotoxicity in rat primary cortical cultures: involvement of L-type calcium channels. Brain Res 654:257-264.

Gaasch JA, Lockman PR, Geldenhuys WJ, Allen DD, Van der Schyf CJ (2007a) Brain iron toxicity: differential responses of astrocytes, neurons, and endothelial cells. Neurochem Res 32:1196-1208.

Gaasch JA, Geldenhuys WJ, Lockman PR, Allen DD, Van der Schyf CJ (2007b) Voltage-gated calcium channels provide an alternate route for iron uptake in neuronal cell cultures. Neurochem Res 32:1686-1693.

Garcia RL, Schilling WP (1997) Differential expression of mammalian TRP homologues across tissues and cell lines. Biochem Biophys Res Commun 239:279-283.

Gee KR, Zhou ZL, Qian WJ, Kennedy R (2002a) Detection and imaging of zinc secretion from pancreatic beta-cells using a new fluorescent zinc indicator. J Am Chem Soc 124:776-778.

Gee KR, Zhou ZL, Ton-That D, Sensi SL, Weiss JH (2002b) Measuring zinc in living cells. A new generation of sensitive and selective fluorescent probes. Cell Calcium 31:245-251.

Gerasimenko O, Tepikin A (2005) How to measure Ca2+ in cellular organelles? Cell Calcium 38:201-211.

Giampa C, DeMarch Z, Patassini S, Bernardi G, Fusco FR (2007) Immunohistochemical localization of TRPC6 in the rat substantia nigra. Neurosci Lett 424:170-174.

Glitsch MD, Bakowski D, Parekh AB (2002) Store-operated Ca2+ entry depends on mitochondrial Ca2+ uptake. Embo J 21:6744-6754.

Godin N, Rousseau E (2007) TRPC6 silencing in primary airway smooth muscle cells inhibits protein expression without affecting OAG-induced calcium entry. Mol Cell Biochem 296:193-201.

Goel M, Sinkins WG, Schilling WP (2002) Selective association of TRPC channel subunits in rat brain synaptosomes. J Biol Chem 277:48303-48310.

Goel M, Sinkins W, Keightley A, Kinter M, Schilling WP (2005) Proteomic analysis of TRPC5- and TRPC6-binding partners reveals interaction with the plasmalemmal Na(+)/K(+)-ATPase. Pflugers Arch 451:87-98.

Gogelein H, Dahlem D, Englert HC, Lang HJ (1990) Flufenamic acid, mefenamic acid and niflumic acid inhibit single nonselective cation channels in the rat exocrine pancreas. FEBS Lett 268:79-82.

Goncalves T, Carvalho AP, Oliveira CR (1991) Antioxidant effect of calcium antagonists on microsomal membranes isolated from different brain areas. Eur J Pharmacol 204:315-322.

Gottlieb P, Folgering J, Maroto R, Raso A, Wood TG, Kurosky A, Bowman C, Bichet D, Patel A, Sachs F, Martinac B, Hamill OP, Honore E (2008) Revisiting TRPC1 and TRPC6 mechanosensitivity. Pflugers Arch 455:1097-1103.

Graham S, Ding M, Sours-Brothers S, Yorio T, Ma JX, Ma R (2007) Downregulation of TRPC6 protein expression by high glucose, a possible mechanism for the impaired Ca2+ signaling in glomerular mesangial cells in diabetes. Am J Physiol Renal Physiol 293:F1381-1390.

Greenwood IA, Helliwell RM, Large WA (1997) Modulation of Ca(2+)-activated Cl- currents in rabbit portal vein smooth muscle by an inhibitor of mitochondrial Ca2+ uptake. J Physiol 505 (Pt 1):53-64.

Greka A, Navarro B, Oancea E, Duggan A, Clapham DE (2003) TRPC5 is a regulator of hippocampal neurite length and growth cone morphology. Nat Neurosci 6:837-845.

Grynkiewicz G, Poenie M, Tsien RY (1985) A new generation of Ca2+ indicators with greatly improved fluorescence properties. J Biol Chem 260:3440-3450.

Guilbert A, Gautier M, Dhennin-Duthille I, Haren N, Sevestre H, Ouadid-Ahidouch H (2009) Evidence that TRPM7 is required for breast cancer cell proliferation. Am J Physiol Cell Physiol.

Guilbert A, Dhennin-Duthille I, Hiani YE, Haren N, Khorsi H, Sevestre H, Ahidouch A, Ouadid-Ahidouch H (2008) Expression of TRPC6 channels in human epithelial breast cancer cells. BMC Cancer 8:125.

Guler AD, Lee H, Iida T, Shimizu I, Tominaga M, Caterina M (2002) Heat-evoked activation of the ion channel, TRPV4. J Neurosci 22:6408-6414.

Gunshin H, Mackenzie B, Berger UV, Gunshin Y, Romero MF, Boron WF, Nussberger S, Gollan JL, Hediger MA (1997) Cloning and characterization of a mammalian proton-coupled metal-ion transporter. Nature 388:482-488.

Hacker K, Medler KF (2008) Mitochondrial calcium buffering contributes to the maintenance of Basal calcium levels in mouse taste cells. J Neurophysiol 100:2177-2191.

Hahn P, Qian Y, Dentchev T, Chen L, Beard J, Harris ZL, Dunaief JL (2004) Disruption of ceruloplasmin and hephaestin in mice causes retinal iron overload and retinal degeneration with features of age-related macular degeneration. Proc Natl Acad Sci U S A 101:13850-13855.

Halliwell B (2006) Oxidative stress and neurodegeneration: where are we now? J Neurochem 97:1634-1658.

Hansen TM, Nielsen H, Bernth N, Moos T (1999) Expression of ferritin protein and subunit mRNAs in normal and iron deficient rat brain. Brain Res Mol Brain Res 65:186-197.

Hara Y, Wakamori M, Ishii M, Maeno E, Nishida M, Yoshida T, Yamada H, Shimizu S, Mori E, Kudoh J, Shimizu N, Kurose H, Okada Y, Imoto K, Mori Y (2002) LTRPC2 Ca2+-permeable channel activated by changes in redox status confers susceptibility to cell death. Mol Cell 9:163-173.

Hardie RC (2007) TRP channels and lipids: from Drosophila to mammalian physiology. J Physiol 578:9-24.

Hardie RC, Minke B (1992) The trp gene is essential for a light-activated Ca2+ channel in Drosophila photoreceptors. Neuron 8:643-651.

Harrison PM, Arosio P (1996) The ferritins: molecular properties, iron storage function and cellular regulation. Biochim Biophys Acta 1275:161-203.

Hassock SR, Zhu MX, Trost C, Flockerzi V, Authi KS (2002) Expression and role of TRPC proteins in human platelets: evidence that TRPC6 forms the store-independent calcium entry channel. Blood 100:2801-2811.

Hentze MW, Muckenthaler MU, Andrews NC (2004) Balancing acts: molecular control of mammalian iron metabolism. Cell 117:285-297.

Hewavitharana T, Deng X, Soboloff J, Gill DL (2007) Role of STIM and Orai proteins in the store-operated calcium signaling pathway. Cell Calcium 42:173-182.

Hidalgo J, Aschner M, Zatta P, Vasak M (2001) Roles of the metallothionein family of proteins in the central nervous system. Brain Res Bull 55:133-145.

Hilgemann DW, Feng S, Nasuhoglu C (2001) The complex and intriguing lives of PIP2 with ion channels and transporters. Sci STKE 2001:RE19.

Hill AJ, Hinton JM, Cheng H, Gao Z, Bates DO, Hancox JC, Langton PD, James AF (2006) A TRPC-like non-selective cation current activated by alpha 1-adrenoceptors in rat mesenteric artery smooth muscle cells. Cell Calcium 40:29-40.

Hill K, Benham CD, McNulty S, Randall AD (2004) Flufenamic acid is a pH-dependent antagonist of TRPM2 channels. Neuropharmacology 47:450-460.

Hisatsune C, Kuroda Y, Nakamura K, Inoue T, Nakamura T, Michikawa T, Mizutani A, Mikoshiba K (2004) Regulation of TRPC6 channel activity by tyrosine phosphorylation. J Biol Chem 279:18887-18894.

Hofmann T, Schaefer M, Schultz G, Gudermann T (2002) Subunit composition of mammalian transient receptor potential channels in living cells. Proc Natl Acad Sci U S A 99:7461-7466.

Hofmann T, Obukhov AG, Schaefer M, Harteneck C, Gudermann T, Schultz G (1999) Direct activation of human TRPC6 and TRPC3 channels by diacylglycerol. Nature 397:259-263.

Hoth M, Fanger CM, Lewis RS (1997) Mitochondrial regulation of store-operated calcium signaling in T lymphocytes. J Cell Biol 137:633-648.

Hu H, Bandell M, Petrus MJ, Zhu MX, Patapoutian A (2009) Zinc activates damage-sensing TRPA1 ion channels. Nat Chem Biol 5:183-190.

Huang GN, Zeng W, Kim JY, Yuan JP, Han L, Muallem S, Worley PF (2006) STIM1 carboxyl-terminus activates native SOC, I(crac) and TRPC1 channels. Nat Cell Biol 8:1003-1010.

Huang WC, Young JS, Glitsch MD (2007) Changes in TRPC channel expression during postnatal development of cerebellar neurons. Cell Calcium 42:1-10.

Hulet SW, Heyliger SO, Powers S, Connor JR (2000) Oligodendrocyte progenitor cells internalize ferritin via clathrin-dependent receptor mediated endocytosis. J Neurosci Res 61:52-60.

Hulet SW, Hess EJ, Debinski W, Arosio P, Bruce K, Powers S, Connor JR (1999) Characterization and distribution of ferritin binding sites in the adult mouse brain. J Neurochem 72:868-874.

Inoue R, Okada T, Onoue H, Hara Y, Shimizu S, Naitoh S, Ito Y, Mori Y (2001) The transient receptor potential protein homologue TRP6 is the essential component of vascular alpha(1)-adrenoceptor-activated Ca(2+)-permeable cation channel. Circ Res 88:325-332.

Inoue R, Jensen LJ, Jian Z, Shi J, Hai L, Lurie AI, Henriksen FH, Salmonsson M, Morita H, Kawarabayashi Y, Mori M, Mori Y, Ito Y (2009) Synergistic Activation of Vascular TRPC6 Channel by Receptor and Mechanical Stimulation via Phospholipase C/Diacylglycerol and Phospholipase A2/{omega}-Hydroxylase/ 20-HETE Pathways. Circ Res.

Jacob C, Maret W, Vallee BL (1998) Control of zinc transfer between thionein, metallothionein, and zinc proteins. Proc Natl Acad Sci U S A 95:3489-3494.

Jardin I, Redondo PC, Salido GM, Rosado JA (2008) Phosphatidylinositol 4,5-bisphosphate enhances store-operated calcium entry through hTRPC6 channel in human platelets. Biochim Biophys Acta 1783:84-97.

Jardin I, Gomez LJ, Salido GM, Rosado JA (2009) Dynamic interaction of hTRPC6 with the Orai1-STIM1 complex or hTRPC3 mediates its role in capacitative or non-capacitative Ca(2+) entry pathways. Biochem J 420:267-276.

Jeong SY, David S (2003) Glycosylphosphatidylinositol-anchored ceruloplasmin is required for iron efflux from cells in the central nervous system. J Biol Chem 278:27144-27148.

Jia Y, Jeng JM, Sensi SL, Weiss JH (2002) Zn2+ currents are mediated by calcium-permeable AMPA/kainate channels in cultured murine hippocampal neurones. J Physiol 543:35-48.

Jia Y, Zhou J, Tai Y, Wang Y (2007) TRPC channels promote cerebellar granule neuron survival. Nat Neurosci 10:559-567.

Jiang D, Sullivan PG, Sensi SL, Steward O, Weiss JH (2001) Zn(2+) induces permeability transition pore opening and release of pro-apoptotic peptides from neuronal mitochondria. J Biol Chem 276:47524-47529.

Jiang DH, Ke Y, Cheng YZ, Ho KP, Qian ZM (2002) Distribution of ferroportin1 protein in different regions of developing rat brain. Dev Neurosci 24:94-98.

Jones LC, Beard JL, Jones BC (2008) Genetic analysis reveals polygenic influences on iron, copper, and zinc in mouse hippocampus with neurobiological implications. Hippocampus 18:398-410.

Jordani MC, Santos AC, Prado IM, Uyemura SA, Curti C (2000) Flufenamic acid as an inducer of mitochondrial permeability transition. Mol Cell Biochem 210:153-158.

Jung S, Strotmann R, Schultz G, Plant TD (2002) TRPC6 is a candidate channel involved in receptor-stimulated cation currents in A7r5 smooth muscle cells. Am J Physiol Cell Physiol 282:C347-359.

Kankaanranta H, Moilanen E (1995) Flufenamic and tolfenamic acids inhibit calcium influx in human polymorphonuclear leukocytes. Mol Pharmacol 47:1006-1013.

Kankaanranta H, Luomala M, Kosonen O, Moilanen E (1996) Inhibition by fenamates of calcium influx and proliferation of human lymphocytes. Br J Pharmacol 119:487-494.

Kawasaki BT, Liao Y, Birnbaumer L (2006) Role of Src in C3 transient receptor potential channel function and evidence for a heterogeneous makeup of receptor- and store-operated Ca2+ entry channels. Proc Natl Acad Sci U S A 103:335-340.

Ke Y, Qian ZM (2007) Brain iron metabolism: neurobiology and neurochemistry. Prog Neurobiol 83:149-173.

Kennard ML, Richardson DR, Gabathuler R, Ponka P, Jefferies WA (1995) A novel iron uptake mechanism mediated by GPI-anchored human p97. Embo J 14:4178-4186.

Keseru B, Barbosa-Sicard E, Popp R, Fisslthaler B, Dietrich A, Gudermann T, Hammock BD, Falck JR, Weissmann N, Busse R, Fleming I (2008) Epoxyeicosatrienoic acids and the soluble epoxide hydrolase are determinants of pulmonary artery pressure and the acute hypoxic pulmonary vasoconstrictor response. Faseb J 22:4306-4315.

Kidane TZ, Sauble E, Linder MC (2006) Release of iron from ferritin requires lysosomal activity. Am J Physiol Cell Physiol 291:C445-455.

Kim AH, Sheline CT, Tian M, Higashi T, McMahon RJ, Cousins RJ, Choi DW (2000) L-type Ca(2+) channel-mediated Zn(2+) toxicity and modulation by ZnT-1 in PC12 cells. Brain Res 886:99-107.

Kim BJ, Jeon JH, Kim SJ, So I, Kim KW (2007) Regulation of transient receptor potential melastatin 7 (TRPM7) currents by mitochondria. Mol Cells 23:363-369.

Kim JY, Saffen D (2005) Activation of M1 muscarinic acetylcholine receptors stimulates the formation of a multiprotein complex centered on TRPC6 channels. J Biol Chem 280:32035-32047.

Kim YH, Koh JY (2002) The role of NADPH oxidase and neuronal nitric oxide synthase in zinc-induced poly(ADP-ribose) polymerase activation and cell death in cortical culture. Exp Neurol 177:407-418.

Kiselyov K, Patterson RL (2009) The integrative function of TRPC channels. Front Biosci 14:45-58.

Kiselyov K, Xu X, Mozhayeva G, Kuo T, Pessah I, Mignery G, Zhu X, Birnbaumer L, Muallem S (1998) Functional interaction between InsP3 receptors and store-operated Htrp3 channels. Nature 396:478-482.

Kiyonaka S, Kato K, Nishida M, Mio K, Numaga T, Sawaguchi Y, Yoshida T, Wakamori M, Mori E, Numata T, Ishii M, Takemoto H, Ojida A, Watanabe K, Uemura A, Kurose H, Morii T, Kobayashi T, Sato Y, Sato C, Hamachi I, Mori Y (2009) Selective and direct inhibition of TRPC3 channels underlies biological activities of a pyrazole compound. Proc Natl Acad Sci U S A 106:5400-5405.

Klomp LW, Farhangrazi ZS, Dugan LL, Gitlin JD (1996) Ceruloplasmin gene expression in the murine central nervous system. J Clin Invest 98:207-215.

Koch E, Chatterjee SS (2001) Hyperforin stimulates intracellular calcium mobilisation and enhances extracellular acidification in DDT1-MF2 smooth muscle cells. Pharmacopsychiatry 34 Suppl 1:S70-73.

Koh JY, Choi DW (1994) Zinc toxicity on cultured cortical neurons: involvement of N-methyl-D-aspartate receptors. Neuroscience 60:1049-1057.

Koh JY, Suh SW, Gwag BJ, He YY, Hsu CY, Choi DW (1996) The role of zinc in selective neuronal death after transient global cerebral ischemia. Science 272:1013-1016.

Kolisek M, Beck A, Fleig A, Penner R (2005) Cyclic ADP-ribose and hydrogen peroxide synergize with ADP-ribose in the activation of TRPM2 channels. Mol Cell 18:61-69.

Kovanen PE, Junttila I, Takaluoma K, Saharinen P, Valmu L, Li W, Silvennoinen O (2000) Regulation of Jak2 tyrosine kinase by protein kinase C during macrophage differentiation of IL-3-dependent myeloid progenitor cells. Blood 95:1626-1632.

Kress GJ, Dineley KE, Reynolds IJ (2002) The relationship between intracellular free iron and cell injury in cultured neurons, astrocytes, and oligodendrocytes. J Neurosci 22:5848-5855.

Kress M, Karasek J, Ferrer-Montiel AV, Scherbakov N, Haberberger RV (2008) TRPC channels and diacylglycerol dependent calcium signaling in rat sensory neurons. Histochem Cell Biol 130:655-667.

Kriegstein AR, Noctor SC (2004) Patterns of neuronal migration in the embryonic cortex. Trends Neurosci 27:392-399.

Krishtal O, Lozovaya N, Fisunov A, Tsintsadze T, Pankratov Y, Kopanitsa M, Chatterjee SS (2001) Modulation of ion channels in rat neurons by the constituents of Hypericum perforatum. Pharmacopsychiatry 34 Suppl 1:S74-82.

Kumar V, Mdzinarishvili A, Kiewert C, Abbruscato T, Bickel U, van der Schyf CJ, Klein J (2006) NMDA receptor-antagonistic properties of hyperforin, a constituent of St. John's Wort. J Pharmacol Sci 102:47-54.

Kuwahara K, Wang Y, McAnally J, Richardson JA, Bassel-Duby R, Hill JA, Olson EN (2006) TRPC6 fulfills a calcineurin signaling circuit during pathologic cardiac remodeling. J Clin Invest 116:3114-3126.

Kwon Y, Hofmann T, Montell C (2007) Integration of phosphoinositide- and calmodulin-mediated regulation of TRPC6. Mol Cell 25:491-503.

Langmade SJ, Ravindra R, Daniels PJ, Andrews GK (2000) The transcription factor MTF-1 mediates metal regulation of the mouse ZnT1 gene. J Biol Chem 275:34803-34809.

Large WA, Saleh SN, Albert AP (2009) Role of phosphoinositol 4,5-bisphosphate and diacylglycerol in regulating native TRPC channel proteins in vascular smooth muscle. Cell Calcium.

Law W, Kelland EE, Sharp P, Toms NJ (2003) Characterisation of zinc uptake into rat cultured cerebrocortical oligodendrocyte progenitor cells. Neurosci Lett 352:113-116.

Lee HM, Kim HI, Shin YK, Lee CS, Park M, Song JH (2003a) Diclofenac inhibition of sodium currents in rat dorsal root ganglion neurons. Brain Res 992:120-127.

Lee YM, Kim BJ, Kim HJ, Yang DK, Zhu MH, Lee KP, So I, Kim KW (2003b) TRPC5 as a candidate for the nonselective cation channel activated by muscarinic stimulation in murine stomach. Am J Physiol Gastrointest Liver Physiol 284:G604-616.

Legendre P, Westbrook GL (1990) The inhibition of single N-methyl-D-aspartate-activated channels by zinc ions on cultured rat neurones. J Physiol 429:429-449.

Lemonnier L, Trebak M, Putney JW, Jr. (2008) Complex regulation of the TRPC3, 6 and 7 channel subfamily by diacylglycerol and phosphatidylinositol-4,5-bisphosphate. Cell Calcium 43:506-514.

Lemos VS, Poburko D, Liao CH, Cole WC, van Breemen C (2007) Na+ entry via TRPC6 causes Ca2+ entry via NCX reversal in ATP stimulated smooth muscle cells. Biochem Biophys Res Commun 352:130-134.

Lepage PK, Boulay G (2007) Molecular determinants of TRP channel assembly. Biochem Soc Trans 35:81-83.

Lepage PK, Lussier MP, Barajas-Martinez H, Bousquet SM, Blanchard AP, Francoeur N, Dumaine R, Boulay G (2006) Identification of two domains involved in the assembly of transient receptor potential canonical channels. J Biol Chem 281:30356-30364.

Lerma J, Martin del Rio R (1992) Chloride transport blockers prevent N-methyl-D-aspartate receptor-channel complex activation. Mol Pharmacol 41:217-222.

Lessard CB, Lussier MP, Cayouette S, Bourque G, Boulay G (2005) The overexpression of presenilin2 and Alzheimer's-disease-linked presenilin2 variants influences TRPC6-enhanced Ca2+ entry into HEK293 cells. Cell Signal 17:437-445.

Leuner K, Kazanski V, Muller M, Essin K, Henke B, Gollasch M, Harteneck C, Muller WE (2007) Hyperforin--a key constituent of St. John's wort specifically activates TRPC6 channels. Faseb J 21:4101-4111.

Levi S, Corsi B, Bosisio M, Invernizzi R, Volz A, Sanford D, Arosio P, Drysdale J (2001) A human mitochondrial ferritin encoded by an intronless gene. J Biol Chem 276:24437-24440.

Li Y, Jia YC, Cui K, Li N, Zheng ZY, Wang YZ, Yuan XB (2005) Essential role of TRPC channels in the guidance of nerve growth cones by brain-derived neurotrophic factor. Nature 434:894-898.

Liao Y, Erxleben C, Abramowitz J, Flockerzi V, Zhu MX, Armstrong DL, Birnbaumer L (2008) Functional interactions among Orai1, TRPCs, and STIM1 suggest a STIM-regulated heteromeric Orai/TRPC model for SOCE/Icrac channels. Proc Natl Acad Sci U S A 105:2895-2900.

Liedtke W, Friedman JM (2003) Abnormal osmotic regulation in trpv4-/- mice. Proc Natl Acad Sci U S A 100:13698-13703.

Lievremont JP, Bird GS, Putney JW, Jr. (2004) Canonical transient receptor potential TRPC7 can function as both a receptor- and store-operated channel in HEK-293 cells. Am J Physiol Cell Physiol 287:C1709-1716.

Lin MJ, Leung GP, Zhang WM, Yang XR, Yip KP, Tse CM, Sham JS (2004) Chronic hypoxia-induced upregulation of store-operated and receptor-operated Ca2+ channels in pulmonary arterial smooth muscle cells: a novel mechanism of hypoxic pulmonary hypertension. Circ Res 95:496-505.

Lintschinger B, Balzer-Geldsetzer M, Baskaran T, Graier WF, Romanin C, Zhu MX, Groschner K (2000) Coassembly of Trp1 and Trp3 proteins generates diacylglycerol- and Ca2+-sensitive cation channels. J Biol Chem 275:27799-27805.

Liu D, Maier A, Scholze A, Rauch U, Boltzen U, Zhao Z, Zhu Z, Tepel M (2008) High glucose enhances transient receptor potential channel canonical type 6-dependent calcium influx in human platelets via phosphatidylinositol 3-kinase-dependent pathway. Arterioscler Thromb Vasc Biol 28:746-751.

Liu DY, Thilo F, Scholze A, Wittstock A, Zhao ZG, Harteneck C, Zidek W, Zhu ZM, Tepel M (2007) Increased store-operated and 1-oleoyl-2-acetyl-sn-glycerol-induced calcium influx in monocytes is mediated by transient receptor potential canonical channels in human essential hypertension. J Hypertens 25:799-808.

Liu X, Bandyopadhyay BC, Singh BB, Groschner K, Ambudkar IS (2005) Molecular analysis of a store-operated and 2-acetyl-sn-glycerol-sensitive non-selective cation channel. Heteromeric assembly of TRPC1-TRPC3. J Biol Chem 280:21600-21606.

Liu X, Wang W, Singh BB, Lockwich T, Jadlowiec J, O'Connell B, Wellner R, Zhu MX, Ambudkar IS (2000) Trp1, a candidate protein for the store-operated Ca(2+) influx mechanism in salivary gland cells. J Biol Chem 275:3403-3411.

Liuzzi JP, Cousins RJ (2004) Mammalian zinc transporters. Annu Rev Nutr 24:151-172.

Liuzzi JP, Aydemir F, Nam H, Knutson MD, Cousins RJ (2006) Zip14 (Slc39a14) mediates non-transferrin-bound iron uptake into cells. Proc Natl Acad Sci U S A 103:13612-13617.

Lockwich TP, Liu X, Singh BB, Jadlowiec J, Weiland S, Ambudkar IS (2000) Assembly of Trp1 in a signaling complex associated with caveolin-scaffolding lipid raft domains. J Biol Chem 275:11934-11942.

Loeffler DA, Connor JR, Juneau PL, Snyder BS, Kanaley L, DeMaggio AJ, Nguyen H, Brickman CM, LeWitt PA (1995) Transferrin and iron in normal, Alzheimer's disease, and Parkinson's disease brain regions. J Neurochem 65:710-724.

Lucas P, Ukhanov K, Leinders-Zufall T, Zufall F (2003) A diacylglycerol-gated cation channel in vomeronasal neuron dendrites is impaired in TRPC2 mutant mice: mechanism of pheromone transduction. Neuron 40:551-561.

Lynes MA, Kang YJ, Sensi SL, Perdrizet GA, Hightower LE (2007) Heavy metal ions in normal physiology, toxic stress, and cytoprotection. Ann N Y Acad Sci 1113:159-172.

Ma HT, Peng Z, Hiragun T, Iwaki S, Gilfillan AM, Beaven MA (2008) Canonical transient receptor potential 5 channel in conjunction with Orai1 and STIM1 allows Sr2+ entry, optimal influx of Ca2+, and degranulation in a rat mast cell line. J Immunol 180:2233-2239.

Malaiyandi LM, Vergun O, Dineley KE, Reynolds IJ (2005) Direct visualization of mitochondrial zinc accumulation reveals uniporter-dependent and -independent transport mechanisms. J Neurochem 93:1242-1250.

Mantyh PW, Ghilardi JR, Rogers S, DeMaster E, Allen CJ, Stimson ER, Maggio JE (1993) Aluminum, iron, and zinc ions promote aggregation of physiological concentrations of beta-amyloid peptide. J Neurochem 61:1171-1174.

Maret W (1994) Oxidative metal release from metallothionein via zinc-thiol/disulfide interchange. Proc Natl Acad Sci U S A 91:237-241.

Maret W, Vallee BL (1998) Thiolate ligands in metallothionein confer redox activity on zinc clusters. Proc Natl Acad Sci U S A 95:3478-3482.

Maroto R, Raso A, Wood TG, Kurosky A, Martinac B, Hamill OP (2005) TRPC1 forms the stretch-activated cation channel in vertebrate cells. Nat Cell Biol 7:179-185.

Maruyama Y, Nakanishi Y, Walsh EJ, Wilson DP, Welsh DG, Cole WC (2006) Heteromultimeric TRPC6-TRPC7 channels contribute to arginine vasopressin-induced cation current of A7r5 vascular smooth muscle cells. Circ Res 98:1520-1527.

McAbee DD (1995) Isolated rat hepatocytes acquire iron from lactoferrin by endocytosis. Biochem J 311 (Pt 2):603-609.

McCarty NA, McDonough S, Cohen BN, Riordan JR, Davidson N, Lester HA (1993) Voltage-dependent block of the cystic fibrosis transmembrane conductance regulator Cl- channel by two closely related arylaminobenzoates. J Gen Physiol 102:1-23.

McDougall P, Markham A, Cameron I, Sweetman AJ (1983) The mechanism of inhibition of mitochondrial oxidative phosphorylation by the nonsteroidal anti-inflammatory agent diflunisal. Biochem Pharmacol 32:2595-2598.

McDougall P, Markham A, Cameron I, Sweetman AJ (1988) Action of the nonsteroidal anti-inflammatory agent, flufenamic acid, on calcium movements in isolated mitochondria. Biochem Pharmacol 37:1327-1330.

McKemy DD, Neuhausser WM, Julius D (2002) Identification of a cold receptor reveals a general role for TRP channels in thermosensation. Nature 416:52-58.

Mederos y Schnitzler M, Storch U, Meibers S, Nurwakagari P, Breit A, Essin K, Gollasch M, Gudermann T (2008) Gq-coupled receptors as mechanosensors mediating myogenic vasoconstriction. Embo J 27:3092-3103.

Medina MA, Martinez-Poveda B, Amores-Sanchez MI, Quesada AR (2006) Hyperforin: more than an antidepressant bioactive compound? Life Sci 79:105-111.

Medvedeva YV, Kim MS, Usachev YM (2008) Mechanisms of prolonged presynaptic Ca2+ signaling and glutamate release induced by TRPV1 activation in rat sensory neurons. J Neurosci 28:5295-5311.

Meguro R, Asano Y, Odagiri S, Li C, Shoumura K (2008) Cellular and subcellular localizations of nonheme ferric and ferrous iron in the rat brain: a light and electron microscopic study by the perfusion-Perls and -Turnbull methods. Arch Histol Cytol 71:205-222.

Meng F, To WK, Gu Y (2008) Role of TRP channels and NCX in mediating hypoxia-induced [Ca(2+)](i) elevation in PC12 cells. Respir Physiol Neurobiol 164:386-393.

Meves H (1994) Modulation of ion channels by arachidonic acid. Prog Neurobiol 43:175-186.

Mizuno N, Kitayama S, Saishin Y, Shimada S, Morita K, Mitsuhata C, Kurihara H, Dohi T (1999) Molecular cloning and characterization of rat trp homologues from brain. Brain Res Mol Brain Res 64:41-51.

Mocchegiani E, Bertoni-Freddari C, Marcellini F, Malavolta M (2005) Brain, aging and neurodegeneration: role of zinc ion availability. Prog Neurobiol 75:367-390.

Moiseenkova-Bell VY, Wensel TG (2009) Hot on the trail of TRP channel structure. J Gen Physiol 133:239-244.

Molina-Holgado F, Hider RC, Gaeta A, Williams R, Francis P (2007) Metals ions and neurodegeneration. Biometals 20:639-654.

Moller CC, Wei C, Altintas MM, Li J, Greka A, Ohse T, Pippin JW, Rastaldi MP, Wawersik S, Schiavi S, Henger A, Kretzler M, Shankland SJ, Reiser J (2007) Induction of TRPC6 channel in acquired forms of proteinuric kidney disease. J Am Soc Nephrol 18:29-36.

Monteilh-Zoller MK, Hermosura MC, Nadler MJ, Scharenberg AM, Penner R, Fleig A (2003) TRPM7 provides an ion channel mechanism for cellular entry of trace metal ions. J Gen Physiol 121:49-60.

Montell C (2005) The TRP superfamily of cation channels. Sci STKE 2005:re3.

Montell C, Rubin GM (1989) Molecular characterization of the Drosophila trp locus: a putative integral membrane protein required for phototransduction. Neuron 2:1313-1323.

Moos T (2002) Brain iron homeostasis. Dan Med Bull 49:279-301.

Moos T, Morgan EH (1998) Evidence for low molecular weight, non-transferrin-bound iron in rat brain and cerebrospinal fluid. J Neurosci Res 54:486-494.

Moos T, Morgan EH (2000) Transferrin and transferrin receptor function in brain barrier systems. Cell Mol Neurobiol 20:77-95.

Moos T, Morgan EH (2004) The metabolism of neuronal iron and its pathogenic role in neurological disease: review. Ann N Y Acad Sci 1012:14-26.

Moos T, Rosengren Nielsen T (2006) Ferroportin in the postnatal rat brain: implications for axonal transport and neuronal export of iron. Semin Pediatr Neurol 13:149-157.

Moos T, Rosengren Nielsen T, Skjorringe T, Morgan EH (2007) Iron trafficking inside the brain. J Neurochem 103:1730-1740.

Moroo I, Ujiie M, Walker BL, Tiong JW, Vitalis TZ, Karkan D, Gabathuler R, Moise AR, Jefferies WA (2003) Identification of a novel route of iron transcytosis across the mammalian blood-brain barrier. Microcirculation 10:457-462.

Morris CM, Candy JM, Keith AB, Oakley AE, Taylor GA, Pullen RG, Bloxham CA, Gocht A, Edwardson JA (1992) Brain iron homeostasis. J Inorg Biochem 47:257-265.

Mueller BK (1999) Growth cone guidance: first steps towards a deeper understanding. Annu Rev Neurosci 22:351-388.

Muller M, Essin K, Hill K, Beschmann H, Rubant S, Schempp CM, Gollasch M, Boehncke WH, Harteneck C, Muller WE, Leuner K (2008) Specific TRPC6 channel activation, a novel approach to stimulate keratinocyte differentiation. J Biol Chem 283:33942-33954.

Mwanjewe J, Grover AK (2004) Role of transient receptor potential canonical 6 (TRPC6) in non-transferrin-bound iron uptake in neuronal phenotype PC12 cells. Biochem J 378:975-982.

Mwanjewe J, Hui BK, Coughlin MD, Grover AK (2001) Treatment of PC12 cells with nerve growth factor increases iron uptake. Biochem J 357:881-886.

Nadler MJ, Hermosura MC, Inabe K, Perraud AL, Zhu Q, Stokes AJ, Kurosaki T, Kinet JP, Penner R, Scharenberg AM, Fleig A (2001) LTRPC7 is a Mg.ATP-regulated divalent cation channel required for cell viability. Nature 411:590-595.

Nasman J, Bart G, Larsson K, Louhivuori L, Peltonen H, Akerman KE (2006) The orexin OX1 receptor regulates Ca2+ entry via diacylglycerol-activated channels in differentiated neuroblastoma cells. J Neurosci 26:10658-10666.

Nemeth E, Tuttle MS, Powelson J, Vaughn MB, Donovan A, Ward DM, Ganz T, Kaplan J (2004) Hepcidin regulates cellular iron efflux by binding to ferroportin and inducing its internalization. Science 306:2090-2093.

Nilius B, Owsianik G, Voets T (2008) Transient receptor potential channels meet phosphoinositides. Embo J 27:2809-2816.

Nilius B, Owsianik G, Voets T, Peters JA (2007) Transient receptor potential cation channels in disease. Physiol Rev 87:165-217.

Nishida M, Onohara N, Sato Y, Suda R, Ogushi M, Tanabe S, Inoue R, Mori Y, Kurose H (2007) Galpha12/13-mediated up-regulation of TRPC6 negatively regulates endothelin-1-induced cardiac myofibroblast formation and collagen synthesis through nuclear factor of activated T cells activation. J Biol Chem 282:23117-23128.

Noh KM, Koh JY (2000) Induction and activation by zinc of NADPH oxidase in cultured cortical neurons and astrocytes. J Neurosci 20:RC111.

Nolte C, Gore A, Sekler I, Kresse W, Hershfinkel M, Hoffmann A, Kettenmann H, Moran A (2004) ZnT-1 expression in astroglial cells protects against zinc toxicity and slows the accumulation of intracellular zinc. Glia 48:145-155.

Numata T, Shimizu T, Okada Y (2007a) TRPM7 is a stretch- and swelling-activated cation channel involved in volume regulation in human epithelial cells. Am J Physiol Cell Physiol 292:C460-467.

Numata T, Shimizu T, Okada Y (2007b) Direct mechano-stress sensitivity of TRPM7 channel. Cell Physiol Biochem 19:1-8.

Ohana E, Segal D, Palty R, Ton-That D, Moran A, Sensi SL, Weiss JH, Hershfinkel M, Sekler I (2004) A sodium zinc exchange mechanism is mediating extrusion of zinc in mammalian cells. J Biol Chem 279:4278-4284.

Oike H, Wakamori M, Mori Y, Nakanishi H, Taguchi R, Misaka T, Matsumoto I, Abe K (2006) Arachidonic acid can function as a signaling modulator by activating the TRPM5 cation channel in taste receptor cells. Biochim Biophys Acta 1761:1078-1084.

Okada T, Inoue R, Yamazaki K, Maeda A, Kurosaki T, Yamakuni T, Tanaka I, Shimizu S, Ikenaka K, Imoto K, Mori Y (1999) Molecular and functional characterization of a novel mouse transient receptor potential protein homologue TRP7. Ca(2+)-permeable cation channel that is constitutively activated and enhanced by stimulation of G protein-coupled receptor. J Biol Chem 274:27359-27370.

Onohara N, Nishida M, Inoue R, Kobayashi H, Sumimoto H, Sato Y, Mori Y, Nagao T, Kurose H (2006) TRPC3 and TRPC6 are essential for angiotensin II-induced cardiac hypertrophy. Embo J 25:5305-5316.

Ordaz B, Tang J, Xiao R, Salgado A, Sampieri A, Zhu MX, Vaca L (2005) Calmodulin and calcium interplay in the modulation of TRPC5 channel activity. Identification of a novel C-terminal domain for calcium/calmodulin-mediated facilitation. J Biol Chem 280:30788-30796.

Ortega R, Moretto P, Fajac A, Benard J, Llabador Y, Simonoff M (1996) Quantitative mapping of platinum and essential trace metal in cisplatin resistant and sensitive human ovarian adenocarcinoma cells. Cellular and Molecular Biology 42:77-88.

Otsuka Y, Sakagami H, Owada Y, Kondo H (1998) Differential localization of mRNAs for mammalian trps, presumptive capacitative calcium entry channels, in the adult mouse brain. Tohoku J Exp Med 185:139-146.

Ottolia M, Toro L (1994) Potentiation of large conductance KCa channels by niflumic, flufenamic, and mefenamic acids. Biophys J 67:2272-2279.

Oudit GY, Trivieri MG, Khaper N, Liu PP, Backx PH (2006) Role of L-type Ca2+ channels in iron transport and iron-overload cardiomyopathy. J Mol Med 84:349-364.

Oudit GY, Sun H, Trivieri MG, Koch SE, Dawood F, Ackerley C, Yazdanpanah M, Wilson GJ, Schwartz A, Liu PP, Backx PH (2003) L-type Ca2+ channels provide a major pathway for iron entry into cardiomyocytes in iron-overload cardiomyopathy. Nat Med 9:1187-1194.

Owsianik G, Talavera K, Voets T, Nilius B (2006a) Permeation and selectivity of TRP channels. Annu Rev Physiol 68:685-717.

Owsianik G, D'Hoedt D, Voets T, Nilius B (2006b) Structure-function relationship of the TRP channel superfamily. Rev Physiol Biochem Pharmacol 156:61-90.

Palmiter RD, Cole TB, Quaife CJ, Findley SD (1996) ZnT-3, a putative transporter of zinc into synaptic vesicles. Proc Natl Acad Sci U S A 93:14934-14939.

Panda S, Nayak SK, Campo B, Walker JR, Hogenesch JB, Jegla T (2005) Illumination of the melanopsin signaling pathway. Science 307:600-604.

Pantopoulos K (2004) Iron metabolism and the IRE/IRP regulatory system: an update. Ann N Y Acad Sci 1012:1-13.

Parekh AB, Putney JW, Jr. (2005) Store-operated calcium channels. Physiol Rev 85:757-810.

Patapoutian A, Tate S, Woolf CJ (2009) Transient receptor potential channels: targeting pain at the source. Nat Rev Drug Discov 8:55-68.

Patapoutian A, Peier AM, Story GM, Viswanath V (2003) ThermoTRP channels and beyond: mechanisms of temperature sensation. Nat Rev Neurosci 4:529-539.

Patel BN, David S (1997) A novel glycosylphosphatidylinositol-anchored form of ceruloplasmin is expressed by mammalian astrocytes. J Biol Chem 272:20185-20190.

Patel BN, Dunn RJ, Jeong SY, Zhu Q, Julien JP, David S (2002) Ceruloplasmin regulates iron levels in the CNS and prevents free radical injury. J Neurosci 22:6578-6586.

Pedersen SF, Owsianik G, Nilius B (2005) TRP channels: an overview. Cell Calcium 38:233-252.

Peier AM, Moqrich A, Hergarden AC, Reeve AJ, Andersson DA, Story GM, Earley TJ, Dragoni I, McIntyre P, Bevan S, Patapoutian A (2002a) A TRP channel that senses cold stimuli and menthol. Cell 108:705-715.

Peier AM, Reeve AJ, Andersson DA, Moqrich A, Earley TJ, Hergarden AC, Story GM, Colley S, Hogenesch JB, McIntyre P, Bevan S, Patapoutian A (2002b) A heat-sensitive TRP channel expressed in keratinocytes. Science 296:2046-2049.

Peppiatt-Wildman CM, Albert AP, Saleh SN, Large WA (2007) Endothelin-1 activates a Ca2+-permeable cation channel with TRPC3 and TRPC7 properties in rabbit coronary artery myocytes. J Physiol 580:755-764.

Perez CA, Huang L, Rong M, Kozak JA, Preuss AK, Zhang H, Max M, Margolskee RF (2002) A transient receptor potential channel expressed in taste receptor cells. Nat Neurosci 5:1169-1176.

Perraud AL, Takanishi CL, Shen B, Kang S, Smith MK, Schmitz C, Knowles HM, Ferraris D, Li W, Zhang J, Stoddard BL, Scharenberg AM (2005) Accumulation of free ADP-ribose from mitochondria mediates oxidative stress-induced gating of TRPM2 cation channels. J Biol Chem 280:6138-6148.

Peters S, Koh J, Choi DW (1987) Zinc selectively blocks the action of N-methyl-D-aspartate on cortical neurons. Science 236:589-593.

Philipp S, Trost C, Warnat J, Rautmann J, Himmerkus N, Schroth G, Kretz O, Nastainczyk W, Cavalie A, Hoth M, Flockerzi V (2000) TRP4 (CCE1) protein is part of native calcium release-activated Ca2+-like channels in adrenal cells. J Biol Chem 275:23965-23972.

Phillips AM, Bull A, Kelly LE (1992) Identification of a Drosophila gene encoding a calmodulin-binding protein with homology to the trp phototransduction gene. Neuron 8:631-642.

Platel JC, Boisseau S, Dupuis A, Brocard J, Poupard A, Savasta M, Villaz M, Albrieux M (2005) Na+ channel-mediated Ca2+ entry leads to glutamate secretion in mouse neocortical preplate. Proc Natl Acad Sci U S A 102:19174-19179.

Poburko D, Lee CH, van Breemen C (2004) Vascular smooth muscle mitochondria at the cross roads of Ca(2+) regulation. Cell Calcium 35:509-521.

Poburko D, Liao CH, Lemos VS, Lin E, Maruyama Y, Cole WC, van Breemen C (2007) Transient receptor potential channel 6-mediated, localized cytosolic [Na+] transients drive Na+/Ca2+ exchanger-mediated Ca2+ entry in purinergically stimulated aorta smooth muscle cells. Circ Res 101:1030-1038.

Pocock TM, Foster RR, Bates DO (2004) Evidence of a role for TRPC channels in VEGF-mediated increased vascular permeability in vivo. Am J Physiol Heart Circ Physiol 286:H1015-1026.

Ponting CP (2001) Domain homologues of dopamine beta-hydroxylase and ferric reductase: roles for iron metabolism in neurodegenerative disorders? Hum Mol Genet 10:1853-1858.

Poronnik P, Ward MC, Cook DI (1992) Intracellular Ca2+ release by flufenamic acid and other blockers of the non-selective cation channel. FEBS Lett 296:245-248.

Poteser M, Graziani A, Rosker C, Eder P, Derler I, Kahr H, Zhu MX, Romanin C, Groschner K (2006) TRPC3 and TRPC4 associate to form a redox-sensitive cation channel. Evidence for expression of native TRPC3-TRPC4 heteromeric channels in endothelial cells. J Biol Chem 281:13588-13595.

Pryor PR, Reimann F, Gribble FM, Luzio JP (2006) Mucolipin-1 is a lysosomal membrane protein required for intracellular lactosylceramide traffic. Traffic 7:1388-1398.

Putney JW, Jr. (1986) A model for receptor-regulated calcium entry. Cell Calcium 7:1-12.

Putney JW, Jr. (2000) Presenilins, Alzheimer's disease, and capacitative calcium entry. Neuron 27:411-412.

Putney JW, Jr. (2007a) New molecular players in capacitative Ca2+ entry. J Cell Sci 120:1959-1965.

Putney JW, Jr. (2007b) Recent breakthroughs in the molecular mechanism of capacitative calcium entry (with thoughts on how we got here). Cell Calcium 42:103-110.

Qian ZM, Wang Q (1998) Expression of iron transport proteins and excessive iron accumulation in the brain in neurodegenerative disorders. Brain Res Brain Res Rev 27:257-267.

Qian ZM, Shen X (2001) Brain iron transport and neurodegeneration. Trends Mol Med 7:103-108.

Qian ZM, Chang YZ, Zhu L, Yang L, Du JR, Ho KP, Wang Q, Li LZ, Wang CY, Ge X, Jing NL, Li L, Ke Y (2007) Development and iron-dependent expression of hephaestin in different brain regions of rats. J Cell Biochem 102:1225-1233.

Qin F (2007) Regulation of TRP ion channels by phosphatidylinositol-4,5-bisphosphate. Handb Exp Pharmacol:509-525.

Qiu X, Kumbalasiri T, Carlson SM, Wong KY, Krishna V, Provencio I, Berson DM (2005) Induction of photosensitivity by heterologous expression of melanopsin. Nature 433:745-749.

Rae JL, Farrugia G (1992) Whole-cell potassium current in rabbit corneal epithelium activated by fenamates. J Membr Biol 129:81-97.

Ramsey IS, Delling M, Clapham DE (2006) An introduction to TRP channels. Annu Rev Physiol 68:619-647.

Rassendren FA, Lory P, Pin JP, Nargeot J (1990) Zinc has opposite effects on NMDA and non-NMDA receptors expressed in Xenopus oocytes. Neuron 4:733-740.

Reiser J, Polu KR, Moller CC, Kenlan P, Altintas MM, Wei C, Faul C, Herbert S, Villegas I, Avila-Casado C, McGee M, Sugimoto H, Brown D, Kalluri R, Mundel P, Smith PL, Clapham DE, Pollak MR (2005) TRPC6 is a glomerular slit diaphragm-associated channel required for normal renal function. Nat Genet 37:739-744.

Riccio A, Medhurst AD, Mattei C, Kelsell RE, Calver AR, Randall AD, Benham CD, Pangalos MN (2002a) mRNA distribution analysis of human TRPC family in CNS and peripheral tissues. Brain Res Mol Brain Res 109:95-104.

Riccio A, Mattei C, Kelsell RE, Medhurst AD, Calver AR, Randall AD, Davis JB, Benham CD, Pangalos MN (2002b) Cloning and functional expression of human short TRP7, a candidate protein for store-operated Ca2+ influx. J Biol Chem 277:12302-12309.

Riera CE, Vogel H, Simon SA, Damak S, le Coutre J (2009) Sensory attributes of complex tasting divalent salts are mediated by TRPM5 and TRPV1 channels. J Neurosci 29:2654-2662.

Rizzuto R, Bernardi P, Pozzan T (2000) Mitochondria as all-round players of the calcium game. J Physiol 529 Pt 1:37-47.

Rodriguez-Linares B, Watson SP (1994) Phosphorylation of JAK2 in thrombin-stimulated human platelets. FEBS Lett 352:335-338.

Rohacs T, Nilius B (2007) Regulation of transient receptor potential (TRP) channels by phosphoinositides. Pflugers Arch 455:157-168.

Roos J, DiGregorio PJ, Yeromin AV, Ohlsen K, Lioudyno M, Zhang S, Safrina O, Kozak JA, Wagner SL, Cahalan MD, Velicelebi G, Stauderman KA (2005) STIM1, an essential and conserved component of store-operated Ca2+ channel function. J Cell Biol 169:435-445.

Roth JA, Garrick MD (2003) Iron interactions and other biological reactions mediating the physiological and toxic actions of manganese. Biochem Pharmacol 66:1-13.

Rothenberger S, Food MR, Gabathuler R, Kennard ML, Yamada T, Yasuhara O, McGeer PL, Jefferies WA (1996) Coincident expression and distribution of melanotransferrin and transferrin receptor in human brain capillary endothelium. Brain Res 712:117-121.

Rouault TA (2001) Systemic iron metabolism: a review and implications for brain iron metabolism. Pediatr Neurol 25:130-137.

Rouault TA, Cooperman S (2006) Brain iron metabolism. Semin Pediatr Neurol 13:142-148.

Rui L, Archer SF, Argetsinger LS, Carter-Su C (2000) Platelet-derived growth factor and lysophosphatidic acid inhibit growth hormone binding and signaling via a protein kinase C-dependent pathway. J Biol Chem 275:2885-2892.

Sadrzadeh SM, Saffari Y (2004) Iron and brain disorders. Am J Clin Pathol 121 Suppl:S64-70.

Saimi Y, Kung C (2002) Calmodulin as an ion channel subunit. Annu Rev Physiol 64:289-311.

Saleh SN, Albert AP, Peppiatt CM, Large WA (2006) Angiotensin II activates two cation conductances with distinct TRPC1 and TRPC6 channel properties in rabbit mesenteric artery myocytes. J Physiol 577:479-495.

Salido GM, Sage SO, Rosado JA (2009) TRPC channels and store-operated Ca(2+) entry. Biochim Biophys Acta 1793:223-230.

Sanchez JA, Garcia MC, Sharma VK, Young KC, Matlib MA, Sheu SS (2001) Mitochondria regulate inactivation of L-type Ca2+ channels in rat heart. J Physiol 536:387-396.

Sandoval AJ, Riquelme JP, Carretta MD, Hancke JL, Hidalgo MA, Burgos RA (2007) Store-operated calcium entry mediates intracellular alkalinization, ERK1/2, and Akt/PKB phosphorylation in bovine neutrophils. J Leukoc Biol 82:1266-1277.

Saris NE, Niva K (1994) Is Zn2+ transported by the mitochondrial calcium uniporter? FEBS Lett 356:195-198.

Schaefer M, Plant TD, Obukhov AG, Hofmann T, Gudermann T, Schultz G (2000) Receptor-mediated regulation of the nonselective cation channels TRPC4 and TRPC5. J Biol Chem 275:17517-17526.

Schalinske KL, Eisenstein RS (1996) Phosphorylation and activation of both iron regulatory proteins 1 and 2 in HL-60 cells. J Biol Chem 271:7168-7176.

Schalinske KL, Anderson SA, Tuazon PT, Chen OS, Kennedy MC, Eisenstein RS (1997) The iron-sulfur cluster of iron regulatory protein 1 modulates the accessibility of RNA binding and phosphorylation sites. Biochemistry 36:3950-3958.

Schindl R, Romanin C (2007) Assembly domains in TRP channels. Biochem Soc Trans 35:84-85.

Schipper HM, Bernier L, Mehindate K, Frankel D (1999) Mitochondrial iron sequestration in dopamine-challenged astroglia: role of heme oxygenase-1 and the permeability transition pore. J Neurochem 72:1802-1811.

Schlondorff JS, Pollak MR (2006) TRPC6 in glomerular health and disease: what we know and what we believe. Semin Cell Dev Biol 17:667-674.

Schumacher PA, Sakellaropoulos G, Phipps DJ, Schlichter LC (1995) Small-conductance chloride channels in human peripheral T lymphocytes. J Membr Biol 145:217-232.

Sensi SL, Yin HZ, Weiss JH (2000) AMPA/kainate receptor-triggered Zn2+ entry into cortical neurons induces mitochondrial Zn2+ uptake and persistent mitochondrial dysfunction. Eur J Neurosci 12:3813-3818.

Sensi SL, Ton-That D, Weiss JH (2002) Mitochondrial sequestration and Ca(2+)-dependent release of cytosolic Zn(2+) loads in cortical neurons. Neurobiol Dis 10:100-108.

Sensi SL, Yin HZ, Carriedo SG, Rao SS, Weiss JH (1999) Preferential Zn2+ influx through Ca2+-permeable AMPA/kainate channels triggers prolonged mitochondrial superoxide production. Proc Natl Acad Sci U S A 96:2414-2419.

Sensi SL, Canzoniero LM, Yu SP, Ying HS, Koh JY, Kerchner GA, Choi DW (1997) Measurement of intracellular free zinc in living cortical neurons: routes of entry. J Neurosci 17:9554-9564.

Sensi SL, Ton-That D, Sullivan PG, Jonas EA, Gee KR, Kaczmarek LK, Weiss JH (2003) Modulation of mitochondrial function by endogenous Zn2+ pools. Proc Natl Acad Sci U S A 100:6157-6162.

Shaw T, Lee RJ, Partridge LD (1995) Action of diphenylamine carboxylate derivatives, a family of non-steroidal anti-inflammatory drugs, on [Ca2+]i and Ca(2+)-activated channels in neurons. Neurosci Lett 190:121-124.

Shi J, Mori E, Mori Y, Mori M, Li J, Ito Y, Inoue R (2004) Multiple regulation by calcium of murine homologues of transient receptor potential proteins TRPC6 and TRPC7 expressed in HEK293 cells. J Physiol 561:415-432.

Shim S, Goh EL, Ge S, Sailor K, Yuan JP, Roderick HL, Bootman MD, Worley PF, Song H, Ming GL (2005) XTRPC1-dependent chemotropic guidance of neuronal growth cones. Nat Neurosci 8:730-735.

Shimamura K, Zhou M, Ito Y, Kimura S, Zou LB, Sekiguchi F, Kitramura K, Sunano S (2002) Effects of flufenamic acid on smooth muscle of the carotid artery isolated from spontaneously hypertensive rats. J Smooth Muscle Res 38:39-50.

Singh BB, Liu X, Tang J, Zhu MX, Ambudkar IS (2002) Calmodulin regulates Ca(2+)-dependent feedback inhibition of store-operated Ca(2+) influx by interaction with a site in the C terminus of TrpC1. Mol Cell 9:739-750.

Singh I, Knezevic N, Ahmmed GU, Kini V, Malik AB, Mehta D (2007) Galphaq-TRPC6-mediated Ca2+ entry induces RhoA activation and resultant endothelial cell shape change in response to thrombin. J Biol Chem 282:7833-7843.

Smith GD, Gunthorpe MJ, Kelsell RE, Hayes PD, Reilly P, Facer P, Wright JE, Jerman JC, Walhin JP, Ooi L, Egerton J, Charles KJ, Smart D, Randall AD, Anand P, Davis JB (2002) TRPV3 is a temperature-sensitive vanilloid receptor-like protein. Nature 418:186-190.

Soboloff J, Spassova M, Xu W, He LP, Cuesta N, Gill DL (2005) Role of endogenous TRPC6 channels in Ca2+ signal generation in A7r5 smooth muscle cells. J Biol Chem 280:39786-39794.

Spahl DU, Berendji-Grun D, Suschek CV, Kolb-Bachofen V, Kroncke KD (2003) Regulation of zinc homeostasis by inducible NO synthase-derived NO: nuclear metallothionein translocation and intranuclear Zn2+ release. Proc Natl Acad Sci U S A 100:13952-13957.

Spassova MA, Hewavitharana T, Xu W, Soboloff J, Gill DL (2006) A common mechanism underlies stretch activation and receptor activation of TRPC6 channels. Proc Natl Acad Sci U S A 103:16586-16591.

Stohs SJ, Bagchi D (1995) Oxidative mechanisms in the toxicity of metal ions. Free Radic Biol Med 18:321-336.

Stonell LM, Savigni DL, Morgan EH (1996) Iron transport into erythroid cells by the Na+/Mg2+ antiport. Biochim Biophys Acta 1282:163-170.

Story GM, Peier AM, Reeve AJ, Eid SR, Mosbacher J, Hricik TR, Earley TJ, Hergarden AC, Andersson DA, Hwang SW, McIntyre P, Jegla T, Bevan S, Patapoutian A (2003) ANKTM1, a TRP-like channel expressed in nociceptive neurons, is activated by cold temperatures. Cell 112:819-829.

Stowers L, Holy TE, Meister M, Dulac C, Koentges G (2002) Loss of sex discrimination and male-male aggression in mice deficient for TRP2. Science 295:1493-1500.

Strubing C, Krapivinsky G, Krapivinsky L, Clapham DE (2003) Formation of novel TRPC channels by complex subunit interactions in embryonic brain. J Biol Chem 278:39014-39019.

Suh BC, Hille B (2005) Regulation of ion channels by phosphatidylinositol 4,5-bisphosphate. Curr Opin Neurobiol 15:370-378.

Suh BC, Hille B (2008) PIP2 is a necessary cofactor for ion channel function: how and why? Annu Rev Biophys 37:175-195.

Sun M, Goldin E, Stahl S, Falardeau JL, Kennedy JC, Acierno JS, Jr., Bove C, Kaneski CR, Nagle J, Bromley MC, Colman M, Schiffmann R, Slaugenhaupt SA (2000) Mucolipidosis type IV is caused by mutations in a gene encoding a novel transient receptor potential channel. Hum Mol Genet 9:2471-2478.

Syyong HT, Poburko D, Fameli N, van Breemen C (2007) ATP promotes NCX-reversal in aortic smooth muscle cells by DAG-activated Na+ entry. Biochem Biophys Res Commun 357:1177-1182.

Tai Y, Feng S, Ge R, Du W, Zhang X, He Z, Wang Y (2008) TRPC6 channels promote dendritic growth via the CaMKIV-CREB pathway. J Cell Sci 121:2301-2307.

Takahashi S, Lin H, Geshi N, Mori Y, Kawarabayashi Y, Takami N, Mori MX, Honda A, Inoue R (2008) Nitric oxide-cGMP-protein kinase G pathway negatively regulates vascular transient receptor potential channel TRPC6. J Physiol 586:4209-4223.

Takeda A (2000) Movement of zinc and its functional significance in the brain. Brain Res Brain Res Rev 34:137-148.

Takeda A (2001) Zinc homeostasis and functions of zinc in the brain. Biometals 14:343-351.

Takei M, Hiramatsu M, Mori A (1994) Inhibitory effects of calcium antagonists on mitochondrial swelling induced by lipid peroxidation or arachidonic acid in the rat brain in vitro. Neurochem Res 19:1199-1206.

Talavera K, Nilius B, Voets T (2008) Neuronal TRP channels: thermometers, pathfinders and life-savers. Trends Neurosci 31:287-295.

Tang J, Lin Y, Zhang Z, Tikunova S, Birnbaumer L, Zhu MX (2001) Identification of common binding sites for calmodulin and inositol 1,4,5-trisphosphate receptors on the carboxyl termini of trp channels. J Biol Chem 276:21303-21310.

Tesfai Y, Brereton HM, Barritt GJ (2001) A diacylglycerol-activated Ca2+ channel in PC12 cells (an adrenal chromaffin cell line) correlates with expression of the TRP-6 (transient receptor potential) protein. Biochem J 358:717-726.

Tessier-Lavigne M, Goodman CS (1996) The molecular biology of axon guidance. Science 274:1123-1133.

Thebault S, Zholos A, Enfissi A, Slomianny C, Dewailly E, Roudbaraki M, Parys J, Prevarskaya N (2005) Receptor-operated Ca2+ entry mediated by TRPC3/TRPC6 proteins in rat prostate smooth muscle (PS1) cell line. J Cell Physiol 204:320-328.

Thebault S, Flourakis M, Vanoverberghe K, Vandermoere F, Roudbaraki M, Lehen'kyi V, Slomianny C, Beck B, Mariot P, Bonnal JL, Mauroy B, Shuba Y, Capiod T, Skryma R, Prevarskaya N (2006) Differential role of transient receptor potential channels in Ca2+ entry and proliferation of prostate cancer epithelial cells. Cancer Res 66:2038-2047.

Thompson KJ, Shoham S, Connor JR (2001) Iron and neurodegenerative disorders. Brain Res Bull 55:155-164.

Trebak M, Hempel N, Wedel BJ, Smyth JT, Bird GS, Putney JW, Jr. (2005) Negative regulation of TRPC3 channels by protein kinase C-mediated phosphorylation of serine 712. Mol Pharmacol 67:558-563.

Treiber K, Singer A, Henke B, Muller WE (2005) Hyperforin activates nonselective cation channels (NSCCs). Br J Pharmacol 145:75-83.

Trost C, Bergs C, Himmerkus N, Flockerzi V (2001) The transient receptor potential, TRP4, cation channel is a novel member of the family of calmodulin binding proteins. Biochem J 355:663-670.

Tseng PH, Lin HP, Hu H, Wang C, Zhu MX, Chen CS (2004) The canonical transient receptor potential 6 channel as a putative phosphatidylinositol 3,4,5-trisphosphate-sensitive calcium entry system. Biochemistry 43:11701-11708.

Ullrich ND, Voets T, Prenen J, Vennekens R, Talavera K, Droogmans G, Nilius B (2005) Comparison of functional properties of the Ca2+-activated cation channels TRPM4 and TRPM5 from mice. Cell Calcium 37:267-278.

Vaca L, Sampieri A (2002) Calmodulin modulates the delay period between release of calcium from internal stores and activation of calcium influx via endogenous TRP1 channels. J Biol Chem 277:42178-42187.

Vannier B, Peyton M, Boulay G, Brown D, Qin N, Jiang M, Zhu X, Birnbaumer L (1999) Mouse trp2, the homologue of the human trpc2 pseudogene, encodes mTrp2, a store depletion-activated capacitative Ca2+ entry channel. Proc Natl Acad Sci U S A 96:2060-2064.

Vargas JD, Herpers B, McKie AT, Gledhill S, McDonnell J, van den Heuvel M, Davies KE, Ponting CP (2003) Stromal cell-derived receptor 2 and cytochrome b561 are functional ferric reductases. Biochim Biophys Acta 1651:116-123.

Vazquez G, Wedel BJ, Trebak M, St John Bird G, Putney JW, Jr. (2003) Expression level of the canonical transient receptor potential 3 (TRPC3) channel determines its mechanism of activation. J Biol Chem 278:21649-21654.

Vazquez G, Wedel BJ, Aziz O, Trebak M, Putney JW, Jr. (2004) The mammalian TRPC cation channels. Biochim Biophys Acta 1742:21-36.

Venkatachalam K, Montell C (2007) TRP channels. Annu Rev Biochem 76:387-417.

Venkatachalam K, Zheng F, Gill DL (2003) Regulation of canonical transient receptor potential (TRPC) channel function by diacylglycerol and protein kinase C. J Biol Chem 278:29031-29040.

Venkatachalam K, Hofmann T, Montell C (2006) Lysosomal localization of TRPML3 depends on TRPML2 and the mucolipidosis-associated protein TRPML1. J Biol Chem 281:17517-17527.

Vig M, Peinelt C, Beck A, Koomoa DL, Rabah D, Koblan-Huberson M, Kraft S, Turner H, Fleig A, Penner R, Kinet JP (2006) CRACM1 is a plasma membrane protein essential for store-operated Ca2+ entry. Science 312:1220-1223.

Voets T, Nilius B (2009) TRPCs, GPCRs and the Bayliss effect. Embo J 28:4-5.

Voets T, Talavera K, Owsianik G, Nilius B (2005) Sensing with TRP channels. Nat Chem Biol 1:85-92.

Vriens J, Nilius B, Vennekens R (2008) Herbal Compounds and Toxins Modulating TRP Channels. Curr Neuropharmacol 6:79-96.

Wang GX, Poo MM (2005) Requirement of TRPC channels in netrin-1-induced chemotropic turning of nerve growth cones. Nature 434:898-904.

Wang HS, Dixon JE, McKinnon D (1997) Unexpected and differential effects of Cl- channel blockers on the Kv4.3 and Kv4.2 K+ channels. Implications for the study of the I(to2) current. Circ Res 81:711-718.

Wang J, Jiang H, Xie JX (2007) Ferroportin1 and hephaestin are involved in the nigral iron accumulation of 6-OHDA-lesioned rats. Eur J Neurosci 25:2766-2772.

Wang J, Weigand L, Lu W, Sylvester JT, Semenza GL, Shimoda LA (2006) Hypoxia inducible factor 1 mediates hypoxia-induced TRPC expression and elevated intracellular Ca2+ in pulmonary arterial smooth muscle cells. Circ Res 98:1528-1537.

Watanabe H, Murakami M, Ohba T, Ono K, Ito H (2009) The pathological role of transient receptor potential channels in heart disease. Circ J 73:419-427.

Watanabe H, Vriens J, Prenen J, Droogmans G, Voets T, Nilius B (2003) Anandamide and arachidonic acid use epoxyeicosatrienoic acids to activate TRPV4 channels. Nature 424:434-438.

Weiss JH, Hartley DM, Koh JY, Choi DW (1993) AMPA receptor activation potentiates zinc neurotoxicity. Neuron 10:43-49.

Weissmann N, Dietrich A, Fuchs B, Kalwa H, Ay M, Dumitrascu R, Olschewski A, Storch U, Mederos y Schnitzler M, Ghofrani HA, Schermuly RT, Pinkenburg O, Seeger W, Grimminger F, Gudermann T (2006) Classical transient receptor potential channel 6 (TRPC6) is essential for hypoxic pulmonary vasoconstriction and alveolar gas exchange. Proc Natl Acad Sci U S A 103:19093-19098.

Welsh DG, Morielli AD, Nelson MT, Brayden JE (2002) Transient receptor potential channels regulate myogenic tone of resistance arteries. Circ Res 90:248-250.

Wessling-Resnick M (2000) Iron transport. Annu Rev Nutr 20:129-151.

Westbrook GL, Mayer ML (1987) Micromolar concentrations of Zn2+ antagonize NMDA and GABA responses of hippocampal neurons. Nature 328:640-643.

White MM, Aylwin M (1990) Niflumic and flufenamic acids are potent reversible blockers of Ca2(+)-activated Cl- channels in Xenopus oocytes. Mol Pharmacol 37:720-724.

Winn MP, Conlon PJ, Lynn KL, Farrington MK, Creazzo T, Hawkins AF, Daskalakis N, Kwan SY, Ebersviller S, Burchette JL, Pericak-Vance MA, Howell DN, Vance JM, Rosenberg PB (2005) A mutation in the TRPC6 cation channel causes familial focal segmental glomerulosclerosis. Science 308:1801-1804.

Worley PF, Zeng W, Huang GN, Yuan JP, Kim JY, Lee MG, Muallem S (2007) TRPC channels as STIM1-regulated store-operated channels. Cell Calcium 42:205-211.

Wu LJ, Leenders AG, Cooperman S, Meyron-Holtz E, Smith S, Land W, Tsai RY, Berger UV, Sheng ZH, Rouault TA (2004a) Expression of the iron transporter ferroportin in synaptic vesicles and the blood-brain barrier. Brain Res 1001:108-117.

Wu X, Babnigg G, Villereal ML (2000) Functional significance of human trp1 and trp3 in store-operated Ca(2+) entry in HEK-293 cells. Am J Physiol Cell Physiol 278:C526-536.

Wu X, Babnigg G, Zagranichnaya T, Villereal ML (2002) The role of endogenous human Trp4 in regulating carbachol-induced calcium oscillations in HEK-293 cells. J Biol Chem 277:13597-13608.

Wu X, Zagranichnaya TK, Gurda GT, Eves EM, Villereal ML (2004b) A TRPC1/TRPC3-mediated increase in store-operated calcium entry is required for differentiation of H19-7 hippocampal neuronal cells. J Biol Chem 279:43392-43402.

Xu H, Ramsey IS, Kotecha SA, Moran MM, Chong JA, Lawson D, Ge P, Lilly J, Silos-Santiago I, Xie Y, DiStefano PS, Curtis R, Clapham DE (2002) TRPV3 is a calcium-permeable temperature-sensitive cation channel. Nature 418:181-186.

Xu SZ, Boulay G, Flemming R, Beech DJ (2006) E3-targeted anti-TRPC5 antibody inhibits store-operated calcium entry in freshly isolated pial arterioles. Am J Physiol Heart Circ Physiol 291:H2653-2659.

Yagami T, Ueda K, Sakaeda T, Itoh N, Sakaguchi G, Okamura N, Hori Y, Fujimoto M (2004) Protective effects of a selective L-type voltage-sensitive calcium channel blocker, S-312-d, on neuronal cell death. Biochemical Pharmacology 67:1153-1165.

Yang J, Goetz D, Li JY, Wang W, Mori K, Setlik D, Du T, Erdjument-Bromage H, Tempst P, Strong R, Barasch J (2002) An iron delivery pathway mediated by a lipocalin. Mol Cell 10:1045-1056.

Yang KT, Chang WL, Yang PC, Chien CL, Lai MS, Su MJ, Wu ML (2006) Activation of the transient receptor potential M2 channel and poly(ADP-ribose) polymerase is involved in oxidative stress-induced cardiomyocyte death. Cell Death Differ 13:1815-1826.

Yasuda N, Akazawa H, Qin Y, Zou Y, Komuro I (2008) A novel mechanism of mechanical stress-induced angiotensin II type 1-receptor activation without the involvement of angiotensin II. Naunyn Schmiedebergs Arch Pharmacol 377:393-399.

Ye B, Maret W, Vallee BL (2001) Zinc metallothionein imported into liver mitochondria modulates respiration. Proc Natl Acad Sci U S A 98:2317-2322.

Yildirim E, Kawasaki BT, Birnbaumer L (2005) Molecular cloning of TRPC3a, an N-terminally extended, store-operated variant of the human C3 transient receptor potential channel. Proc Natl Acad Sci U S A 102:3307-3311.

Yin HZ, Weiss JH (1995) Zn(2+) permeates Ca(2+) permeable AMPA/kainate channels and triggers selective neural injury. Neuroreport 6:2553-2556.

Yin HZ, Ha DH, Carriedo SG, Weiss JH (1998) Kainate-stimulated Zn2+ uptake labels cortical neurons with Ca2+-permeable AMPA/kainate channels. Brain Res 781:45-55.

Young KW, Bampton ET, Pinon L, Bano D, Nicotera P (2008) Mitochondrial Ca2+ signalling in hippocampal neurons. Cell Calcium 43:296-306.

Yu Y, Fantozzi I, Remillard CV, Landsberg JW, Kunichika N, Platoshyn O, Tigno DD, Thistlethwaite PA, Rubin LJ, Yuan JX (2004) Enhanced expression of transient receptor potential channels in idiopathic pulmonary arterial hypertension. Proc Natl Acad Sci U S A 101:13861-13866.

Yuan JP, Zeng W, Huang GN, Worley PF, Muallem S (2007) STIM1 heteromultimerizes TRPC channels to determine their function as store-operated channels. Nat Cell Biol 9:636-645.

Zagranichnaya TK, Wu X, Villereal ML (2005) Endogenous TRPC1, TRPC3, and TRPC7 proteins combine to form native store-operated channels in HEK-293 cells. J Biol Chem 280:29559-29569.

Zapater P, Moreno J, Horga JF (1997) Neuroprotection by the novel calcium antagonist PCA50938, nimodipine and flunarizine, in gerbil global brain ischemia. Brain Res 772:57-62.

Zecca L, Youdim MB, Riederer P, Connor JR, Crichton RR (2004) Iron, brain ageing and neurodegenerative disorders. Nat Rev Neurosci 5:863-873.

Zhang L, Saffen D (2001) Muscarinic acetylcholine receptor regulation of TRP6 Ca2+ channel isoforms. Molecular structures and functional characterization. J Biol Chem 276:13331-13339.

Zhang L, Guo F, Kim JY, Saffen D (2006) Muscarinic acetylcholine receptors activate TRPC6 channels in PC12D cells via Ca2+ store-independent mechanisms. J Biochem 139:459-470.

Zhang P, Land W, Lee S, Juliani J, Lefman J, Smith SR, Germain D, Kessel M, Leapman R, Rouault TA, Subramaniam S (2005) Electron tomography of degenerating neurons in mice with abnormal regulation of iron metabolism. J Struct Biol 150:144-153.

Zhang Y, Li B, Chen C, Gao Z (2009) Hepatic distribution of iron, copper, zinc and cadmium-containing proteins in normal and iron overload mice. Biometals 22:251-259.

Zhang Y, Hoon MA, Chandrashekar J, Mueller KL, Cook B, Wu D, Zuker CS, Ryba NJ (2003) Coding of sweet, bitter, and umami tastes: different receptor cells sharing similar signaling pathways. Cell 112:293-301.

Zhang Z, Tang J, Tikunova S, Johnson JD, Chen Z, Qin N, Dietrich A, Stefani E, Birnbaumer L, Zhu MX (2001) Activation of Trp3 by inositol 1,4,5-trisphosphate receptors through displacement of inhibitory calmodulin from a common binding domain. Proc Natl Acad Sci U S A 98:3168-3173.

Zhou J, Du W, Zhou K, Tai Y, Yao H, Jia Y, Ding Y, Wang Y (2008) Critical role of TRPC6 channels in the formation of excitatory synapses. Nat Neurosci 11:741-743.

Zhu MX (2005) Multiple roles of calmodulin and other Ca(2+)-binding proteins in the functional regulation of TRP channels. Pflugers Arch 451:105-115.

Zitt C, Zobel A, Obukhov AG, Harteneck C, Kalkbrenner F, Luckhoff A, Schultz G (1996) Cloning and functional expression of a human Ca2+-permeable cation channel activated by calcium store depletion. Neuron 16:1189-1196.

APPENDIX

1. Synchrotron Radiation

In a number of specialized cases, X-ray analysis experiments make use of synchrotron sources. Synchrotron radiation (SR) is produced by high-energy (GeV) relativistic electrons or positrons circulating in a storage ring (Figure APPX 1). This is a very large, quasi-circular vacuum chamber where strong magnets force the particles on closed trajectories. X-ray is produced during the continuous acceleration of the particles. SR sources are several orders of magnitude brighter than X-ray tubes, have a natural collimation in the vertical plane and are linearly polarized in the plane of the orbit. The spectral distribution is continuous when the emission of radiation is induced by bending magnets (Figure APPX 2A). When more sophisticated magnetic arrays called undulators are used to produce the radiation, much intenser X-ray beams can be generated. The photons are emitted in specific energy bands called harmonics (Figure APPX 2B). This type of insertion device is used at ESRF ID22 beamline where our experiments were carried out. By changing undulator parameters such as the gap width and the magnetic field strength, the energy of the harmonics can be adjusted so that the output flux of an undulator in a specific energy range can be optimized. In view of their quasi-monochromatic nature, undulator sources therefore are more suitable for performing μXRF experiments involving monochromatic primary micro-beams, of which the energy can optionally be tuned. An additional advantage is the high degree of polarization of synchrotron radiation, which greatly reduces the scatter-induced spectral backgrounds when the detector is placed at 90 degree to the primary beam and in the storage ring plane.

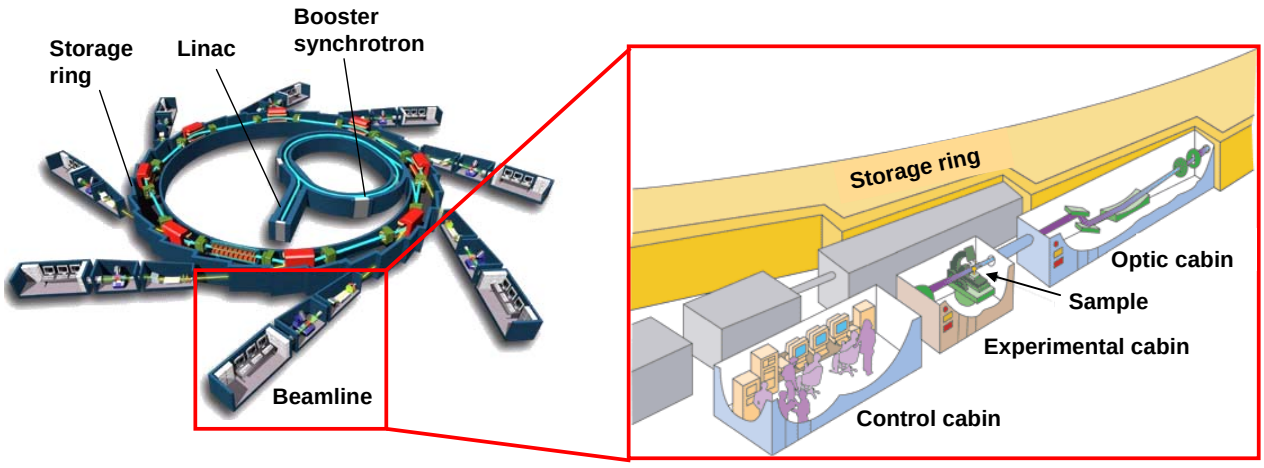

Figure APPX 1 Scheme of synchrotron radiation facility and a synchrotron beamline

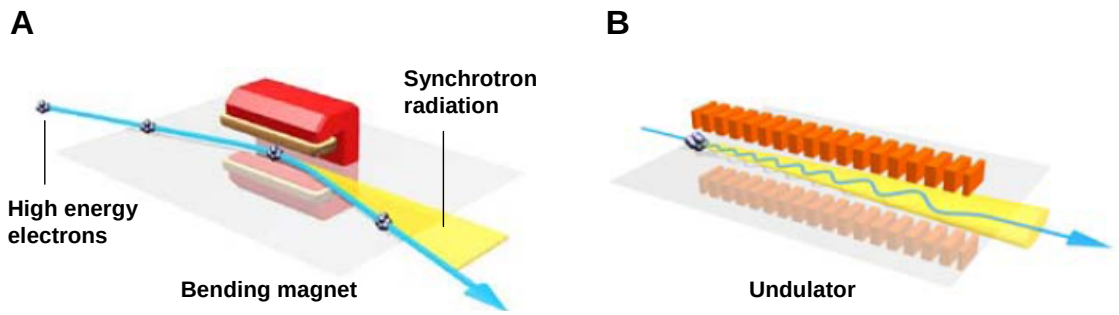

Figure APPX 2 Synchrotron radiation generated by the bending magnets (A) or by an undulator (B)

2. X-ray fluorescence

X-ray fluorescence analysis (XRF) is a powerful analytical tool for the spectrochemical determination of almost all the elements present in a sample. When a sample is irradiated with X-rays, the source X-rays may undergo either scattering or absorption by sample atoms. The latter phenomenon is known as the photoelectric effect. When an atom absorbs the source X-rays, the incident radiation dislodges electrons from the innermost shells of the atom, creating vacancies. The electron vacancies are filled by electrons cascading in from the outer shells. The outer shells electrons have higher energy than the inner shell electrons, and they give off energy as they cascade down into the inner shell vacancies (Figure APPX 3). This rearrangement of electrons results in the emission of characteristic X-rays of a given atom. The emission of X-rays, in this manner, is termed X-ray fluorescence. An X-ray source can excite characteristic X-rays from an element only if the source energy is greater than the absorption edge energy for the particular line group of the element, that is, the K absorption edge, L absorption edge or M absorption edge energy.

A typical emission pattern, also called an emission spectrum, for a given metal has multiple intensity peaks generated from the emission of K, L or M shell electrons. Each characteristic X-ray line is defined with the letter K, L or M, which signifies which shell has the original vacancy, and with a subscript alpha (α) or beta (β), which indicates the higher shell from which electrons fall to fill the vacancy and produce the X-ray. For example, a K_α line is produced by a vacancy in the K shell filled by an L shell electron, whereas a K_β line is produced by a vacancy in the K shell filled by an M shell electron. The K_α transition is on average 6 to 7 times more probable than the K_β transition; therefore, the K_α line is approximately 7 times intenser than the K_β line for a given element, making the K line the choice for quantitation purposes. The relationship between emission wavelength and atomic

number is known, thus isolation of individual characteristic lines allows the identification of an element and give estimates on the elemental concentrations from characteristic line intensities. Therefore, XRF is a powerful technique for determining the chemical composition of a sample.

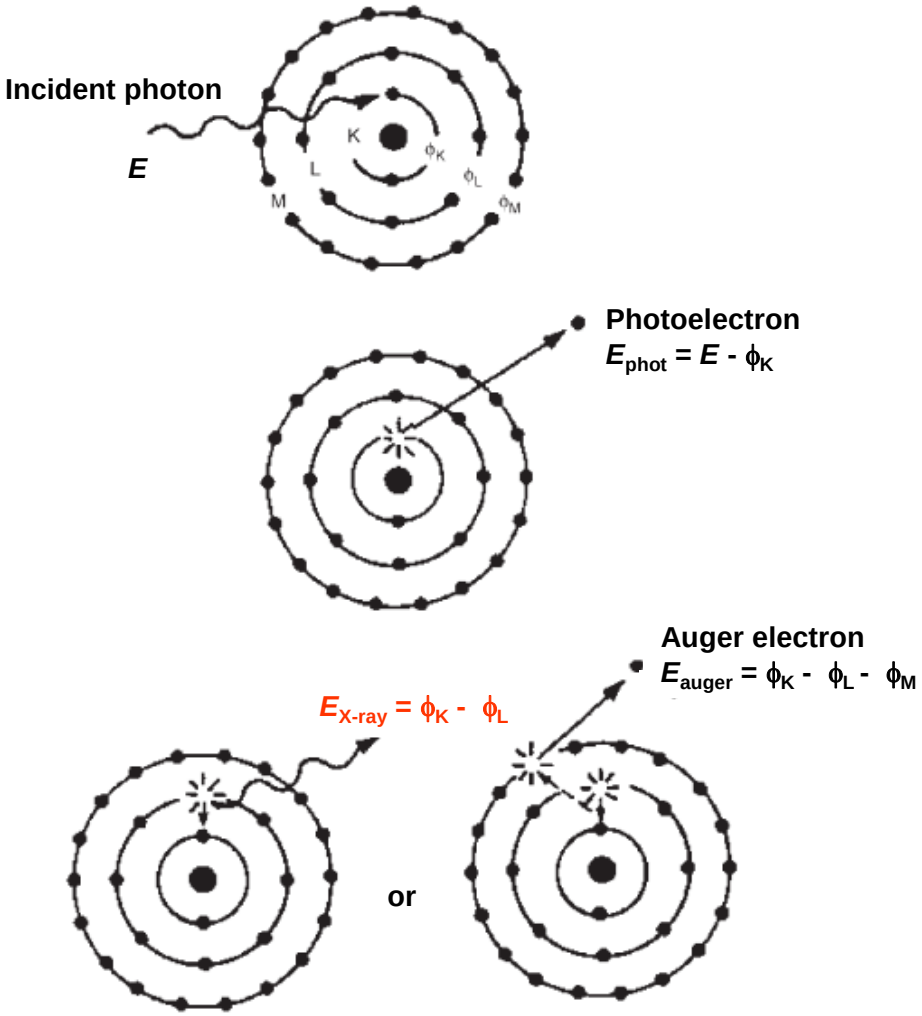

Figure APPX 3 Photoelectric ionization and emission of X-ray fluorescence

Photoelectric ionization can be followed by either radiative relaxation, causing the emission of characteristic fluorescent X-rays or non-radiative relaxation, involving the emission of Auger electrons.

3. Experimental set-up

In the XRF nanoprobe, the brilliant X-ray beam is focused to a small spot size down to 100 nm, and the sample (see Section 7.4) placed onto a piezoelectric stage with displacement accuracy in the nanometer range is then scanned. At each pixel, the fluorescence of each element is measured by an energy resolving detector (Figure APPX 4). The incident beam

intensity is varying with time and intensity normalization is required and achieved using a silicium-based PIN-diode as counter which is put just in front of the sample. A schematic view of the XRF nanoprobe beamline at ESRF is shown in Figure APPX 5.

Worldwide, only one similar nanoprobe end-station exists, which is situated at the Argonne Synchrotron in the USA. There are only few spatially resolved techniques available to map trace elements within samples of varying origins, among which the XRF synchrotron nanoprobe is the most sensitive muti-elemental technique with limit of detection in the order of the attogram in a 100 × 100 nm spot within a single cell.

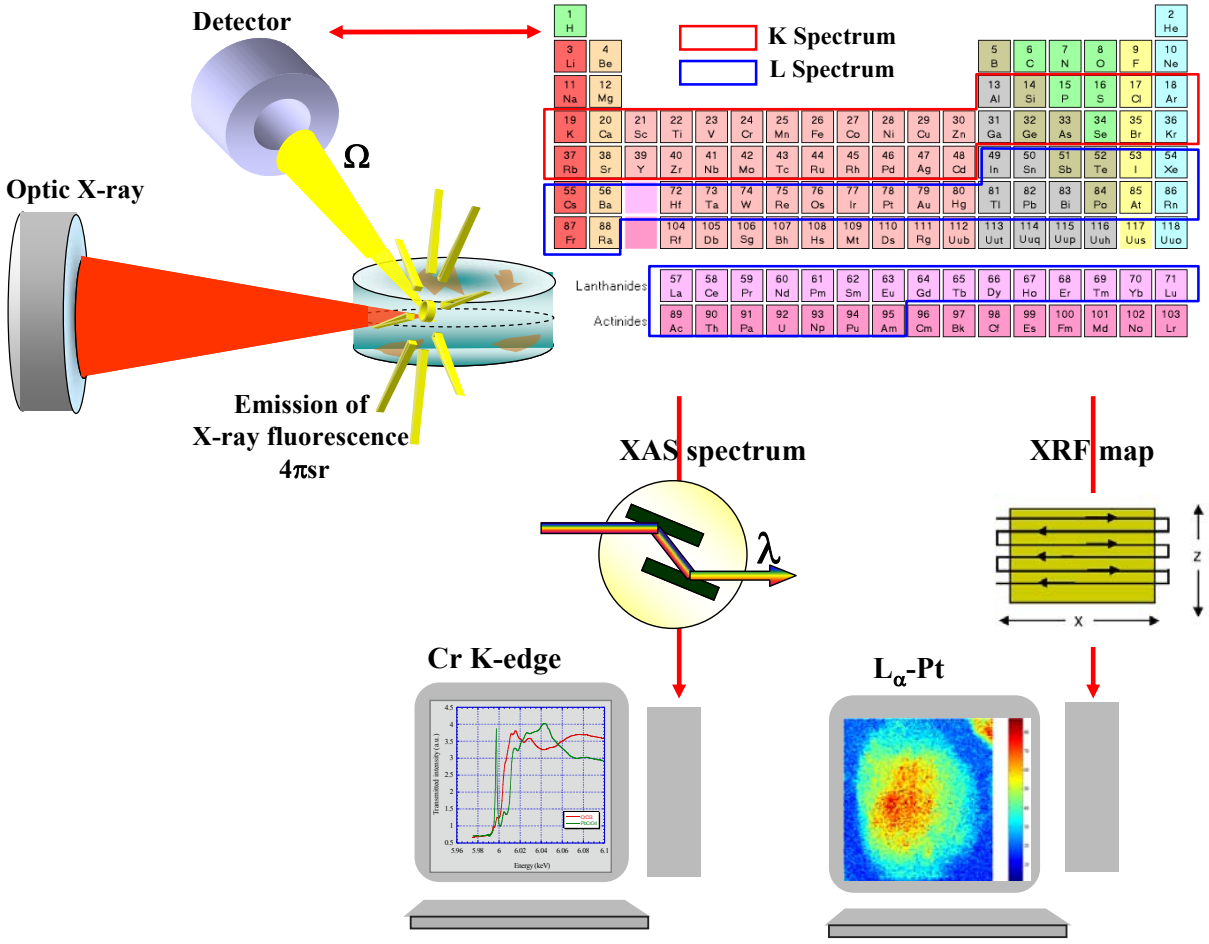

Figure APPX 4 A schematic view of data collection for obtaining 2D XRF maps or X-ray absorption spectroscopy (XAS)

In X-ray fluorescence mapping mode, only a small fraction of the isotropic fluorescence emission is collected by the detector solid angle Ω . The energy range of ID22 microprobe or nanoprobe (ID22NI) allows the detection of all elements of Z > 23 by using their K- or L- emission spectrum. The XRF maps are generated by continuous scanning of sample through the focused beam which is fixed.

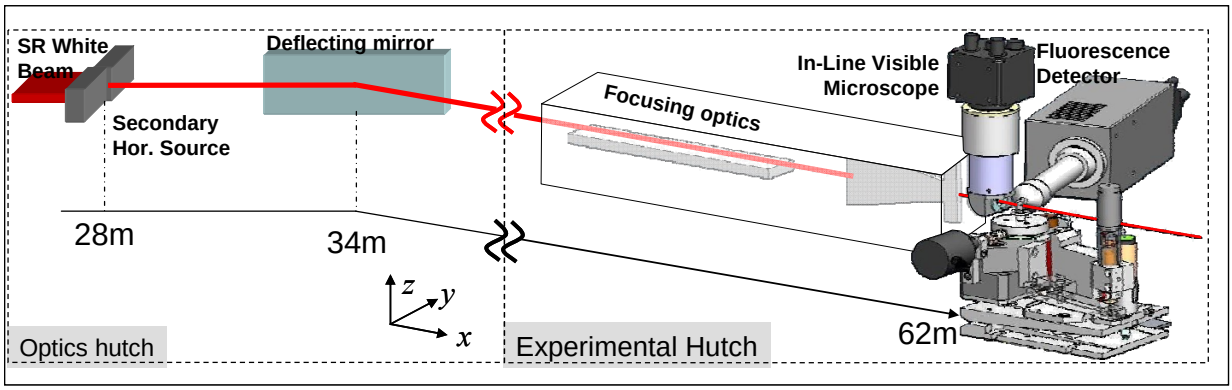

Figure APPX 5 A schematic view of the XRF nanoprobe beamline at ESRF

4. Data processing

The process to convert experimental XRF data into analytically useful information (i.e concentration values of elemental constituents) relies first on the evaluation of the spectral data, whereby the net intensities of the X-ray peaks are determined (essentially the background contribution is carefully subtracted from the spectrum followed by individual peaks deconvolution using fitting algorithm), peak overlap (if any) between X-ray lines of different elements are corrected and the X-ray intensities are converted into concentration data, i.e. the quantification. In our case some assumptions can be made to simplify the quantification process: parallel beam approximation, homogeneous sample and the absence of matrix effects (absorption-enhancement effects). This is justified when working with very thin samples like cells containing trace metals (e.g. diluted high Z elements in a thin low-Z matrix mainly carbon), resulting in simplified equation for concentration calculation (Bohic et al., 2001). XRF data can be normalized against a standard having similar matrix and elemental concentration. For this, we used a thin disc of a NIST SRM 1577 bovine liver with certified concentration to calibrate the experimental data. The data processing is performed using the free software PyMca developed at ESRF (Solé et al., 2007).

References

Bohic S, Simionovici A, Snigirev A, Ortega R, Deves G, Heymann D, Schroer CG (2001) Synchrotron hard x-ray microprobe: Fluorescence imaging of single cells. Applied Physics Letters 78:3544-3546.

Solé VA, Papillon E, Cotte M, Walter P, Susini J (2007) A multiplatform code for the analysis of energy-dispersive X-ray fluorescence spectra. Spectrochimica Acta Part B: Atomic Spectroscopy 62:63-68.

RESUME

Les canaux TRPC6 sont des canaux cationiques non sélectifs qui peuvent être activés par le diacylglycérol (DAG). Ils sont présents dans de nombreux tissus et types cellulaires, notamment dans le cortex de souris embryonnaire (à E13). Des expériences d'imagerie calcique réalisées sur des neurones de cortex de souris en culture ont révélé la présence de canaux cationiques activés par le DAG. Ils sont perméables aux ions Ca^{2+}, Na^{+}, Ba^{2+} et Mn^{2+}. L'entrée de Ca^{2+} via ces canaux est indépendante de la protéine kinase C et elle est bloquée par le SKF-96365 et le Gd^{3+}. Par ailleurs, l'acide flufénamique augmente l'amplitude des réponses calciques induites par le DAG. Des expériences d'électrophysiologie réalisées avec la technique du *patch-clamp* en configuration cellule entière ont montré que l'hyperforine, un activateur des canaux TRPC6, donne naissance à un courant cationique non sélectif, confirmant ainsi l'existence de canaux de type TRPC6 dans les neurones corticaux.

Des analyses quantitatives en spectrométrie d'émission atomique à plasma couplé inductif, en spectrométrie d'absorption atomique et en fluorescence X avec la nanosonde synchrotron (μ-SXRF) révèlent que la surexpression de TRPC6 dans les cellules HEK-293 s'accompagne d'une augmentation du contenu intracellulaire en zinc, en soufre et en manganèse. Les résultats obtenus avec des sondes fluorescentes sensibles au zinc et au fer indiquent que les canaux TRPC6 peuvent transporter ces cations. Par ailleurs, les expériences en μ-SXRF montrent que l'activation des canaux TRPC6 en présence de fer induit une accumulation de ce métal dans les cellules HEK et les neurones.

Au cours de notre étude, nous avons également mis en évidence l'action de deux agents (l'acide flufénamique et l'hyperforine), couramment utilisés pour modifier l'activité des canaux TRPC6, sur la physiologie mitochondriale et l'homéostasie des métaux. En effet, l'acide flufénamique et l'hyperforine non seulement modifient le fonctionnement des canaux TRPC6 mais ils exercent aussi une action de type découplante sur les mitochondries, provoquant une libération de Ca^{2+} et de Zn^{2+} à partir de ces organelles.

Mots clés : neurones de cortex, cellules HEK-293, TRPC6, diacylglycérol, acide flufénamique, hyperforine, rayonnement synchrotron, fluorescence X, fer, zinc, cuivre, manganèse